THE CHARLESTON METAMORPHIC GROUP: PALEOZOIC AND CRETACEOUS DEFORMATION AND METAMORPHISM, AND DEVELOPMENT OF THE PAPAROA METAMORPHIC CORE COMPLEX

A thesis

submitted in partial fulfillment

of the requirements for the degree

of

Master of Science in Geology

in the

University of Canterbury

by

Kathryn J. Lewthwaite

University of Canterbury

1995

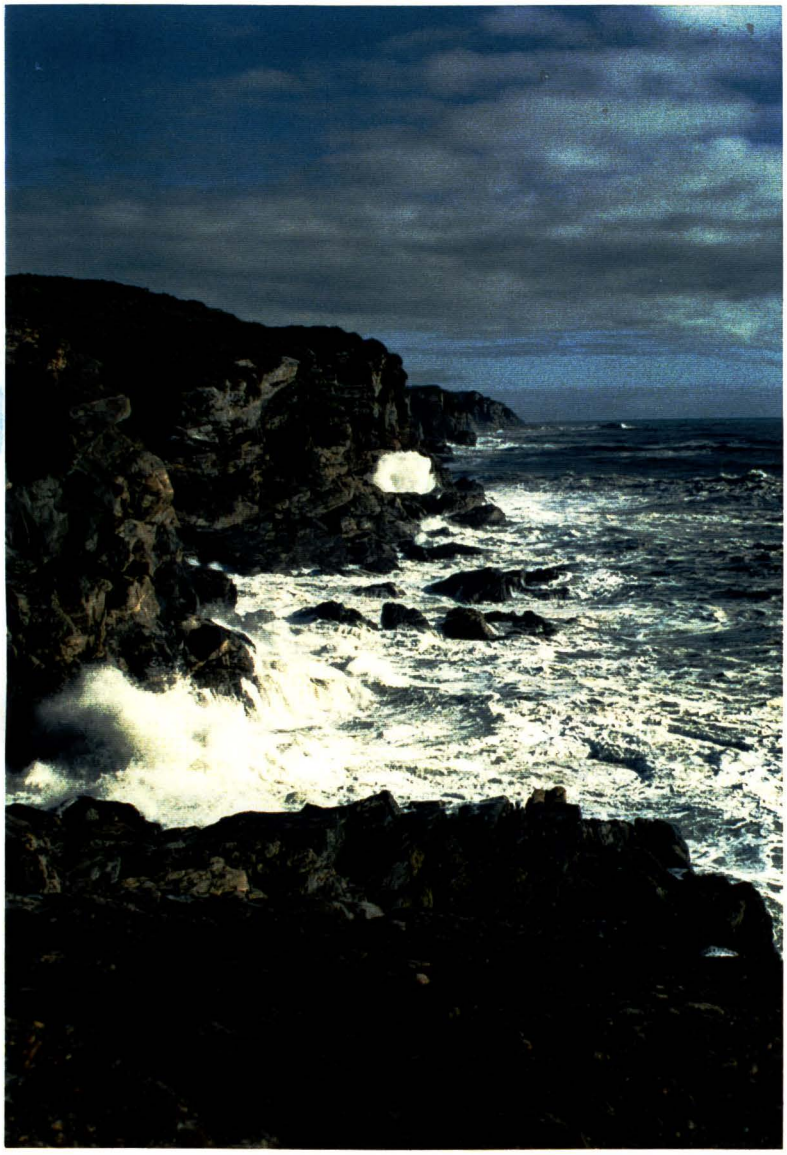

Frontispiece: Coastal view from cliffs below the Charleston Cemetery.

TO GOD

ABSTRACT

The Charleston Metamorphic Group exposed in the Paparoa Range and along the coast to the west has recently been interpreted as the lower plate of an exhumed metamorphic core complex (Paparoa Metamorphic Core Complex), developed during NNE-SSW-oriented extension in the mid-Cretaceous. A detailed fabric analysis of the Charleston Metamorphic Group exposed along the coast between Cape Foulwind and south of Belfast Creek was undertaken to test this hypothesis.

On the southern limb of the proposed core complex, mylonites of the Morrisey Creek Mylonite Zone, Deep Creek Mylonite Zone and near the mouth of the Four Mile River possess generally NE-SW-trending stretching lineations. Shear-sense indicators within these mylonitic rocks show predominantly a top-to-the-SW sense of shear. NE-SW-trending lineations and top-to-the-SW shear-sense indicators found in these mylonitic rocks sub-parallel the trend of lineations and direction of shearing recorded in mylonites underlying the Pike Detachment Fault in the southern Paparoa Range.

South of the MCMZ, south of White Horse Creek, mylonitized migmatites record a top-to-the-NE sense of shear overprinted by top-to-the-SW fabrics. Top-to-the-NE senses of shear possibly record the development of an early top-to-the-NE detachment fault.

On the northern limb of the proposed core complex, mylonitized syenogranite-monzogranite in the Siberia Bay Mylonite Zone and monzogranitic gneiss at the south Tauranga Bay Headland possess stretching lineations which trend from NE-SW to ENE-WSW. Most shear-sense indicators record a top-to-the-NE/ENE sense of shear, associated with movement on the overlying Ohika Detachment Fault. However, C-, S, and C′-planes which record a top-to-the-NE/ENE sense of shear in the Siberia Bay Mylonite Zone and Tauranga Bay monzogranitic gneiss have been reactivated during a later top-to-the SW/WSW movement which can possibly be attributed to the overprinting of fabrics associated with the Ohika Detachment Fault by fabrics associated with movement on the Pike Detachment Fault, or the development of conjugate C′-planes near the axis of the core complex.

This study has shown quartz c-axis preferred orientations to be unreliable shear-sense indicators.

Intrusion of mid-Cretaceous magmas around Charleston imposed important local controls on the ductile deformation of the lower plate, forming the WNW-ESE-trending arches. Opposing senses of shear on either side of these arches suggests that ductile deformation at these localities was controlled by the uprise of magma rather than the movement of the overlying detachment faults.

Post-mylonitic granitoid intrusion is recorded throughout the mylonite zones. In the Siberia Bay Mylonite Zone, post-mylonitic pegmatite intrusion has been accompanied by localised post-mylonitic intrusion of syenogranite-monzogranite. Extreme post-mylonitic brittle deformation is recorded on the coast south of White Horse Creek.

NNW-SSE-trending lineations found in the monzogranitic gneiss at Cape Foulwind and paragneiss near Charleston, and top-to-the-NW/NNW shear-sense indicators associated with

NW-NNW-trending mylonitic lineations south of White Horse Creek may be of Paleozoic or Cretaceous age.

A two stage model for core complex development is proposed. The first stage involves the formation of regional, conjugate listric normal faults. The second stage envisages growth and eventual dominance of the Pike Detachment over the Ohika Detachment and a possible third southern detachment.

TABLE OF CONTENTS

LIST OF FIGURES

ACKNOWLEDGEMENTS

My sincere thanks to my supervisor, Associate Professor David Shelley, for his advice during the research stage of this project, his willingness to read and re-read draft chapters and his enthusiasm for petrofabric analysis. My thanks also to Dr Roddie Muir, who suggested new ways of solving problems which occurred during the course of this work, who always encouraged me to pursue the "theory of least astonishment", and whose cheerfulness was greatly appreciated.

Todd Waight and Associate Professor Steve Weaver are thanked for illuminating discussions on the granitoids of the Western Province.

Rob Spiers went far beyond the call of duty making thin section upon thin section, and Michael Finnemore fielded many a cry about 'that Rockware program'. Their help was greatly appreciated. Kerry Swanson is thanked for advice and help with photography.

Financial support from the Mason Trust Fund and University of Canterbury Masters Scholarship which paid for field expenses and thesis production and is most appreciated.

Greg Bell and Andrew Rennie are thanked for their West Coast hospitality and access to their land.

Big thankyous must go to fellow students Nicola Litchfield for her friendship and help in the field, and Kay Cooper, for being a sympathetic fellow U-stage sufferer. Nicola Dodunski is thanked for her confidence that I would finish on time, and Greg Sheppard and Tim Jowett are thanked for hacking outside the room. Thanks to Craig Farrow who spent his Saturday spell-checking and reference-checking this thesis.

Finally, special thanks and deep gratitude goes to my family for their support and encouragement during the years of study, and for absorbing all that stress in the last two months of this thesis.

CHAPTER ONE

INTRODUCTION

1.1 The Paparoa Metamorphic Core Complex

The Paparoa Metamorphic Core Complex was first proposed by Tulloch and Kimbrough (1987, 1989) to explain the juxtaposition of low grade metasedimentary rocks of the Greenland Group and high grade metamorphic rocks of the Charleston Metamorphic Group in the Paparoa Range. In this model, (Fig 1.1), Tulloch and Kimbrough suggest that the Greenland Group and overlying terrestrial conglomerates of the Pororari Group comprise the upper plate of a core complex, separated from the lower plate, or Charleston Metamorphic Group, by low angle detachment faults during the mid-Cretaceous extension which preceeded rifting of New Zealand from Australia. Two detachment faults were recognised: the Ohika Detachment Fault and the Pike Detachment Fault. According to Tulloch and Kimbrough (1989), mylonites underlying the Ohika Detachment Fault in the lower Buller Gorge record a top-to-the-NE sense of shear, while in the SW Paparoa Range, mylonites associated with the Pike Detachment Fault record a top-to-the-SSW sense of shear. Tulloch and Kimbrough further proposed that the extension direction during core complex formation was NNE-SSW based on similarly trending, regionally consistent stretching lineations in mylonitic rocks of the lower plate.

The NNE-SSW extension required by the Paparoa Metamorphic Core Complex model is supported by WNW-trending mid-late Albian (110-95 Ma) sedimentary basins of the upper plate in the southern Paparoa Range (Laird 1994) and WNW-ESE-trending late Cretaceous lamprophyre dykes. However, no further work has been published regarding the kinematic analysis of the lower plate of the Paparoa Metamorphic Core Complex.

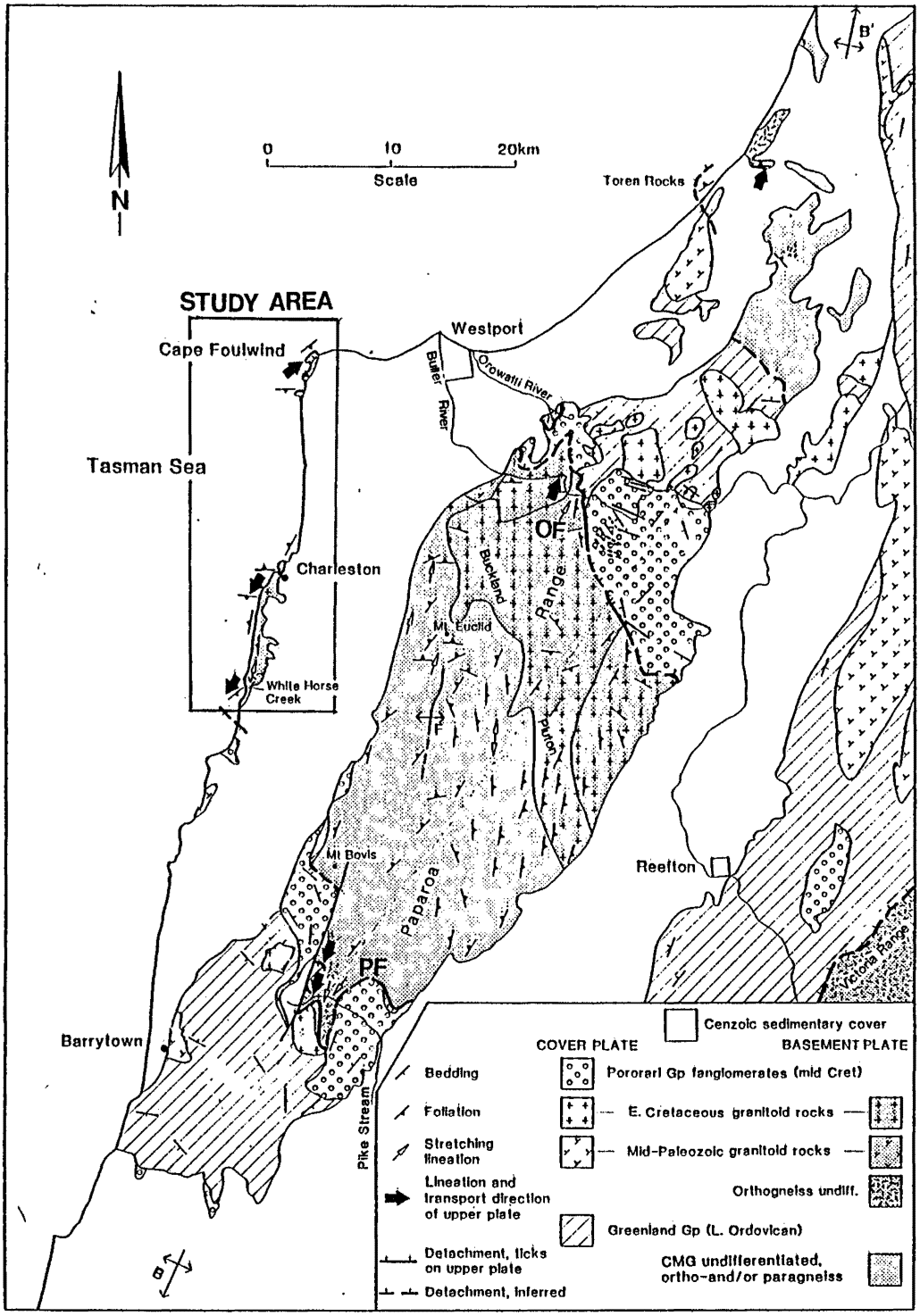

Fig. 1.1 The Paparoa Metamorphic Core Complex model proposed by Tulloch and Kimbrough (1989) showing proposed movement directions of the upper plate and location of the Pike Detachment (PF) and Ohika Detachment (OF), and location of study area.

1.2 Regional Geology

The South Island of New Zealand is divided into two provinces, separated by a complex belt of dismembered arcs known as the Median Tectonic Zone (Bradshaw 1993) and offset by 480 km along the Alpine Fault. The Western Province consists of the Buller and Takaka Terranes, separated by the Anatoki Thrust (Fig 1.2). The Buller Terrane comprises Ordovician shales, siltstones and quartz-rich sandstones of the Greenland Group, and amphibolite facies mixed ortho- and paragneisses and migmatites, which, in part, comprise the Charleston Metamorphic Group. To the east, the Takaka Terrane consists of tectonic slices of Ordovician carbonates, Silurian quartzites and Cambrian sandstones, mudstones, conglomerates, volcanics and volcanogenic sediments (Cooper 1989). According to Muir et al (1994a), the Western Province is a fragment of Gondwana with clear relationships to Antarctica and Australia.

The Eastern Province, which lies to the east of the Median Tectonic Zone, contains generally younger arc-volcanics, volcanogenic sediments and Permian-Mesozoic accretionary complexes which developed as a result of convergence along the Gondwana Margin (Bradshaw 1989).

Low grade metasedimentary rocks of the Western Province are cut by three NNE-trending batholiths and several isolated plutons (Fig 1.2). Tulloch (1988) divided the granitoid rocks of the Western Province into three suites based on age, geochemical characteristics, mineralogy and granite type. The Karamea Suite comprises Devonian-Carboniferous S-type biotite and two-mica granitoids and is confined to the Buller Terrane. Granitoids of mid- Cretaceous age comprise the Separation Point and the Rahu Suites. Granitoids of the Separation Point Suite are characterised by biotite ± hornblende monzogranites to diorites with I-type geochemical characteristics (Muir et al 1994a) and occur in both the Buller and Takaka Terranes. The Rahu Suite is of a transitional I/S-type character dominated by granites and granodiorites and is restricted to the Buller Terrane (Muir et al 1994a). Granitoids of mid-Cretaceous age (114-109 Ma) also occur in the Hohonu Ranges (Waight 1995) and are geochemically similar to the Rahu Suite granitoids.

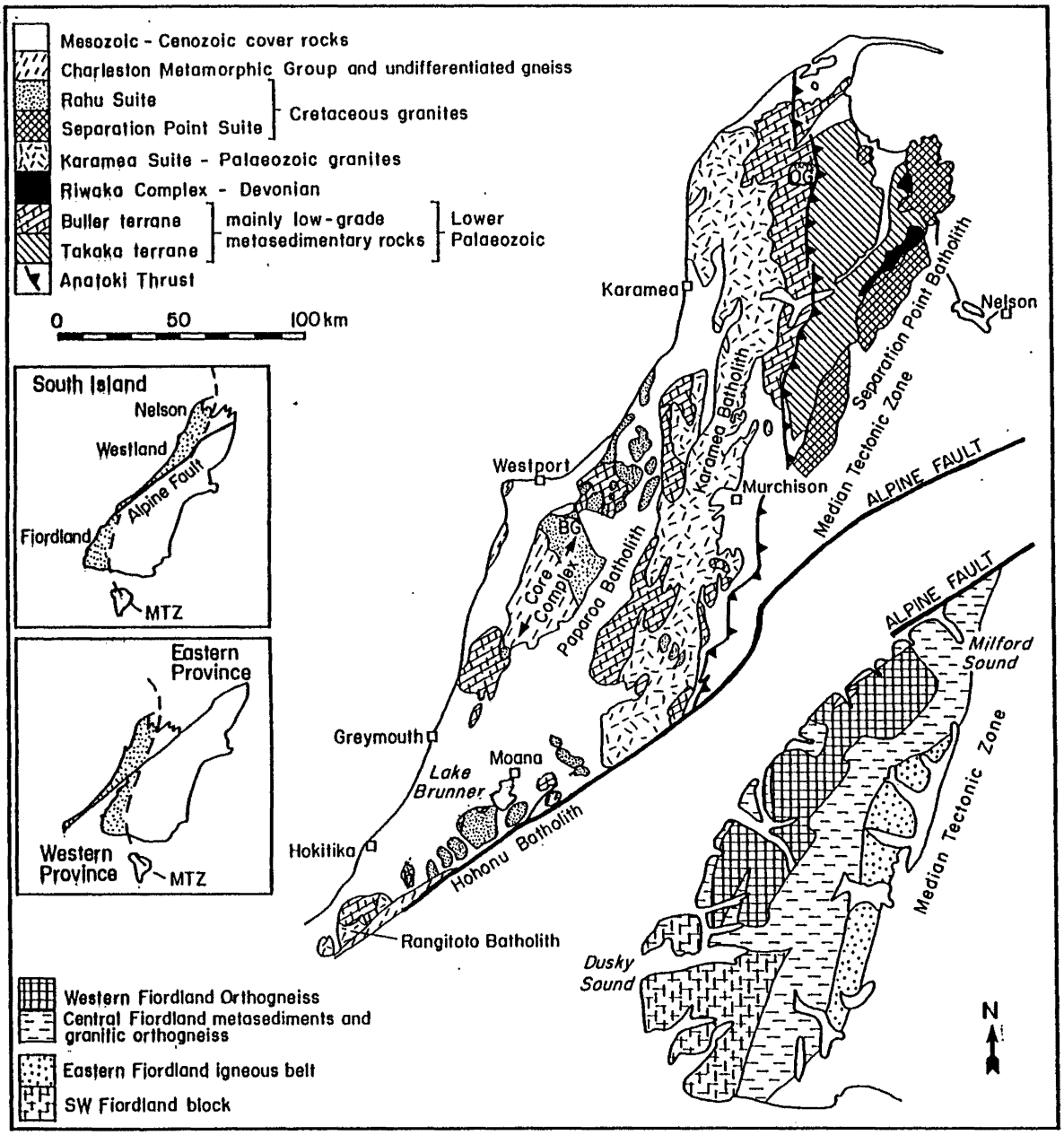

Fig. 1.2 Geology of the Western Province modified from Waight (1995) and Muir et al (1994a).

1.3 Definition of the Charleston Metamorphic Group

Metamorphic rocks exposed along the coast south of Charleston and in the Paparoa Range were first named Charleston Gneiss by Grindley et al (1959) and later, Constant Gneiss by Bowen (1964). Nathan (1975) renamed the Constant Gneiss the "Charleston Metamorphic Group", but excluded from his definition the deformed granitoids of Paleozoic emplacement age at Cape Foulwind and the younger Red Jacket Granite.

Tulloch and Kimbrough (1989) regarded the Charleston Metamorphic Group as "not characterised by a particular age or metamorphic grade, but by a regional ductile deformation" and suggested that Nathan's original definition be extended to include similarly deformed units such as the Buckland Granite and Windy Point Granite, or be restricted to the high grade metasedimentary component. Tulloch and Kimbrough favoured the former option.

However, in this field area, granitoids of Paleozoic and Cretaceous emplacement age, and paragneisses and migmatites are characterised by a moderate to high grade of metamorphism of possibly a range of ages, the last moderate to high grade metamorphic event being the ductile deformation during the Cretaceous. Therefore, the Charleston Metamorphic Group is defined here as granitoids of Paleozoic and Cretaceous emplacement age, and paragneisses and migmatites of moderate to high metamorphic grade and uncertain age which have undergone a ductile deformation in the Cretaceous. Thus, the deformed monzogranites at Cape Foulwind, the Windy Point Granite, Buckland Granite and Red Jacket Granite, which possess a tectonic foliation related to a moderate to high grade metamorphic event of Cretaceous age are included in the Charleston Metamorphic Group.

1.4 Thesis Objectives

This thesis was undertaken to investigate, in detail, the structures and kinematic indicators in the lower plate rocks in order to test the Paparoa Metamorphic Core Complex model and NNE-SSW directed extension proposed by Tulloch and Kimbrough (1987, 1989).

These objectives were achieved through the following studies:

1) Structural mapping of the Charleston Metamorphic Group from Cape Foulwind to just south of Belfast Creek, including foliations, lineations and mesoscopic folds.

2) Petrofabric studies in Cretaceous mylonitic zones and gneisses in order to interpret a sense of shear by using kinematic indicators including quartz c-axis fabrics.

3) Structural, kinematic and textural descriptions of structurally anomalous, generally migmatitic areas including the Red Jacket Granite.

1.5 Location of Study

The study area is located 11 km west of Westport around the Tauranga Bay and Cape Foulwind headlands, and 18 km to the south, from Parsons Hill, just north of Charleston to south of Belfast Creek, encompassing 3 km^2 of Paparoa National Park (Fig 1.1).

Outcrop is generally restricted to the rugged coastline, road cuttings, river beds and very limited inland exposures. Cape Foulwind, Tauranga Bay and the Charleston coast are easily accessible. However, to the south, access to the coast is only possible at the mouth of Deep Creek, and between the Four Mile River and Red Jacket Creek. In this study area, inland exposures of Charleston Metamorphic Group are unconformably overlain by Tertiary and gold-bearing Quaternary sediments (Map 1). Mining of the raised Quaternary

gold-bearing black sands and gravels during the early nineteen hundreds has left historically interesting relics that were discovered during traverses from State Highway 6 to the coast. However, much of the area is now densely vegetated with gorse, manuka and towards the south, subtropical rainforest.

The New Zealand Fur Seal inhabits much of the coastline and two particularly large colonies occur at Cape Foulwind and at the mouth of Deep Creek. Access to some areas of coast, heavily populated in seals, was difficult.

1.6 Previous Works.

1.6.1 Geology

The first geological explorations of the northwest coast of the South Island were those by Charles Heaphy and Thomas Brunner in 1846 and 1847; the first regional geological report to be published was by Julius von Haast in 1864. Crystalline schists along the Buller River and muscovite in gneisses near Charleston were described by Haast (1865), Hector (1865) and Cox (1882). Commercial mining of muscovite during 1911-1912 was described by Morgan and Bartrum (1915).

Bartrum (1914) and Morgan and Bartrum (1915) described gneiss from the Paparoa Range, inliers of granite or gneissic rock from Cape Foulwind to south of Charleston, and "lit-par-lit or injection gneisses" at the mouth of the Nile River, noting undulatory extinction of quartz and bending of mica lamellae. Morgan and Bartrum (1915) considered most of the granite and gneiss to be of the same age, but the reservation was made that the sedimentary gneiss could be "perhaps Precambrian of age, unconformably underlying Ordovician greywackes and argillites".

Early research into the relative age of gneissic rock and Paleozoic sediments was hindered because no contact between the two could be found (Henderson 1917), and because the age of the Greenland Group itself was not established until lower Ordovician

Graptolitic fauna were discovered by Cooper (1974). However, Henderson (1917), Wellman (1956), Reed (1958), and Grindley et al (1959) speculated that the Charleston Metamorphic Group gneisses were older than the plutonic rocks of the same region. Suggate (1957) disputed other workers suggesting that granitic and gneissic rock in the Paparoa Range constitutes one complex batholith, intruded into the Greenland Group sediments. Grindley et al (1961) assigned a tentative Precambrian age to granite-gneiss exposed at Charleston based on "high metamorphic grade and intense deformation" and suggested granitic rock in the northern Paparoa Range was intrusive into both the gneiss and Greenland Group.

In 1967, Laird described a "gradational contact" between the Greenland Group and the Charleston Metamorphic Group in the southern Paparoa Range, concluding that the gneiss was metamorphosed Greenland Group. Laird (1967) assigned an upper Jurassic age to gneissification, folding and erosion of the Greenland Group. Later evaluation of this contact led Hume (1977) to suggest that the gneiss was not, in fact, metamorphosed Greenland Group but that the Greenland Group was unconformably deposited on top of the gneiss. However, both Laird (1967) and Hume (1977), made the reservation that a thrust contact could not be ruled out; a tectonic contact has since been favoured by Laird (1988).

The structure and petrography of the gneiss near Charleston and Cape Foulwind was first described in detail by Shelley (1970, 1972) who distinguished three phases of plutonism and structural development. The first phase was associated with NNW-SSE folds; the second with ESE-WNW folds and the third with NE-SW trending structures and formation of mylonites, probably during the Cretaceous. Shelley proposed that the metasedimentary layers and enclaves represented metamorphosed Greenland Group and noted that the principal regional structural feature to explain was the marked contrast in attitude between the subhorizontal foliation and metasedimentary layers in the gneisses, and the subvertical cleavage and tight generally upright folding of the nearby Greenland Group. The structure of the gneiss was explained by "simple flattening parallel to bedding with little penetrative movement" and on the basis of fold vergence, Shelley (1972) proposed the development of "mantled gneiss domes", with the overlying Greenland

Group sliding off the high points of such domes. Shelley (1970, 1972) suggested that the formation of the domes occurred in the Ordovician.

Tulloch and Kimbrough (1987, 1989) re-interpreted the contact between the Greenland Group and the Charleston Metamorphic Group in the Southern Paparoa Range. Tulloch and Kimbrough (1987) suggested that high grade gneisses of the Charleston Metamorphic Group constitute the lower plate of an exhumed metamorphic core complex centred on the Paparoa Range, separated from lower greenschist facies Greenland Group sediments by low angle detachment faults proposing that extension was oriented along NNE-SSW lines. Further studies of the Charleston Metamorphic Group in the Paparoa Range by White (1994) record peak metamorphic conditions of 600 ± 50°C and 4 ±1 kb and uplift rates of the order of 0.6-1.0 mm/a for rocks of the lower plate.

1.6.2 Geochronology

Reconnaissance Rb-Sr geochronology of the west-Nelson area by Aronson (1965, 1968) indicated two main periods of metamorphic and plutonic activity at approximately 350-370 Ma and 100-120 Ma. Paleozoic magmatism has since been refined into two periods; mid Devonian (380 Ma) and early Carboniferous (330 Ma) (Muir et al 1994a).

Orthogneiss at Charleston records Cretaceous crystallisation ages of 114 ± 18 Ma (Kimbrough and Tulloch 1989) and 95-120 Ma (Ireland 1992). However ages as young as 95 Ma conflict with a Rb-Sr date of 108 Ma on undeformed pegmatite from Charleston (recalculated from Aronson 1968). Muir (pers. comm.) suggests that the 120-95 Ma ages of Ireland (1992) have high associated errors and that crystallization of the magmas probably occurred at around 110 Ma. A late Precambrian isochron of 680 ± 21 Ma (Adams 1975a) is now considered to be a scatterchron of varied rock types indicating source rock age rather than an age of gneissification (Tulloch and Brathwaite 1986).

K-Ar and $^{40}Ar/^{39}Ar$ dating methods have also produced Cretaceous ages for lower plate gneisses and granites in the Paparoa Range (Spell and Mc Dougall. pers. comm). Zircon U-Pb dating of the ductilely deformed Buckland Granite in the northern Paparoa Range at

109.6 ± 1.7 Ma (Muir et al 1994a) suggests that ductile deformation associated with the formation of the Paparoa Metamorphic Core Complex was occurring at around 109 Ma in the Paparoa Range. Undeformed pegmatite at Charleston (108 Ma; recalculated from Aronson 1968) and lamprophyre dykes dated at 86-80 Ma (Adams and Nathan 1978) suggest that ductile deformation had ceased by approximately 108 Ma at Charleston and 86 Ma in the Paparoa Range.

Ion microprobe analysis of paragneiss zircons rims from near Charleston give minimum ages of 380-400 Ma and probably represent the Ordovician Metamorphism of the Greenland Group (Ireland 1992).

1.7 Methods

1.7.1 Field Work

Approximately 8 weeks of field work were undertaken during January, June and September 1994, and December-January 1995. Outcrops were initially located using Sheets S23 and S30 Foulwind and Charleston (Nathan 1975) and the structural map published by Shelley (1970). Foliations and lineations were measured using a Sunto compass. Although the West Coast is known for wet weather and sandflies, field work was not unpleasant due to the warm climate and a good insect repellent. Few days were lost to rain.

1.7.2 Petrographic Techniques

From the study area, 76 oriented specimens were collected. From these specimens thin sections were cut parallel to the dominant lineation (parallel to the axis of greatest finite strain X) and at right angles to the foliation plane (ie in the plane containing the axis of greatest finite strain, X, and the axis of least finite strain, Z). Textural studies of some specimens required an additional section to be cut perpendicular to both the lineation and foliation.

All shear-sense indicators were observed in XZ thin sections and quartz c-axes in this section were measured on a universal stage using techniques outlined in Shelley (1993). Wherever possible, at least 250 individual quartz grains were measured. The crystallographic data were plotted on equal area lower hemisphere stereonet projections and contoured using the Rockware structural data software package.

1.8 Thesis Organisation

On the basis of location, lithology, structure and texture, the Charleston Metamorphic Group is divided into six broad groups of rocks: mylonites; Charleston, Deep Creek and Four Mile River orthogneisses; Cape Foulwind and Tauranga Bay orthogneisses; the Red Jacket Granite and similar lithologies; paragneisses and migmatites of sedimentary origin; and hornfelsic lithologies.

In Chapter 2, the lithologic character and mineralogy of the six groups are briefly outlined. Structural and petrofabric analysis of mylonitic rocks that are of significance to the core complex model are discussed in Chapter 3. Chapters 4, 5, and 6 are divided into areas of structural similarity, and not necessarily by lithological character. Chapter 4 describes the orthogneisses and paragneiss lithologies outcropping around Charleston and at the mouth of the Four Mile River. The structural and petrofabric analysis of orthogneisses at Cape Foulwind and Tauranga Bay are outlined in Chapter 5. Chapter 6 outlines the structural development of the Red Jacket Granite, and the surrounding coastal migmatites of sedimentary origin south White Horse Creek. After a brief description of hornfelsic lithologies in Chapter 7, the origin of true and apparent shear reversals are discussed in Chapter 8. Finally, a discussion and model for the development of the Paparoa Metamorphic Core Complex, and future work follows in Chapter 9, and brief conclusions in Chapter 10.

In this thesis, kinematic analysis relies heavily on the interpretation of shear-sense indicators. The remainder of this chapter briefly introduces common shear-sense indicators found in mylonitic zones.

1.9 Mylonite Zones and Shear-sense Indicators

1.9.1 Introduction

In fault zones below the brittle-ductile transition, mylonitization of quartz-feldspar-mica rocks involves both crystal-plastic deformation and cataclasis. However, crystal-plasticity dominates producing ductile deformation on a regional, outcrop and thin section scale. In these ductile shear zones quartz undergoes plastic deformation and commonly dynamic recrystallization accommodating large amounts of strain. At the same time, rigid grains such as feldspar and garnet undergo cataclastic deformation to form porphyroclasts, and sheet silicates become bent and cataclased. This strain partitioning produces unique fabrics visible in hand specimen and thin section which may be used to determine sense of shear such as S-, C- and C′-planes, porphyroclast systems and fracture patterns, oblique quartz shape-preferred orientations, asymmetric microfolds and quartz c-axis fabrics.

1.9.2 S-, C- and C′- Planes

Two anastomosing foliations called C- and S-planes (Berthé et al 1979) commonly occur in sheared granitoids (Fig 1.3). The C-plane develops as a result of localised high shear strains, parallel to, or at a low angle to the shear zone wall (Shelley 1993). The S-plane is related to the accumulation of finite strain in zones not subject to intense shearing (Lister and Snoke 1984), and develops at a high angle to the maximum compressive stress direction. The S-plane is initially oriented at 45° to the C-plane but may rotate into parallelism with the C-plane and shearing progresses. The relative configuration of C-and S-planes allows shear sense to be determined.

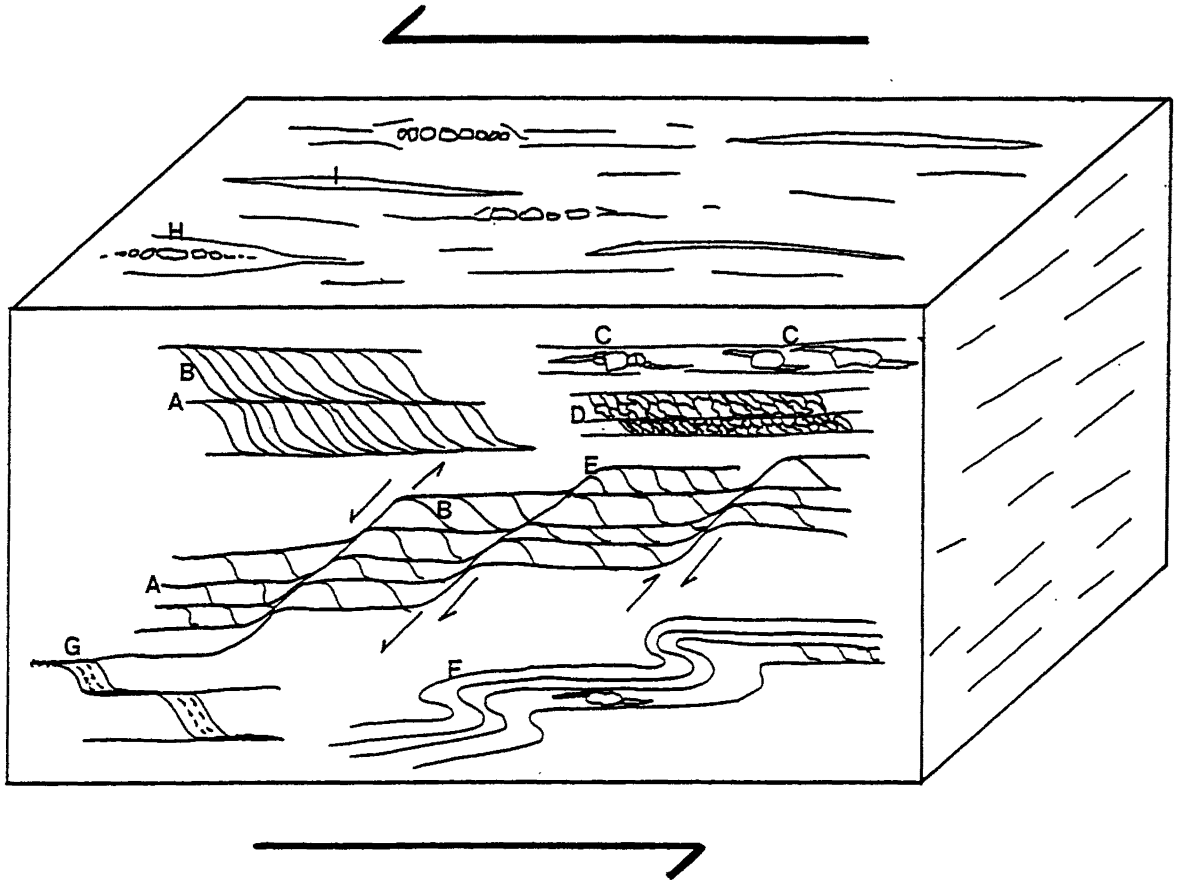

A = C-plane
B = S-plane
C = σ-type porphyroclast
D = oblique quartz shape-preferred orientation
E = C′-plane
F = asymmetric microfolds
G = mica fish
H = boudinaged porphyroclast
I = quartz ribbon

Fig 1.3 Common shear-sense indicators in a mylonite undergoing a simple shear.

C′-planes, also termed shear bands (White et al 1980), extensional crenulation cleavages (Platt and Vissers 1980), asymmetric extensional shear bands (Hanmer and Passchier 1991) and synthetic Riedel shears (Shelley 1993) are usually oriented between 15°and 20° to the mylonitic foliation. If well developed, C′-planes may constitute a foliation or cleavage. However, their development is typically discontinuous when compared with C-planes. During non-coaxial deformation one set of C′-planes develop, synthetic to the mylonitic foliation (White et al 1980; Platt and Vissers 1980; Gapais and White, 1982; Simpson and Schmid 1983; Blumenfeld and Bouchez, 1988). However, during coaxial deformation, conjugate sets of C′-planes have been recorded (Law et al 1986). The synthetic relationship of the C′-plane to foliation during non-coaxial deformation enables them to be used as kinematic indicators (Fig 1.3).

1.9.3 Porphyroclast Systems

In quartz-feldspar-mica mylonites, porphyroclasts of feldspar and mica, usually muscovite, are preserved. Passchier and Simpson (1986) divided porphyroclast systems into two groups: σ- and δ-types (Fig. 1.4). σ-type porphyroclasts systems behave passively during shearing and are characterised by simple stair-stepped wedge shaped tails. These clasts have been divided into σ_a- and σ_b-types. σ_a-type porphyroclasts lie isolated in a homogeneous matrix, around which the foliation is distorted (Passchier and Simpson 1986) and include mica-fish in type II S-C mylonites. σ_b-type clasts occur in aggregates within a heterogeneous fabric and usually form the S-plane, enclosed by the C-plane (Passchier and Simpson 1986).

According to Passchier and Simpson (1986), δ-type porphyroclast systems are characterised by a component of rotational strain during which the tails become wrapped around the porphyroclast, and a sense of shear may be determined by the stair stepping symmetry, which is the same for σ- and δ- type systems for a particular sense of vorticity.

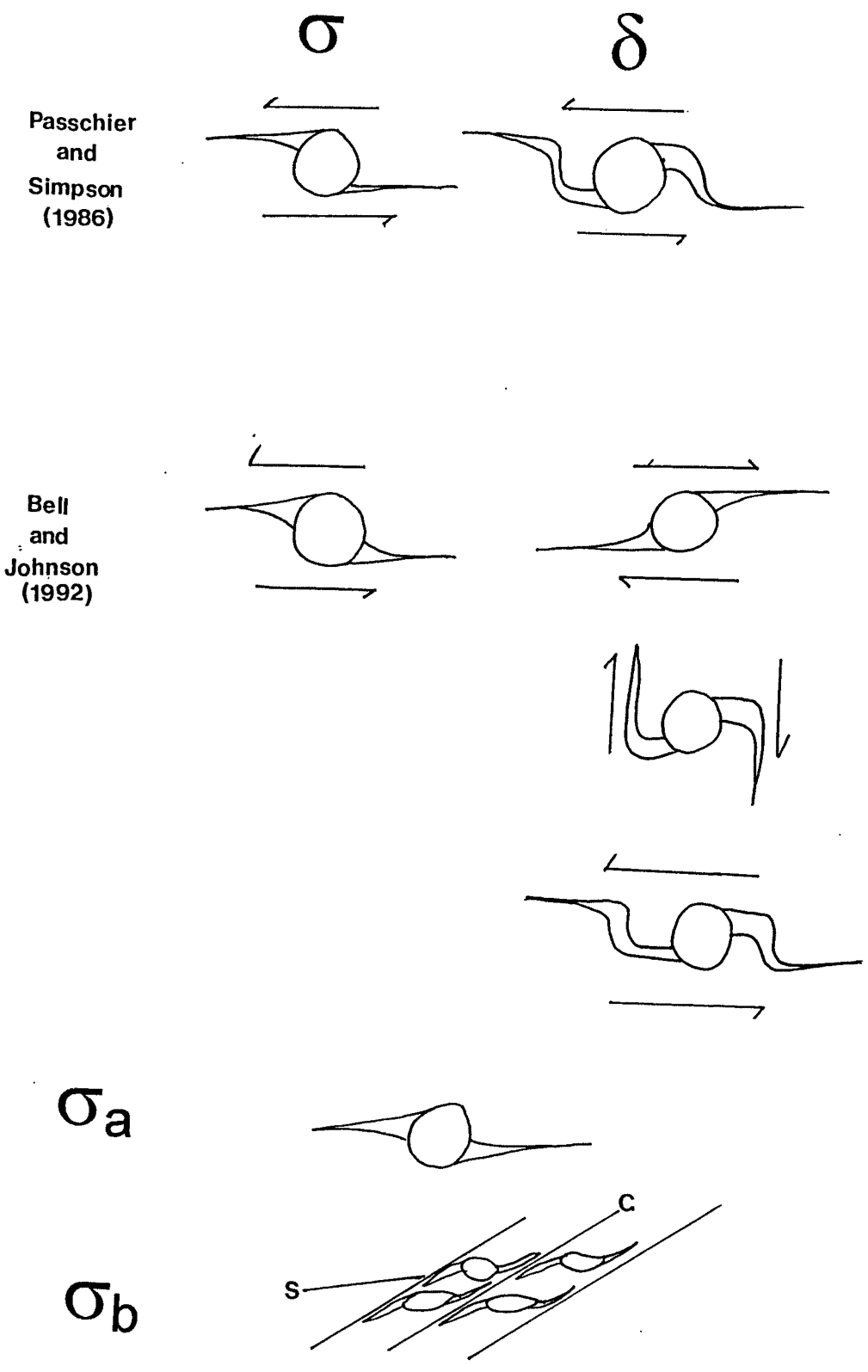

Fig. 1.4 The shear-sense interpretation of σ-type and δ-type porphyroclasts according to Passchier and Simspon (1986) and Bell and Johnson (1992). Bell and Johnson (1992) suggest that δ-type porphyorpclast systems are the result of overprinting of orthogonal foliation-forming events and do not represent a single simple shear-sense. Also given are schematic examples of σ_a and σ_b-type porphyroclast systems after Passchier and Simpson (1986).

However, δ-type porphyroclast systems have recently been re-interpreted by Bell and Johnson (1992) who suggest these porphyroclast systems are formed by the overprinting effects of orthogonal foliation forming events, rather than recording a rotational component of strain, and that a simple single shear-sense cannot be attributed to the formation of δ-type porphyroclast systems (Fig. 1.4). Although controversy remains over the use of δ-typeporphyroclast systems, both Bell and Johnson (1992) and Passchier and Simpson (1986) agree on the direction of shearing recorded by σ-type porphyroclast systems.

1.9.4 Oblique Quartz Shape-preferred Orientations

In S-C mylonites, quartz ribbons which lie along the C-plane or mylonitic foliation sometimes contain slightly elongate quartz crystals which are oriented with their long axes at an angle to the quartz-ribbon boundary. These oblique quartz shape-preferred orientations are a result of repeated cycles of dynamic recrystallization (Lister and Snoke 1984). In the literature, oblique quartz shape-preferred orientations have been termed S_B foliations by Law et al (1984). However, this shape-preferred orientation of quartz rarely forms a continuous foliation and this terminology has not been retained here. A consistent sense of obliquity is observed between the oblique quartz shape-preferred orientations and the C-plane which can be used to indicate a sense of shear (Simpson and Schmidt 1983; Law et al 1986).

1.9.5 Porphyroclast Fracture Patterns

A) *Parallel Displacements.*

During deformation, feldspars may fracture in such a way that the displaced crystal walls remain parallel to each other. Parallel displacements have been subdivided by Hippertt (1993) into microshears (where the displacement occurs exclusively along fracture planes), and parallel pull-aparts (where gaps between the fragments may occur).

According to Simpson and Schmid (1983) and Simpson (1986), the sense of movement of a rigid object along fractures during deformation depends on the initial orientation of the microfracture relative to the kinematic framework. This initial orientation is often difficult to determine and parallel displacements can give ambiguous results. Hippertt (1993) recommends that parallel displacements only be used if the precursor fractures lie at a low angle to the flow plane.

B) *'V'-pull-aparts*

The 'V'-pull-apart is characterised by a 'V'-shaped gap between feldspar fragments infilled with a quartz, or quartz-mica aggregate. In non-coaxial regimes, the 'V' shape is formed by synthetic rotation of small fragments, while larger fragments of the same porphyroclast either do not rotate, or rotate more slowly (Hippertt 1993).

According to Hippertt (1993), the asymmetry of the 'V'-pull-apart relative to the shear plane, and the foliation deflection within the pull-apart, can be used as a shear-sense indicator in non-coaxial regimes provided the pull-apart is adjacent to a principal shear surface such as those parallel to the shear-zone boundary. This new shear-sense indicator has not been widely used in the literature, and its reliability as such has been tested against other indicators in this work (section 3.9).

1.9.6 Asymmetric Microfolds

In heterogeneously deformed mylonites, perturbation in flow may produce asymmetric microscopic or mesoscopic folds. These folds can be used as shear-sense indicators if the initial orientation of the foliation prior to folding is known (Bell and Johnson 1992, see Fig. 29). However, this is not often the case and shear-sense based on fold asymmetry may be difficult to determine. According to Hanmer and Passchier (1991), fold asymmetry will depend on the style of folding (sheath or drag), and the scale of folding, as the symmetry of minor folds on a major fold will change from 'S' to 'Z' across a major axial plane. Hanmer and Passchier suggest that fold asymmetry should only be use if regionally consistent, representing a regional sense of shear.

1.9.7 Quartz c-axis Fabrics

Under greenschist and lower amphibolite facies conditions of metamorphism, quartz may undergo plastic deformation by basal <a> slip, and to a lesser degree, prism <a> and rhombohedral <a> slip. At temperatures greater than 650°C, prism <c> slip may also become important (Mainprice et al 1986). During plastic deformation by basal <a> slip, c-axes rotate to lie at high angles to quartz ribbons in mylonitic rocks. This c-axis preferred orientation is common and may be observed on insertion of a sensitive tint plate or by measurement on the universal stage in the XZ plane of the rock sample.

In an attempt to understand quartz plastic deformation, some researchers undertook numerical simulations on polycrystalline aggregates assuming both homogeneous deformation and compliance with von Mises criterion (Lister et al 1978; Lister and Williams 1979; and Lister and Hobbs 1980); and heterogeneous strain incorporating pressure solution, grain boundary sliding and dynamic recrystallization (Etchecopar 1977: Etchecopar and Vassuer 1987). From these simulations it was discovered that coaxial deformation histories produced symmetric quartz c-axis fabrics with respect to foliation, which can be related to a range of strain regimes (Lister and Hobbs 1980; Schmid and Casey 1986; Fig. 1.5A). However, during progressive simple shear asymmetric crossed girdles and single girdles with respect to foliation were produced, the obliquity of which may be used to determine the sense of shear in non-coaxial regimes (Fig. 1.5B) (Lister and Hobbs, 1980; Etchecopar and Vassuer 1987).

In this thesis, c-axis fabrics are classified as small-circle girdles, single girdles, crossed girdles or as fabrics dominated by point maxima. Crossed girdle fabrics are subdivided into type I crossed girdles and type II crossed girdles (Fig. 1.5B). Fabrics that contain strong point maxima concentrations of c-axes are classified with reference to Fig. 1.5B(d).

The kinematic interpretation of girdle fabrics in natural examples are possibly complicated by non-random initial c-axis distributions, late coaxial overprints (Lister and Williams 1979) and heterogeneous deformation that may depart from progressive simple shear (Law et al 1990). However, when used in conjunction with other shear-sense

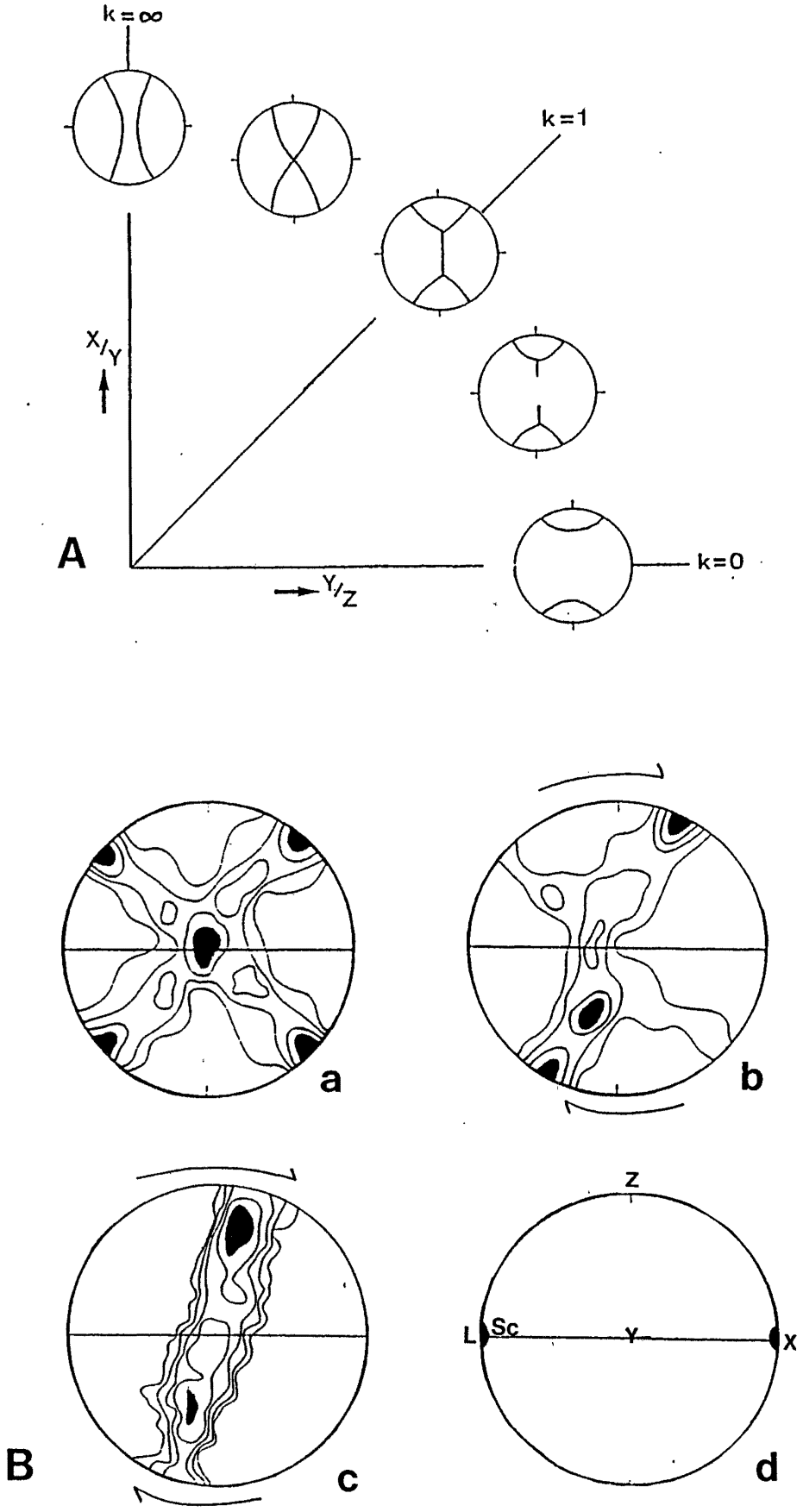

Fig. 1.5 A) Sketch of the main features of pole figure for quartz c-axes expected for coaxial deformation within different area of the Flinn diagram. K=1 corresponds to plane strain; k>1 implies constriction, k<1 implies flattening. Modified from Schmid and Casey (1986). B) Examples of a type II crossed girdle (a) and type I crossed girdle (b) from the Saxony granulite terrain (Lister and Dornsiepen 1982), and single a girdle fabric (c) from Etchecopar and Vasseur (1987); bold arrows indicate shear-sense. Relationship of the schistosity (Sc) and lineation (L) to the kinematic axes of finite strain, X, Y and Z.

indicators, quartz fabric analysis becomes a powerful tool for unwrapping deformational histories in complexly deformed terrains.

CHAPTER TWO

LITHOLOGIC DESCRIPTIONS AND MINERALOGY

2.1 Introduction

The Charleston Metamorphic Group contains ortho- and paragneisses, migmatites, mylonites and deformed granitoids which are variable in mineralogy and texture. The descriptions that follow are based on field observations and thin section analysis. Mineral percentages are visually estimated and plagioclase anorthite content determined by refractive index methods outlined in Shelley (1985). Thin sections housed in the University of Canterbury collection, and sample localities are listed in Appendix A.

2.2 Mylonitic Rocks

2.2.1 Morrisey Creek Mylonite Zone (MCMZ)

Mylonites and flinty mylonites outcrop along the coast for 1.5 km north of White Horse Creek and inland along the Morrisey Creek. In outcrop, layers of dynamically recrystallized quartz, mylonitized biotite-rich granitoids and leucogranites up to 3 m wide commonly occur, although biotite-rich granitoid mylonites predominate (Fig 2.1A and B). Feldspar porphyroclasts up to 5 mm long can also been seen in outcrop. Quartz-feldspar-muscovite pegmatites and aplites deformed during mylonitization occur as pods up to 15 cm wide or as deformed layers (Fig 2.1C). Post-mylonitic pegmatites up to 3 m wide cross-cut the mylonitic foliation.

Along White Horse Creek itself and for approximately 200 m north, the mylonites have suffered post-mylonitic brittle faulting and are bleached pale pink in colour.

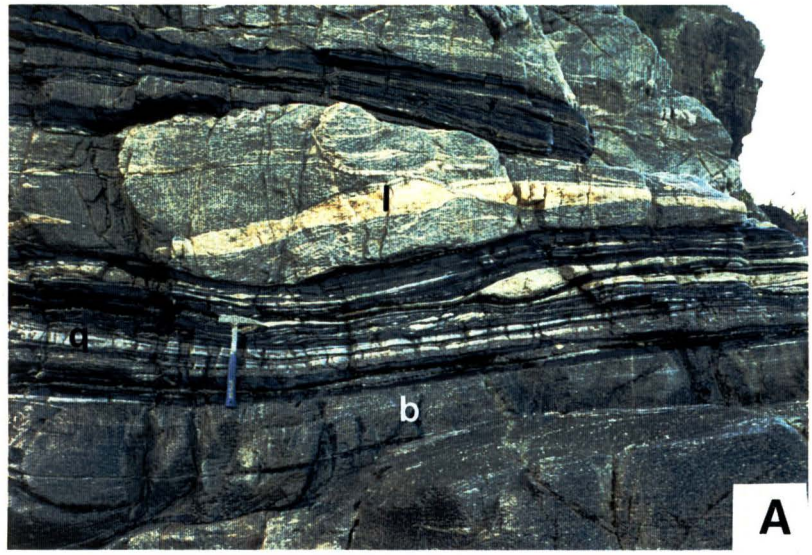

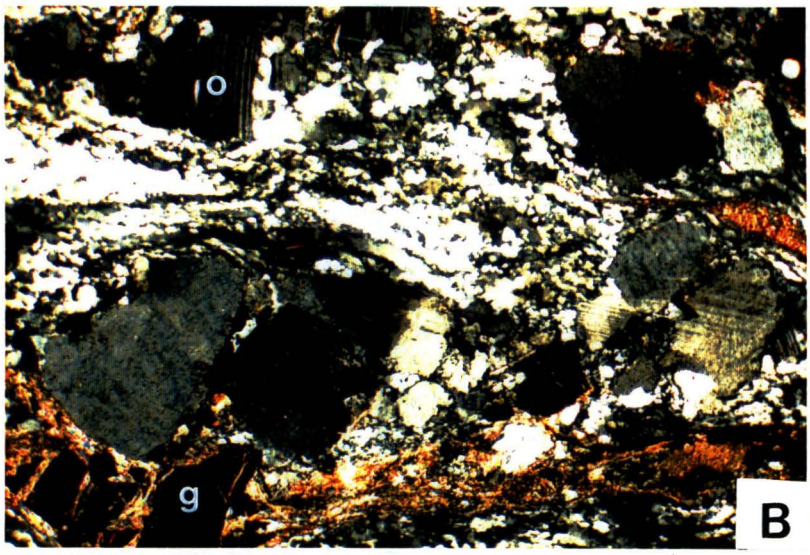

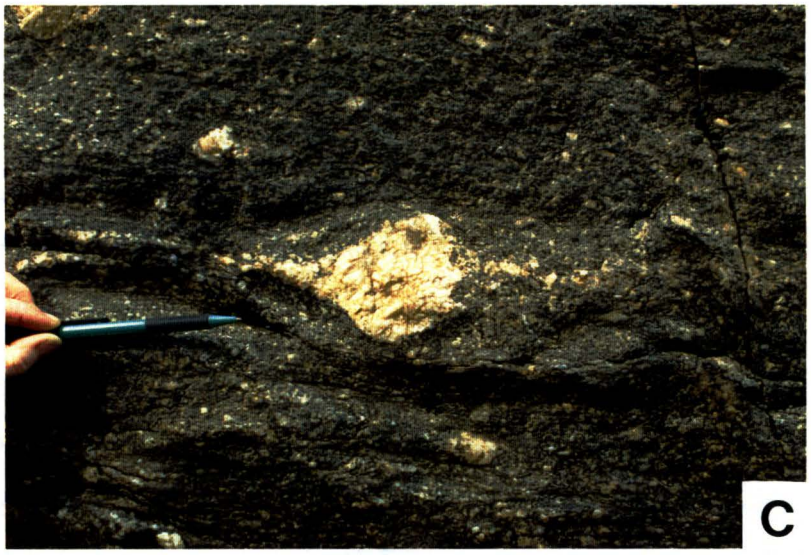

Fig. 2.1 Mylonites in the MCMZ. A) Biotite-rich granitoid mylonites (b), layers of dynamically recrystallized quartz (q) and mylonitized leucogranites (l); hammer length=33cm). B) Biotite-rich granitoid mylonite under cross polarised light; o=oligoclase, g=garnet; view 2.9 mm across. C) Deformed pegmatite; pencil length=14cm.

Quartz: Quartz comprises between 15 and 40% of most mylonites, except for MC5, a mylonitized vein which contains 92% quartz and mylonitized leucogranited, MC2, which possesses 50% quartz.

Four textural types of quartz occur (Fig 2.2):

1) extremely elongate, high aspect ratio, plastically deformed quartz ribbons up to 3 mm long possessing serrated boundaries, well developed undulatory extinction and little grainsize reduction due to dynamic recrystalization;
2) dynamically recrystallized ribbons, sometimes possessing oblique quartz shape-preferred-orientions, containing equant to slighty elongate quartz grains as small as 0.01 mm with serrated grain boundaries and little undulose extinction;
3) grains up to 3 mm long and 0.5 mm wide which do not typically form ribbons, but may possess undulose extinction and serrated grain boundaries;
4) equant 0.3 mm quartz grains associated with the retrogade alteration of K-feldspar to muscovite and quartz.

Plagioclase: The Morrisey Creek mylonites contain up to 30% plagioclase of predominantly oligoclase composition (An 15-30%) except for MC5, a mylonitized vein which lacks plagioclase altogether and samples WH44, WH43 and WH41 which contain andesine. Plagioclase porphyroclasts are elongate, up to 5 mm long, with albite and pericline twinning, lightly sericitised and sometimes recrystallized. Cataclasis may be extreme resulting in boudinage and undulatory extinction (Tullis and Yund 1987). Large oligoclase porphyroclasts in WH32a exhibit patch-like antiperthite of cross-hatched twinned microcline.

K-feldspar: Porphryoclasts up to 5 mm long of microcline comprise 5-18% of the mylonites and display Carlsbad and cross-hatched twinning. K-feldspar porphyroclasts are typically cataclased, boudinaged and possess recrystallised and myrmekitized grain boundaries. Perthitic texture is rare.

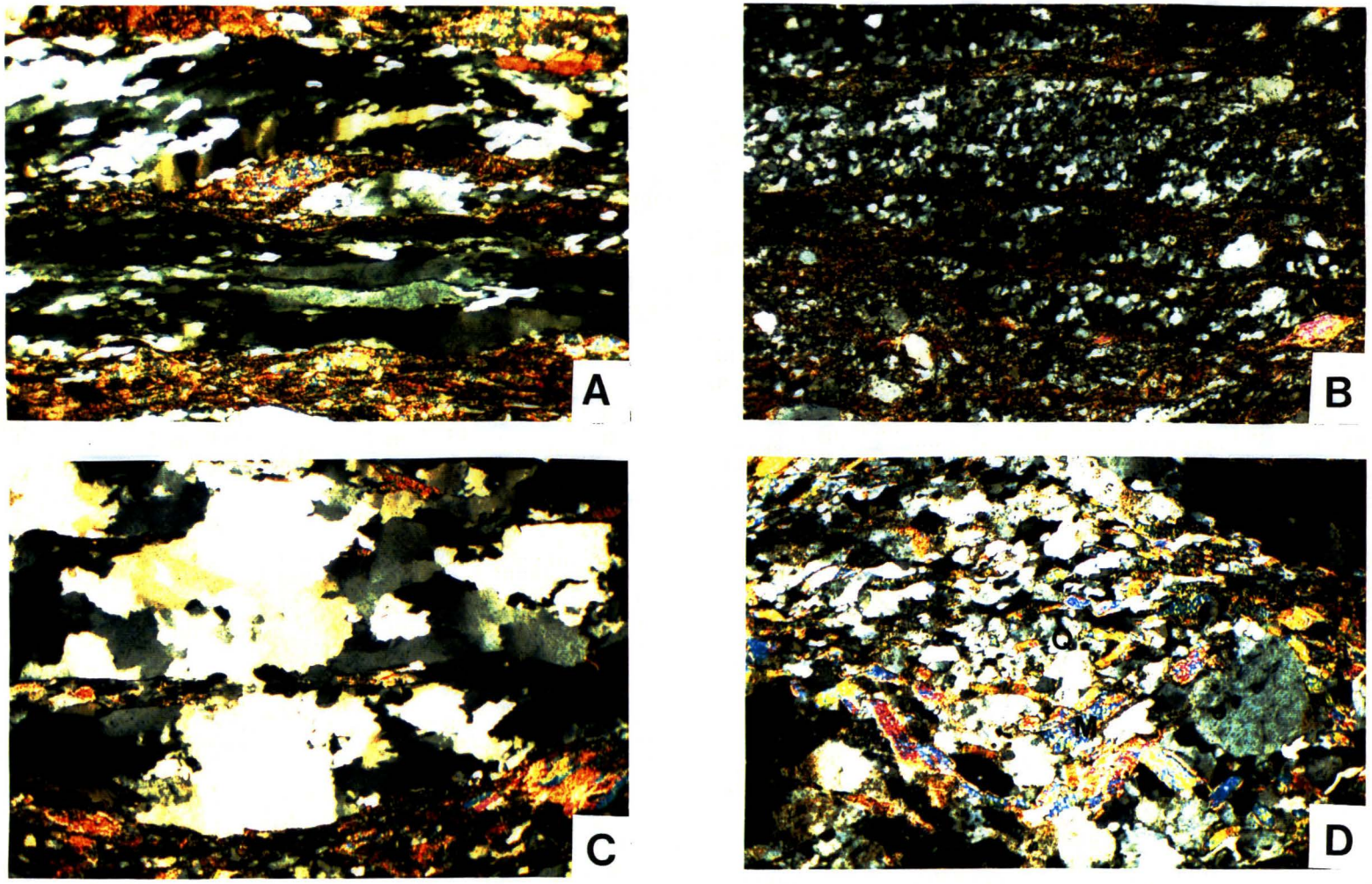

Fig. 2.2 Four textural types of quartz in the MCMZ, crossed polarised light, view=2.9 mm across. A) type 1 quartz; B) type 2 quartz; C) type 3 quartz; D) type 4 quartz; Q=quartz, M=muscovite.

Mica: Red-brown biotite comprises between 10 and 43% of most mylonites. MC5 (mylonitized vein) and MC2 (mylonitized leucogranite) possess no biotite. In coarse grained mylonites (WH35, WH36, WH37 and WH38), biotite is predominantly recrystallized and may be up to 4 mm long. However, in most mylonites, biotite has undergone cataclasis and kinking resulting in undulatory extinction and extreme grainsize reduction.

Muscovite crystals up to 1 mm long constitutes between 2 and 20% of the mylonites. Two textural types of muscovite occur:

1) pre and syn-mylonitic cataclased muscovite which exhibits kinking, undulatory extinction and may form mica fish
2) post-mylonitic euhedral to subhedral muscovite produced during retrograde alteration of K-feldspar to muscovite and quartz.

Centimeter wide layers of mica in hand specimen and thin section consist predominantly of cataclased or recrystallized biotite with minor muscovite.

Accessory Minerals: Apatite (tr-3%) occurs in all mylonites as anhedral to euhedral, rounded, elongate or hexagonal sections up to 1.5 mm across, or as needles. Equant to elongate cataclased garnets up to 1 mm long are found in WH234, WH32a, MC5 and MC2. Trace amounts of chlorite occur as minor retrograde replacement of biotite; epidote and zircon occur in most samples as small euhedral to subhedral grains. Calcite and sericite are common alteration products of plagioclase and calcite is often found filling minor cracks and veins. Hematite and opaques occur in trace amounts.

2.2.2 Four Mile River Mylonites

Biotite-rich mylonitic rocks outcrop along the coast south of the Four Mile River and appear mineralogically and texturally similar to the Morrisey Creek mylonites (Fig 2.3A)

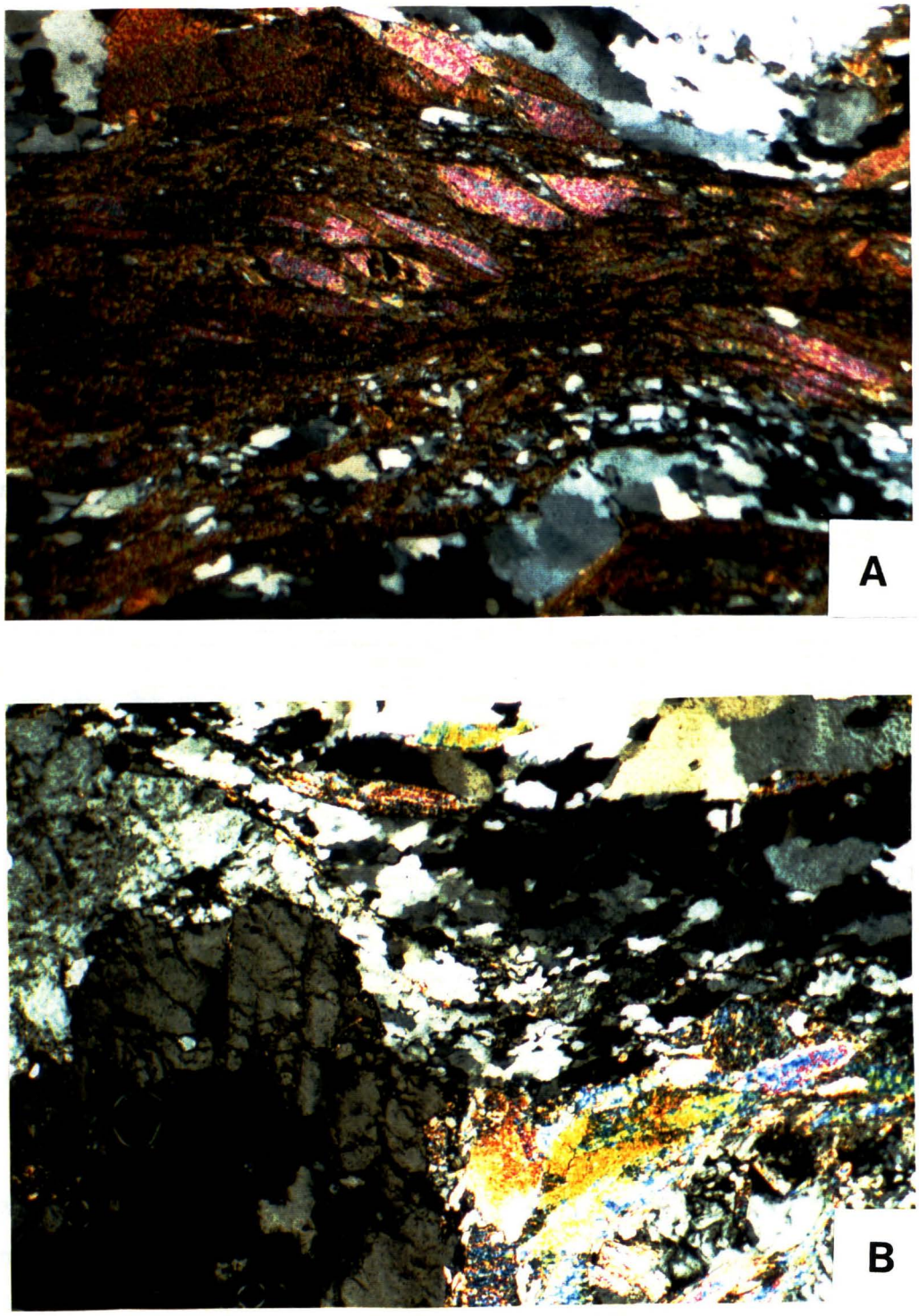

Fig. 2.3 A) Biotite-rich granitoid mylonite from near the mouth of the Four Mile River; cross polarised light; view across=2.9 mm. B) Mylonitized leucogranite from the DCMZ; cross polarized light; view across=2.9 mm.

and may simply be a continuation of the MCMZ. Post-mylonitic pegmatites up to 3 m wide cross-cut and post-date the mylonitic foliation and contain 30 cm long K-feldspar crystals.

Quartz: Two mylonite samples, FM15 and FM17, contain up to 35% quartz, deformed into dynamically recystallized ribbons approximately 0.5 mm wide which exhibit undulatory extinction and serrate grain boundaries.

Feldspar: Calcic oligoclase (approx. 20%) forms equant to elongate porphyroclasts between 0.2 and 3 mm long which may be cataclased and exhibit undulatory extinction. Deformation pericline and albite twinning is common; normal zoning is found in plagioclase crystals in FM15. Cataclased K-feldspar porphyroclasts comprise only 2-5% of both samples, are up to 0.25 mm long, and may be either cross-hatched twinned microcline (FM17), or orthoclase (FM15).

Mica: Muscovite (up to 18%) exhibits a large range of grainsizes and occurs as pre and syn-mylonitic cataclased and kinked grains and mica fish or as post-mylonitic clumps replacing K-feldspar. Cataclased and kinked red-brown biotite comprises up to 35% of the mylonites and ranges from 0.2 to 2 mm in length. Layers of biotite and minor muscovite up to 2 mm thick occur in thin section.

Accessory Minerals: Trace amounts of epidote, retrograde chlorite, zircon and apatite occur in both FM15 and FM17. Apatite comprises rounded to elongate grains 0.25 mm long. Garnet is found in trace amounts in FM17.

2.2.3 Deep Creek Mylonite Zone (DCMZ)

Mylonitized granites s.s., and biotite-rich mylonites occur inland where the Coast Road crosses Deep Creek and to the SW. Outcrops are poor and well weathered, particularly

inland, south of Deep Creek. Where the road crosses Deep Creek folded felsic layers up to 0.5 m are seen in the road cutting.

Mylonitized Granite: Mylonitised granite (DC5; Fig 2.3B) contains 40% quartz, 23% microcline, 18% plagioclase and 12% muscovite. Green-brown biotite, epidote, apatite, garnet and chlorite occur in trace amounts. Equant to elongate quartz grains, generally 0.25 mm, exhibit serrated grain boundaries and undulose extinction or occassionally triple point junctions suggesting a component of both dynamic and static recrystalization. Ribbons are poorly developed. Normally zoned plagioclase of generally oligoclase composition and cross-hatched twinned microcline form cataclased, recrystallized and sericitzed porphryoclasts up to 3 mm long and 1 mm wide. Large muscovite crystals up to 2 mm long have been cataclased and, in places, form mica fish.

Biotite-rich Granitoid Mylonites: Biotite-rich granitoid mylonites DC3 and R20 contain fine-grained dynamically recrystallized quartz ribbons bound by mica. Quartz ribbons up to 3 mm wide in sample DC3 possesses a weak quartz shape-preferred orientation. DC3 displays normally zoned, albite and pericline twinned porphyroclasts up to 5 mm long of labradorite composition (20%). K-feldspar is absent. Biotite (35%) may be up to 5 mm long or finely cataclased. Apatite, chlorite, epidote and zircon occur in trace amounts.

R20 contains 50% dynamically recrystallized quartz which forms ribbons up to 0.7 mm wide bound by muscovite. Pericline and albite twinned plagioclase (An 27-40%) forms elongate porphyroclasts typically 0.6 mm long, and matrix grains 0.4 mm long. Plagioclase exhibits little undulatory extinction and cataclasis. Muscovite (20%) comprises 0.7 mm wide layers composed mainly of mica fish. Red-brown biotite (18%) may be up to 1.2 mm long and cataclased. Apatite (3%) occurs as 0.75 mm elongate anhedral porphyroclasts. Trace amounts of chlorite, epidote and zircon are present.

2.2.4 Siberia Bay Mylonite Zone (SBMZ)

Mylonitized grey syenogranite-monzogranite outcrops in central and southern Siberia Bay, south of Cape Foulwind. In outcrop, the mylonites are generally fine-grained except

for megacrysts of K-feldspar (8%) which have undergone extreme boudinage (Fig 2.4A). The necks of the boudinaged megacrysts are infilled with quartz and the total length of feldspar boudins and quartz infill may exceed 10 cm. Mylonitization is best developed in central Siberia Bay, although primary igneous textures are present in thin section. Undeformed outcrops of syenogranite-monzogranite occur in the north of Siberia Bay and undeformed quartz-feldspar-tourmaline pegmatites and quartz-feldspar-muscovite veins generally parallel foliation.

Quartz: Quartz (15-50%) occurs as ribbons which mantle feldspar porphyroclasts recrystallized to 0.25-0.75 mm equidimensional grains (Fig 2.4B). Quartz also occurs as lensoid pods 1 mm wide which are generally statically recrystallized, but also dynamically recrystallized exhibiting serrated grain boundaries or undulose extinction. The retrograde metamorphic reaction of K-feldpsar to muscovite and quartz has produced 0.01 mm equant quartz grains possessing triple point junctions.

Plagioclase: Plagioclase (An 5-12%) comprises between 5 and 15% of the Siberia Bay mylonites. Porphyroclasts of plagioclase may be sericitized, cataclased and boudinaged but still exhibit igneous features including Carlsbad and albite twinning, oscillatory and continous normal zoning and rare euhedral crystal form.

K-feldspar: Orthoclase and microcline (18-40%) porphryoclasts occur as extremely boudinaged megacrysts up to 15 cm long. In thin section, K-feldspar is perthitic, cross-hatched and Carlsbad twinned and contain quartz blebs possibly representing eutectic crystallization (Fig 2.4D). Metamorphic reaction of K-feldspar occurs along deformation bands and at the edge of the porphryoclasts producing 0.01-0.06 mm new grains. In some cases, extreme metamorphic reaction has obliterated porphyroclasts altogether producing layers of small new grains of plagioclase, muscovite and quartz up to 3 mm wide (Fig 2.4C).

Micas: Red-brown biotite (7-20%) occurs as 0.2 to1 mm grains in clots with decussate texture, smeared out to form a foliation or as single kinked crystals exhibiting undulatory

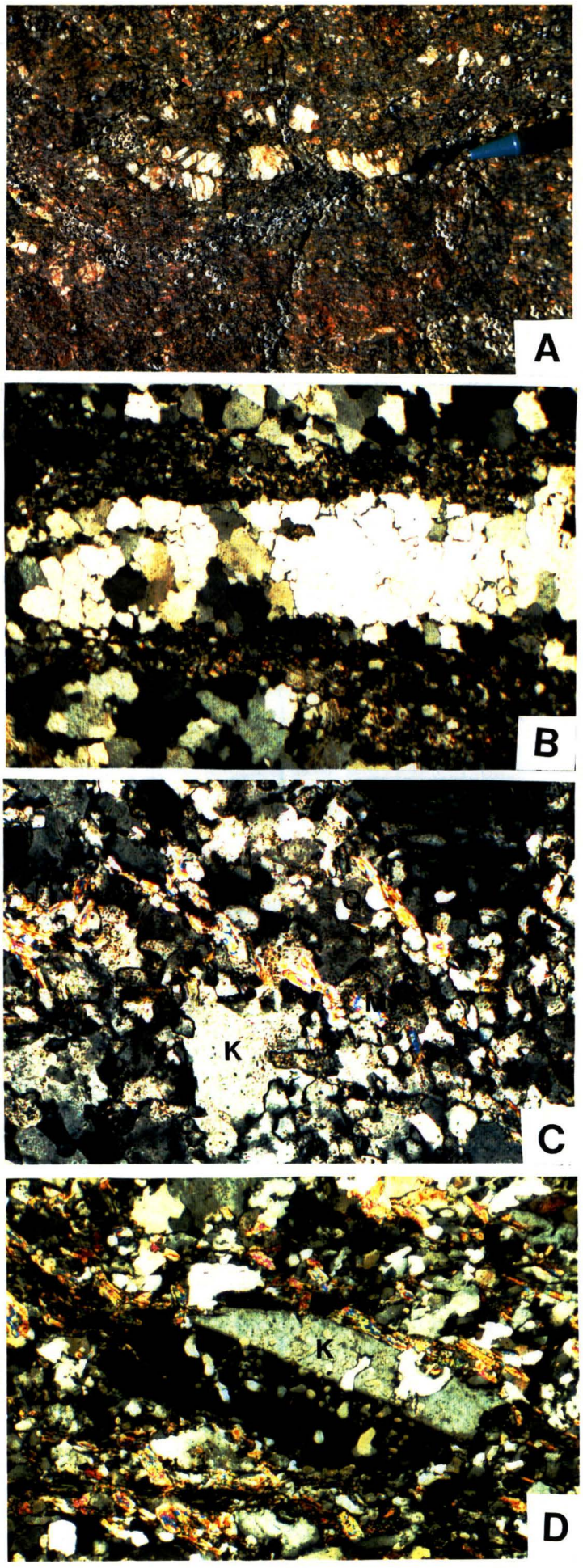

Fig. 2.4 A) K-feldspar megacrysts which have undergone boudinage in the SBMZ. Boudin necks infilled with quartz; view across=18cm. B) Recrystallized quartz ribbons in SBMZ; crossed polarised light; view across=2.9 mm. C) Retrograde metamorphic reaction of K-feldspar (K) to muscovite (M) and quartz (Q); cross polarised light; view across= 1.2 mm. D) Carlsbad twinned K-feldspar (K) displaying quartz blebs; cross polarised light; view across=2.9 mm.

extinction. Muscovite (2-8%) generally occurs as cataclased 0.5 mm long crystals or mica fish. Muscovite is locally enriched in shear bands and also replaces K-feldspar where it forms euhedral 0.1 mm crystals of random orientation (Fig 2.4C).

Accessory Minerals: Biotite, rutile, tourmaline, zircon and epidote occur in trace amounts. Apatite occurs as 0.5 mm anhedral, rounded crystals. Chlorite occurs as a retrograde alteration of biotite.

2.3 Charleston, Deep Creek and Four Mile River Orthogneisses.

2.3.1 Introduction

Orthogneisses of granitic, granodioritic and tonalitic composition outcrop around Charleston and the mouth of the Four Mile River and Deep Creek. In Constant Bay, two-mica granite intrudes biotite-tonalite. However, a tectonic foliation defined by an alignment of mica cuts both lithologies and is described further in Chapter 4. At the mouth of the Four Mile River, schistose two-mica granite occurs as cliffs up to 50 m high. Its relationship to mylonitic and other rocks is unclear. Along the coast and in the bed of Deep Creek, foliated biotite-tonalites predominate, intruded by two phases of pegmatites. The first phase of pegmatite intrusion is characterised by folding and is cross-cut and displaced by undeformed second-phase pegmatites.

Granodiorites, locally mylonitized, and biotite-tonalites also outcrop at Parsons Hill. A migmatite of granodioritic composition occurs near Constant Bay and mechanically mixed orthogneiss and migmatites outcrop at the mouth of the Nile River (Chapter 4; section 4.3).

2.3.2 Two-Mica Granitic Gneiss

Quartz: Two-mica granitic gneiss (Fig 2.5A) may contain up to 45% elongate quartz as long as 1 mm. Quartz may comprise poorly formed, statically recrystallized ribbons or layers, in which quartz-quartz boundaries possess triple junction geometry, or individual elongate quartz grains. Extinction is sharp or slightly undulose and subgrain formation is poor (Fig 2.5A).

Feldspar: Plagioclase (5-7%) ranges in composition from An 22-45% but is generally andesine. Crystals are of the order of 1 mm in diameter and equant, possess albite and pericline twins and occasionally are oscillatory zoned. In general, porphyroclast development is poor. K-feldspar (27-30%) is microcline and occurs as 2 mm long equant grains, cross-hatched and Carlsbad twinned and only rarely porphyroclastic. K-feldspar may be recrystallized and exhibit fine perthite.

Mica: Muscovite (10-15%) up to 3 mm long may be cataclased to form mica-fish. Green-brown biotite (5-7%) occurs as cataclased crystals as long as 1mm.

Accessory Minerals: Trace amounts of apatite, chlorite, garnet, zircon and epidote occur.

2.3.3 Tonalitic Gneiss

Quartz: Quartz comprises between 20 and 35% of the tonalitic gneiss and may be up to 4 mm long and elongate, but is usually between 0.25 and 2 mm long. At Parsons Hill and in Joyce and Constant Bay, the tonalitic gneisses sometimes posssess granitic texture, being equigranular and quartz displays sharp extinction and possesses no recrystallization (Fig 2.5B). However, quartz may also exhibit undulatory extinction, deformation lamellae

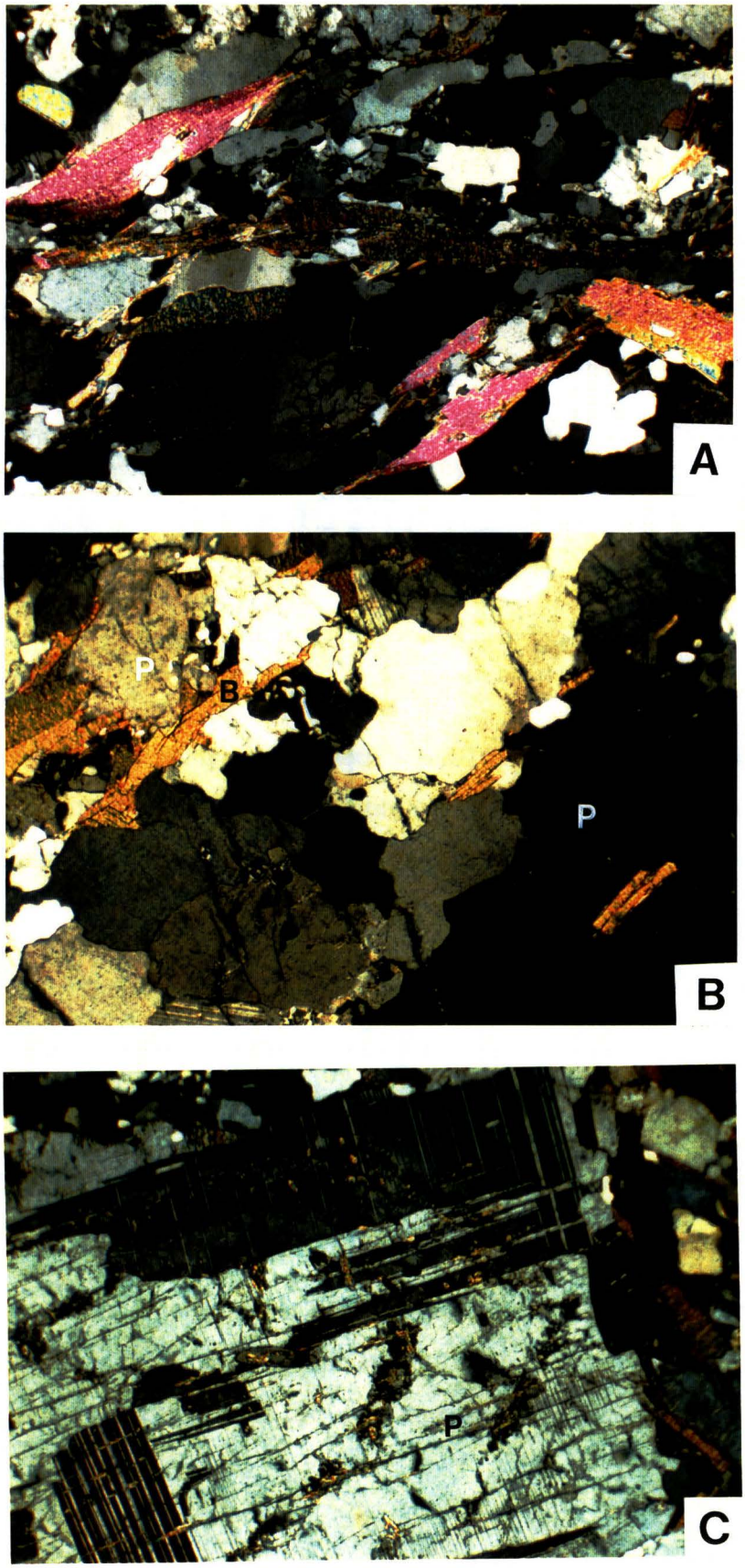

Fig. 2.5 A) Two-mica granitic gneiss; crossed polarised light; view across =3.3 mm. B) Biotite-tonalite granitic texture; B=biotite; P=plagioclase; crossed polarised light; view across=3.3 mm. C) Phenocrysts of plagioclase in biotite tonalite displaying three growth zones; P=plagioclase; crossed polarised light; view across=3.3mm.

and serrated grain boundaries suggesting dynamic recrystallization, or strain-free grains with triple point junctions suggesting at least some static recrystallization. Ribbons are poorly developed.

Plagioclase: Plagioclase (35-55%) forms either equant to slightly elongate euhedral to anhedral phenocrysts up to 8 mm long and 5 mm wide, or subhedral to anhedral matrix crystals between 3.5 mm and 0.3 mm long. Both phenocrysts and matrix plagioclase possess oscillatory zoning and albite and pericline twinning. Phenocrysts of plagioclase may exhibit up to three growth zones (Fig 2.5C). Phenocrysts range from An 30-55% (labradorite-andesine) and matrix plagioclase ranges from An 15-45% (oligoclase-andesine).

Mica: Green-brown biotite comprises between 3 and 20% of the tonalites and occurs as clumps or single grains up to 2 mm long. Biotite is only weakly cataclased. Muscovite is occasionally present (up to 5%) as 1.2 mm long cataclased crystals.

Accessory Minerals: Subhedral crystals of allanite comprise up to 3% of the tonalites. K-feldspar, apatite, zircon, and epidote occur in trace amounts.

2.3.4 Granodioritic Gneiss

Gneiss of granodioritic composition outcrops at Parsons Hill. In outcrop and thin section, shear zones up to 1 cm wide exhibit mylonitic textures. However, these are volumetrically insignificant and granitic texture is dominant in thin section.

Typically, quartz (25-38%) occurs as 2 mm long rounded to elongate grains with generally sharp extinction. Subhedral to anhedral plagioclase (30%) up to 5 mm long and 3 mm wide is oligoclase to andesine, normally zoned with albite and pericline twinning. Microcline (15-17%) phenocrysts up to 4 mm are perthitic and exhibit undulatory

extinction and cross-hatched twinning. Green-brown biotite (10-18%) up to 2 mm long and muscovite (5%) up to 1.2 mm long also occur. Epidote, apatite, chlorite, zircon, rutile, opaques and iron oxides occur in trace amounts.

2.4 Cape Foulwind-Tauranga Bay Orthogneisses

2.4.1 Cape Foulwind Monzogranitic Gneiss

Around Cape Foulwind, dark grey, coarse biotite-rich monzogranite containing megagcrysts of K-feldspar and plagioclase up to 5 cm long is variably deformed (Fig 2.6A and B). Aligned megagcrysts may be concentrated into layers up to 50 cm wide, which probably represent a magmatic foliation and layering. However, a biotite preferred orientation produces a tectonic foliation. The relationships between these foliations is described in Chapter 5.

Quartz (40%) forms ribbons with either small dynamically recrystallized crystals or statically recrystallized grains exhibiting triple point junctions. Plagioclase (25%, An 7-12%) up to 4.2 mm long are zoned, cataclased, Carlsbad and albite twinned and contain inclusions of biotite and muscovite. Cross-hatched twinned microcline (15%), up to 5 cm long, exhibits undulatory extinction, boudinage, dynamic recrystallization and myrmekitization as well as thin string perthite. Microcline poikilitically encloses small albite twinned plagioclase crystals. Red-brown biotite (15-20%) up to 1 mm long forms decussate clots or single crystals imparting a foliation. Muscovite is less common than biotite, froms crystals up to 0.5 mm long and may replace K-feldspar. Apatite (3%) occurs as anhedral, slightly elongate crystals up to 0.25 mm long. Epidote, zircon and chlorite occur in trace amounts.

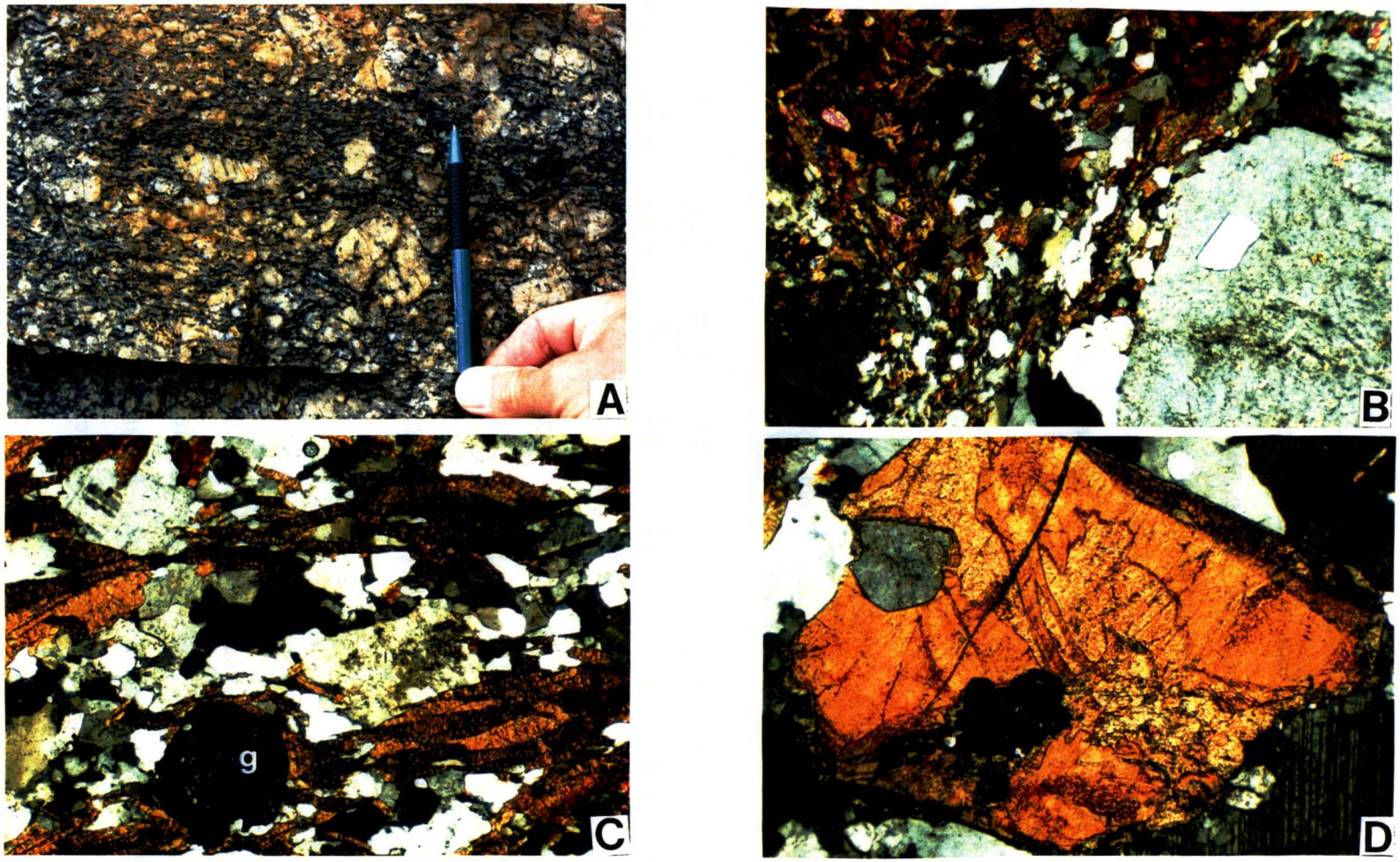

Fig. 2.6 A) Typical view of Cape Foulwind monzogranitic gneiss showing megacrysts of feldspar. Pencil length=14 cm. B) Typical view of Cape Foulwind monzogranitic gneiss under crossed polarised light; view across=2.9 mm. C) Typical view of Tauranga Bay monzogranitic gneiss, g=garnet; crossed polarised light; view across=2.9 mm. D) Allanite; crossed polarised light; view across=2.9 mm.

2.4.2 Tauranga Bay Monzogranitic Gneiss

Deformed grey, coarse-grained, biotite-rich monzogranitic gneiss outcrops at the south Tauranga Bay headland. The gneiss comprises 20% quartz with grains up to 1 mm long and exhibiting undulose extinction, subgrain formation and in some cases, triple point junctions. However, ribbons are poorly developed. Plagioclase (20-25%) ranges from An 7-20% and possesses Carlsbad, albite and occasionally pericline twins. Anhedral phenocrysts up to 1 cm long and matrix crystals 0.2 mm long possess continous normal zoning. Orthoclase (12-15%) occurs as 0.5 mm anhedral matrix crystals and subhedral phenocrysts up to 2 mm long which are sometimes Carlsbad twinned. Green-brown biotite comprises between 25 and 35% of the Tauranga Bay gneiss as 4 mm long crystals producing an anastomosing foliation, or decussate clots up to 0.8 mm wide.

Hexagonal and tabular apatite up to 0.2 mm long and porphyroblastic garnet enclosing quartz and biotite comprise 3% of the gneiss respectively (Fig 2.6C). Allanite comprises up to 2 % of the monzogranitic gneiss and occurs as euhedral to subhedral crytals up to 3 mm long (Fig 2.6D). Zircon, epidote, xenotime, hornblende and chlorite occur in trace amounts.

2.5 The Red Jacket Granite and Similar Lithologies

Gneissose leucocratic granitoids are exposed south of White Horse Creek. The largest of these is the Red Jacket Granite, mapped by Nathan (1975) and outcropping around Belfast Creek. Although this granitic body locally cross-cuts layering in adjacent migmatites (Fig. 2.7A), it has also undergone deformation, has an irregular distribution and locally forms sills within the migmatites such that mapping its outer contact is difficult.

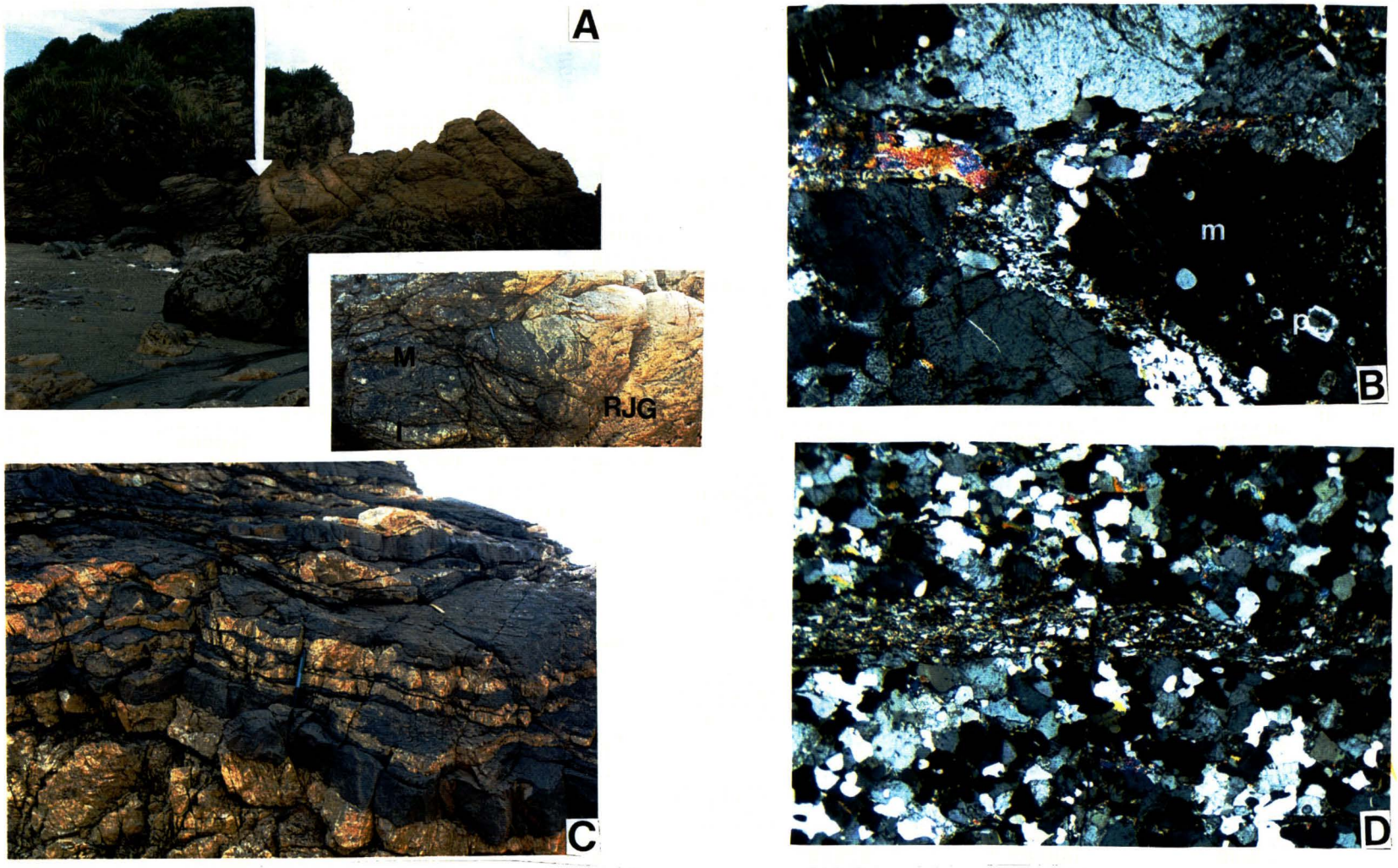

Fig. 2.7 A) Contact between Red Jacket Granite and migmatites of sedimentary origin (arrow); length of outcrop=12 m. Inset shows cross-cutting relationship of Red Jacket Granite (RJG) and migmaitite layering (M=mesosome, l=leucosomes); pencil=14cm.B) Red Jacket Granite; crossed polarised light; m=microcline, p=plagioclase; view across=5.3 mm.C)Sills of Red Jacket Granite within paragneiss country rock; pencil length=14 cm. D) equigranular textures of sill; crossed polarised light; view across=5.3 mm.

The Red Jacket Granite and two leucocratic granitic bodies north of Belfast Creek (samples RJG2, RJG3, and B29) possess 20-30% quartz up to 2 mm long with dynamically recrystallized grain boundaries and undulatory extinction. Anhedral to subhedral plagioclase (An 25-34%) phenocrysts up to 4 mm long may be strongly boudinaged, heavily sericitized and exhibit albite and pericline twinning. Microcline (18-40%) is cross-hatch twinned, coarsely perthitic, and poikilitically encloses 0.2 mm subhedral zoned plagioclase crystals, muscovite and rounded blebs of quartz (Fig. 2.7B). Some microcline has since been altered to muscovite and quartz and where this reaction is intense, muscovite may comprise 20% of the rock. Samples RJG1 and RJG2 are biotite poor. However, a smaller granitoid body, B29, possesses up to 20% biotite due to mixing with paragneiss country rock. Trace amounts of opaques, apatites and iron oxides occur.

Sills: Sills of leucocratic granitic rocks up to 0.5 m wide lie parallel or oblique to the foliation south of Red Jacket Creek (Fig. 2.7C) In the field, these are difficult to differentiate from leucosomes but tend to be weathered a creamy orange. These sills appear

texturally similar to the Red Jacket Granite, but may contain generally finer grained, more equidimensional mosaics (Fig. 2.7D). The textures of such sills are discussed further in section 6.7.2.

Most sills contain up to 40% dynamically recrystallized quartz, 25% plagioclase of oligoclase-andesine composition, between 10 and 30% boudinaged, myrmekitized and recrystallized microcline, 20% muscovite and up to 5% poikiloblastic anhedral rounded garnets containing inclusions of quartz. Sample B18f contains alternating layers approximately 2 mm wide of muscovite-rich and muscovite-poor leucogranite separated by muscovite-rich shear zones up to 0.75 mm wide (Fig. 2.7D). Similar shear zones are found in B27 and impart a weak foliation to both specimens.

2.6 Mylonitized Migmatites of Sedimentary Origin

Migmatites of sedimentary origin outcrop south of White Horse Creek, at the mouth of the Nile and Four Mile Rivers and below the northern Charleston Cemetery (Fig. 2.8A). Paragneiss lithologies also outcrop inland, south of Deep Creek. Late brittle faulting and deformation has affected most of the rocks south of White Horse Creek, and breccia zones up to 20 m wide cross-cut the migmatites. Biotite is commonly altered to opaques and calcite thoughout the area (Fig. 2.8B).

The stromatic migmatites contain up to 50% coarse-grained leucosomes of variable thickness bounded by thin biotite selvages, or melanosomes, no more than .1 or 2 mm wide. From south of Belfast Creek to White Horse Creek, the proportion of leucosome decrease. Mesosomes vary in thickness and appear simply as biotite schist or gneiss. Post-migmatitic mylonitization is recorded in migmatites south of White Horse Creek, particularly in the mesosomes. In these rocks, quartz may form statically recrystallized quartz ribbons up to 1mm wide which mantle cataclased feldpsar porphyroclasts as large as 5 mm long and 2 mm wide. Feldspar porphyroclasts have undergone significant post-mylonitic recrystallization and replacement by muscovite and quartz.

Leucosomes: Quartz (up to 50%) occurs as dynamically recystallized crystals up to 4 mm long exhibiting undulose extinction and serrated grain boundaries or statically recrystallized grains possessing triple junctions and sharp extinction. Plagioclase crystals up to 1 mm long, may comprise around 25% of leucosomes (Fig. 2.8C) and are of oligoclase-andesine composition (An 27-32%). Plagioclase is Carlsbad and albite twinned, weakly zoned, weakly boudinaged and lightly sericitized. Some leucosomes contain up to 10% orthoclase clasts up to 7 mm long partially replaced by muscovite and quartz or myrmekite. Muscovite may, in fact, comprise up to 15% of leucosomes where this retrograde alteration of orthoclase is extreme. Biotite, calcite and iron oxides occur in trace amounts.

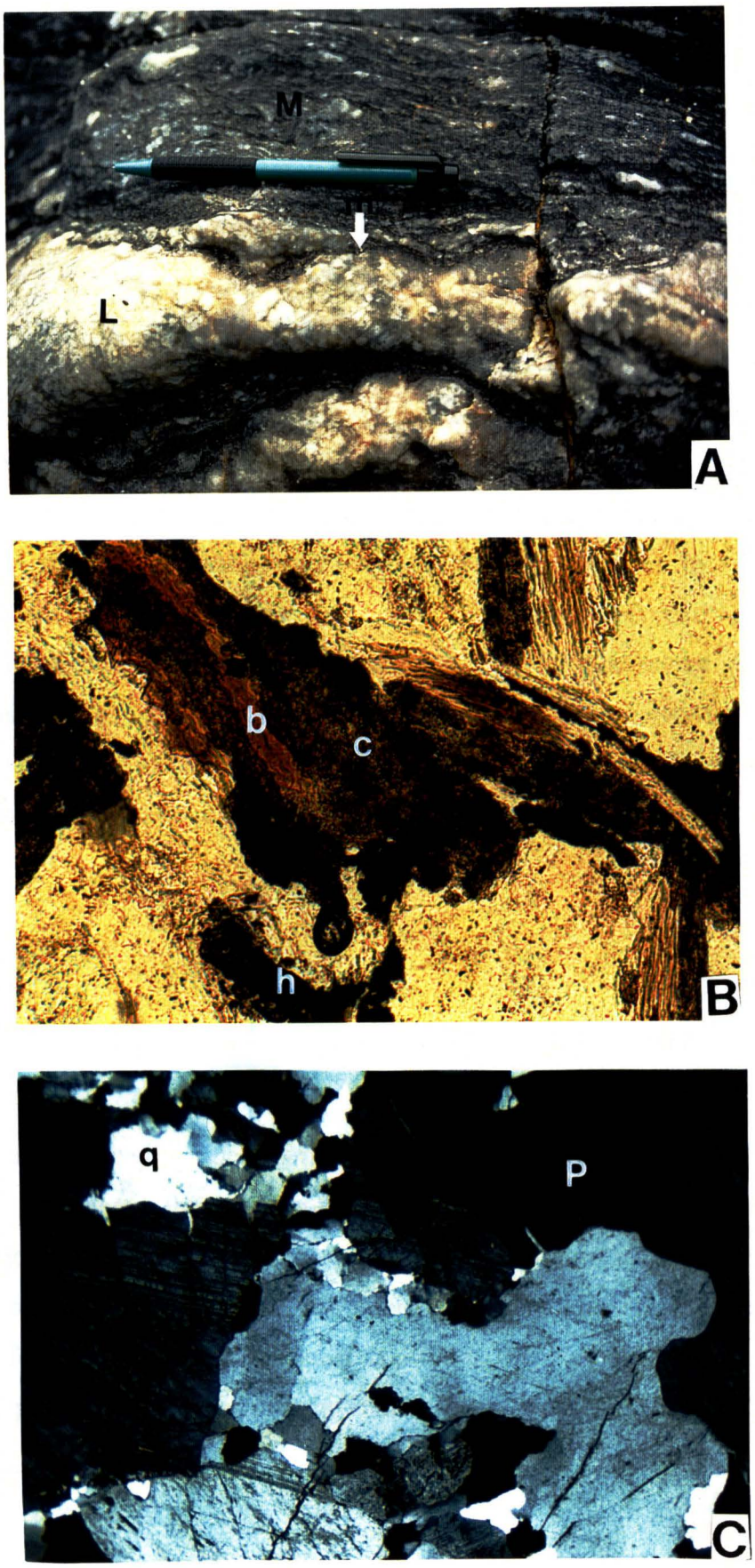

Fig. 2.8 A) Migmatite displaying leucosome (L),mesosome (M) and melanosome (m; arrow); pencil length=14 cm. B) Alteration of biotite (b) to calcite (c) and hematite (h); plane polarised light; view across=1.2 mm. C) Typical leucosome; P=plagioclase, q=quartz; crossed polarised light; view across=5.3 mm.

Melanosomes: Biotite and muscovite crystals up to 0.5 mm long comprise thin melanosomes no more than 2 mm wide (Fig. 2.8A). Micas display post-migmatitic cataclasis and undulose extinction. Quartz, feldspar and iron oxides may also be present.

Mesosomes: Mesosomes contain between 20 and 40% quartz as statically recrystallized crystals exhibiting triple point junctions and sharp extinction or dynamically recrystallized grains forming poor ribbons possessing and oblique quartz shape-preferred orientations. Most quartz crystals are elongate and up to 2 mm long. Plagioclase (An 20-45%) comprises 15-25% of most mesosomes as elongate to equant crystals up to 1 mm long exhibiting albite and pericline twinning and weak normal zoning. Orthoclase and microcline up to 8 mm long and 6 mm wide constitute 5-35% of most mesosomes. Both orthoclase and microcline may be replaced by muscovite, quartz and myrmerkite. Apatite (tr-3%) may occur rounded anhedral grains up to 0.45 mm. Epidote, zircon, calcite, rutile, allanite, sillimanite and a yellow carbonate occur in trace amounts.

2.7 Hornfelsic Lithologies

Layers and pods of even grained biotite-rich hornfelsic to shistose rock of variable thickness occurs throughout the study area (Fig. 2.9A) These layers possess sharp, schistose, or gradational boundaries with the country rock and are mineralogically and texturally monotonous, except for those in Tauranga Bay which exhibit a more diverse mineralogy. K-feldspar is absent from most hornfelses. Most hornfelses exhibit little deformation except for some boudinage or mylonitization in the Morrisey Creek Mylonite Zone.

Quartz: Quartz (20-45%) is generally equant to elongate, up to 1 mm long and may possess undulatory extinction and serrated grain boundaries, or triple point junctions and sharp extinction.

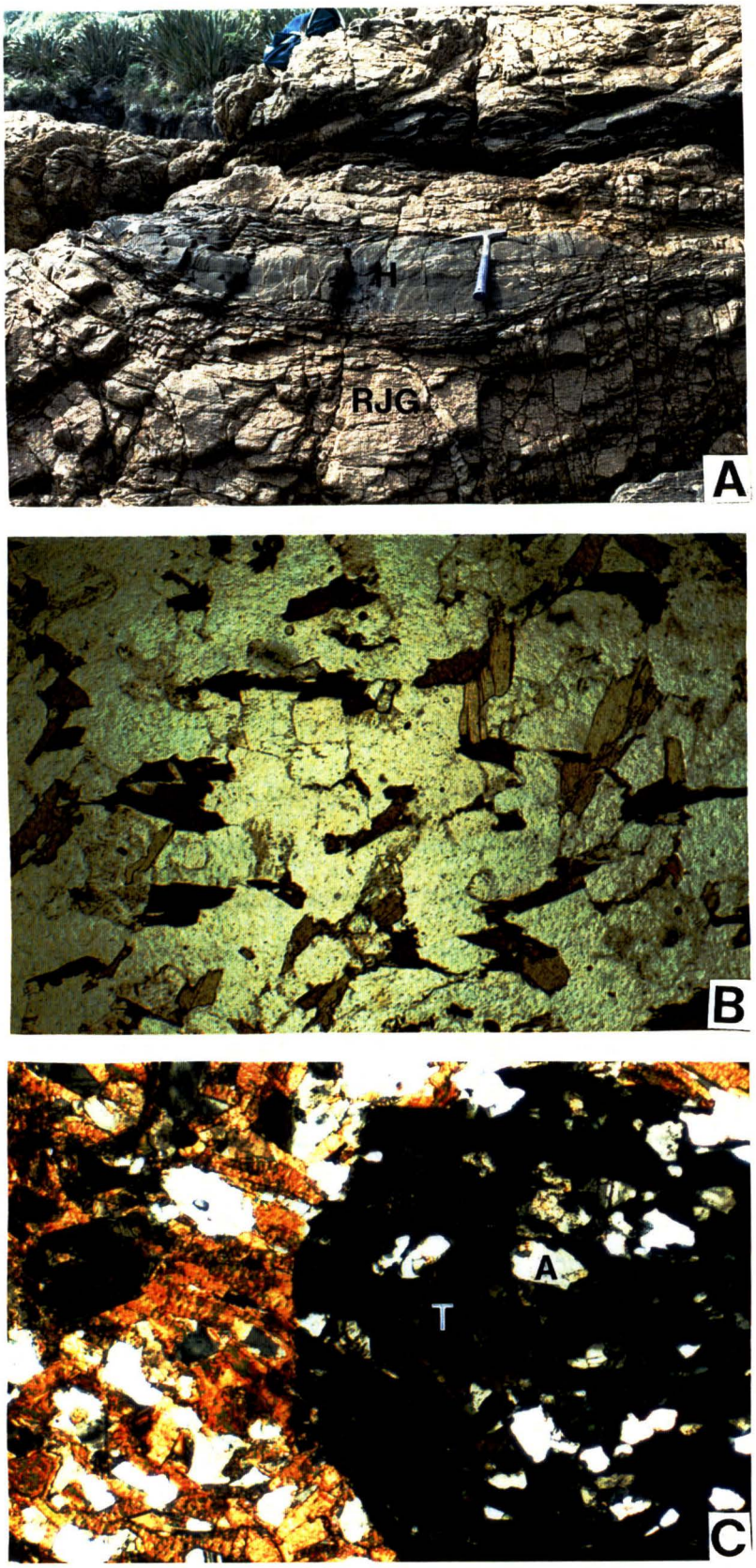

Fig. 2.9 A) Hornfelsic pod (H) in the Red Jacket Granite (RJG); hammer length=33cm. B) Hornfelsic texture in section cut at right angles to the lineation; plane polarised light; view across=2.9 mm. C) Tourmaline porphyroblasts (T) enclosing albite (A); crossed polarised light; view across=2.9 mm.

Plagioclase: Plagioclase ranges from An 20-32% around Charleston, Morrisey Creek and in the southern migmatites. However, at the Tauranga Bay headland, plagioclase is typically albite-oligoclase, ranging from An 5-20%. Plagioclase is equant, no larger than 1 mm, ocasionally normally zoned, lightly sericitized and albite and pericline twinned.

Biotite: Biotite comprises between 20 and 45% of hornfelsic layers and is red-brown in samples from the Morrisey Creek Mylonite Zone, green-brown at Charleston and an intermediate colour at Tauranga Bay. Usually between 0.2-0.5 mm long, biotite imparts a hornfelsic texture in sections cut at right angles to lineation and sometimes in the section parallel to lineation (Fig. 2.9B). In Tauranga Bay, an even-grained core of plagioclase and quartz and minor K-feldspar and titanite lacks biotite.

Accessory Minerals: Apatite, zircon, calcite, muscovite, allanite, opaques, epidote, chlorite and titanite occur in trace amounts in most hornfels. In some hornfels, allanite may be reduced to a near metamict state. Trace amounts of sillimanite were found in hornfelses from the southern migmatites. Tourmaline porphyroblasts up to 3 cm long comprise 10% of sample HFTBA, a hornfels from Tauranga Bay (Fig. 2.9C).

CHAPTER THREE

THE MYLONITE ZONES

3.1 Introduction

Mylonitic zones are formed throughout the study area and the petrofabric and structural analysis of four specific areas are described and discussed here: the Morrisey Creek Mylonite Zone (MCMZ) which outcrops around Morrisey Creek and along the coast as far south as White Horse Creek; the Four Mile River mylonites which are exposed on the coast south of the Four Mile River mouth; the Deep Creek Mylonite Zone (DCMZ) which outcrops where State Highway 6 crosses Deep Creek and to the south of Deep Creek; and the Siberia Bay Mylonite Zone (SBMZ), located in the centre and south of Siberia Bay near Cape Foulwind.

The MCMZ, Four Mile River mylonites and DCMZ contain predominantly biotite-rich granitoid mylonites. In addition, the MCMZ also contains mylonitized leucogranites and veins. Mylonitized leucogranite also occurs in the DCMZ. The SBMZ contains mylonitized syenogranite-monzogranite.

The MCMZ, Four Mile River mylonites and the DCMZ lie on the southern limb of the Paparoa Metamorphic Core Complex and, according to the model proposed by Tulloch and Kimbrough (1989), should simply record a top-to-the-SSW sense of shear. However, SBMZ lies on the northern flank of the proposed core complex where Tulloch and Kimbrough (1989) propose a top-to-the-NE sense of shear.

3.2 Foliations and Lineations in the Mylonite Zones

Mylonites from the MCMZ, near the Four Mile River and the DCMZ are type II S-C mylonites possessing a gently dipping anastomosing foliation defined by a mica shape preferred orientation and aligned quartz ribbons. The foliation orientation is variable but generally dips gently to the SW in the MCMZ, gently to moderately SW near the mouth of the Four Mile River and is flat to gently dipping near Deep Creek. Towards the centre of the MCMZ superficially homogeneous slaty mylonites display a more planar foliation and weaker than normal stretching lineation due to successive repeated cycles of mylonitization and nucleation of phyllosilicates.

Within the MCMZ, DCMZ and near the mouth of the Four Mile River, stretching lineations are defined by linear trails of cataclased mica and boudinaged feldspar, and a linear preferred orientation of quartz ribbons on the foliation surface. These lineations trend generally NE-SW (Fig. 3.1A; Map 1 and Map 3). Slickenfibres in poorly exposed outcrops south of Deep Creek also trend NE-SW. Where State Highway 6 crosses Deep Creek, the stretching lineation trends ENE-WSW. In both the Deep Creek and Morrisey Creek mylonites multiple mica-defined lineations may lie oblique to the stretching lineation.

Mylonitized syenogranite-monzogranite in Siberia Bay exhibits a foliation defined by aligned primary and secondary biotite, quartz ribbons and cataclased feldspar which dips gently to moderately to the east. Stretching lineations are defined by a linear preferred orientation of mica, quartz ribbons and cataclased feldspar megacrysts and trend NE-SW to ENE-WSW. Boudinaged feldspar megacrysts in the plane of the foliation contain cracks filled with quartz oriented at a high angle to the lineation. Extension directions recorded by this cracking trend generally NE (Figs. 3.1B and C).

South of the mouth of the Four Mile River mylonitization is heterogeneously developed. Where mylonitization is poorly developed dominantly migmatitic rocks possess a moderate to steeply dipping foliation (S1). In one outcrop, a biotite-defined mylonitic

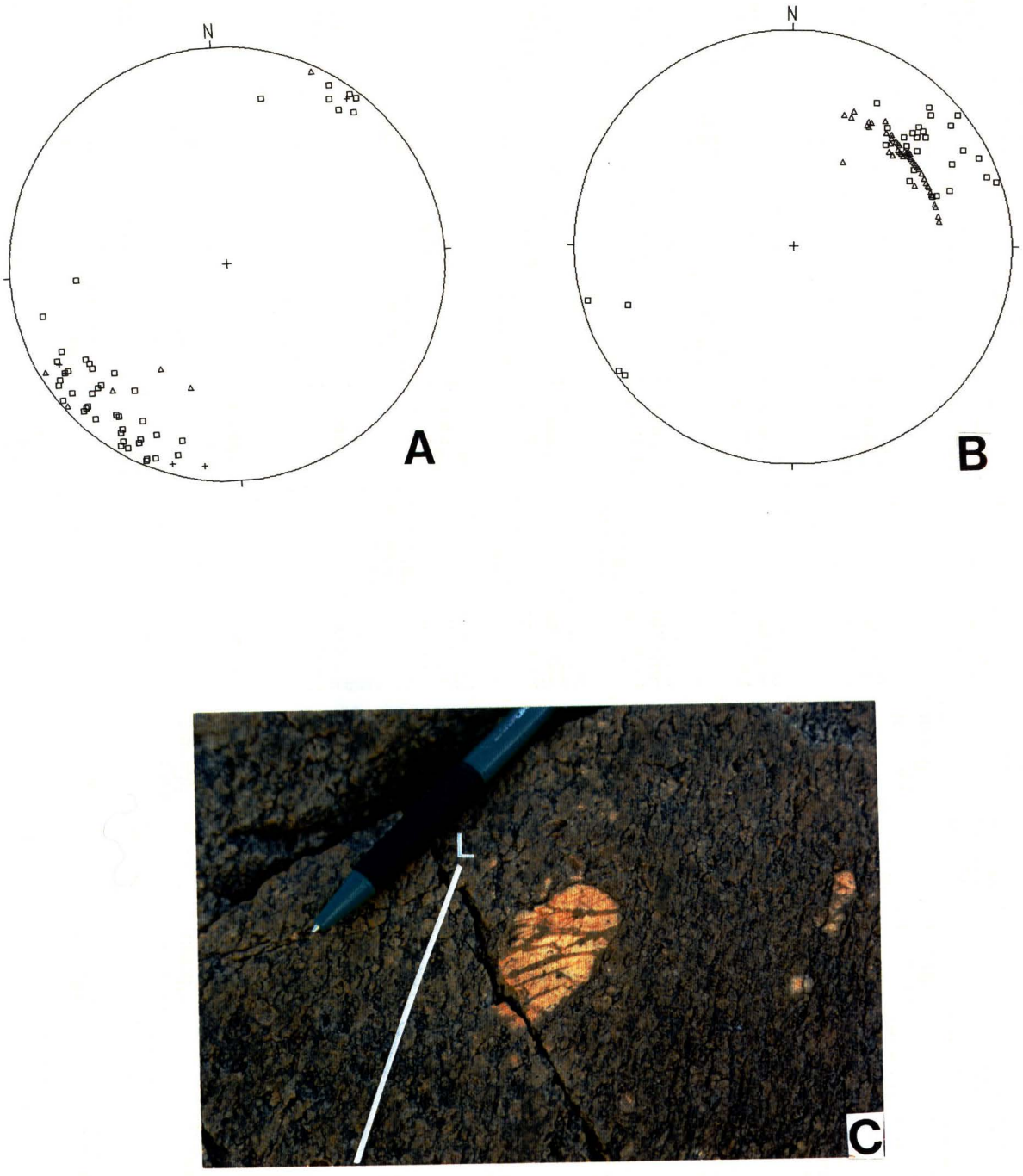

Fig. 3.1 A) Poles to lineations from the MCMZ (squares), Four Mile River mylonites (triangles) and DCMZ (crosses). B) Poles to lineations from the SBMZ (squares) and trend and plunge of feldspar cracks (triangles). C) Cracks in K-feldspar megacrysts at high angles to the lineation (L). Feldspar length=3.5 cm.

foliation dipping gently to the SW (S2) crosscuts a migmatitic foliation which dips moderately to the NE (S1).

3.3 Shear-sense Indicators

3.3.1 C-, S- and C′-planes

The MCMZ and DCMZ

Within all the mylonite zones the C-plane is defined as the dominant mesoscopic foliation of aligned cataclased muscovite, biotite and feldspar, and quartz ribbon boundaries. Dominant C-plane formation is characteristic of type II S-C mylonites (Lister and Snoke 1984).

In the MCMZ, sigmoidal S-planes are defined by mica fish, porphyroclast systems and finely cataclased mica which lie between 15° and 38° to the C-planes. Mylonites from the DCMZ contain S-planes defined by mica fish (DC5, R20) and aligned biotite (DC3) which lie between 18° and 25° to the C-planes (Fig. 3.2A). C-S plane geometries displayed in the MCMZ and DCMZ record a top-to-the-SW sense of shear.

C′-planes in both the MCMZ and DCMZ constitute either a true crenulation (Fig. 3.2B) or a shear plane oriented between 8° and 48° to the mylonitic foliation (C plane). Mica fish and quartz ribbons may be displaced along these shear planes. DC5 and R20, from the DCMZ display an alignment of mica along the C′-plane. C′-planes are best developed in mica-rich layers, but are generally discontinuous. Crenulations may also form as a response to heterogeneous deformation around porphyroclasts. However, these are not true C′-planes and die out away from the parent porphyroclast.

Analysis of mica-fish shape preferred orientations in sample WH31 (MCMZ) by Shelley (1995) suggests that the true planes of maximum shearing stress parallel to the shear zone boundary are the C′-planes, oriented about 25° to the C-planes. During progressive simple shear, the mylonitic foliation (defined by the C-plane) lies at some angle (α) to the

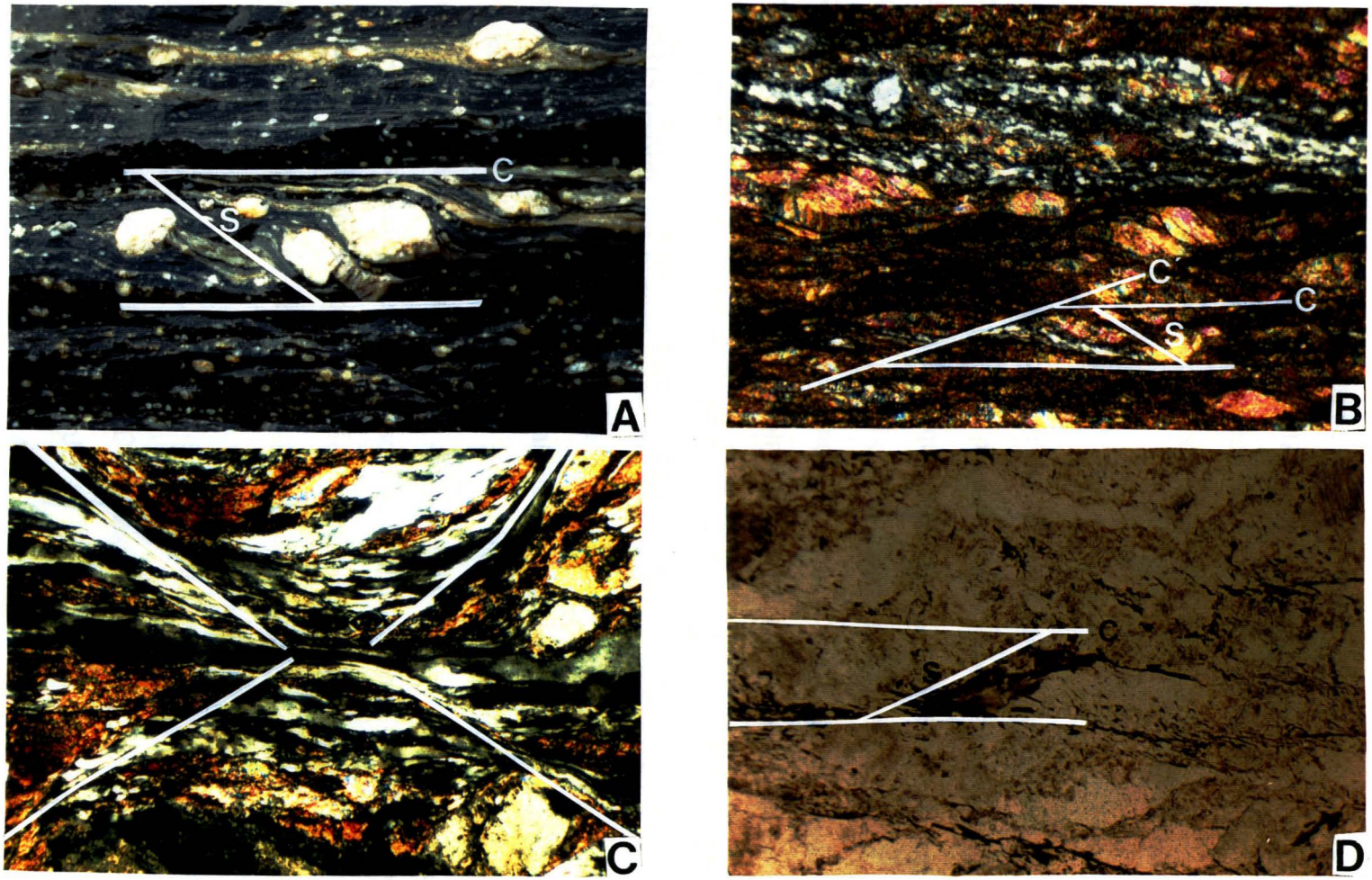

Fig. 3.2 A) C-S planes in MCMZ showing top-to-the-SW shear-sense indicators; viewed towards NW; view across=8 cm. B) C-, S-, and C′-planes (crenulation) showing top-to-the-SW shear-sense in MCMZ;crossed polarised light; viewed towards NW; C) conjugate C′-planes (white lines) (MCMZ); crossed polarised light; viewed towards NW. D) C-S planes in SBMZ showing top-to-the-NE sense of shear; note reactivated foliation along C-plane (3.3.5); viewed towards NW. B), C) and D) view across= 2.9 mm.

shear zone boundary and rotates towards the shear zone boundary or C′-plane with increasing strain (Fig 3.3).

One set of C′-planes synthetic to the mylonitic foliation (C-plane) has developed in most mylonites from the MCMZ and DCMZ and are consistent with a top-to-the-SW sense of shear during a non-coaxial deformation. Sample WH2 (MCMZ) contains conjugate C′-planes suggesting a component of coaxial deformation (Fig. 3.2C).

The Four Mile River Mylonites

Mylonites from near the mouth of the Four Mile River display a more complex C-S plane development. FM17 contains C-planes defined by the mesoscopic mylonitic foliation and S-planes of cataclased mica and quartz ribbons. S-planes lie at approximately 23° to the C- planes. C′-planes constitute both an asymmetric crenulation and a shear plane oriented synthetically between 19° and 29° to the C-plane. The C′-plane displaces the mylonitic foliation and feldspar porphyroclast tails. C-, S- and C′-plane geometries in FM17 show a top-to-the-SW sense of shear.

FM15 records two periods of C- and S-plane development. 'Old' C- and S-planes of recrystallized mica are consistent with a top-to-the-SW sense of shear. However, later developed C- and S-planes of finely cataclased mica, and asymmetric crenulations or C′-planes developed in these fine-grained zones, show a top-to-the-NE sense of shear. This suggests that the movement direction changed from top-to-the-SW sense of shear to a top-to-the-NE sense of shear during some later deformation. In fact, 'old' S-planes of muscovite are variably kinked or buckled, consistent with a change in orientation of the maximum principal compressive stress direction ($\sigma 1$) (Fig. 3.4).

The SBMZ

In the Siberia Bay Mylonite Zone, C-, S- and C′-planes are defined by three differing foliations. The C-plane may be regarded as the mylonitic foliation characterised by a preferred orientation of quartz ribbons, cataclased feldspars and sometimes an alignment of mica. The S-plane is oriented between 17° and 39° to the C-plane and is defined by

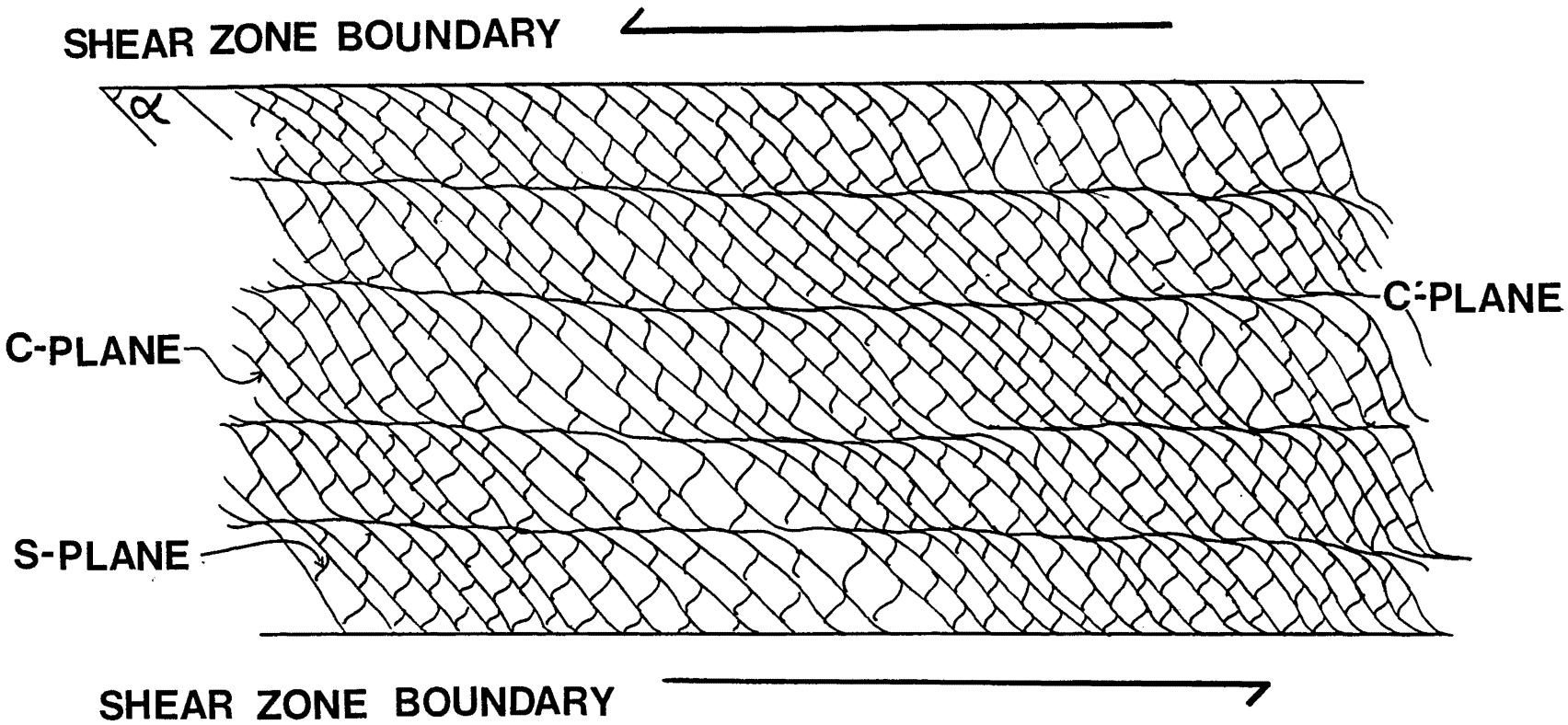

Fig. 3.3 Diagrammatic representation of the possible relationship of C-, S- and C′-planes to the shear zone boundary.

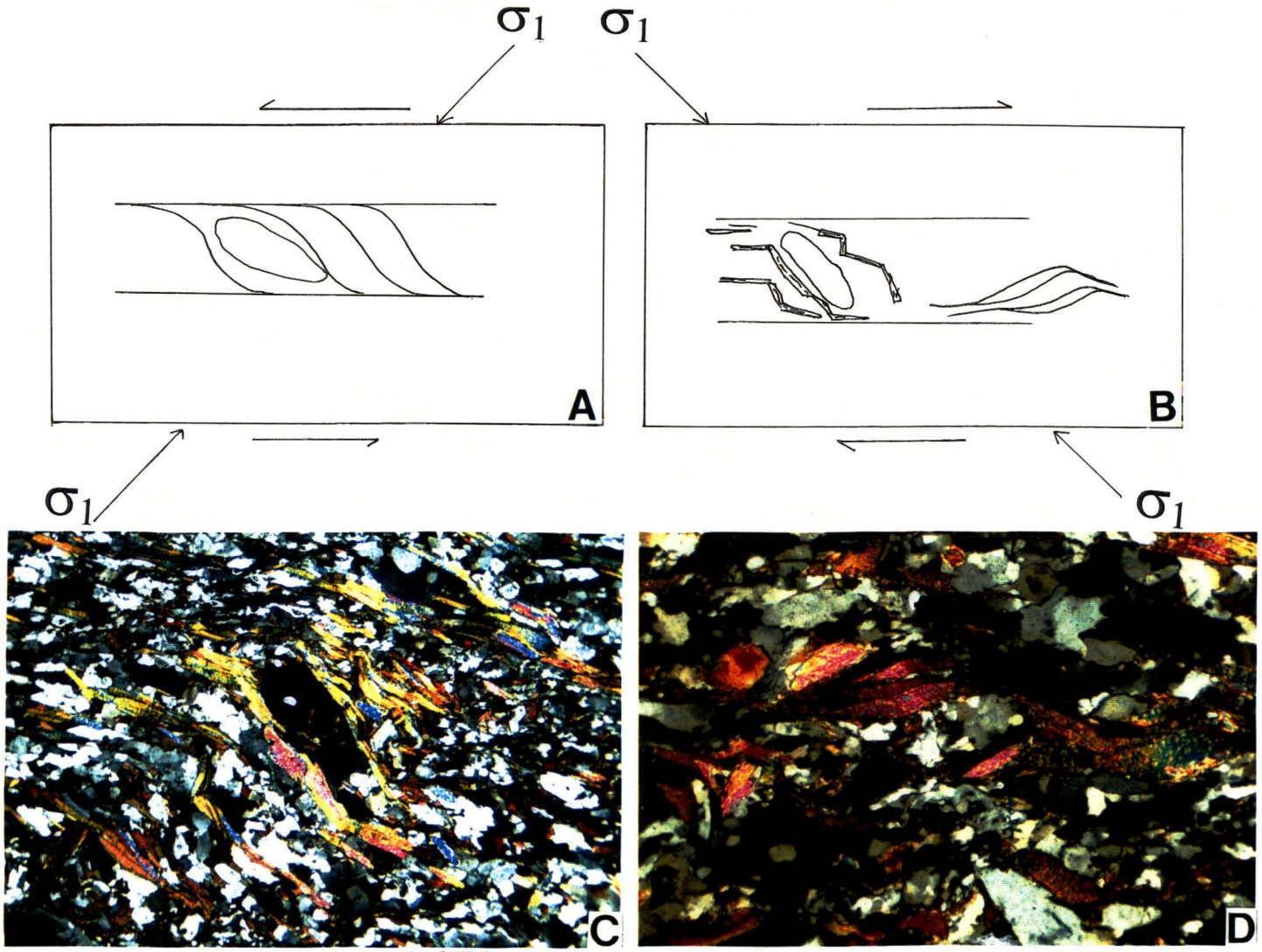

Fig. 3.4 Shear reversal from mylonites at the mouth of the Four Mile River. A) S-C planes and porphyroclast systems formed under a top-to-the-SW shearing. B) kinking of 'old' S-planes and the development of top-to-the-NE fabric elements during later top-to-the-NE shearing. C) example of top-to-the-SW porphyroclast and kinked S-planes; crossed polarised light; viewed to the NW; view across=5.3 mm.D) top-to-the-NE fabric elements;crossed polarised light; viewed to NW; view across=2.9 mm.

cataclased muscovite and minor biotite. A shear plane of cataclased biotite and minor muscovite, oriented synthetically between 20° and 57° to the C-plane, constitutes the C′-plane. In some cases, the C′-plane occurs as a more dominant foliation than the C-plane and displaces porphyroclast tails and the mylonitic foliation. The C′-plane only rarely occurs as an asymmetric crenulation. Gross C-, S- and C′-plane geometries in the SBMZ suggest a top-to-the-NE/ENE sense of shear (Fig. 3.2D).

3.3.2 Porphyroclast Systems

The MCMZ, DCMZ and Four Mile River Mylonites

In the MCMZ, DCMZ and mylonites south of the Four Mile River mouth, σ-type porphyroclasts of feldspar, garnet and apatite display wedge shaped tails of predominantly fine grained cataclased or newly crystallized biotite and dynamically recrystallized quartz. Occasionally tails of cataclased feldspar extend from feldspar parent porphyroclasts. Most porphyroclast systems are σ_a-type exhibiting predominantly stair-stepped tail geometries (Fig. 3.5A, B, C and D) (Hanmer and Passchier 1991). In-plane tails and pseudo δ-type porphyroclasts form where porphyroclast tails are locally displaced by C′-planes. In feldspar-rich mylonites σ_b-type porphyroclasts may also occur. σ_a-type porphyroclasts in coarse grained mylonites which outcrop for 200 m north of the centre of the MCMZ contain tails of recrystallized biotite and muscovite.

One characteristic of many σ-type porphyroclasts is the asymmetric distribution of recrystallized muscovite on porphyroclast boundaries oriented at a high angle to the maximum principal compressive stress direction. This suggests localised volume loss by the removal of soluble matrix components such as quartz and the concentration of muscovite which later becomes recrystallized (Fig. 3.5B).

All σ_a-type porphyroclasts and isolated σ_b-type porphyroclasts in the MCMZ and DCMZ possess an internal stair-stepping asymmetry consistent with a top-to-the-SW sense of shear, except for one porphyroclast from the DCMZ which shows a top-to-the-

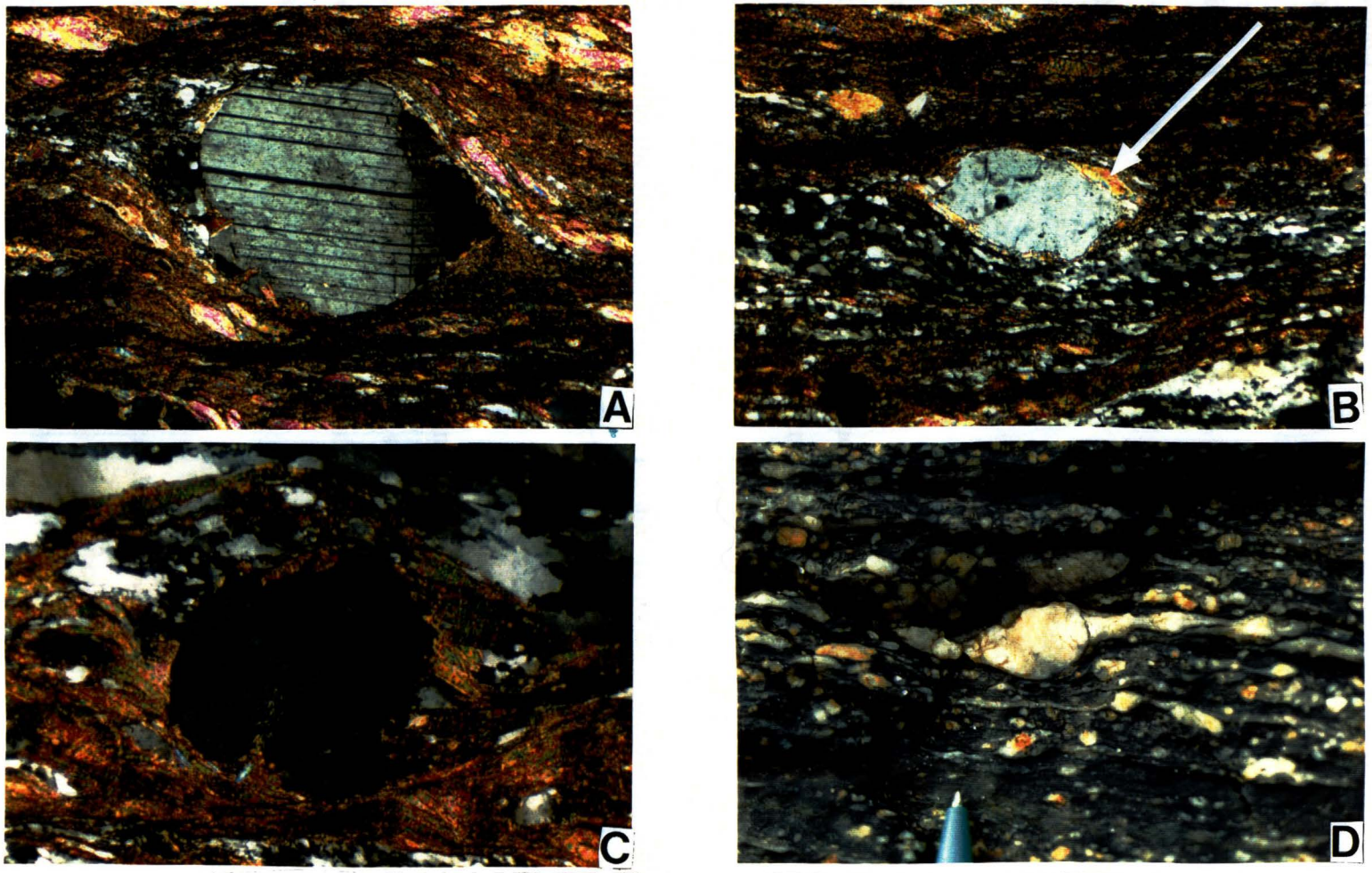

Fig. 3.5 A) and B) MCMZ: σ_a-type oligoclase porphyroclast systems displaying a top-to-the-SW sense of shear. Note asymmetric distribution of muscovite around porphyroclast boundary in B) crossed polarised light; view across=2.9 mm. C) σ_a-type porphyroclast system from Four Mile River mylonites displaying a top-to-the-SW shear-sense; crossed polarised light; view across=2.9 mm. D) σ_a-type porphyroclast system from MCMZ in outcrop showing top-to-the-SW sense of shear; view across=6 cm. A, B and C are viewd to the NW, D viewed to the SE.

NE sense of shear. Top-to-the-SW senses of shear recorded by porphyroclast systems are supported by C-, S- and C′-plane development in outcrop and thin section. Porphyroclasts in samples FM17 and FM15, from near the mouth of the Four Mile River also show an asymmetry consistent with a top-to-the-SW sense of shear.

Mica fish constitute a special type of σ_a-type porphyroclast which are best developed in mica-rich mylonites containing layers of cataclased mica up to 0.5 cm wide. Muscovite fish are by far the most common variety and occur as isolated porphyroclasts or complex aggregates of cataclased muscovite crystals (Fig 3.6A). Most mica fish display their {001} cleavage planes lying nearly parallel to the C-plane or tilted back against the sense of shear by up to 30°, although sample DC5 contains mica fish with their {001} cleavage planes oriented up to 49° to the C-plane. Some mica fish possess tails of cataclased or newly crystallized mica which stair step from one fish to the next. However, in highly sheared biotite-rich layers muscovite fish may lack tails altogether (Fig. 3.6B).

Muscovite fish have multiplied by movement along listric normal microfaults oriented antithetically to the shear sense and along cleavage fractures. In addition, muscovite fish have multiplied by displacement along C′-planes oriented synthetically to the bulk shear sense (Fig. 3.6C).

Mica fish in the MCMZ, DCMZ and in sample FM17 possess an internal asymmetry which shows a consistent top-to-the-SW sense of shear. However, FM15 contains mica fish which show a top-to-the-NE sense of shear (Fig. 3.4) associated with the development of 'new' C-S planes of cataclased mica.

In addition to mica fish recorded in thin section, boudinaged pegmatites in outcrop show fish-like forms when viewed in outcrops that are parallel to the stretching lineation. One such example from the MCMZ (Fig. 3.6D) shows asymmetric pegmatite boudins consistent with a top-to-the-SW sense of shear.

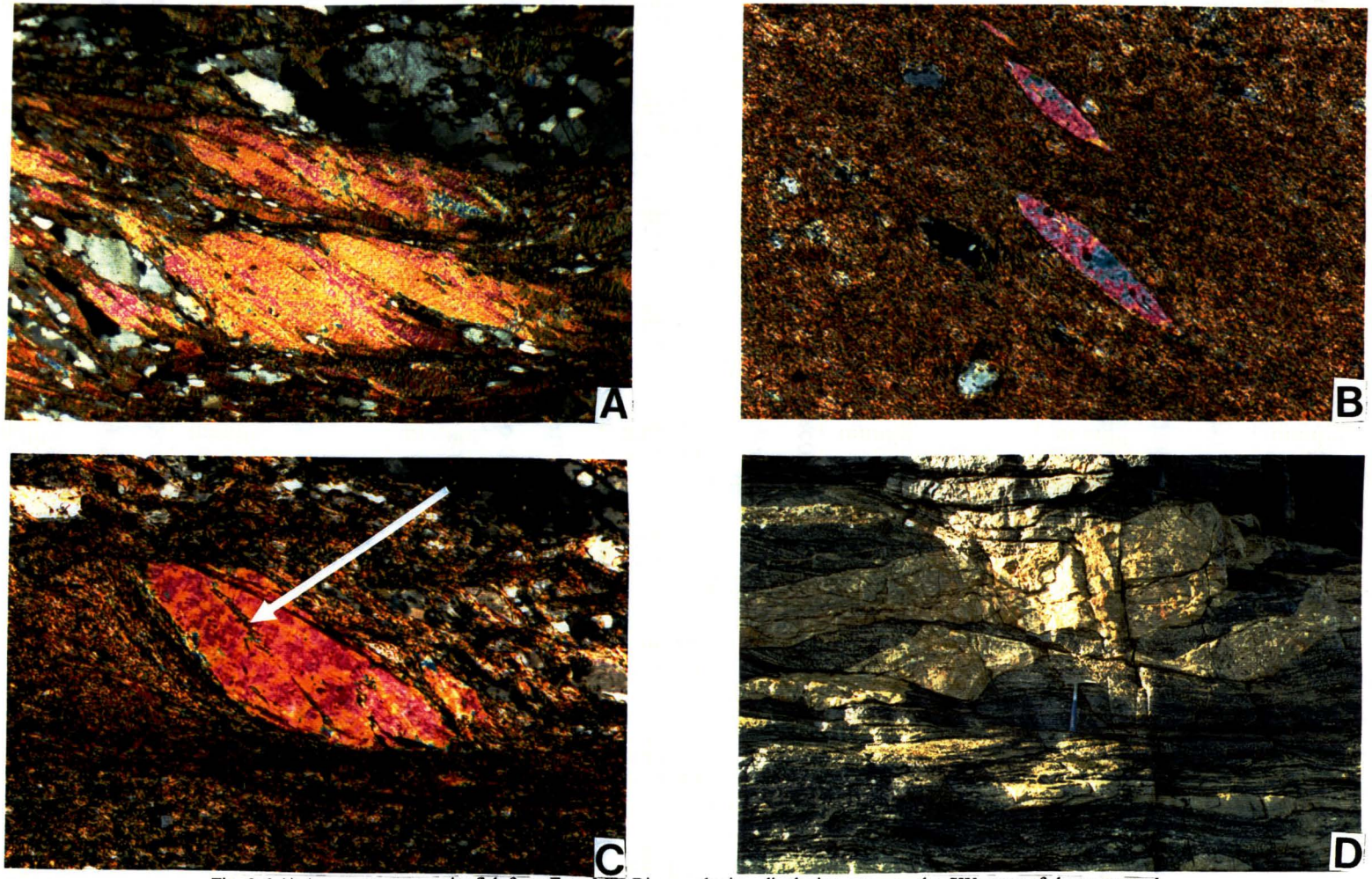

Fig. 3.6 A) Aggregate muscovite fish from Four Mile River mylonites displaying a top-to-the-SW sense of shear; crossed polarised light; view across=2.9 mm.
B) Muscovite fish from MCMZ displaying top-to-the-SW shear-sense and lacking tails of cataclased mica. View across=1.2 mm.
C) Muscovite fish from MCMZ showing a top-to-the-SW sense of shear; note listric normal microfault (arrow). View across=1.2 mm.
D) Deformed 'pegmatite fish' in MCMZ showing a top-to-the-SW sense of shear. Hammer length=33 cm.
A,B, and C are viewed to the NW. D is viewed to the SE.

The SBMZ

In the SBMZ σ_a-type porphyroclasts of predominantly microcline and plagioclase are variably developed. CFS33, CFS4, CFS38 and CFS2 contain σ_a-type porphyroclasts with tails of cataclased mica, quartz, cataclased feldspar and asymmetrically deflected quartz ribbons. These porphyroclast systems show an asymmetry consistent with a top-to-the-NE/ENE sense of shear (Fig. 3.7A and B). CFS27 and CFS31 contain poorly developed σ_a-type porphyroclast systems exhibiting both top-to-the-SW/WSW and top-to-the-NE/ENE senses of shear. Feldspar porphyroclasts in CFS3 are obliterated by cataclasis and metamorphic crystallisation and cannot be interpreted in regard to shear sense .

Mica fish are composed of both biotite and muscovite. Muscovite and biotite fish are generally large single crystals with short tails of cataclased mica. The {001} cleavage planes lie parallel to or up to 40° to the C-plane and are sometimes sigmoidal in shape tracing the S-plane (Fig. 3.7C). One muscovite fish in CFS27 has undergone cleavage slip showing a top-to-the-NE/ENE sense of shear (Fig. 3.7D).

CFS33, CFS27, CFS4, CFS3 and CFS2 contain mica fish and biotite lozenges consistent with a top-to-the-NE/ENE sense of shear. Mica fish in CFS31 are poorly developed but two mica fish may be interpreted in terms of shear sense; one exhibits a top-to-the-NE/ENE sense of shear, the other, top-to-the-SW/WSW. Asymmetric lozenge-shaped biotite aggregates possess tails of biotite smeared along the C- or C′-plane and indicate a sense of shear consistent with C-, S- and C′-planes in any one sample.

3.3.3 Oblique Quartz Shape-preferred Orientations

Dynamically recrystallised quartz ribbons in the MCMZ may display a quartz shape-preferred orientation oblique to the mylonite foliation (C-plane). In any one thin section, quartz ribbons may display no quartz shape-preferred orientation or a range of quartz shape-preferred orientations aligned synthetically from 7° to 50° to the mylonitic foliation. This suggests cycles of recrystallization such that equant dynamically recrystallised quartz grains become elongate under strain to form an oblique quartz shape-

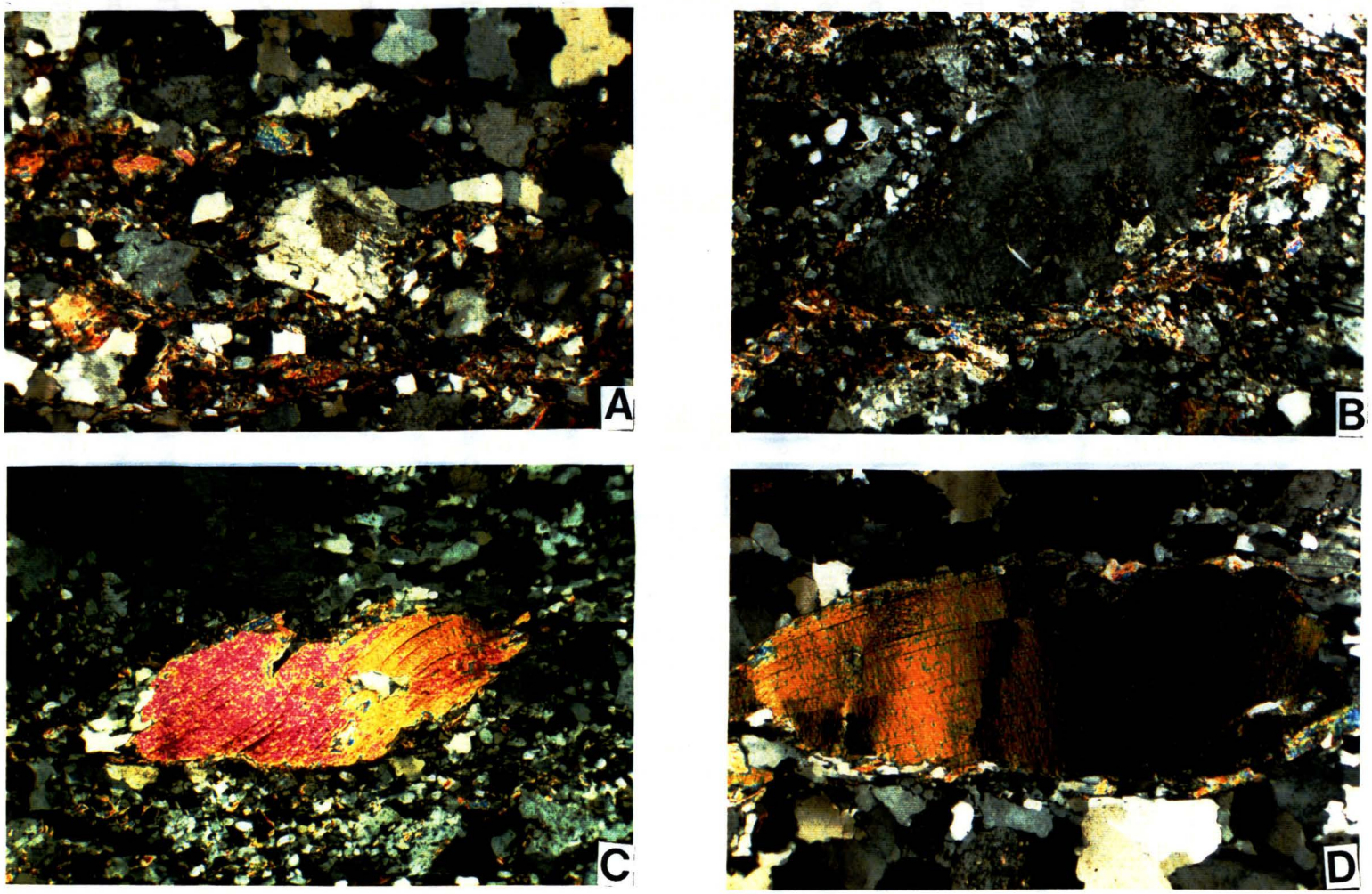

Fig. 3.7 A) and B): σ_a-type feldspar porphyroclast systems from the SBMZ, displaying top-to-the-NE/ENE shear-senses. C) Top-to-the-NE muscovite fish showing sigmoidal cleavage tracing the S-plane (SBMZ). D) cleavage slip in muscovite fish recording a top-to-the-NE shear-sense. View across A, B, C and D = 2.9 mm. Crossed polarised light; viewed towards the NW or NNW.

preferred orientation. The quartz shape-preferred orientation then rotates towards the C-plane with increasing strain. As dynamic recrystallization continues new strain free grains are produced, which in turn undergo strain and form new quartz shape preferred orientations. In this scenario, quartz shape preferred-orientations that lie closest to the C-plane represent the oldest cycle of recrystallization (Lister and Snoke 1984). The oblique quartz shape-preferred orientations throughout the MCMZ show a consistent top-to-the-SW shear-sense (Fig. 3.8).

Oblique quartz shape-preferred orientations are variably developed in the DCMZ and are oriented between 24° and 37° to the C-planes. A consistent sense of obliquity with respect to the mylonitic foliation suggests a top-to-the-SW sense of shear in all samples from the Deep Creek mylonites.

The Four Mile River mylonites display more than one period of oblique quartz shape-preferred orientation development. FM17 contains quartz shape-preferred orientations oriented synthetically between 19° and 44° from the C-plane which show an asymmetry consistent with a top-to-the-SW sense of shear. A top-to-the-SW sense of shear is supported by other fabric elements within the thin section. However, FM15 displays weakly developed oblique quartz shape-preferred orientations associated with the late development of top-to-the-NE fabric elements.

The SBMZ possesses oblique quartz shape-preferred orientations which record a top-to-the-SW/WSW sense of shear, sometimes associated with reactivated C-, S- and C′-planes. These fabrics are discussed in section 3.3.5.

3.3.4 Porphyroclast Fracture Patterns

The Siberia Bay mylonites contain megacrysts of predominantly microcline which have been cataclased and boudinaged to form 'books' of feldspar. However, when viewed in perpendicular to the NE-SW stretching lineation, feldspar books in close proximity show opposite senses of shear (Fig. 3.9A). Feldspar 'books' are inherently difficult to interpret in terms of shear sense and opposing shear senses may be the result of differing initial

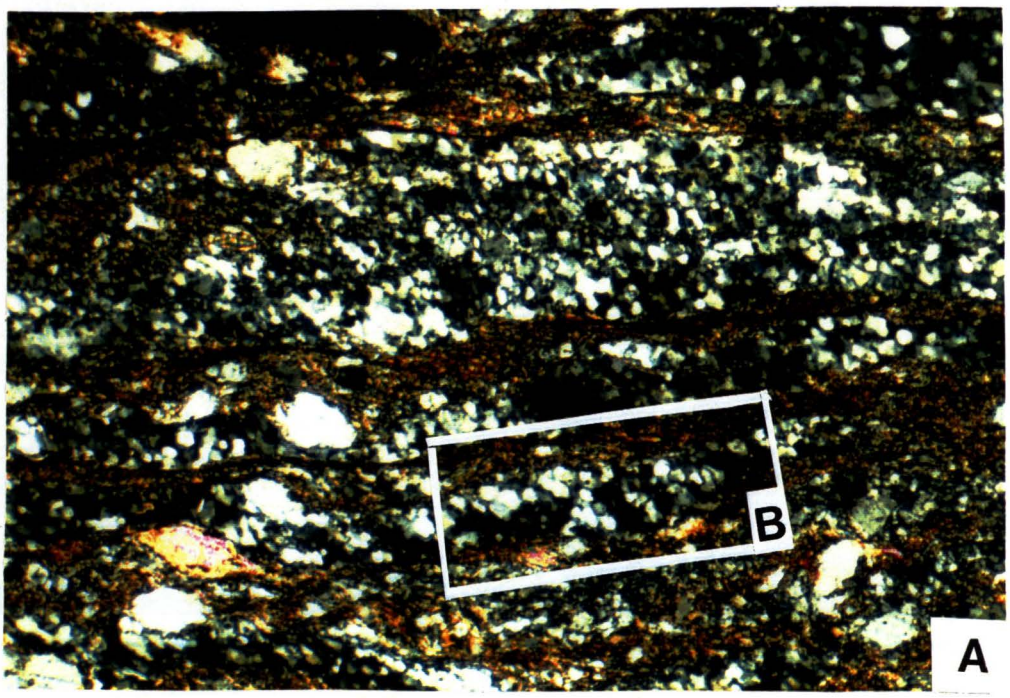

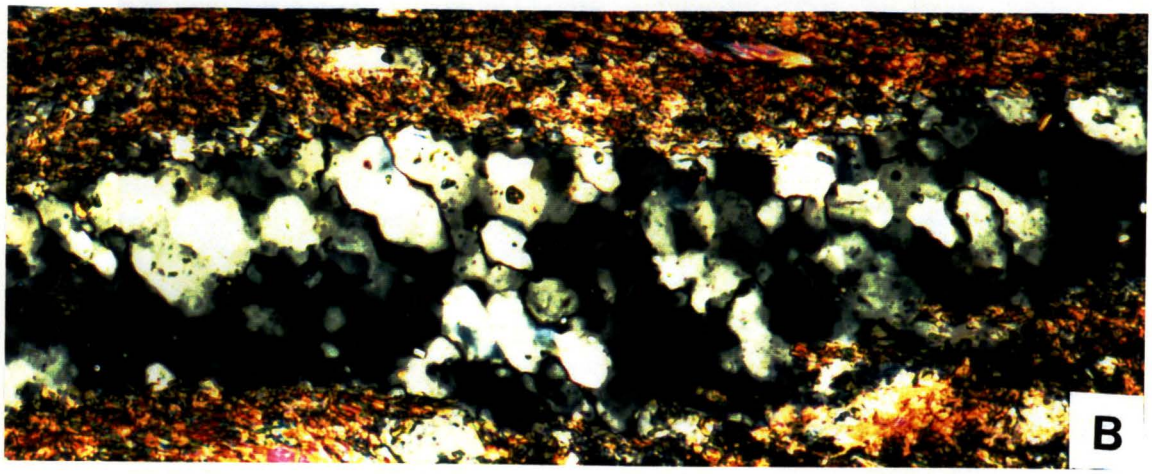

Fig. 3.8 A) Finegrained dynamically recrystallized quartz ribbons displaying oblique quartz shape preferred orientations recording a top-to-the-SW sense of shear; crossed polarised light; view across=2.9 mm. B) Close up of dynamically recrystallized quartz grains recording a top-to-the-SW shear-sense; crossed polarised light; view across=1.4 mm. A and B viewed towards NW.

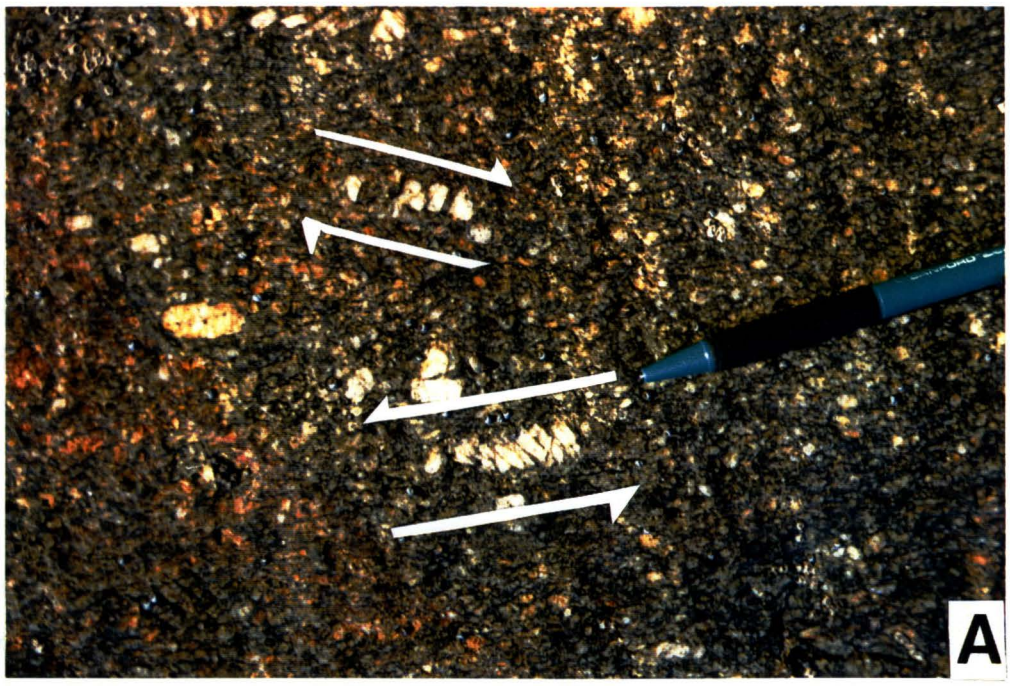

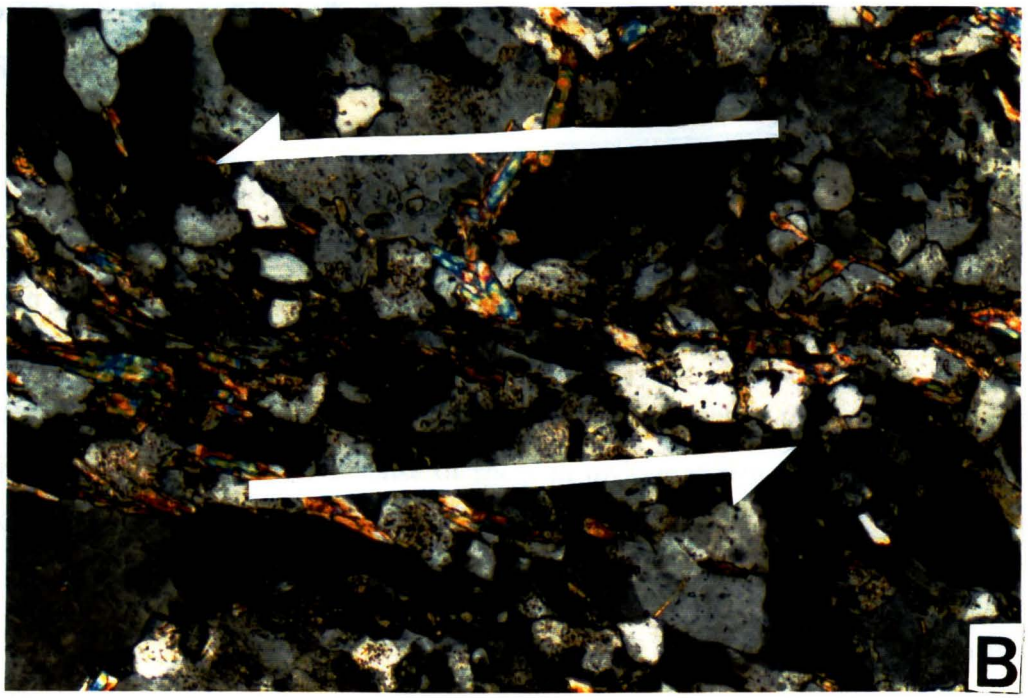

Fig. 3.9 A) Feldspar 'books' from the SBMZ showing conflicting shear-senses; viewed towards SE; view across=22 cm. B) Foliation deflection along C-plane showing top-to-the-SW sense of shear in SBMZ. Viewed towards NW; crossed polarised light; view across=1.2 mm.

feldspar orientations relative to the kinematic framework (Simpson and Schmid 1983). True opposing shear senses from feldspar fracture patterns cannot, therefore, be unequivocally established.

3.3.5 Reactivated C-, S- and C′-planes and Quartz Shape-preferred Orientations in the SBMZ

In the SBMZ S-planes, C′-planes and especially C-planes sometimes exhibit a sigmoidal foliation deflection consistent with a top-to-the-SW/WSW sense of shear (Figs. 3.2D and 3.9B). A top-to-the-SW/WSW sense of shear contradicts top-to-the-NE/ENE senses of shear recorded by the gross C-, S- and C′-plane geometries, some mica fish and most feldspar porphyroclasts. Associated with this localised foliation deflection is the development of oblique quartz shape-preferred orientations consistent with a top-to-the SW/WSW sense of shear.

Some samples contain a quartz shape-preferred orientation at 50° to the C-plane which is not spatially associated with reactivated C-, S- or C′-planes. This quartz shape- preferred orientation also records a top-to-the-SW/WSW sense of shear.

The origin of reactivated C-, S- and C′-planes and quartz shape-preferred orientations suggesting a top-to-the-SW/WSW sense of shear in mylonites which record a gross top-to-the-NE/ENE sense of shear is discussed in Chapter 8.

3.4 Quartz c-axis Fabric Analysis

3.4.1 The MCMZ

General Descriptions

MC1, MC2, DS833 and WH231 display type I crossed girdles (Fig. 3.10). Small circle c-axis girdles are either asymmetrically or symmetrically disposed about the axis of least finite strain (Z) and intersect connecting girdles between 30° and 45° from Z.

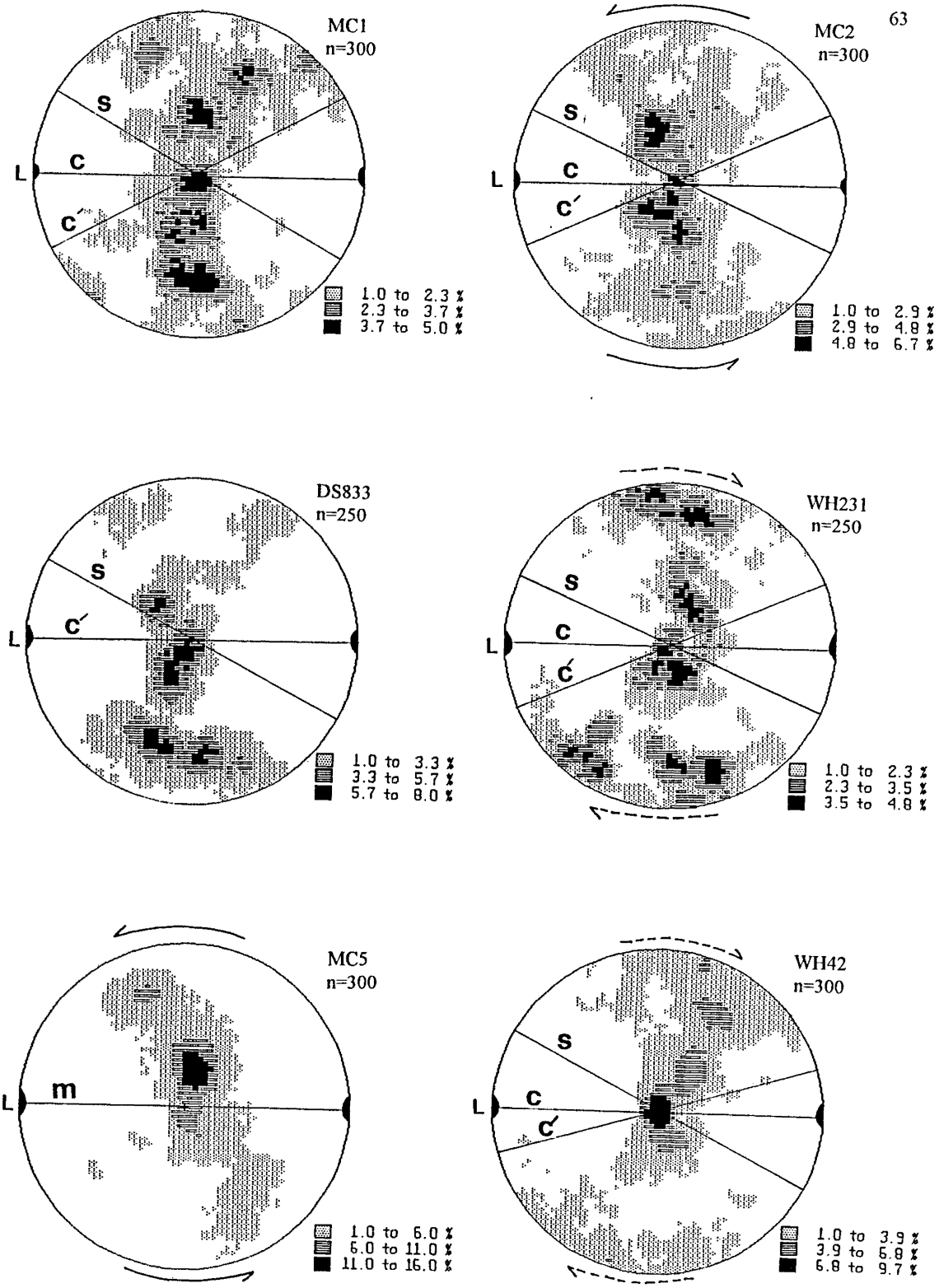

Fig. 3.10 Contoured lower hemisphere equal area projections of quartz c-axis orientations from the MCMZ; c=C-plane, s= S-plane, c′= C′-plane, L=lineation. Mylonitized vein MC5 displays a mylonitic foliation (m), but no C-S planes; the mylonitic foliation parallels the C-plane in surrounding granitoid mylonites. All quartz fabrics are viewed towards the NW. Bold arrows show true sense of shear; dashed arrows show apparent shear-sense; shear-sense discussed in text.

Mylonitized vein MC5, biotite-rich granitoid mylonite WH42 and coarse-grained mylonites WH35, WH36 and WH38 display well defined single girdles with a distinct asymmetry with respect to the C-plane (Figs. 3.10 and 3.11). WH42 and WH36 display peaks at the Y axis (the axis of intermediate finite strain). WH38 contains a girdle distribution of c-axes and a maxima intermediate between X (the axis of greatest finite strain) and Z (the axis of least finite strain), approximately 30° from the circumference of the stereonet. MC5 displays a strong girdle concentration of c-axes.

WH31, WH233 and WH234 display poorly defined girdles with discrete point maxima (Fig. 3.11). WH233 contains two maxima oriented symmetrically about Z. WH31 is characterised by a strong peak near the Y axis and WH234, near the Z axis. Ribbon mylonite WH2 and mylonitized leucogranite WH32a display fabrics intermediate between type I crossed girdle and single girdle geometries (Fig. 3.12). WH37 (Fig. 3.12) contains a strongly asymmetric fabric similar to "double girdle fabrics" recorded by Keep and Hansen (1994).

WH43 and WH44 appear texturally similar to mylonitized migmatites that outcrop south of White Horse Creek, and show incoherent fabrics that cannot be classified as type I or type II crossed girdles or interpreted in terms of a sense of shear (Fig. 3.12).

Glide Systems.

Quartz c-axis maxima concentrations at the Y axis are attributed to the prism <a> glide systems (Starkey 1979). Girdles of c-axes oriented at a high angle to X and maxima disposed at or around Z can be attributed to dominant basal <a> glide. Most quartz fabrics in the MCMZ have undergone a combination of basal <a>, prism <a> and possibly rhombohedral <a> glide. However, prism <a> glide seems to dominate, as in WH42 for example, producing discrete c-axis concentrations at the Y axis.

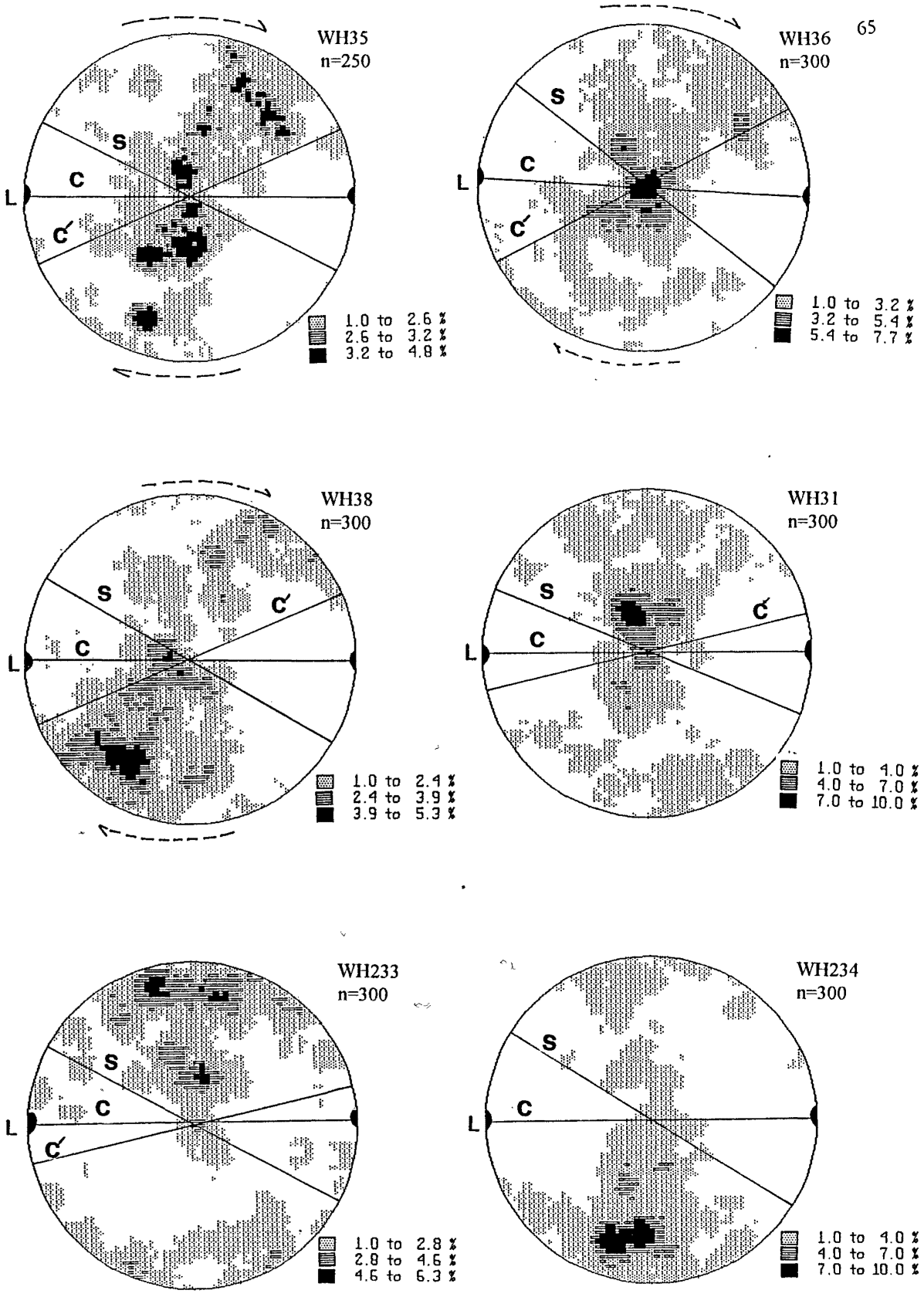

Fig. 3.11 Contoured lower hemisphere equal area projections of quartz c-axis orientations from the MCMZ; c=C-plane, s=S-plane, c′=C′-plane, L=lineation. All quartz fabrics are viewed towards the NW. Dashed arrows show apparent shear-sense; shear-sense discussed in text.

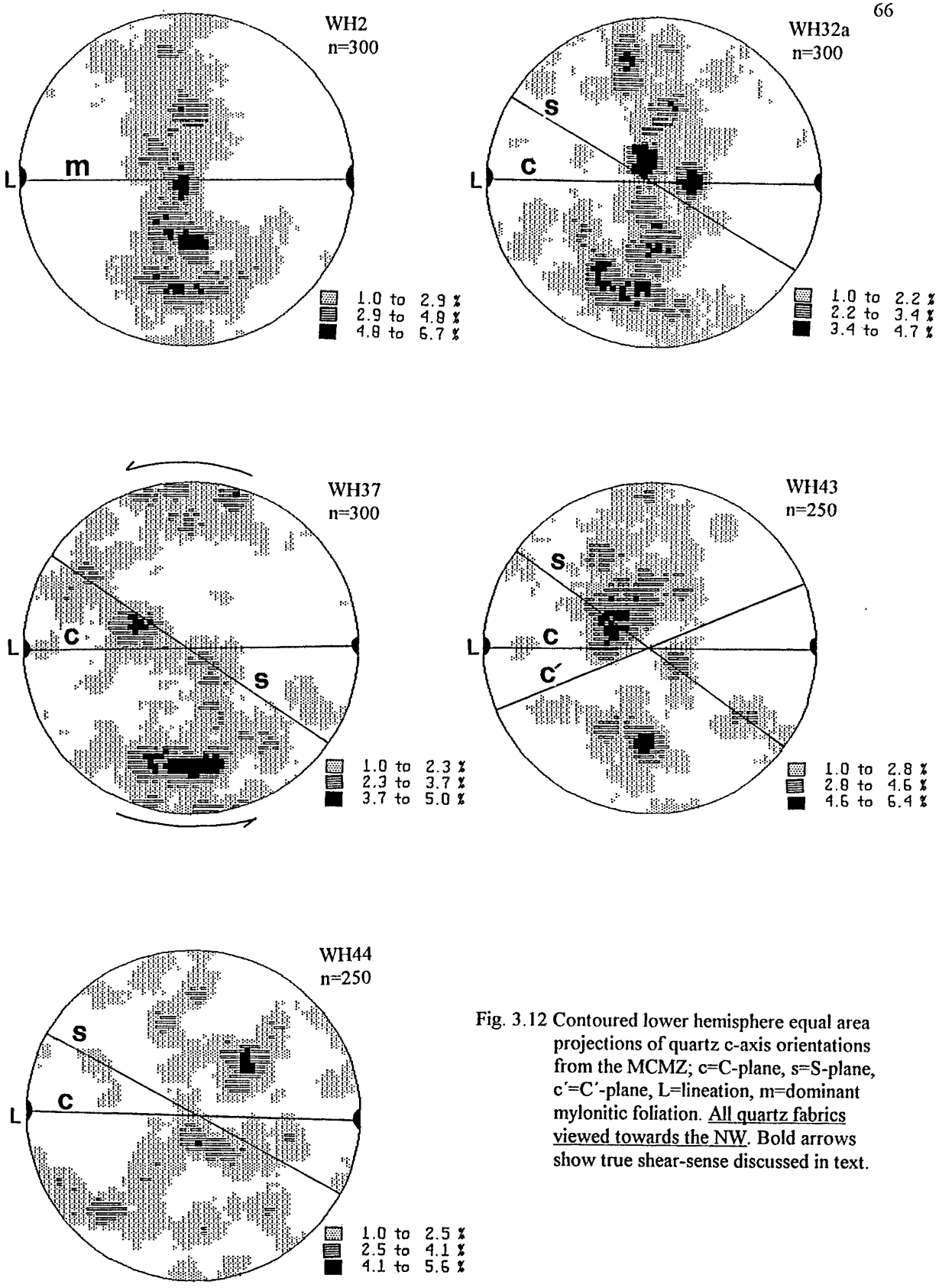

Fig. 3.12 Contoured lower hemisphere equal area projections of quartz c-axis orientations from the MCMZ; c=C-plane, s=S-plane, c′=C′-plane, L=lineation, m=dominant mylonitic foliation. All quartz fabrics viewed towards the NW. Bold arrows show true shear-sense discussed in text.

Sense of Shear from the Quartz c-axis Fabrics

WH37 and MC5 show strongly asymmetric fabrics with respect to mylonitic foliation indicating a top-to-the-SW sense of shear consistent with fabric elements in thin section. WH2 displays a symmetric fabric with respect to foliation suggesting coaxial deformation, supported by the presence of conjugate C′-planes in thin section (Fig. 3.2C).

WH31, WH233, WH234 and WH32a display girdles that are not asymmetric and do not seem to suggest any sense of shear (Figs 3.11 and 3.12). However, fabric elements such as mica fish, C-, S- and C′-planes and asymmetric porphyroclasts are well developed in thin section indicating that the above samples underwent a predominantly non-coaxial strain history.

Type I crossed girdles MC2 and MC1 (Fig. 3.10) appear slightly asymmetric with respect to C-plane and suggest a top-to-the-SW sense of shear, consistent with other fabric elements in thin section.

Biotite-rich granitoid mylonite WH231 displays a type I crossed girdle which appears to record top-to-the-NE sense of shear, contradicting well developed mica fish and other fabric elements in thin section. North of the centre of the MCMZ, coarse-grained mylonites containing recrystallized mica (WH35, WH36, and WH38; Fig 3.11) and biotite-rich granitoid mylonite WH42 (Fig. 3.10) possess strongly asymmetric single girdle fabrics which also appear to record a top-to-the-NE sense of shear. Top-to-the-NE movement directions contradict top-to-the-SW senses of shear shown by mica fish, porphyroclast systems, C-, S- and C′-planes and oblique shape-preferred orientations. Such a problem is not uncommon and similar occurrences have been reported by Law et al (1994) and Keep and Hansen (1994). The origin of apparent shear reversals in the MCMZ are discussed further in Chapter 8.

3.4.2 The Four Mile River Mylonites

FM17 and FM15 display type II crossed girdles centred about the Y axis (Fig. 3.13). FM17 cannot be interpreted in terms of a sense of shear. FM15 exhibits two broad girdles

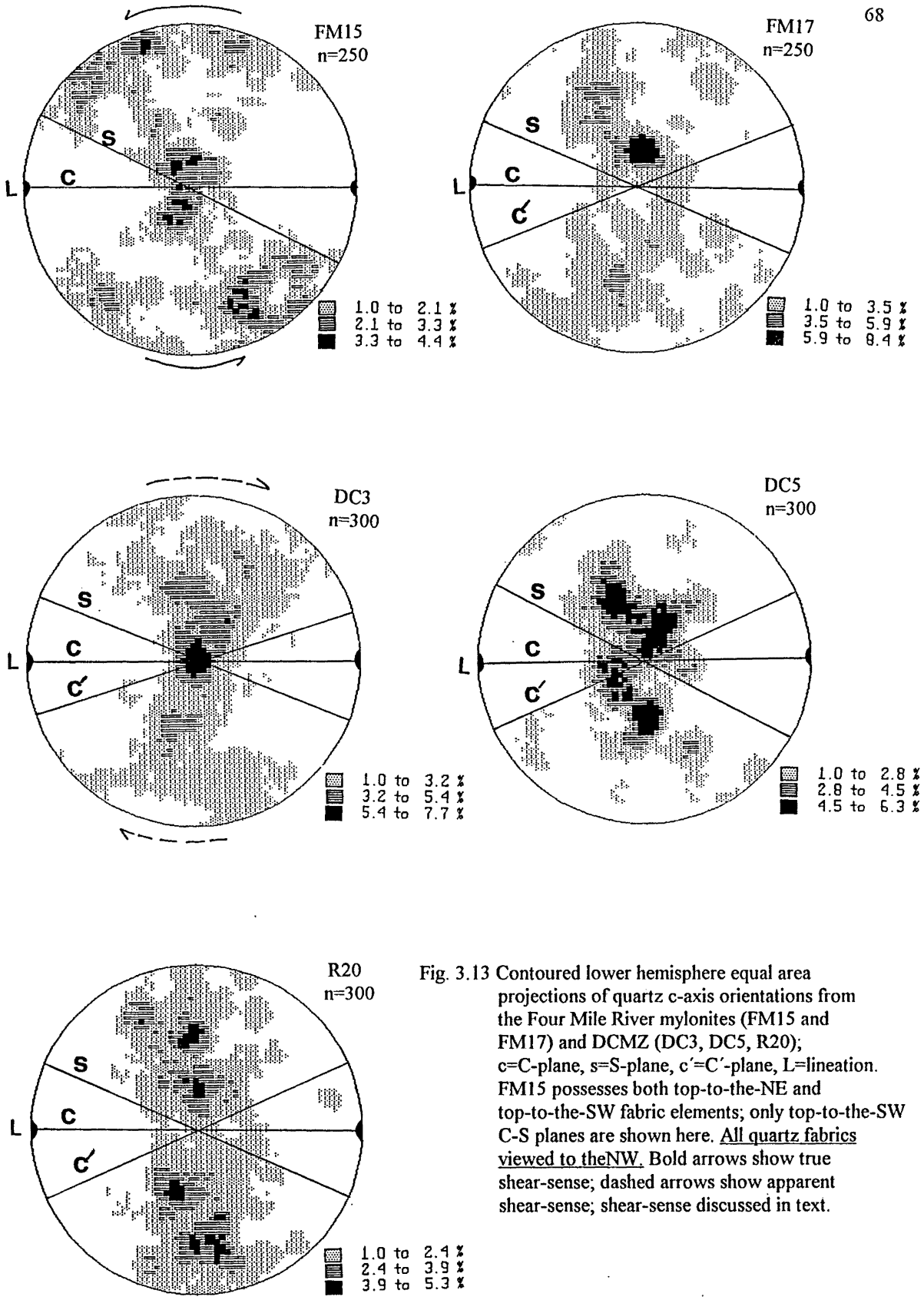

Fig. 3.13 Contoured lower hemisphere equal area projections of quartz c-axis orientations from the Four Mile River mylonites (FM15 and FM17) and DCMZ (DC3, DC5, R20); c=C-plane, s=S-plane, c′=C′-plane, L=lineation. FM15 possesses both top-to-the-NE and top-to-the-SW fabric elements; only top-to-the-SW C-S planes are shown here. All quartz fabrics viewed to theNW. Bold arrows show true shear-sense; dashed arrows show apparent shear-sense; shear-sense discussed in text.

containing a weak concentration of c-axes at the Y axis and oriented approximately 35° from Z. Type II crossed girdles have been attributed to a combination of basal <a> and prism <a> glide (Lister and Dornsiepen 1982). The c-axis fabric from FM15 contains one girdle with a higher concentration of c-axes than the other. This girdle is asymmetrically disposed to the mylonitic foliation (C-plane) suggesting a top-to-the-SW sense of shear. The remaining weaker girdle could represent either those quartz grains in unfavourable orientations for slip during SW shearing, or c-axes which have been rotated during later top-to-the-NE movements recorded by C-, S- and C′- planes of cataclased mica and oblique quartz shape-preferred orientations.

3.4.3 The DCMZ

DC3 displays a well defined type I crossed girdle containing a maxima at the Y axis (Fig. 3.13). This suggests a predominance of prism <a> glide (Feuten 1992). DC5 and R20 show poorly defined quartz c-axis fabrics with variable maxima orientations and are hesitantly interpreted here as type I crossed girdles (Fig. 3.13). DC3 is clearly asymmetric with respect to the C-plane and records a top-to-the-NE sense of shear. If R20 and DC5 can be interpreted as similar type I crossed girdles, they also display an asymmetry consistent with movement to the NE.

A top-to-the-NE sense of shear determined by quartz c-axis fabrics contradicts top-to-the-SW shear-sense indicators in thin section suggesting that the apparent shear reversals recorded in some mylonites of the MCMZ may be widespread. The origin of the c-axis fabrics reported from the DCMZ are discussed further in Chapter 8.

3.4.4 The SBMZ

In the SBMZ quartz occurs as coarse-grained recrystallized ribbons and as fine-grained individual grains associated with mica. The following discussion is divided into two sections: section A describes c-axis fabrics from samples containing only coarsely recrystallized quartz ribbons; section B describes domainal quartz fabrics found in CFS27 and within a shear zone in sample CFS4.

A) *Coarse-grained Quartz c-axis Preferred Orientations.*

CFS33 and CFS38 display type II crossed girdles (Fig. 3.14). However in CFS33 part of one girdle is missing. CFS38 and CFS33 type II crossed girdles exhibit one dominant girdle which contains a high number of c-axes but lack discrete maxima. The dominant girdle in both CFS38 and CFS33 are asymmetric with respect to the dominant mylonitic foliation (C-plane) and suggest a top-to-the-NE/ENE sense of shear.

CFS31 and CFS2 display single c-axis girdles (Fig. 3.14). The CFS2 fabric pattern displays a strong maxima in the XZ plane, and a very weak maximum at the Y axis which have been attributed to basal <a> glide and prism <a> glide respectively (Feuten et al 1991). CFS31 contains a broad girdle with no discrete maxima and a peculiar concentration of c-axes at the lineation. A concentration of c-axes at the lineation has not been reproduced from other coarse-grained quartz in the mylonites. These maxima are regarded as not significant.

CFS31 and CFS2 single girdles, (Fig. 3.14), are both asymmetric with respect to the mylonitic foliation (C-plane) suggesting a top-to-the-NE/ENE sense of shear, consistent with C-, S- and C′-plane geometries in CFS31 and both C-, S- and C′-planes and porphyroclast systems in CFS2.

Coarse-grained quartz from CFS4a contains four broad concentrations of c-axes consistent with basal <a> glide (Fig. 3.14). Maxima in the NE and SW quadrants of the steroenet contain a large proportion of c-axes, which suggests a top-to-the-NE/ENE sense of shear, consistent with C-, S- and C′-planes in thin section.

CFS3 exhibits a poorly defined quartz c-axis fabric which could be interpreted as either two small circle girdles or a type II crossed girdle (Fig. 3.14) This fabric cannot be interpreted in terms of sense of shear.

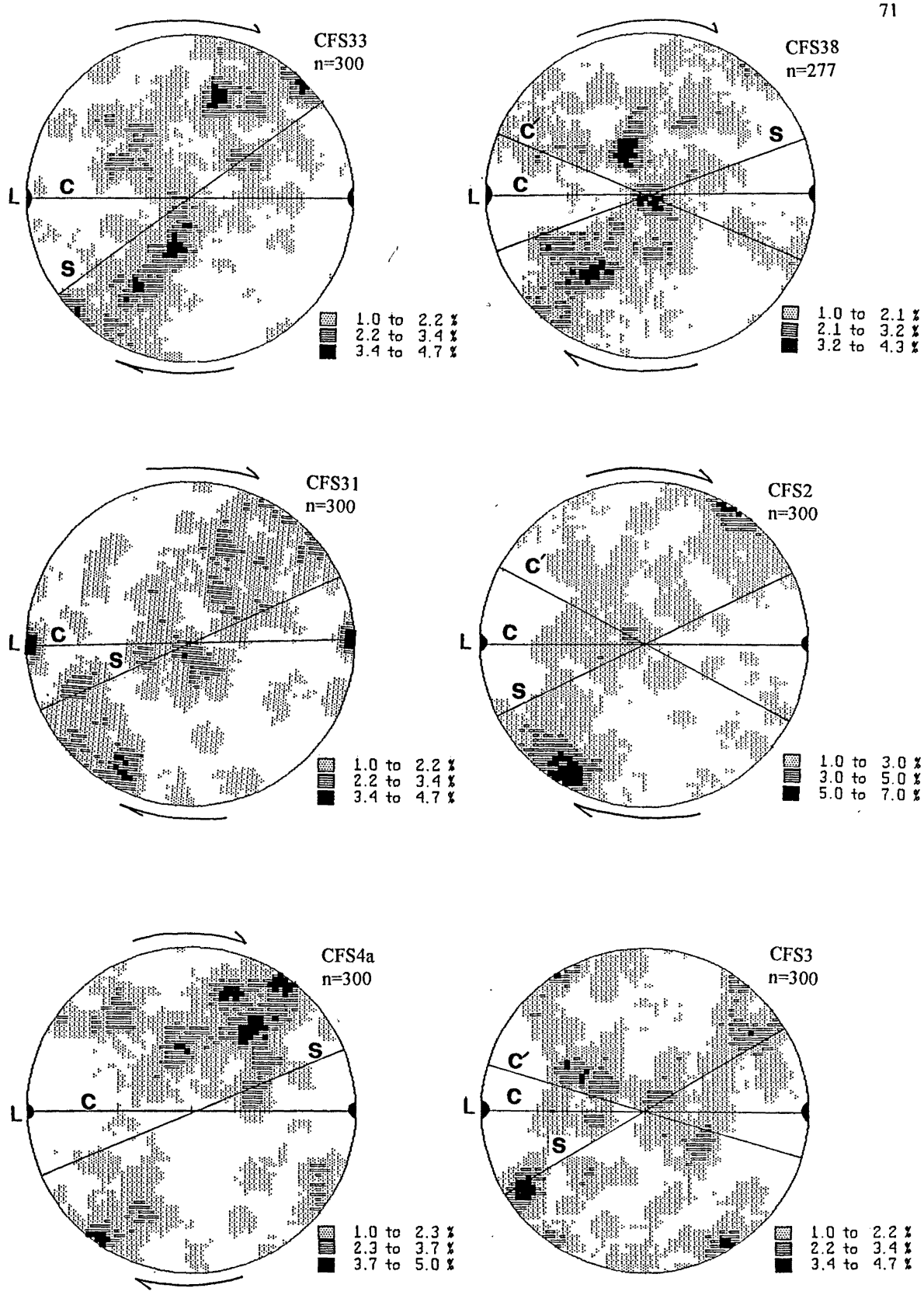

Fig. 3.14 Contoured lower hemisphere equal area projections of quartz c-axis orientations from the SBMZ; c=C-plane, s=S-plane, c′=C′-plane, L=lineation. Fabrics viewed to the NW/NNW. Bold arrows show true shear-sense; shear-sense discussed in text.

B) *Domainal Quartz Fabrics and Shear Zone Development*

In the south of Siberia Bay dark coloured fine-grained discrete layers up to 2 cm wide lie parallel or slightly oblique to the mylonitic foliation and contain a sigmoidal foliation deflection consistent with shear zone formation. Although dark coloured in outcrop, the shear zones are composed primarily of muscovite and quartz with lesser amounts of biotite and plagioclase, suggesting the dark colour is due to a grainsize reduction rather than any concentration of mafic minerals.

One such shear zone in sample CFS4 displays irregular but discrete boundaries with the deformed syenogranite-monzogranite country rock. Recrystallized quartz ribbons in the shear zone form a mylonitic foliation or C-plane. Within the quartz ribbons, quartz grain boundaries lie at a high angle to foliation and are in part controlled by small mica flecks aligned parallel to the foliation within the quartz ribbons. Muscovite is deformed into fish occasionally displaced along C′-planes. Muscovite fish and C-, S- and C′-plane geometries suggest a top-to-the-NE/ENE sense of shear.

The shear zone boundaries are characterised by a concentration of 0.05 mm, slightly elongate individual quartz crystals bound by fine-grained biotite (Fig. 3.15A) This concentration of fine grains towards the shear zone boundaries contradicts shear zones described in the literature which display a decrease in grainsize towards the centre of the shear zones, due to increasing strain, dynamic recrystallization and cataclasis. (Vauchez 1987; Lloyd et al 1992). Although the fine quartz grains appear to be associated with a disaggregation of quartz ribbons, no evidence for cataclasis of the quartz ribbons can be found in thin section.

Sample CFS27 also contains domains of fine-grained quartz and mica (Fig. 3.15B). These layers do not form discrete shear zones such as those in CFS4. However they do appear to be involved in a shearing process by which coarse-grained quartz ribbons are partly smeared along the foliation. Although some quartz grains have undergone recrystallization to form equant crystals occasionally possessing triple junctions, other

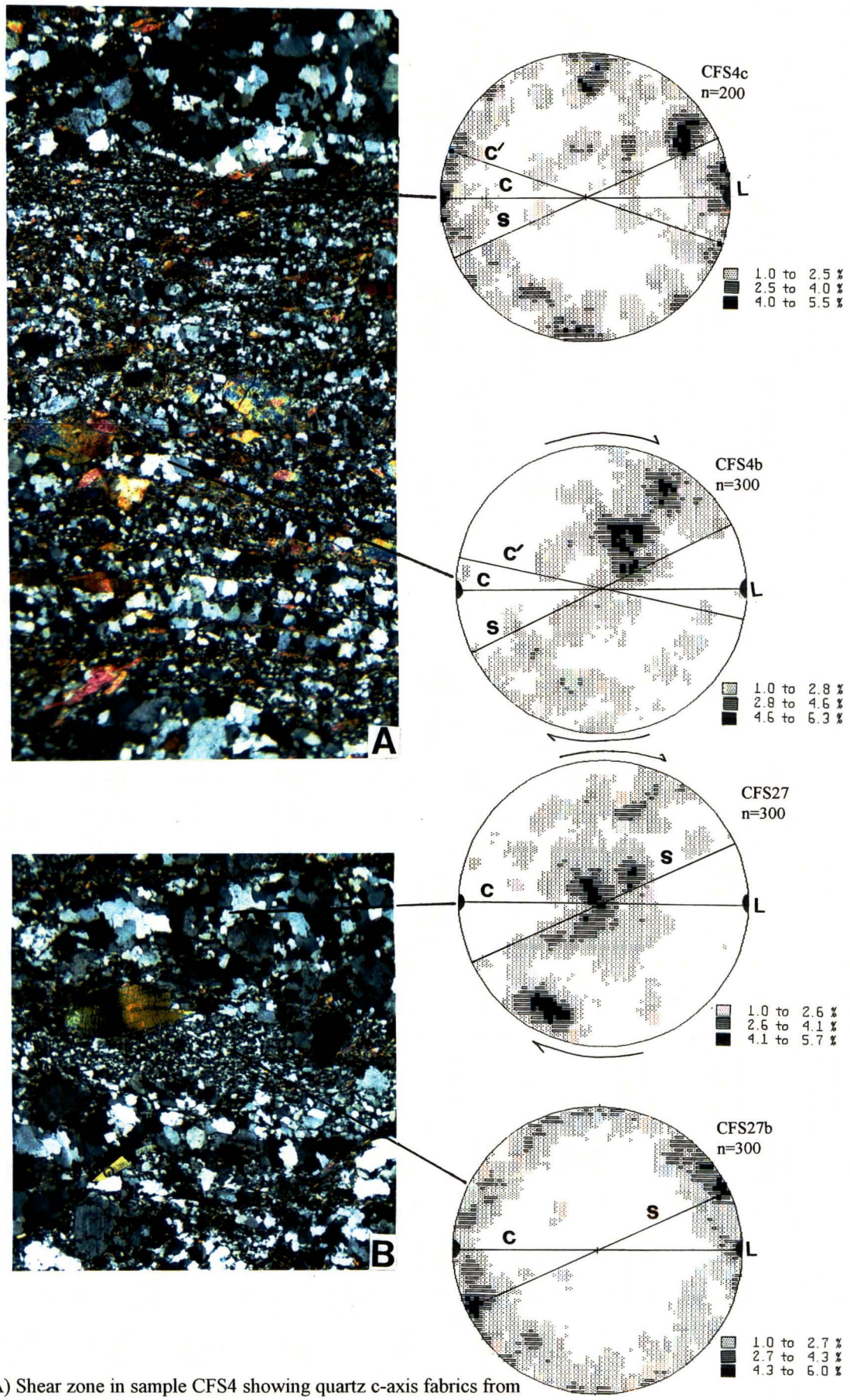

Fig. 3.15 A) Shear zone in sample CFS4 showing quartz c-axis fabrics from fine-grained quartz-mica areas (CFS4c) and coarser-grained ribbons in shear zone (CFS4b); crossed polarised light; view across width if photo=4.2 mm. B) Sample CFS27 showing fine-grained quartz-mica areas and coarse-grained quartz ribbons; crossed polarised light; view across=4.2 mm. Quartz c-axis fabrics are from fine-grained layers (CFS27b) and coarse grained layers (CFS27). Fabrics viewed towards the NW/NNW; c=C-plane, s=S-plane, c′=C′-plane, L=lineation.

fine grains of quartz are somewhat elongate in the plane of foliation. Within the same sample coarse-grained recrystallized quartz ribbons are prominent.

Associated with a decrease in grain size and an increase in mica content in both the shear zone in sample CFS4 and in fine-grained quartz-mica layers in CFS27, is a change in c-axis preferred orientation (Fig. 3.15). Within the shear zone in CFS4, coarser-grained quartz ribbons display a girdle concentration of c-axes at a high angle to and asymmetric to the mylonitic foliation (C-plane). This is consistent with a top-to-the-NE/ENE sense of shear shown by other shear zone fabric elements. However fine-grained quartz bounded by biotite at the shear zone boundary exhibits a girdle at right angles to the foliation and containing the lineation (girdle CFS4c; Fig. 3.15).

In the same manner, coarse-grained quartz ribbons in CFS27 display a single girdle with broad maxima concentrations at the Y axis and maxima in the XZ plane consistent with a top-to-the-NE/ENE sense of shear and a combination of basal <a> and prism <a> glide (girdle CFS27; Fig. 3.15). Fine-grained layers of mica and quartz exhibit a girdle of c-axes at high angles to the foliation and containing the lineation (CFS27b; Fig 3.15). The c-axis fabric of CFS27b is remarkably similar to the fabric of CFS4c except that the c-axes appear to be asymmetric about the lineation.

Origin of c-axis girdles at high angles to foliation and containing the lineation.

Basal <a>, rhombohedral <a> or prism <a> slip cannot account for c-axis girdles at a high angle to the foliation and containing the lineation. Prism <c> slip has been advocated as a means of producing c-axes near the lineation. However, Lister and Dornsiepen (1982), Behr (1980) and Hippertt (1994) suggest that this slip system can be activated only under high amphibolite or granulite facies conditions. Mainprice et al (1986) suggests that prism <c> slip requires temperatures in excess of 650°C. Feldspar megacrysts and phenocrysts in CFS27 have only undergone a brittle deformation. If the metamorphic conditions were high amphibolite facies or granulite facies, feldspar would have been expected to undergo plastic deformation rather than cataclasis.

Alternatively, grain boundary sliding may disturb or randomise fabrics (Starkey and Cutforth 1978). However, the fabrics shown by fine-grained mica layers show a change in crystallographic preferred orientation rather than a randomisation by grain boundary sliding.

Recently Hippertt (1994) described c-axis preferred orientations and petrofabrics of highly sheared quartz-mica layers in greenschist facies phyllonites. Hippertt (1994) found that the fabrics displayed by fine-grained quartz crystals associated with high amounts of sericite show a concentration of c-axes at a low angle to the stretching lineation. However, mica-poor quartz domains recorded fabrics consistent with crystal plastic processes. Hippertt (1994) concluded that solution transfer and possibly grain growth was an important process particularly in mica-rich layers. Mica-rich layers, may in fact favour solution transfer as preferential solution of quartz occurs along boundaries in contact with the {001} plane of phyllosilicates (Bell and Cuff 1989). According to Hippertt (1994) dissolution or solution transfer in mica-rich quartz layers results in a concentration of grains with c-axes parallel or at low angles to the lineation unfavourably oriented to undergo solution.

Selective dissolution of quartz grains in mica-rich quartz layers may possibly explain the fabric recorded by CFS27b, which contains a concentration of c-axes near the lineation. However, the fabric of CFS4c contains a girdle distribution of quartz c-axes that cannot be attributed simply to dissolution or grain growth. However, dissolution may still explain the concentration of micas associated with fine grained quartz.

Alternatively, there is the possibility that c-axis fabrics from the fine-grained zones may represent shearing along NW-SE lines. However, this is unlikely because the rock specimens appear only to record an ENE-WSW to NE-SW-trending stretching lineations and no NW-SE stretching lineations occur in the Siberia Bay mylonitic rocks. In addition, the coarser-grained quartz ribbons within the same samples clearly record movement along NE-SW to ENE-WSW lines rather than NW-SE lines.

The origin of c-axis girdles at high angles to foliation and containing the lineation is not clearly understood and more research is needed to explain fabrics inconsistent with basal or prism slip.

3.5 Folding associated with Mylonitization

3.5.1 Intrafolial Folds

The MCMZ, DCMZ and Four Mile River mylonites contain numerous folds of variable morphology. By far the most common are intrafolial folds of the mylonitic foliation. Intrafolial folds are characteristically tight to isoclinal gently-inclined gently-plunging folds or isolated fold hinges within the foliation (Fig. 3.16 A). Folds of this morphology may trend at a range of angles, or parallel to the stretching lineation and probably initiated at high angle to $\sigma 3$. Those folds now with axes parallel to the lineation have been subsequently rotated towards $\sigma 3$ during progressive deformation (Cobbold and Quinquis 1980; Ghosh and Sengupta 1987; Berthe′ and Brun 1980; Malavielle 1987). Where State Highway 6 crosses Deep Creek an isoclinal syn-mylonitic recumbent fold exposed in the road cutting trends parallel to the stretching lineation and contains a reactivated mylonitic foliation in the hinge region.

No unequivocal sheath folds were found in either the MCMZ, DCMZ or in mylonites south of the mouth of the Four Mile River.

3.5.2 Asymmetric Folds

In the MCMZ, folds of mylonitic foliation with hinges trending at high angles to the lineation occur in both outcrop and thin section. Folds of this trend occurr throughout the MCMZ and are consistently asymmetric and overturned towards the SW. This consistent sense of overturning suggests that this style of folding records a top-to-the-SW sense of shear (Figs. 3.16 B and C). This conclusion is supported by C-, S-, and C′-planes and porphyroclast systems (sections 3.3.1 and 3.3.2).

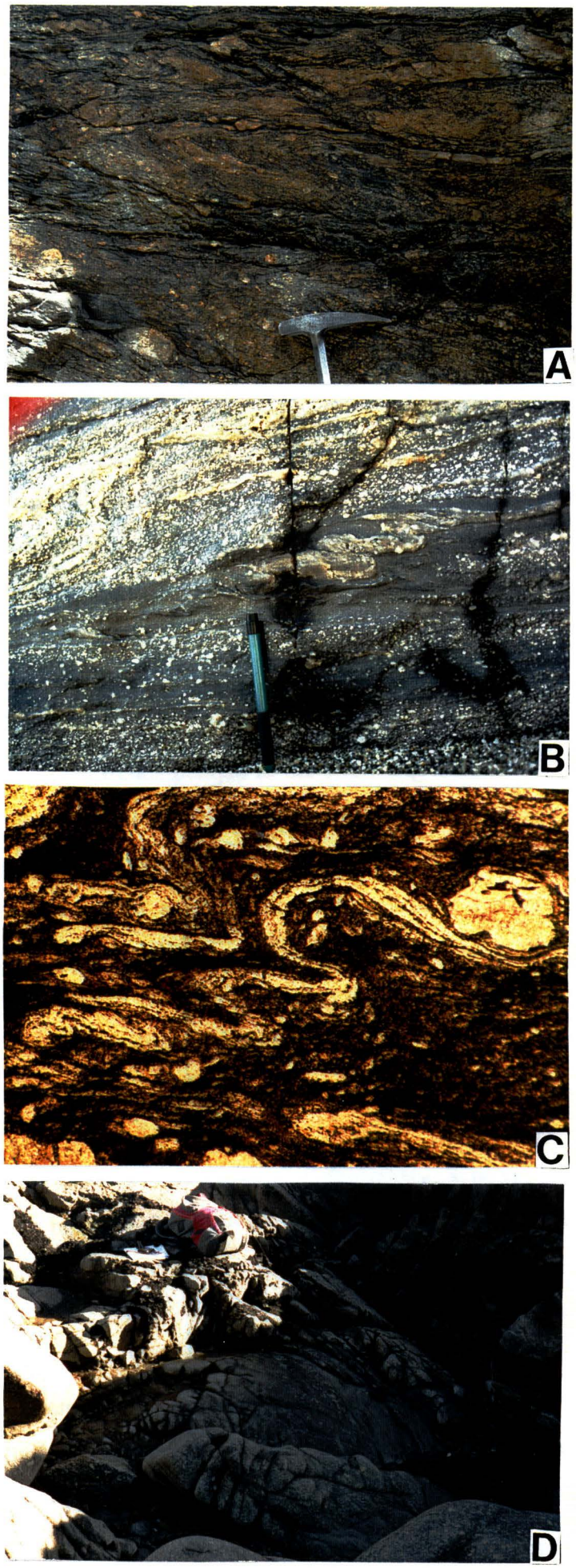

Fig. 3.16 A) Isolated fold hinges in the mylonitic foliation (MCMZ). Hammer head length=15 cm. B) and C) Asymmetric folds trending at high angles to the lineation from the MCMZ consistent with a top-to-the-SW sense of shear; viewed towards the NW; B) pencil length= 14 cm; C) plane polarised light; view across= 2.9 mm.

In the small area of outcrop along the coast south of the Four Mile River, folds of mylonitic foliation trend at a high angle to the lineation and are asymmetric recording a top-to-the-SW sense of shear. In thin section, isoclinal microfolds of the foliation are poorly developed and difficult to interpret in regard to sense of shear. No asymmetric folds were observed in the SBMZ or DCMZ.

3.5.3 Arch Structures

In contrast to the MCMZ, Four Mile River mylonites and DCMZ, the SBMZ contains few fold structures. No asymmetric folds of mylonitic foliation occur in outcrop or thin section. One folded pegmatite outcrops in the south of Siberia Bay; the fold axis trends NE-SW and a subhorizontal axial-planar foliation was developed.

In the centre of Siberia Bay, two 2m wide arch-like open upright folds of mylonitic foliation occur, one of which trends oblique to the stretching lineation and one parallel to the stretching lineation. The arch-like fold structures (Fig. 3.16 D) consist of well-foliated syenogranite-monzogranite overlying less deformed granite of the same composition. A range of origins may be advocated: a perturbation of flow around a lesser deformed pod of syenogranite-monzogranite; a local rise of magma during or after the main mylonite-forming event or, in the case of the arch parallel to lineation, localised constriction. The origin of arch-like structures are discussed further in section 3.6.

3.5.4 Buckle folds

In addition to asymmetric folds of the mylonitic foliation and intrafolial folds, mesoscopic open upright folds of the mylonitic foliation, which parallel the lineation, outcrop in the centre of the MCMZ (Fig. 3.17 A and B). M-type parasitic folds in the hinges of the open upright buckle folds suggest buckling associated with some component of longitudinal strain (Ramsay 1967). According to Bell and Hammond (1984), open folds of this nature could not have been rotated from initially high angles to become parallel to $\sigma 3$ without becoming tight to isoclinal. Similar folds are described from the Mojave Metamorphic Core Complex by Fletcher and Bartley (1994), who attribute these folds to

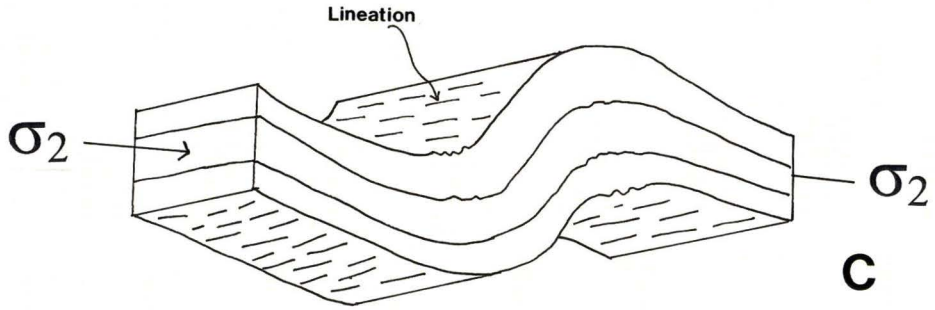

Fig 3.17 A) Buckle fold viewed parallel to the stretching lineation. B) M-type folds in the hinge of the buckle fold shown in A. Hammer length= 33 cm. C) schematic diagram of fold in relation to the lineation.

a local or regional constrictive strain where $\sigma 1 > \sigma 2 > \sigma 3$. In fact, local constriction in extension-related mylonite zones may be a natural consequence of heterogeneous deformation and the development of an anastomosing foliation.

3.6 Post-mylonitic Structures

In the MCMZ, box and kink folds of variable orientation are concentrated in fissile thinly layered rocks south of the unnamed headland north of White Horse Creek and in road cuttings around White Horse Creek. Some kink bands with horizontal axes of variable orientation also occur in the SBMZ. Kink bands in both areas possess cataclastically failed hinge lines and represent a late stage semi-brittle deformation (Fig. 3.18 A).

Mesoscopic and microscopic scale brittle normal faults containing hematitic and chloritic infill occur throughout the MCMZ. Most trend NW-SE and indicate extension (Fig. 3.18 B). Some occur as normal and reverse conjugate pairs. One single reverse fault outcrops in the centre of the MCMZ. In the SBMZ, similar small-scale brittle faults occasionally infilled with quartz trend NW-SE (perpendicular to the stretching lineation) and dip NE or SW. This orientation is consistent with NE-SW-oriented extension.

Post-mylonitic quartz-feldspar-muscovite antitaxial veins parallel the foliation in the centre of the SBMZ. Such foliation-parallel veins have been described in the literature and may be attributed to the precipitation of quartz in low pressure pull-aparts (Sawyer and Robin 1986).

Undeformed quartz-feldspar-muscovite pegmatites cross-cut the mylonitic foliation in the MCMZ and near the mouth of the Four Mile River. Some are up to 5 m wide and contain arrow head feldspars up to 5 cm long (Fig. 3.18C). In Siberia Bay, undeformed post-mylonitic quartz-feldspar-tourmaline pegmatites lie oblique or parallel to the mylonitic foliation.

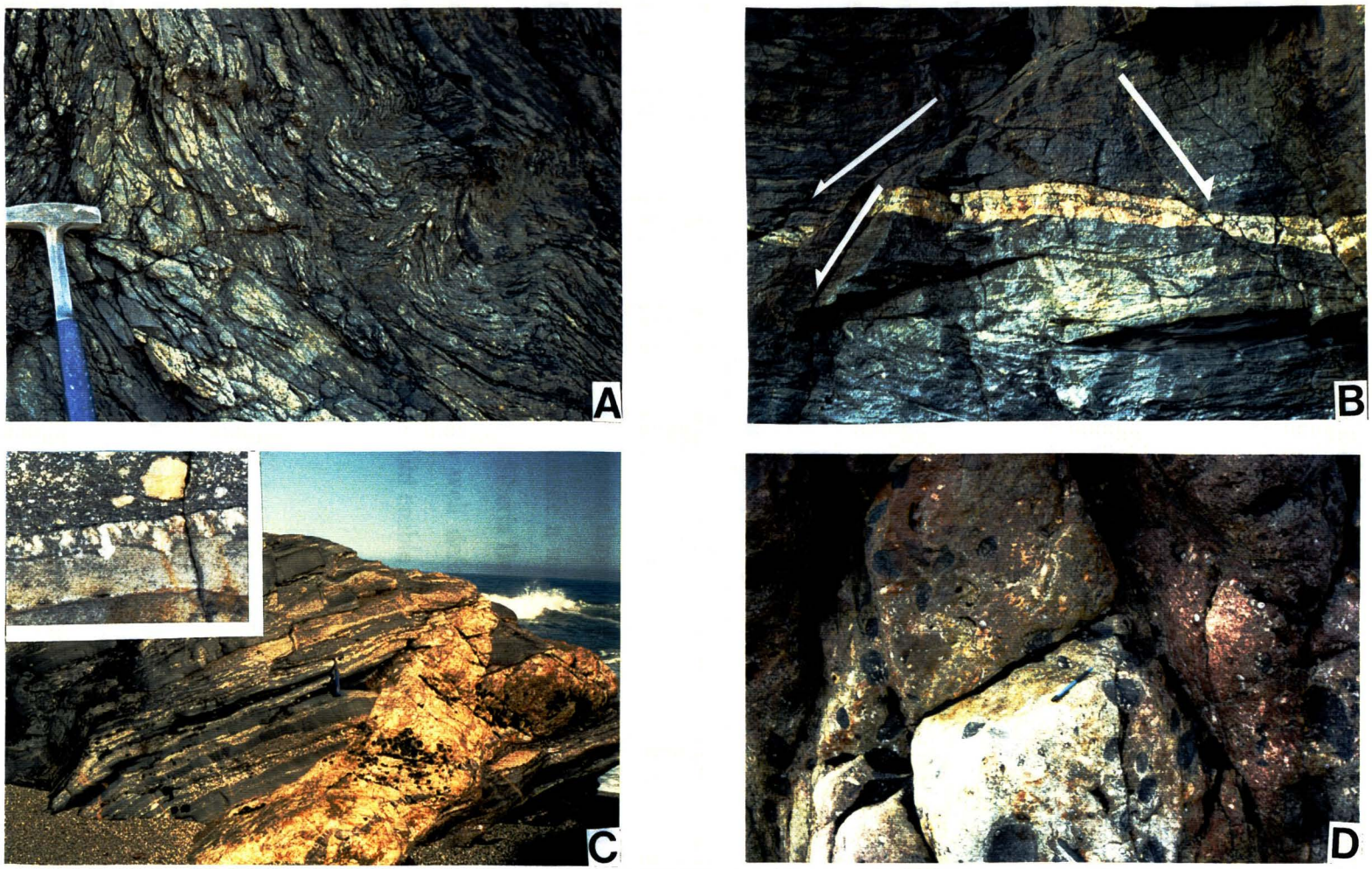

Fig. 3.18 Post-mylonitic structures. A) Box folds in the MCMZ, view across= 80 cm. B) Normal brittle faults; view across=3.2 m; viewed towards the NW. C) Undeformed pegmatites cross cutting the mylonitic foliation in the MCMZ; hammer length=33 cm; inset shows arrow head feldspar. D) Undeformed Siberia Bay syenogranite-monzogranite; pencil length=14 cm.

Post-mylonitic granitoid intrusion and the origin of arch-like structures in the SBMZ

Undeformed syenogranite-monzogranite outcrops at the northern end of Siberia Bay. The syenogranite-monzogranite lacks a foliation and lineation and rounded xenoliths included in the granite suggest that the granite has not undergone any component of flattening (Fig. 3.18 D). The presence of undeformed granite only 200 m away from centre of the SBMZ is difficult to reconcile with simple strain partitioning and suggests that the undeformed granite may be post-tectonic.

In light of this argument, arch structures in the centre of the SBMZ (section 3.5.3) are interpreted not as constrictional folds or a simple strain partitioning, but as a local uprise of magma which perturbed the overlying rock. This interpretation is supported by the incidence of lesser deformed granite below well foliated and deformed mylonites of the same composition (Fig. 3.16D), and undeformed syenogranite-monzogranite and pegmatites within the mylonite zone.

Although the crystallisation age of the surrounding Cape Foulwind Granite has been dated at 327.3 ± 6.2 Ma (Muir et al 1994a) and the Siberia Bay pluton appears geochemically related to the Cape Foulwind Granite (Smith 1992), it cannot necessarily be assumed that undeformed portions of the Siberia Bay syenogranite-monzogranite are also mid-Paleozoic. Indeed, it is difficult to reconcile a mid-Paleozoic crystallisation age with the undeformed nature of some parts of the Siberia Bay pluton, particularly when the mid-Paleozoic Cape Foulwind Granite appears well deformed. Dating of the undeformed Siberia Bay syenogranite-monzogranite would enable further conclusions to be drawn.

3.7 Mineralogical, Textural and Fabric Variations across the MCMZ

Mineralogical, textural and fabric variations occur along the coast from White Horse Creek to the northern most outcrop of the Morrisey Creek mylonites. These gross variations appear to reflect an increase in strain towards the flinty mylonites, which are located about 150 m south of the mouth of Morrisey Creek and a rapid, but heterogeneous decrease in strain and/or an increase in temperature from the flinty mylonites northwards.

With increasing strain from White Horse Creek towards the flinty mylonites, elongate quartz grains deformed into ribbons with aspect ratios up to 14.4/1 (WH2; type 1 quartz ribbons (section 2.2.1)) become increasingly dynamically recrystallized and undergo a reduction in grainsize, aspect ratio and degree of undulose extinction (WH234; type 2 quartz ribbons (section 2.2.1)). Quartz grains display serrated grain boundaries, and oblique quartz shape-preferred orientations develop with repeated recrystallization and strain. Approximately 150 metres south of the mouth of Morrisey Creek, flinty mylonites display extreme dynamic recrystallization containing quartz grains as small as 0.01 mm which display triple point junctions and aspect ratios approaching 1/1.

Feldspar porphyroclasts and mica undergo increasing boudinage and cataclasis towards the centre of the mylonite zone which results in a decrease in porphyroclast grainsize with increasing strain. However, there is little reduction in the volume percentage of porphyroclasts in thin section, except in biotite-rich layers which may contain only 10% porphyroclasts. Feldspar porphyroclasts display mostly elongate grain shapes in sections parallel to the stretching lineation in lower strain rocks, but with increasing boudinage, shapes become more equidimensional.

S-planes appear to rotate towards C-planes with increasing strain. However, this is difficult to document because the angle between S- and C-planes in any one thin section also depends on the proportion of porphyroclasts. Feldspar-rich mylonites, even in the centre of the mylonite zone, display little decrease in the angle between the C- and S-planes as feldspars partly control C- and S-plane development. In contrast to C- and S-planes, C′- planes rotate towards the C-planes with increasing strain and form angles as small as 8° in the flinty mylonites.

From the flinty mylonites of the MCMZ northwards the mylonites quickly coarsen and display recrystallized mica and little grainsize reduction due to cataclasis. Quartz ribbons display undulatory extinction and sometimes oblique quartz shape preferred orientations, although most quartz grains have undergone only some dynamic recrystallization and show little grainsize reduction. Quartz aspect ratios range from 1/1 to 10/1.

S-planes lie at relatively high angles to the C-planes (up to 54°) in the coarse grained mylonites and where developed, C′-planes lie between 21° and 24° to the C-plane.

Around the mouth of the Morrisey Creek and for 200 m north, mylonites show variable grainsizes depending on the degree of mylonitization. Type 3 quartz (section 2.2.1) has only undergone a moderate amount of dynamic recrystallization and displays serrated grain boundaries, aspect ratios between 1/1 and 4/1 and coarse quartz shape preferred orientation development. In places, type 2 quartz predominates showing intense grainsize reduction by dynamic recrystallization. Micas show a moderate amount of cataclasis and mica fish are occasionally developed.

The S-planes form angles between 12° and 38° to the C-planes. C′-planes range from 13° to 43° to the C-planes.

Across the mylonite zone, the anorthite content of plagioclase increases from oligoclase to andesine (WH41, WH44 and WH43) and possibly reflects a general increase in basicity towards the north of the parent granitoids rather than being simply due to mylonitization. In the most mylonitized granitoids there is a conspicuous lack of albitisation of the plagioclase feldspar suggesting that the conditions during the early periods of mylonitisation were those of the amphibolite facies. A later reduction in the temperature to greenschist facies conditions is recorded by the nucleation of abundant biotite and the rare retrograde alteration of biotite to chlorite, although conversion of oligoclase-andesine to albite does not occur.

The rapid increase in grainsize to the north of the centre of the mylonite zone may be due to an increase in temperature. Pegmatite intrusion is concentrated in this area and temperatures during and after mylonitic deformation may have been high inducing a coarse recrystallization of the surrounding mylonites. These coarse-grained mylonites may also reflect a general increase in temperature towards the centre of the core complex, associated with the intrusion of granitoid bodies such as those at Charleston (Chapter 4).

3.8 Summary of the Mylonite Zones

Lineations in the MCMZ, DCMZ and Four Mile River mylonites trend generally NE-SW. Lineations in the SBMZ trend from NE-SW to ENE-WSW. Evidence for predominantly simple shear (asymmetric quartz fabrics, oblique quartz shape-preferred orientations, asymmetric porphyroclast systems and mica fish) show that these lineations parallel the movement direction.

C-, S- and C′-planes, porphyroclast systems, oblique quartz shape-preferred orientations and fold asymmetries record a top-to-the-SW sense of shear for the MCMZ and DCMZ.

Quartz c-axis fabrics in the MCMZ and DCMZ are dominated by type I crossed girdles and single girdles. While some quartz fabrics are asymmetric with respect to the foliation consistent with a top-to-the-SW sense of shear, others appear to record top-to-the-NE senses of shear. The origins of these apparent reversals of shear sense are discussed in Chapter 8.

The Four Mile River mylonites record two stages of C-S plane development. Coarse grained C-S planes of recrystallized mica show a top-to-the-SW sense of shear while fine grained cataclased C-S planes and mica fish record a top-to-the-NE sense of shear. Two quartz fabrics from the Four Mile River mylonites are variably defined type II crossed girdles.

Fabric elements in the SBMZ record predominantly a top-to-the-NE/ENE sense of shear although reactivated C-, S- and C′ planes and some oblique quartz shape preferred orientation record a top-to-the-SW/WSW sense of shear. The origin of top-to-the-SW/WSW senses of shear in the SBMZ are discussed in Chapter 8. Quartz fabrics from the SBMZ are dominated by type II crossed girdles and single girdles. Fine-grained quartz associated with mica record anomalous girdles at a high angle to the foliation and containing the lineation.

Post-mylonitic intrusion of pegmatites which cross-cut the mylonitic foliation occur in the MCMZ and near the mouth of the Four Mile River. In Siberia Bay, post-mylonitic

pegmatites lie oblique or parallel to the foliation. In addition to pegmatite intrusion, the SBMZ has undergone a localised post-mylonitic intrusion of syenogranitic-monzogranitic magmas.

Brittle deformation such as kink and box folding and small scale faulting has overprinted the semi-ductile deformation.

3.9 'V'-pull-aparts as Shear-sense Indicators

Hippertt (1993) proposed that the asymmetry of 'V'-pull-aparts relative to the shear plane, as well as the foliation deflection within the gaps, can be used to evaluate the sense of shear along active shear surfaces adjacent to the 'V'-pull-apart (section 1.9.5). Hippertt also stated that the local shear sense determined from 'V'-pull-aparts was always the same as the overall shear sense determined from S-C foliations and other independent shear sense indicators.

In the following discussion 'V'-pull-aparts from four samples of the MCMZ exhibiting unequivocal shear sense from mica fish, feldspar porphyroclasts and C-, S- and C′-planes are assessed. Within all 'V'-pull-aparts, some quartz has grown with c-axes parallel to the extension direction, but some has undergone a ductile deformation producing c-axes at a high angle to the foliation.

MC1 and MC2 contain well developed shear sense indicators suggesting a top-to-the-SW sense of shear. 'V'-pull-aparts in MC1 show an asymmetry consistent with this sense of shear (Fig. 3.19A). The direction and amount of rotation can be deduced from rotated twin planes and the shape-preferred orientation of quartz crystals within the 'V'-pull-

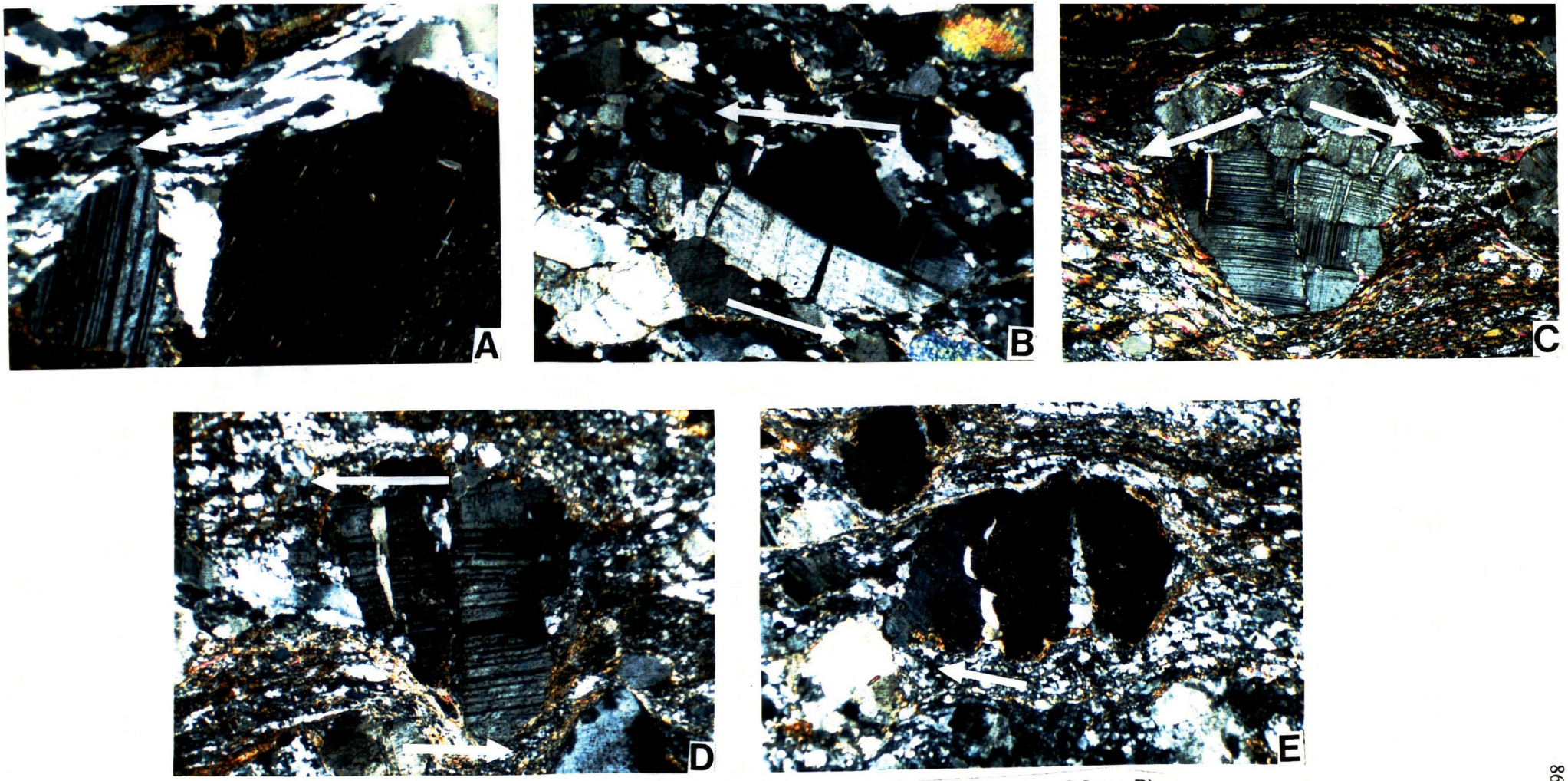

Fig. 3.19 A) 'V'-pull-apart from MC1 showing a top-to-the-SW shear-sense; view across=2.5 mm. B) 'V'-pull-apart from MC2 showing a top-to-the-SW sense of shear; view across= 2.5 mm. C) 'V'-pull-aparts showing a flattening around a large porphyroclast; view across=6 mm. D) 'V'-pull-apart showing top-to-the-SW shear-sense; view across= 2.9 mm. E) 'V'-pull-apart from the same section as D) but inconsistent with a top-to-the-SW shear-sense; view across=2.9 mm. All sections in crossed polarised light and viewed to the NW.

apart. Well developed 'V'-pull-aparts in MC2 (Fig 3.19B) occur within a K-feldspar porphyroclast lying along the S-plane. This suggests that the S-plane has become a plane of shearing: the direction of shear is consistent with a top-to-the-SW sense of shear.

WH31 and WH233 also contain well developed mica fish, feldspar porphyroclast systems and C-, S- and C′-planes which suggest top-to-the-SW sense of shear during a clearly non-coaxial deformation. However, one large porphyroclast in WH31 exhibits 'V'-pull-aparts which appear to show a more coaxial component of strain when compared with non-coaxial shear sense indicators (Fig. 3.19C). Mica fish above and below the porphyroclast show a top-to-the-SW sense of shear. It is suggested here that large porphyroclasts may undergo a more coaxial component of strain and that 'V'-pull-aparts in large porphyroclasts can give anomalous results.

'V'-pull-aparts in WH233 generally show an asymmetry consistent with a top-to-the-SW sense of shear (Fig. 3.19D). However the 'V'-like pull-apart shown in Fig. 3.19E is inconsistent with the bulk shear sense and probably only represents a local sense of shear.

In conclusion, 'V'-pull-aparts only record a localised sense of shear around feldspar porphyroclasts. This localised sense of shear only sometimes conforms to the bulk shear sense or may reflect a more coaxial component around large porphyroclasts. It is therefore risky to use 'V'-pull-aparts as sole indicators of a bulk shear-sense. However, they may be used to better understand strain partitioning along S-, C- and C′-planes or between domains of coaxial and non-coaxial strain in rocks undergoing bulk simple shear.

3.10 Strain Softening in the Mylonite Zones

Ductile shear zones or mylonite zones mark areas that have undergone localised strain softening, which enables the zone to accommodate a local or regional strain rate that the country rock cannot accommodate by bulk deformation (White et al 1980). Processes that enable a rock to accommodate strain are termed strain softening processes. Strain softening processes typically involve a reduction in grainsize (dynamic recrystallization;

metamorphic crystallisation), a change in deformation mechanism, reorientation of 'hard' grains into orientations for easy slip during progressive deformation and processes such as shear heating and water-weakening of quartz.

The mylonite zones within the Charleston Metamorphic Group display softening processes dominated by grainsize reduction. These are as follows:

Cataclasis: Cataclasis, particularly of feldspar, but also of mica and garnet produces small grains that can be easily reoriented for further deformation or smeared out along the foliation. Cataclasis also enables metamorphic, typically water-rich fluids to penetrate the feldspar porphyroclasts promoting further strain softening by metamorphic reaction (see following discussion).

Dynamic Recrystallization: Dynamic recrystallization of quartz produces strain-free quartz grains as small as 0.01 mm. These small strain-free grains easily accommodate further strain by ductile deformation, and potentially at least, grain-boundary sliding, although quartz from dynamically recrystallized mylonites in the Charleston Metamorphic Group have strong crystallographic preferred orientations suggesting that grain boundary sliding did not occur.

Metamorphic Reaction: In the mylonite zones retrograde metamorphic reaction breaks down K-feldspar and crystallises muscovite and quartz. Newly crystallized small grains of muscovite and strain-free quartz may accommodate further strain through cataclasis and ductile deformation respectively. Phillips et al (1972) suggest the following reaction:

$$3KAlSi_3O_8 + H_2O \rightarrow KAl_2(Al,Si_3)O_{10}(OH)_2 + 6SiO_2 + K_2O$$

K-feldspar muscovite quartz

In the mylonite zones, this reaction rarely goes to completion and relic K-feldspars are common. The crystallisation of biotite is especially common and also produces small grains easily able to accommodate strain.

Sericitization of plagioclase is moderately well developed throughout the mylonite zones and weakens large porphyroclasts so that they can more easily undergo cataclastic deformation. In fact, sericitization may be driven by the reaction of K-feldspar to muscovite and quartz which releases K_2O (see above reaction), which in turn can be utilised during the replacement of plagioclase.

CHAPTER FOUR

THE CHARLESTON ORTHOGNEISSES AND PARAGNEISS, AND FOUR MILE RIVER ORTHOGNEISS

4.1 Introduction

Orthogniess and paragneiss lithologies are exposed along the coast around Charleston, Parsons Hill and the Four Mile River. Orthogneiss and paragneiss lithologies appear to record somewhat distinctive metamorphic histories and the following discussion is divided into two sections: orthogneiss lithologies and paragneiss lithologies. Petrographic descriptions of both these lithologies have been given in Chapter 2, sections 2.3 and 2.6.

4.2 Orthogneiss Lithologies

4.2.1 Introduction

Gneiss of tonalitic, granitic and granodioritic composition, and granodioritic migmatites outcrop around Charleston, Deep Creek, Parson Hill and the mouth of the Four Mile River (Map 1). Field evidence suggests that the biotite tonalite is intruded by the two-mica granite (Fig. 4.1A). However, both orthogneiss lithologies display a tectonic foliation defined primarily by a shape-preferred orientation of green biotite and muscovite. South of Deep Creek and around the Four Mile River mouth, the foliation dips moderately to gently SW and W respectively. At the mouth of Bromielaw Creek the foliation dips gently NNE forming a broad macroscopic WNW-ESE-trending arch, centred near Deep Creek. A smaller WNW-ESE trending arch is centred to the north, on Parson Hill. These two broad arch structures form the phase two Charleston and minor arches of Shelley (1970). In the bed of Deep Creek, within the centre of the Charleston Arch, coarse-

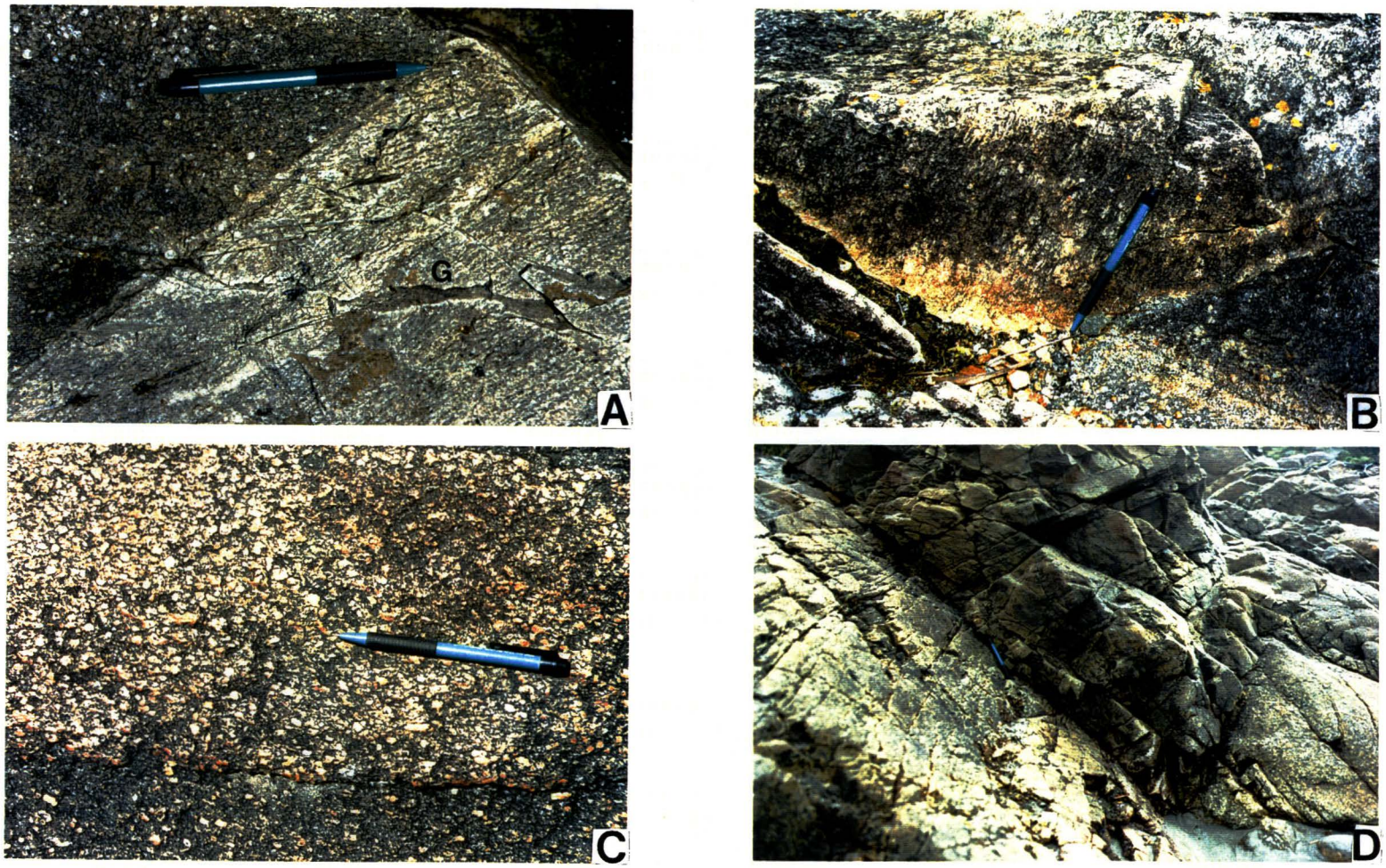

Fig. 4.1 A) Tonalitic gneiss (T) cut by granitic gneiss (G). Note tectonic foliation imprinted on both gneisses, parallel to trend of pencil. B) NE-SW-trending stretching lineation. C) WNW-ESE-trending feldspar-defined lineation. D) WNW-ESE-trending fold. Pencil length= 14cm.

grained biotite-tonalites exhibit a vertical foliation defined by a shape-preferred orientation of biotite and an alignment of plagioclase phenocrysts up to 1 cm long.

Around the greater Charleston area and the mouth of the Four Mile River, a NE-SW-trending stretching lineation is defined by elongate quartz crystals, grooves on feldspar porphyroclasts/phenocrysts and a shape-preferred orientation of mica (Fig. 4.1B). Slickenfibres in Constant Bay and at the mouth of Deep Creek also trend NE-SW. In addition to NE-SW-trending stretching lineations, orthogneiss at the mouth of Deep Creek and near Constant Bay records a WNW-ESE linear shape-preferred orientation of feldspar porphyroclasts/phenocrysts and a population of WNW-ESE to WSW-ESE-trending recumbent subhorizontal open folds (Figs. 4.1C and D). In areas where both NE-SW and WNW-ESE-trending lineations coexist, the NE-SW stretching lineation is defined, at least in part, by grooves on feldpsar crystals suggesting it formed later than the feldspar-defined WNW-ESE lineation.

At the mouth of Deep Creek, folded quartz-feldspar-muscovite pegmatites are cross-cut and displaced by younger, undeformed pegmatites of the same composition defining two periods of pegmatite intrusion. Pegmatite fold axes trend anywhere from NE-SW to NW-SE.

4.2.2 The Northern Limb of the Charleston Arch

Shear-sense Indicators

Granitic gneiss: Medium-grained two-mica granitic gneiss outcropping around Constant Bay and Joyce Bay possesses moderately well defined C- and S- planes. C-planes are defined by a shape-preferred orientation of cataclased mica and an alignment of quartz layers which forms a dominant mesoscopic schistosity. Sigmoidal S- planes in samples C1 and C3 lie anywhere between 20° and 50° to the C-planes and are formed by an alignment of muscovite occasionally deformed into mica fish, and poorly developed feldspar porphyroclast systems. C′-planes are generally absent, but may be present as a shape-preferred orientation of chloritized biotite oriented synthetically to the C-plane. A predominance of chloritized biotite along the C′-plane suggests development during

retrograde, probably greenschist facies conditions. C-, S- and rare C′-planes in both sample C1 and C3 possess a geometry consistent with a top-to-the-NE sense of shear (Fig. 4.2A).

Feldspar porphyroclast systems are poorly developed in sample C1 but sample C3 contains some σ_b-type porphyroclasts and σ_a-type porphyroclasts oriented along the S-plane (Fig. 4.2A). Muscovite fish possess tails of cataclased or newly-crystallized muscovite and are oriented so that their {001} cleavage planes lie either nearly parallel to the C-plane or tilted back against the plane of shearing by up to 30°. Feldspar porphyroclasts possess recrystallized muscovite asymmetrically disposed about the porphyroclast boundaries oriented at a high angle to the maximum principal compressive stress direction. σ-type feldspar porphyroclasts and asymmetric mica fish are consistent with a top-to-the-NE sense of shear (Fig. 4.2B). No shape-preferred orientation of quartz oblique to the C-plane or asymmetric microfolds occur in thin section.

Folds of granitic gneiss within the biotite tonalite occur on the northern limb of the Charleston Arch in weathered road sections north of Charleston (Fig. 4.2C). These folds are overturned towards the NE and therefore show a top-to-the-NE sense of shear for the northern limb of the Charleston Arch. A top-to-the-NE sense of shear recorded by fold asymmetry supports the same sense of shear recorded by the fabric elements in both samples C1 and C3.

Biotite-tonalites: Coarse-grained biotite-rich tonalitic gneiss outcropping in Constant and Joyce Bay, on the northern limb of the Charleston Arch lacks well developed microscopic structures which may be used to determine a sense of shear. A schistosity is defined by an alignment of biotite. However C-, S- and C′-planes are poorly developed. Large crystals of muscovite and hence muscovite fish are absent from the tonalitic gneiss. Around the mouth of Bromielaw Creek and in the creek bed, tonalites possess a schistosity defined by aligned micas. In thin section the tonalites exhibit dominantly granitic texture (DC8). Quartz displays undulose extinction and deformation lamellae but little dynamic recrystallisation and grain-size reduction. Chloritized biotite records retrograde greenschist facies metamorphic conditions. However plagioclase is only lightly

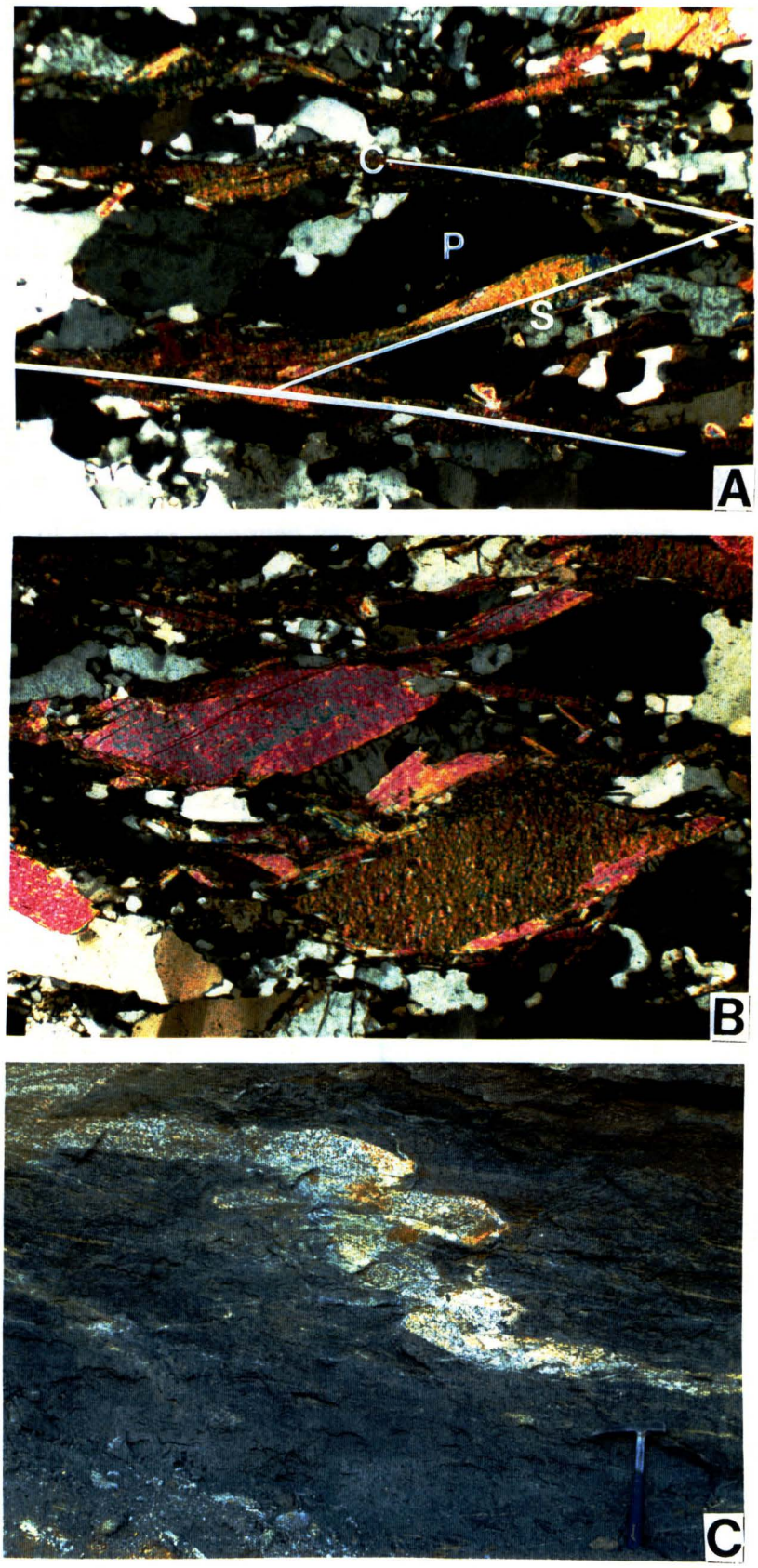

Fig. 4.2 A) C-S planes in granitic gneiss displaying a top-to-the-NE sense of shear; P=plagioclase porphyroclast system; crossed polarised light; viewed toward the NW; view across=2.9 mm. B) Muscovite fish in granitic gneiss showing a top-to-the-NE shear-sense; viewed towards the NW; crossed polarised light; view across=2.9 mm. C) Asymmetric folds viewed towards NW; hammer length=33cm.

sericitized. C-, S- and C′-planes, feldspar porphyroclast systems and mica fish are ill defined and there is no indication of a sense of shear.

Granodioritic-migmatites: Just south of Constant Bay is a small area of irregularly layered mica-rich migmatite of granodioritic composition. In thin section (C10), well developed C- and S-planes are defined by a shape-preferred orientation of abundant but poorly cataclased mica. The C′-plane occurs as an asymmetric crenulation cleavage displacing the migmatitic foliation. σ_a-type feldspar prophyroclasts perturb the foliation in such a way as to exhibit an asymmetry consistent with a top-to-the-SW sense of shear. Long thin crystals of mica are deformed into elongate mica fish which lie along the S-plane. All porphyroclast systems and C-, S- and C′-planes suggest a top-to-the-SW sense of shear.

A top-to-the-SW sense of shear recorded by microscopic structures in the granodioritic migmatite is inconsistent with clear top-to-the-NE senses of shear recorded by C-, S- and C′-planes, porphyroclast systems and asymmetric folds in other lithologies on the northern side of the Charleston Arch. The SW shear-sense probably reflects a localised sense of shear developed during flow of the migmatite rather than a regionally significant sense of shear.

Quartz c-axis Fabric Analysis

Most naturally occuring quartz c-axis fabrics in the literature are measured from fine-grained dynamically recrystallized mylonitic rocks: coarse-grained gneisses are less well documented. Feuten (1992) describes quartz c-axis fabrics from coarse-grained gneisses in the Thompson Belt and records well defined fabrics dominated by type I crossed girdles and type II crossed girdles. However, fabrics from the medium- and coarse-grained orthogneiss on the northern limb of the Charleston Arch are generally indistinct and only one quartz fabric, from the mouth of Bromielaw Creek, can be used to determine a sense of shear.

Within the granitic gneiss, quartz displays undulose extinction and some deformation lamellae but little dynamic recrystallization or grainsize reduction. Sample C1 (Fig. 4.3)

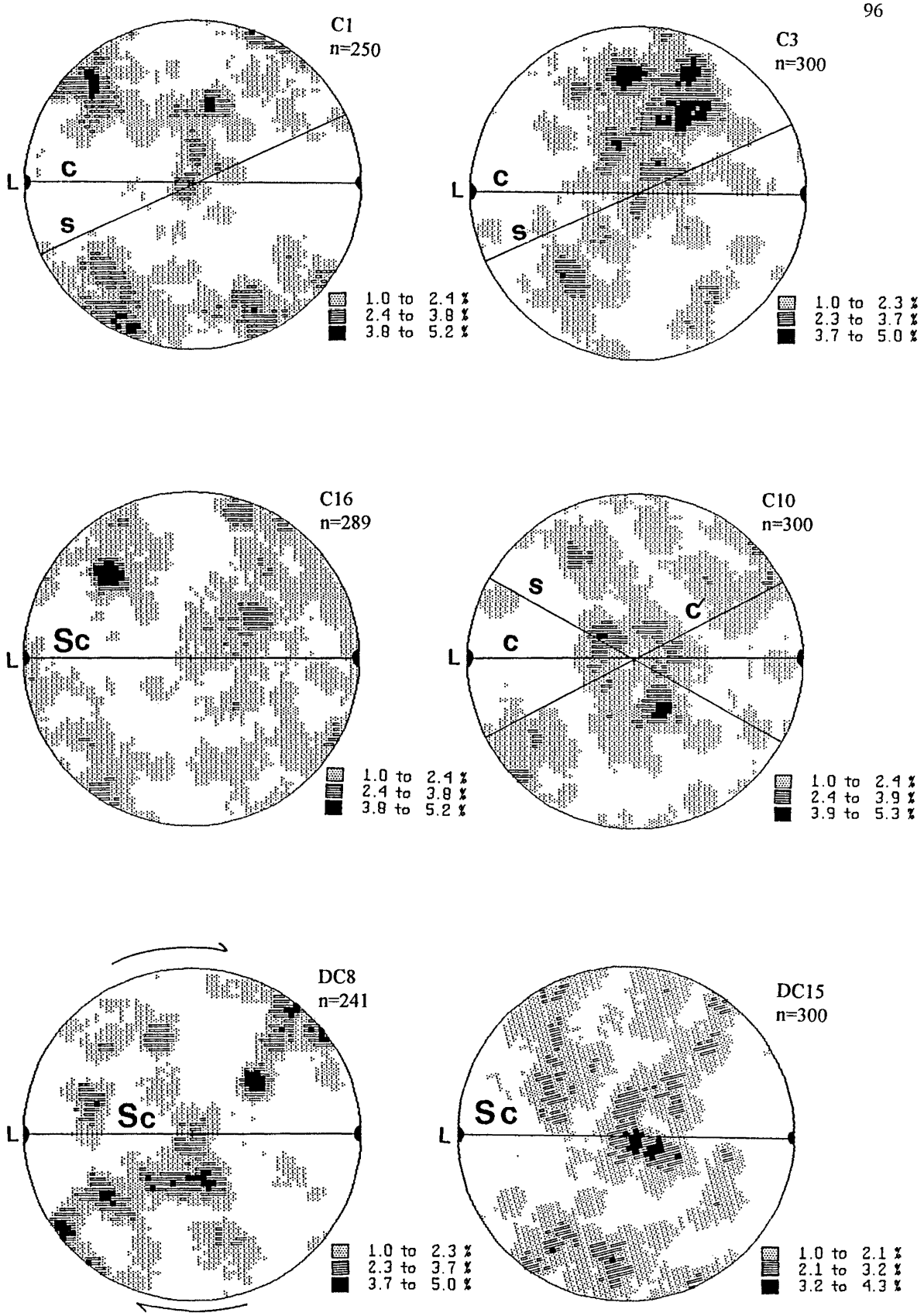

Fig. 4.3 Contoured lower hemisphere equal area projections of quartz c-axis orientations from the northern limb of the Charleston Arch (C1, C3, C16, C10, DC8) and the axis of the arch, in Deep Creek (DC15). All fabrics are viewed towards the NW. c=C-plane, s=S-plane, c'=C'-plane, Sc=schistosity, L=lineation. Bold arrows show shear-sense; shear-sense discussed in text .

contains four broad maxima intermediate between X and Z, and a weak maxima at the Y axis. Although C-S planes consistent with a top-to-the-NE sense of shear are found in thin section, the quartz fabric is symmetrically disposed with respect to the schistosity, recording a more coaxial component of strain. Sample C3, which contains well defined C-S planes and porphyroclast systems, exhibits an ill-defined quartz c-axis fabric that is difficult to classify and cannot be interpreted in regards to shear-sense (Fig. 4.3). Coarse-grained biotite-tonalite C16 also displays a poorly-defined quartz fabric that is impossible to interpret (Fig. 4.3).

From south of Constant Bay, C10, a granodioritic migmatite displays a fabric with a broad maxima at the Y axis and a weak girdle distribution of c-axes. Although this fabric appears to record a top-to-the-NE sense of shear, the fabric is generally indistinct and a top-to-the-NE sense of shear is not unequivocal (Fig. 4.3).

At the mouth of Bromielaw Creek, tonalite sample DC8 (Fig. 4.3) displays a c-axis fabric dominated by a single girdle asymmetrically disposed to the schistosity consistent with a top-to-the-NE sense of shear. A top-to-the-NE sense of shear is supported by other shear-sense indicators on the northern limb of the Charleston Arch.

4.2.3 The Centre of the Charleston Arch

In the bed of Deep Creek, coarse grained porphyritic biotite-rich tonalites possess a steeply dipping to vertical foliation defined by an alignment of large, zoned plagioclase phenocrysts/porphyroclasts and a biotite shape-preferred orientation. Shelley (1970) suggested that this represents the vertical rise of magma in the centre of the Charleston Arch. This conclusion is supported by σ_a-type porphyroclasts of plagioclase in DC15 which possess short tails of quartz and biotite and asymmetrically perturb the foliation, consistent with the vertical movement of magma within the centre of the Charleston Arch. Although sample DC15 contains a quartz c-axis fabric that cannot be classified as either a type I or type II crossed girdle (Fig. 4.3), the quartz fabric is consistent with a combination of basal <a> and prism <a> glide rather than prism <c> slip which would be expected if the

foliation was simply a syn-magmatic one. This suggests that the foliation is partly tectonic in origin.

To the south of Deep Creek the foliation quickly flattens to become gently to moderately dipping towards the south-west. Orthogneiss lithologies immediately south of Deep Creek along the coast and in road cuttings do not contain well developed shear-sense indicators.

4.2.4 The Parsons Hill Arch

At Parsons Hill north of Charleston, variably deformed granodioritic and tonalitic gneiss contains a foliation defined by a preferred orientation of mica. In general, thin sections of the gneiss display predominantly granitic texture (PH3) and quartz crystals display both sharp and undulose extinction, the later associated with minor plastic deformation but no dynamic recrystallisation.

In such coarse-grained rocks gross fabric elements are best seen in outcrop. On the southern limb of the Parsons Hill Arch, C′-planes are represented by broad asymmetric crenulations oriented approx. 40° to the C-plane (Fig. 4.4A). At closer inspection well developed C- and S- planes are displaced along a C′-plane foliation consistent with a top-to-the-SW sense of shear (Fig. 4.4B).

Although the orthogneiss is generally poorly deformed, a sheath fold is exposed on the cliffs at Parsons Hill suggesting some component of rotational strain. On the rock platform at Parsons Hill, highly sheared layers up to 1cm wide parallel the foliation in the granodioritic gneiss. In outcrop, the shear zones are preferentially weathered giving the rocks a layered appearance. In thin section, the shear-zones contain fine-grained quartz ribbons and cataclased biotite with minor cataclased muscovite and elongate feldspar porphyroclasts. Sample PH1 contains a shear zone which displays C-planes defined by cataclased mica and sigmoidal S-planes by quartz-ribbons. Sericitized σ_a-type plagioclase porphyroclasts and chloritized biotite suggests deuteric alteration during retrograde

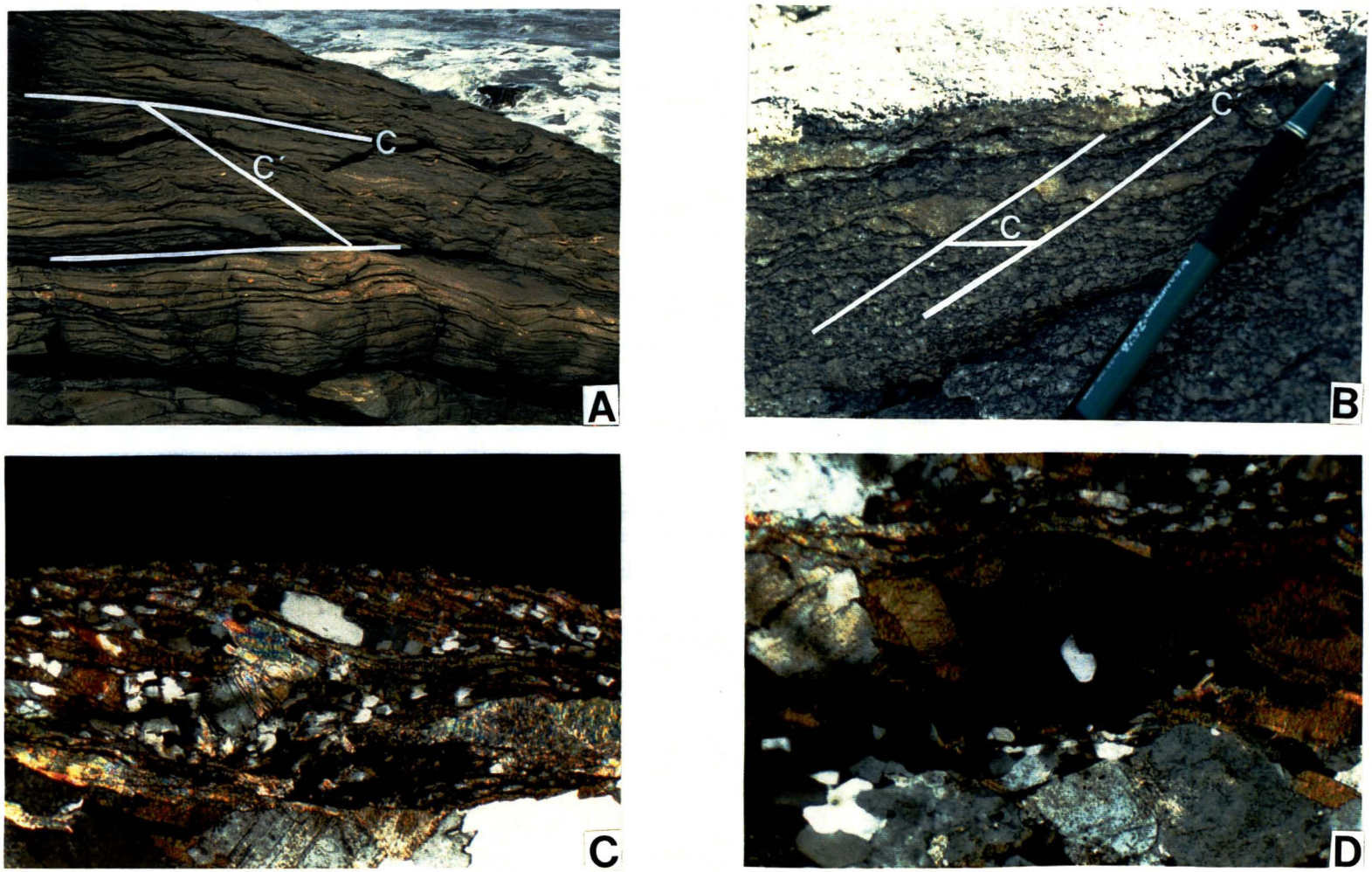

Fig. 4.4 Fabric elements on southern limb of the Parsons Hill Arch. A)Development of broad C′-planes and C-planes; viewed towards the SE; view across=3.5 m. B) C and C′-planes, showing a top-to-the-SW sense of shear; viewed towards the NW; pencil length=14 cm. C) and D) top-to-the-SW porphyroclast systems in thin section; crossed polarised light; viewed towards the NW; view across=2.9 mm.

metamorphism. C-S planes and asymmetric porphyroclasts are consistent with a top-to-the-SW sense of shear for the southern limb of the Parsons Hill Arch (Fig. 4.4C and D). A top-to-the-SW sense of shear from shear-zone fabric elements in thin section supports the same shear-sense recorded by gross fabric elements in outcrop.

On top of Parsons Hill the foliation is horizontal, defining the axis of the Parsons Hill Arch. To the north, coarse-grained homogeneous but foliated gneiss displays granitic texture (sample C40), dips to the NW and contains a NE-SW-trending stretching lineation. On the northern side of the Parsons Hill Arch Shelley (1970) records WNW-ESE-trending folds that are overturned to the north.

Quartz c-axis Fabric Analysis

Coarse-grained biotite granodiorites PH1 and PH3 display poorly defined quartz fabrics (Fig. 4.5). The c-axis fabric recorded by PH1 cannot be classified or used as a kinematic indicator. However, PH3 contains a single girdle fabric asymmetric with respect to the C-plane consistent with a top-to-the-NE sense of shear. A top-to-the-NE sense of shear conflicts with vague top-to-the-SW C-S planes and porphyroclast systems in thin section. However, sample PH3 was taken from almost horizontal gneiss on top of Parsons Hill and has probably undergone essentially a combination of both shear-senses during a bulk coaxial flattening.

Sample C40, from just north of Parsons Hill, displays a poorly defined quartz c-axis fabric that cannot be interpreted in terms of a sense of shear (Fig. 4.5).

4.2.5 Four Mile River Granitic Gneiss

Introduction

Gneiss of granitic composition outcrops along the coast and in cliff sections at the mouth of the Four Mile River. In outcrop, the granitic gneiss possesses a schistosity defined by a shape-preferred orientation of muscovite. Stretching lineations trend NE-SW, defined primarily by a linear-preferred orientation of muscovite.

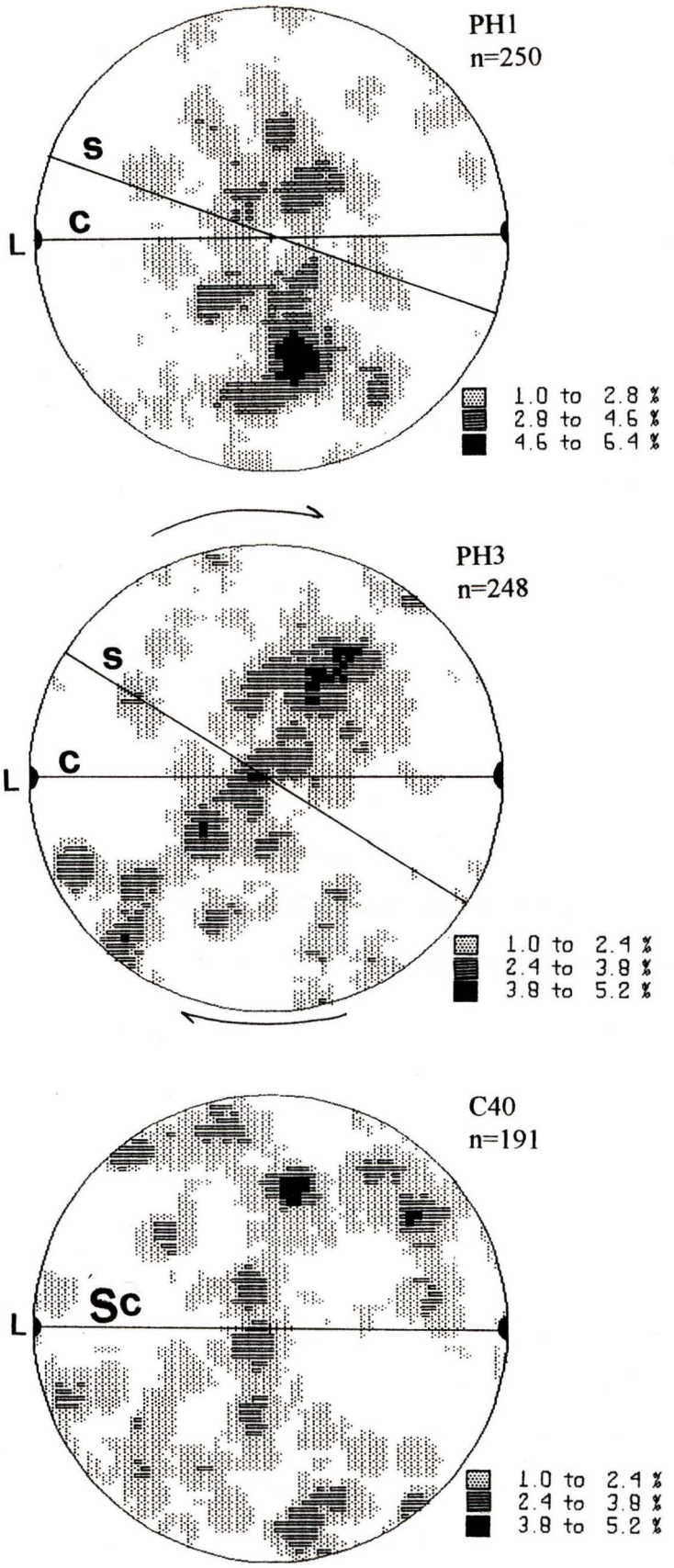

Fig. 4.5 Contoured lower hemisphere equal area projections of quartz c-axis orientations from Parsons Hill. All fabrics viewed towards the NW. C=C-plane, s=S-plane, Sc=schistosity, L=lineation. Shear-sense discussed in text.
Bold arrows indicate shear-sense.

Shear-sense Indicators

C- and S-planes are variably developed in thin section (Fig. 4.6A). C-planes are defined by the alignment of finely cataclased muscovite. S-planes are defined by occasional feldspar porphyroclast systems and a shape-preferred orientation of mica sometimes deformed into mica-fish. S-planes are typically oriented up to 38° to the C-plane. C-S plane geometry is consistent with a top-to-the-SW sense of shear.

The C-planes appear to contain a foliation of finely cataclased muscovite which is deflected along the C-plane. Associated with this foliation deflection is the development of a shape-preferred orientation of quartz oblique to the C-plane. Both the foliation deflection within the C-plane and shape-preferred orientation of quartz are consistent with the top-to-the-SW sense of shear, recorded by other fabric elements.

Feldspar σ_a-type porphyroclasts occur both in outcrop and thin section (Fig. 4.6B). The asymmetric porphyroclasts deflect the surrounding mica-defined foliation and possess tails of mica and quartz. Muscovite fish possess short tails of cataclased muscovite and cleavage planes oriented up to 30° from the C-plane. Both muscovite fish and σ_a-type feldspar porphyroclast systems show an asymmetry consistent with a top-to-the-SW sense of shear.

Quartz c-axis Fabric Analysis

Granitic orthogneiss at the mouth of the Four Mile River contains quartz exhibiting undulose extinction and a moderate amount of dynamic recrystallization and grainsize reduction. FM12 exhibits an unusual quartz c-axis fabric that cannot be classified as either a type I or type II crossed girdle (Fig. 4.7). No shear-sense can be determined from this fabric. However, FM22 possesses a c-axis fabric dominated by a concentration of c-axes at the Y axis which can be attributed to prism <a> glide (Feuten 1992) (Fig. 4.7). In addition, a weak girdle of c-axes is asymmetrically disposed to the C-plane consistent with a top-to-the-SW sense of shear. A top-to-the-SW sense of shear is consistent with C-S planes and porphyroclast systems in thin section and supports top-to-the-SW indicators from the Four Mile River biotite-rich granitoid mylonites.

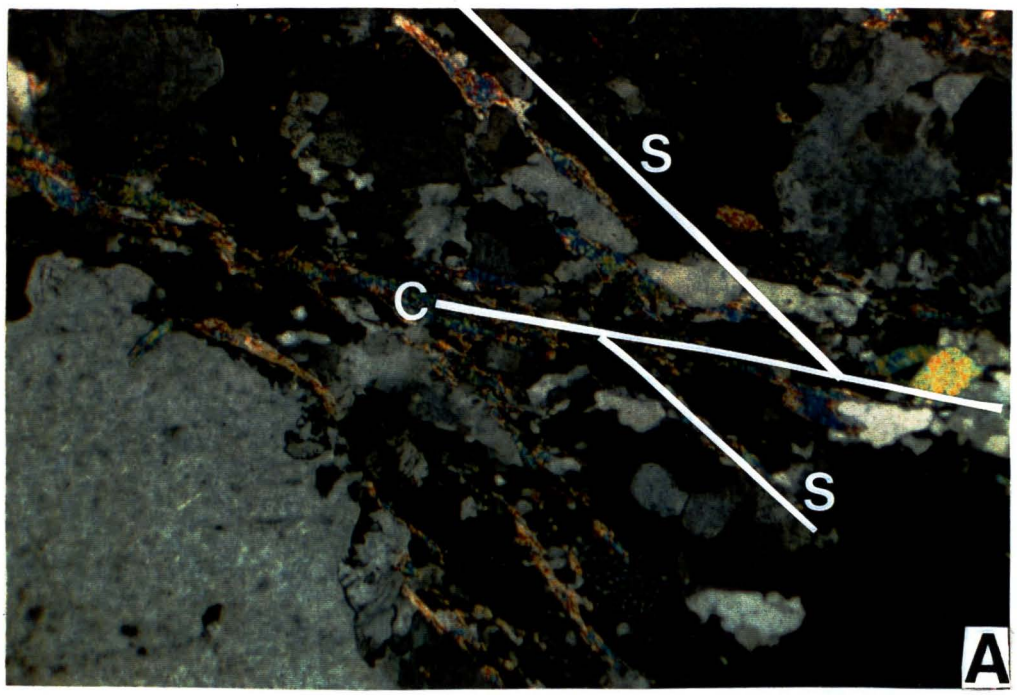

Fig. 4.6 A) C-S planes in granitic gneiss at the mouth of the Four Mile River displaying top-top-the-SW sense of shear; viewed towards NW; view across=2.9 mm. B) Feldspar porphyroclast system and C-S planes in outcrop (Four Mile River) displaying top-to-the-SW shear-sense; porphyroclast=1cm long; viewed towards the SE.

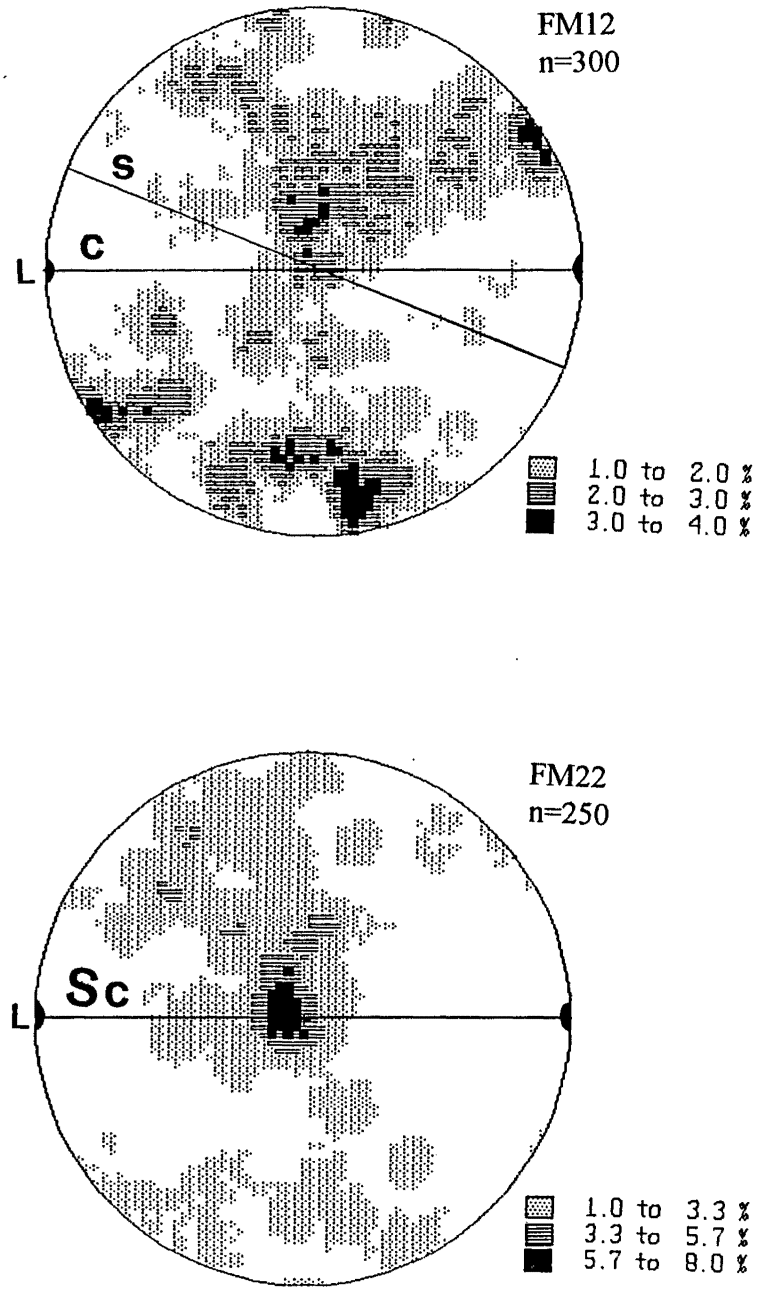

Fig. 4.7 Contoured lower hemisphere equal area projections of quartz c-axis orientations from granitic gneiss at the mouth of the Four Mile River; s=S-plane, c=C-plane, Sc=schistosity, L=lineation. Both fabrics viewed towards the NW. Bold arrows indicate shear-sense.

4.3 Paragneiss Lithologies and Migmatites of Sedimentary Origin

On the cliffs below the Charleston Cemetery (on the northern limb of the Charleston Arch) stromatic migmatites of sedimentary origin contain centimetre-wide leucosomes of plagioclase and quartz bound by 1-2 mm wide melanosomes of red-brown biotite and minor muscovite. Mesosomes appear essentially as paragneiss containing predominantly red-brown biotite, feldspar and quartz and traces of sillimanite. Red-brown biotite suggests a sedimentary origin for the migmatites.

Three periods of structural development are recorded in outcrop. The earliest recorded structures are NNW-SSE-trending lineations which are folded into NE-SW orientations about WNW-ESE to WSW-ENE-trending horizontal folds. This suggests that NNW-SSE lineations predate WNW-ESE to WSW-ENE- trending structures: the same relationship was noted by Shelley (1970). In addition, a NE-SW stretching lineation throughout the migmatites is defined by a preferred orientation of biotite and quartz crystallographic and shape-preferred orientation.

Within the mesosomes, σ_a-type plagioclase porphryroclasts display tails of recrystallized biotite, which possess an asymmetry recording a top-to-the-NE sense of shear, consistent with most other samples from the northern limb of the Charleston Arch. Sample C28 contains quartz c-axes oriented at a high angle to the foliation forming a type I crossed girdle. Although no sense of shear can be determined from sample C28, it suggests that NE-SW trending lineations record a quartz-stretching lineation developed during a post-migmatitic deformation related to the development of the Charleston Arch.

Kimbrough and Tulloch (1989) sampled a mixed ortho- and paragneiss from north of the Nile River, just below Parsons Hill. U-Pb zircon analysis recorded a heterogeneous zircon population and discordant U-Pb data which was interpreted to be the result of the mixed parentage of the sample. Similar mixed ortho- and paragneisses outcrop at the mouth of the Nile River where gneiss of different parentage is clearly discernible: paragneiss lithologies contain red-brown biotite while orthogneiss contains green biotite. Asymmetric folds of layered gneiss at the mouth of the Nile River are overturned towards the SW

consistent with a top-to-the-SW sense of shear for the northern limb of the Charleston Arch.

4.4 Timing of Structural Development

U-Pb zircon analysis of bulk zircon separates from the biotite-tonalite at Charleston records a 114 ± 18 Ma crystallisation age for the biotite-tonalite magmas (Kimbrough and Tulloch 1989). Although the granitic-gneiss clearly intrudes the biotite-tonalite, microprobe dating of zircon growth zones by Ireland (1992) record similar zircon systematics for these two lithologies. According to Ireland, Cretaceous rims on the zircons do not represent one single event, but have an age range from 120 Ma to 95 Ma. However, ages as young as 95 Ma conflict with a muscovite Rb-Sr age of 108 Ma for undeformed pegmatite from the Charleston area (recalculated from Aronson 1968). Muir (pers. comm.) suggests that 120-95 Ma ages of Ireland (1992) have high associated errors, and that the Charleston orthogneiss lithologies probably crystallized around 110 Ma.

In contrast, paragneiss outcropping around Charleston and the Nile River record a Paleozoic event. The youngest age zircon rims within the paragneiss are 380-400 Ma (Ireland 1992) while a monazite from the paragneiss records a 350 Ma age (Ireland pers. comm.).

NE-SW stretching lineations and WNW-ESE-WSW-ENE-trending structures recorded in both ortho- and paragneiss lithologies around Charleston postdate the crystallisation age of orthogneiss at Charleston (around 110 Ma) but predate 108 Ma, recorded by an undeformed pegmatite (recalculated from Aronson 1968). However, the age of NNW-SSE-trending lineations are largely unconstrained. They may be of Paleozoic age postdating the youngest paragneiss zircon rim at 380-400 Ma. In this case, the absence of NNW-SSE lineations from the orthogneiss lithologies may simply be beacause their development predated the emplacement of the grantitic bodies. Alternatively, NNW-SSE lineations may be of Cretaceous age predating the intrusion of the magmas near Charleston. However, the NNW-SSE lineations may also be of Cretaceous age postdating

the crystallization of orthogneiss, but destroyed by mobilization of the orthogneiss lithologies during later NE-SW movements.

CHAPTER FIVE

CAPE FOULWIND-TAURANGA BAY ORTHOGNEISSES

5.1 Introduction

The Cape Foulwind granite complex crops out 11 km west of Westport. The complex contains three subgroups of granitic rocks: Cape Foulwind monzogranite, which outcrops from Siberia Point northwards and in the north of Tauranga Bay; Siberia Bay syenogranite-monzogranite, which is exposed in Siberia Bay; and the less felsic Tauranga Bay monzogranite, which outcrops at the headland south of Tauranga Bay. In general, these granitoids have been deformed and may be called granitic gneisses.

Zircon U-Th-Pb isotopic systems indicate that the Cape Foulwind monzogranite crystallized 327±6.2 Ma ago (Muir et al 1994a). Aronson (1965, 1968) derived a U-Pb age of 330 Ma for a sample of augen gneiss from Tauranga Bay, and a Rb-Sr age of 100 Ma for biotite and feldspar phases from the same area. The biotite and feldspar age of 100 Ma was interpreted to represent the age of the last deformation which affected the rocks.

Petrographic studies of the granite complex indicate an S-type character for the Cape Foulwind monzogranite and Siberia Bay syenogranite-monzogranite, and an ambiguous I/S-type character for the Tauranga Bay monzogranite exposed at the headland south of Tauranga Bay (Smith 1992). However, these geochemical studies give an A-type designation for the Cape Foulwind granite which suggests that the granite formed in a late- or post-orogenic setting. A coherence in geochemistry between the three plutonic phases has been interpreted to represent emplacement over a short period of time (Smith 1992). However, the Siberia Bay syenogranite-monzogranite, which in part is undeformed has yet to be dated and the structural analysis herein suggests that the assumption that all these granitoids are Paleozoic may not be warranted.

5.2 Structure

The granitic gneiss which outcrops around Cape Foulwind and Tauranga Bay contains two foliations. The first is defined by a shape-preferred orientation of feldspar megacrysts, biotite and xenoliths, and the second predominantly by biotite. The first foliation is parallel to phase layering within the granitic gneiss, (Fig. 5.1A and Map 2), and generally strikes ENE-WSW and dips to the south, but may also dip towards the north in the northern outcrops at Cape Foulwind. A preferred orientation of megacrysts and xenoliths parallel to phase layering within the granitic gneiss suggests that the foliation is, at least in part, magmatic in origin (Paterson et al 1989). However, ground mass minerals record a component of solid-state flow: quartz has been plastically deformed and somewhat dynamically recrystallized, and biotite has undergone varying amounts of cataclasis. A combination of solid-state flow and magmatic flow suggests that the first foliation may record a tectonic overprint on a crystallising magma body.

At Siberia Point, the first foliation contains quartz-rodding and mica shape-preferred lineations which trend NNW-SSE (Fig. 5.1B and Map 2). Shelley (1972) also records NNW-SSE-trending lineations at the south Tauranga Bay headland. In both of these areas, biotite-rich xenoliths are oblate within the plane of foliation suggesting a component of flattening associated with the first foliation development.

In the quarry below the Cape Foulwind lighthouse and along the coast north of Siberia Point, outcrops of Cape Foulwind monzogranite display a second, predominantly biotite-defined foliation. In the quarry, a northerly-dipping first foliation is cross-cut by a poorly-defined nearly horizontal second foliation. However, most coastal outcrops record a south-dipping first foliation deflected by a north-dipping second foliation in a manner consistent with the development of C- and S-planes (Fig. 5.1C and D). Associated with the development of the second foliation are lineations of rodded quartz, a mica-preferred orientation and grooves on feldspar porphyroclasts which trend NE-SW (Fig. 5.1E).

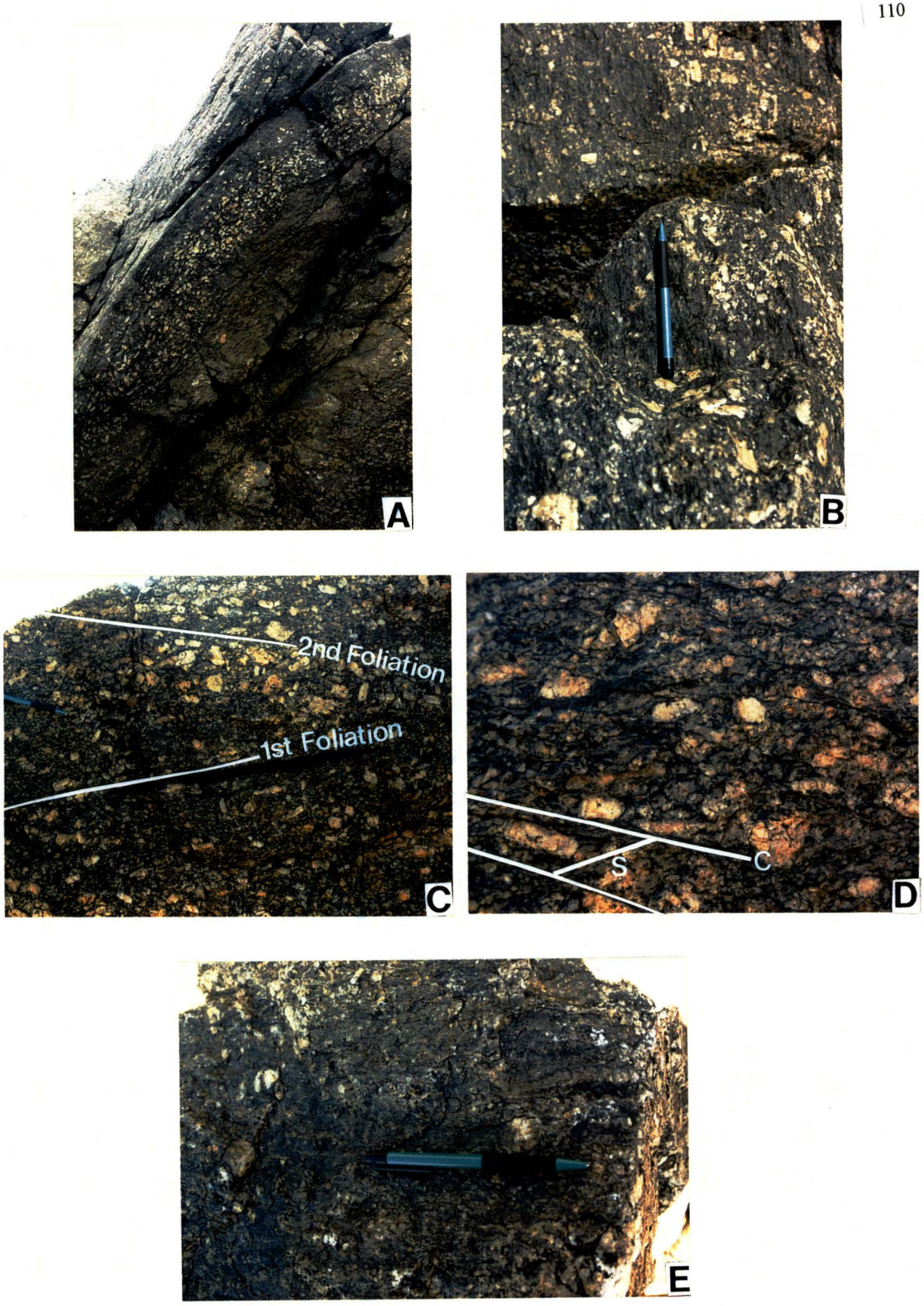

Fig.5.1 A) First foliation parallel to phase layering in Cape Foulwind monzogranitic gneiss; view across=3 m. B) NNW-SSE-trending lineations in plane of first foliation. C) First and second foliations; Cape Foulwind monzogranitic gneiss; pencil length=14 cm. D) C-S planes in Cape Foulwind monzogranitic gneiss; view across=12 cm;viwed to NW. E) NE-SW-trending lineations in plane of second foliation; pencil length=14 cm.

At the south Tauranga Bay headland, ENE-WSW-trending lineations predominate although the dominant foliation is the first foliation aligned parallel to xenoliths and megacrysts within the gneiss.

The Siberia Bay syenogranite-monzogranite appears to record only the second foliation and all lineations trend nearly NE-SW to ENE-WSW. Undeformed parts of the Siberia Bay pluton do not exhibit the first foliation or NNW-SSE-trending lineations which suggests that crystallisation some of the Siberia Bay syenogranite-monzogranite post-dates the development of NNW-SSE lineations and hence the Cape Foulwind and Tauranga Bay monzogranites.

5.3 Shear-sense Indicators

5.3.1 Tauranga Bay Monzogranitic Gneiss

Recrystallized monzogranitic biotite-gneiss, which outcrops at the south Tauranga Bay headland, contains a complex array of internal structures. Two periods of C-S plane development are displayed in thin sections cut parallel to a ENE-WSW-trending lineation. 'Old' C-planes are defined by an alignment of recrystallized biotite and associated S-planes by an alignment of biotite and elongate plagioclase porphyroclasts. The 'old' S-C planes are clearly visible in handspecimen and record a top-to-the-ENE sense of shear.

However, in thin section (TB3b and TB5) 'new' C-S planes which record a top-to-the-WSW sense of shear are developed in addition to 'old' C-S planes which record a top-to-the-NE shear-sense. σ_a-type porphyroclasts of plagioclase which lie along the 'new' S-planes display asymmetric tails of biotite and quartz that are deflected along the 'new' C-planes consistent with a top-to-the-WSW sense of shear (Fig. 5.2A). C-planes associated with this later-developed fabric fold and kink 'old' S-planes which have been caught up during the development of 'new' C-planes (Fig. 5.2B and C). Kinked and folded 'old' S-planes are consistent with this reversal in shear-sense from 'old' top-to-the-ENE to 'new' top-to-the-WSW.

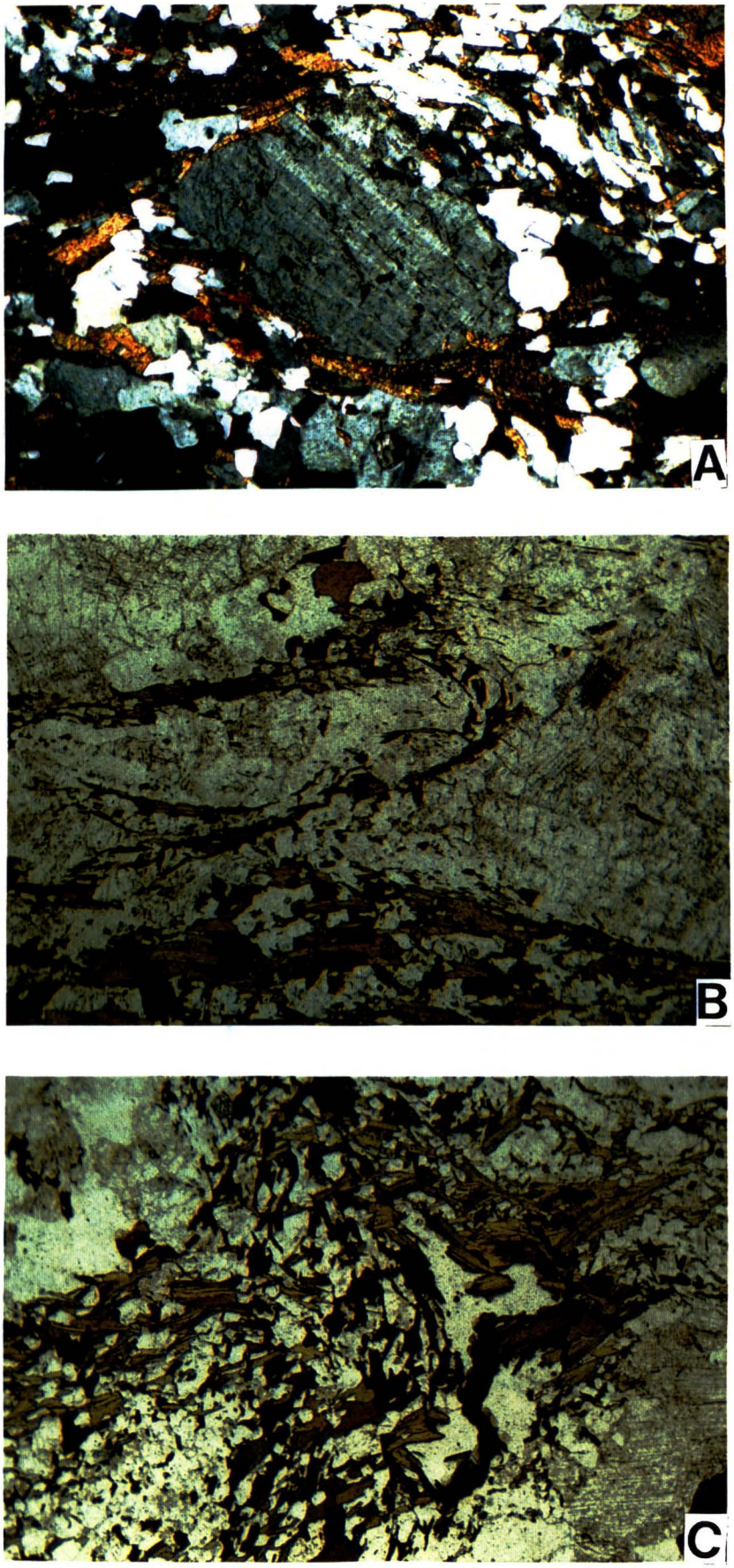

Fig. 5.2 A) σ-type porphyroclast system displaying a top-to-the-WSW sense of shear; crossed polarised light; view across=2.9 mm. B) and C) 'Old' top-to-the-ENE S-plane which have been folded and kinked by the development of top-to-the-WSW fabrics; plane polarised light; viewed to the NNW; field of view=6 mm.

Abundant schistose xenoliths within the Tauranga Bay gneiss contain two pervasive biotite-defined foliations which form weak but distinct C-S planes. In sample TB3b, one such xenolith contains C-S planes which record a top-to-the-WSW sense of shear. A top-to-the-WSW sense of shear is consistent with later-developed C-S planes within the Tauranga Bay orthogneiss.

Biotite involved in both 'old' and 'new' C-S plane development has been thoroughly recrystallized. This suggests that the temperature was at least moderate, even after deformation ceased.

Quartz c-axis Fabric Analysis

Orthogneiss samples from Tauranga Bay (TB3b and TB5) contain anhedral quartz crystals which display undulose extinction and occasionally form ribbons. The quartz c-axis fabrics from both samples can possibly be regarded as type II crossed girdles (Fig. 5.3): a sense of shear cannot be determined from either fabric. Indistinct quartz fabrics are, in fact, to be expected if a true reversal in shear sense occurred during the rocks deformational history as recorded by C-S planes.

5.3.2 Cape Foulwind Monzogranitic Gneiss

The coarse-grained nature of deformed orthogneiss around Cape Foulwind makes thin section analysis of shear-sense indicators difficult. In coastal outcrops below the Cape Foulwind lighthouse, most C-S planes viewed in sections parallel to the NE-SW-trending lineation show a top-to-the-NE sense of shear (Fig. 5.1D). In thin section (CF51), the gneiss displays narrow shear zones containing C-, S- and C′-planes of cataclased mica, and quartz shape-preferred orientations which support the sense of shear determined from gross C-S planes in outcrop. Deformed pegmatite (CF50) displays coarse-grained partly recrystallized muscovite fish that are asymmetric consistent with a top-to-the-NE sense of shear.

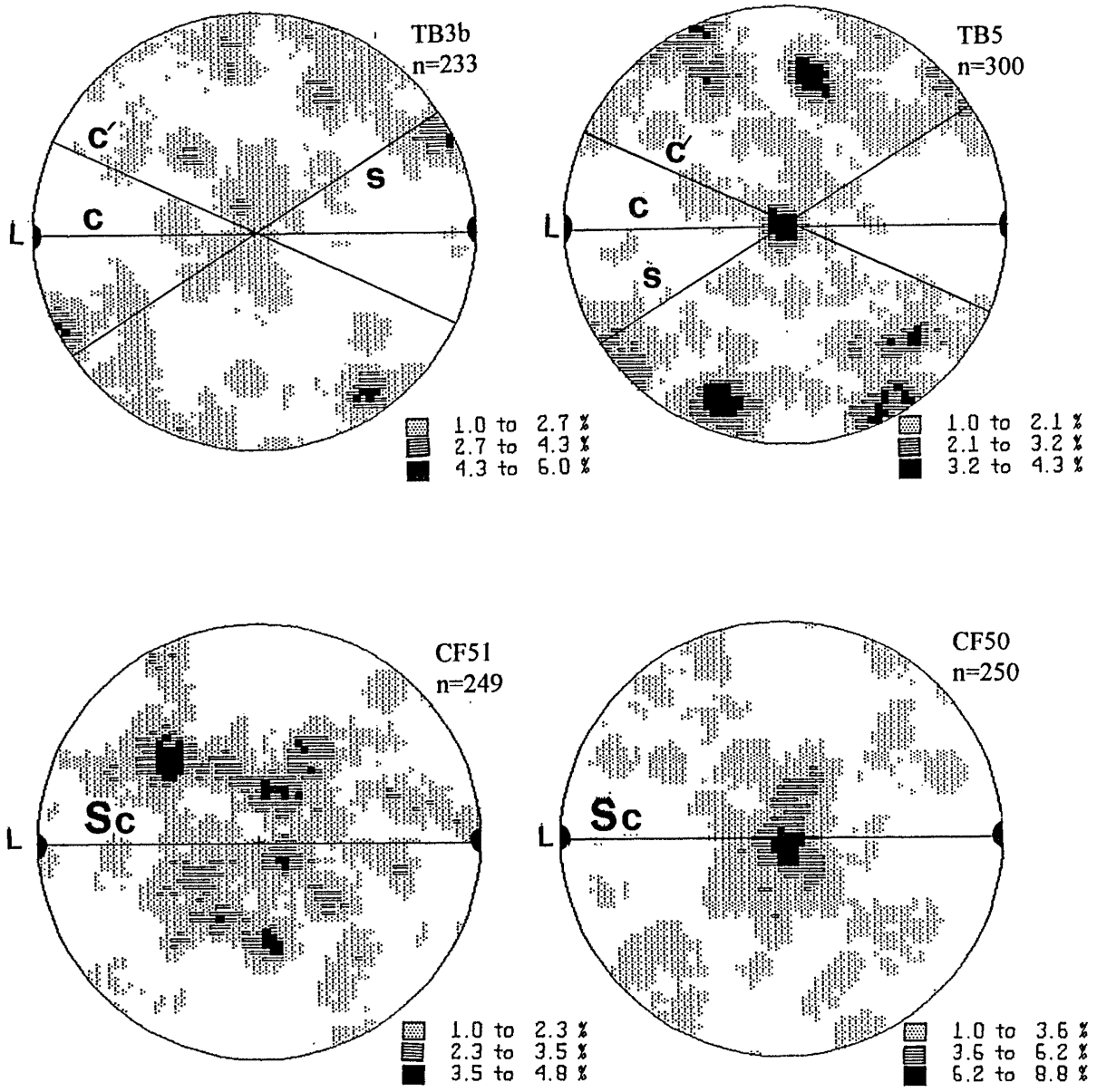

Fig. 5.3 Contoured lower hemisphere equal area projections of quartz c-axis orientations from the gneiss at Tauranga Bay (TB3b and TB5) and Cape Foulwind (CF51 and CF50); c=C-planes, s=S-planes, c′=C′-planes, L=lineation, Sc=schistosity. TB3b and TB5 possess both top-to-the-ENE and top-to-the-WSW C-S planes; only top-to-the-ENE C-S planes are shown on these fabrics. Fabrics are viewed either to the NW (CF50 and CF51) or NNW (TB3b and TB5).

Quartz c-axis Fabric Analysis

Sample CF51 displays an indistinct quartz c-axis fabric that cannot be classified or used as a kinematic indicator (Fig. 5.3). CF50 possesses a type II crossed girdle with a maxima at the Y axis recording a combination of basal <a> and prism <a> glide. No sense of shear can be determined from CF50 (Fig. 5.3).

5.4 Discussion

The two opposing senses of shear recorded in orthogneiss at the headland south of Tauranga Bay (early top-to-the-ENE and later top-to-the-WSW) are also recorded in the SBMZ where top-to-the-NE/ENE shear-sense indicators are overprinted by top-to-the-SW/WSW shear-sense indicators (Chapter 3; section 3.3.5). At Tauranga Bay, the last event affecting the rocks has been dated at 100 Ma (Aronson 1965), which suggests the deformation associated with top-to-the-WSW sense of shear is of Cretaceous age.

NNW-SSE- trending lineations at Siberia Point, which occur in the plane of the first foliation, appear to predate NE-SW-trending lineations. The association of the first foliation with aligned megacrysts and xenoliths suggests development close to the time of magma crystallisation: hence NNW-SSE lineations may be as old as 327 Ma. Alternatively, a Cretaceous deformation predating the NE-SW lineations may have been preferentially taken up along the first foliation. The absence of NNW-SSE lineations from the Siberia Bay syenogranite-monzogranite implies that either the NNW-SSE lineations predated intrusion of the Siberia Bay pluton, or that they post-dated the intrusion of the syenogranitic-monzogranitic magmas but been destroyed by later NE-SW to ENE-WSW movements recorded by the SBMZ. The presence of undeformed granite in the north of Siberia Bay suggests that some of the Siberia Bay syenogranite-monzogranite may have been emplaced after the mylonitic deformation.

The timing of similar NNW-SSE lineations around Charleston are broadly constrained between 380-400 Ma (youngest zircon rim recorded in paragneiss lithologies; Ireland 1992) and 108 Ma (age of undeformed pegmatite; recalculated from Aronson 1968).

CHAPTER SIX

THE RED JACKET GRANITE AND ADJACENT MIGMATITES

6.1 Introduction

Variably mylonitized migmatites outcrop in the most southern part of the field area, south of White Horse Creek. A biotite-defined foliation generally parallels the migmatitic layering, has variable strike and dips gently to steeply to the south or east (Map 3). On the coast immediately south of the Red Jacket Creek, lineations which trend NNW-SSE to NW-SE (Map 3) are defined by either elongate leucosomes and a preferred orientation of mica, or quartz-rodding and grooves on feldspar porphyroclasts (Fig. 6.1A). In coastal outcrops between Red Jacket Creek and White Horse Creek, some biotite and muscovite lineations record a more northerly trend. However, the dominant lineation is oriented NNW-SSE. In fact there is a distinct abrupt change from NNE-SSW-trending lineations in the MCMZ to typically NNW-SSE lineations in outcrops south of the White Horse Creek Fault.

Around Belfast Creek, the foliation and migmatitic layering dips moderately to steeply SW but appears to rotate around the main body of Red Jacket Granite to dip north or east in the extreme south of the area. A linear preferred orientation of leucosomes and biotite shapes trend NW-SE: some quartz rods, biotite crystals and feldspar grooves trend dominantly NE-SW but also WNW-ESE. Outcrops of unequivocal Red Jacket Granite appear to contain only NE-SW or WNW-ESE-trending muscovite-defined lineations.

6.2 Structure

In coastal outcrops south of White Horse Creek the migmatites are complexly deformed. Fold structures are highly variably in morphology and orientation and NNW-SSE-trending folds can be difficult to discern from WNW-ESE-trending folds. NNW-SSE

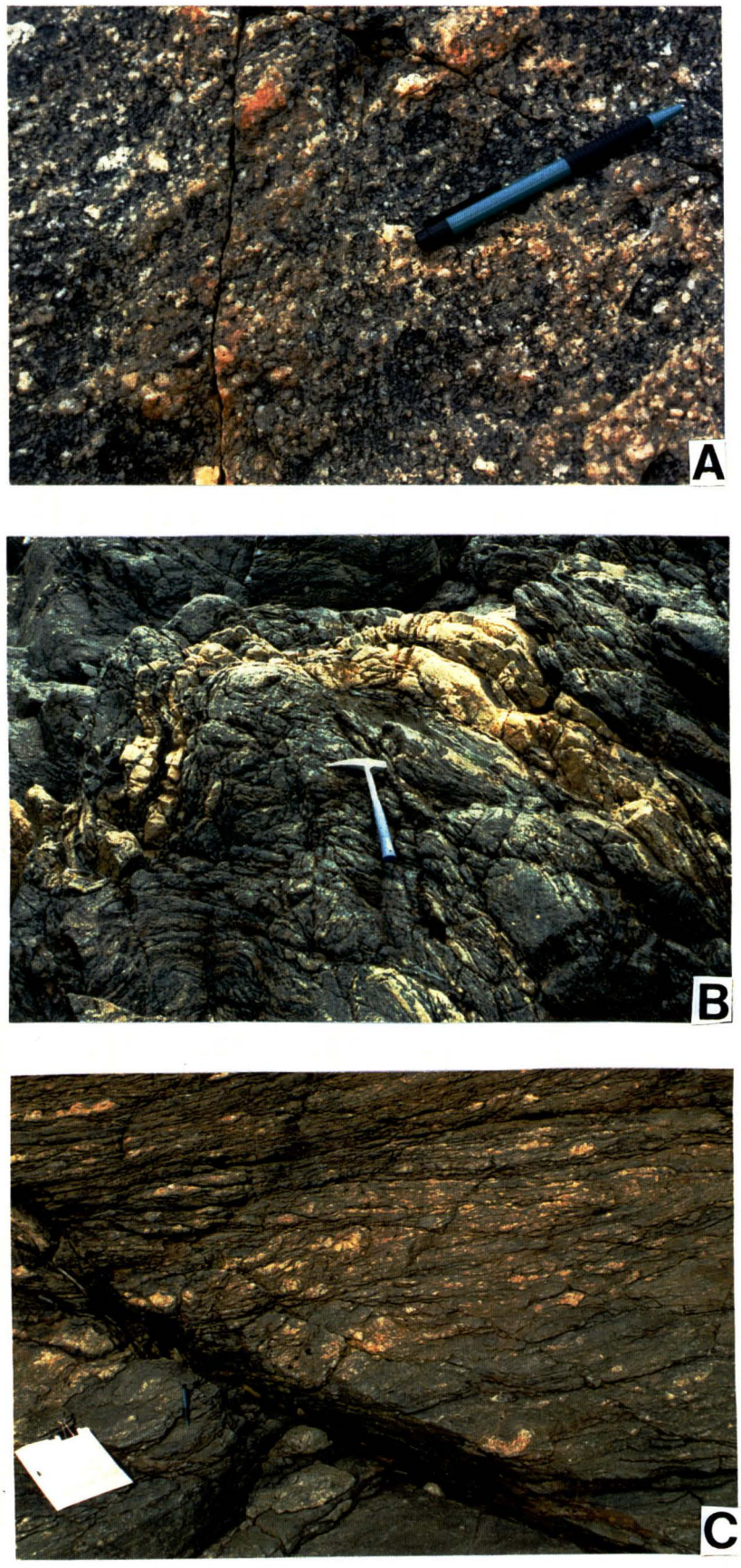

Fig. 6.1 A) NW-SE-trending lineations; pencil length=14 cm. B) E-W-trending buckle of the layering; hammer length=33cm.C) isoclinal fold of a mylonitic foliation; pencil length=14 cm.

trending folds occur as recumbent or gently inclined, sub-horizontal to gently plunging crenulations of the migmatitic layering, which trend parallel to the dominant lineation. No axial planar structures are associated with folds of this morphology and orientation.

In addition to NNW-SSE folds, close to open buckles of the layering with axes trending between 90° and 116° (predominantly WNW-ESE) outcrop on the coast north of Red Jacket Creek. One such fold (Fig. 6.1B) trends E-W and folds NW-SE-trending lineations into NE-SW orientations. Broad buckles of the gneiss which trend WNW-ESE also lack any axial-planar structures.

Around Belfast Creek, folds of the migmatitic foliation trend either NNW-SSE, ENE-WSW or NE-SW. Folds within the homogeneous but deformed Red Jacket Granite are more difficult to discern. Three folds were recognised: one trended NE-SW, the other two WNW-ESE. No NNW-SSE folds were recorded within the main body of the Red Jacket Granite.

NE-SW-trending folds that parallel associated NE-SW-trending lineations vary in morphology from open buckles to nearly isoclinal recumbent folds which may display axial-planar structures such as fracture cleavage or an axial-planar foliation. One NE-SW-trending fold folds a foliation of mylonitic origin rather than migmatitic layering (Fig. 6.1C).

Asymmetric folds with fold axes parallel to the overall strike of the surrounding migmatitic layering occur throughout the area. A traditional interpretation of asymmetric folds such as that shown in Fig. 6.2A would record a down-dip sense of movement. However, new strain field diagrams proposed by Bell (1985), where deformation is partitioned into zones of progressive shortening and zones of progressive shearing, suggest that the opposite may be true, at least for some folds. The centre of the fold in Fig. 6.2A is significantly thicker than the limbs of the fold which have undergone a greater amount of strain. When interpreted in terms of strain partitioning, the fold gives an up-dip movement direction. If this scenario is true, the orientation of the foliation within the thickened part of the fold will record the foliation orientation prior to folding. A pre-

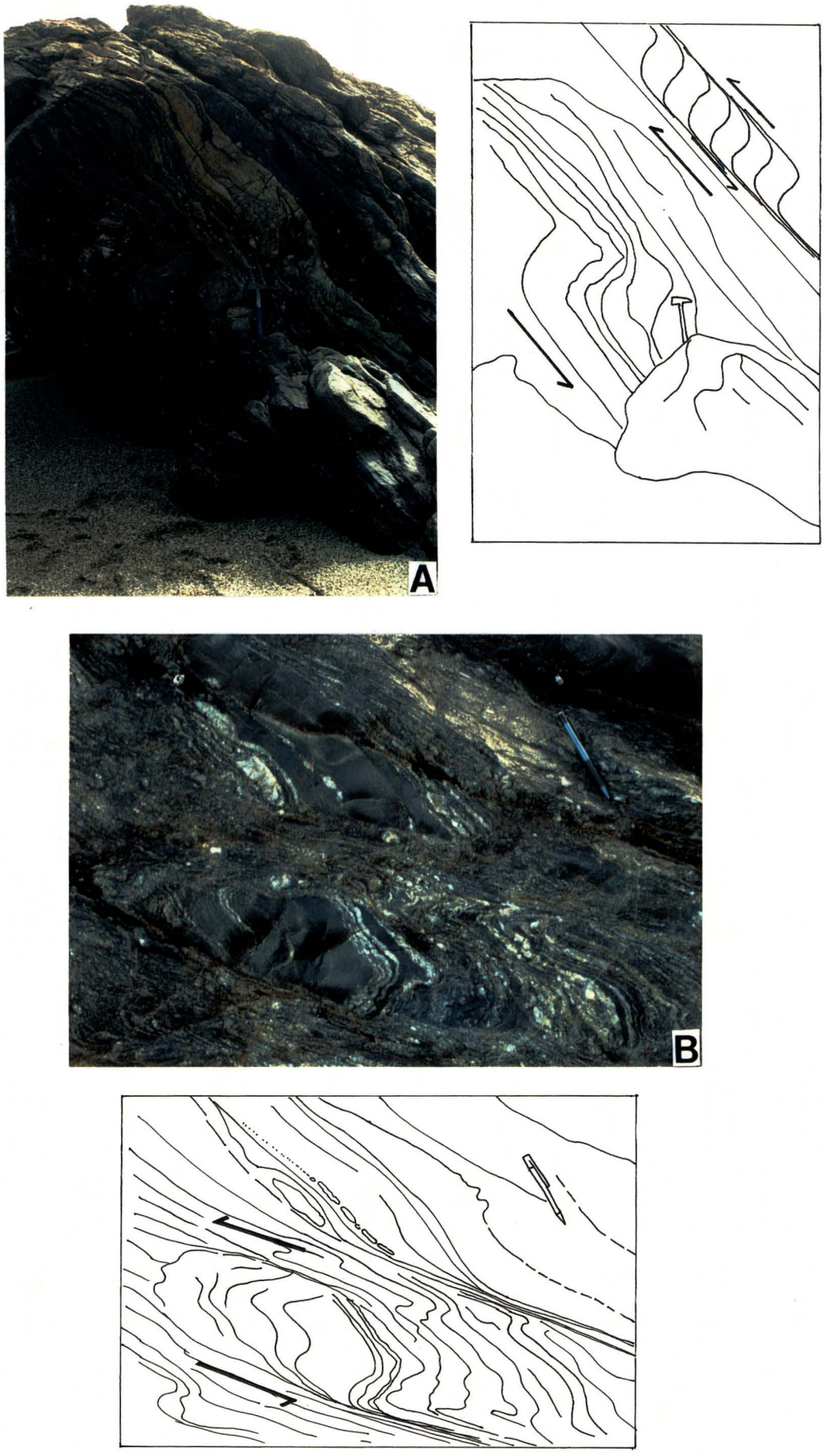

Fig. 6.2 A) Asymmetric fold of the migmatitic layering and strain partitioning interpretation; hammer length=33 cm. B) Pods of low-strain hornfelsic lithologies preserved by strain partitioning; pencil length=14 cm.

existing foliation is also preserved in the south of the area where strain partitioning has been extreme. Pods of low-strain migmatite (typically hornfels-type layers) record a layering oriented at an angle to the foliation recorded within high-strain zones surrounding the pods. A strain partitioning interpretation is sketched in Fig. 6.2B.

Although an up-dip movement direction is recorded for folds such as those in Fig. 6.2A, the orientation of the folds such as these south of White Horse Creek vary with the strike and dip of the migmatitic layering and a consistent sense of shear cannot be determined.

6.3 Post-ductile Brittle Deformation

Migmatites and mylonitized migmatites have undergone severe post-ductile brittle deformation. Zones of brecciated rocks up to 20 m wide cut the migmatites: one such zone trends NNW-SSE (Map 3). Quartz veins abound, particularly in the Red Jacket Granite. These veins have variable trend and appear predominantly post-tectonic. However, some veins are folded about axes of variable orientation. Kink bands are common along the coast south of White Horse Creek and in road cuttings.

A conspicuous feature of the rocks around White Horse Creek is extreme brecciation and silicification. Alteration of biotite to calcite and hematite gives the rocks a pale pink colour. In the bed of White Horse Creek, the foliation becomes more steeply dipping and rocks containing NE-SW-trending lineations appear in close proximity to rocks containing NNW-SSE lineations. The brecciation, alteration and juxtaposition of two texturally structurally different areas of rock suggest that a fault outcrops along the White Horse Creek. The White Horse Creek Fault does not affect the Tertiary sedimentary rocks unconformably overlying the high grade metamorphic rocks and is considered to be of Cretaceous age. The attitude of the fault and the sense of throw cannot be determined with any certainty, although section 6.6 shows that the rocks on the south side of the fault are probably upthrown.

6.4 Shear-sense Indicators

6.4.1 Just North of Belfast Creek to White Horse Creek

From just north of Belfast Creek to White Horse Creek some migmatitic outcrops have been intensely mylonitized and contain quartz-rodding, boudinaged feldspar and mica lineations that trend NW-SE and NNW-SSE. However, the degree of mylonitization generally decreases towards the south. C-S planes in mylonitized samples (B3, B5, B25, WH24, WH50, WH51) are defined primarily by a preferred orientation of recrystallized mica: S-planes lie up to 48° to the C-planes. C′-planes are defined as a recrystallized muscovite and/or biotite foliation oriented synthetically between 29° and 21° to the C-plane, or an asymmetric crenulation of the mica-defined C-plane. Gross C-, S- and C′-plane geometries are consistent with a top-to-the-NW/NNW sense of shear.

Cataclased plagioclase and K-feldspar porphyroclasts within B3, B5, B25, WH24, WH50 and WH51 are always σ_a-type and possess tails of predominantly recrystallized biotite and sometimes recrystallized quartz: one porphyroclast displayed tails of myrmekitized feldspar. Asymmetric tail geometries and deflected statically recrystallized quartz ribbons record a top-to-the-NW/NNW sense of shear consistent with C-, S- and C′-planes (Fig. 6.3A and B). No muscovite fish were found in the mylonitized migmatites: muscovite appears predominantly as late-tectonic kinked crystals or post-tectonic fine grains replacing K-feldspar porphyroclasts.

In addition to gross C-S plane geometries and porphyroclast systems which record a top-to-the NW/NNW sense of shear, samples B3, B5, B25, WH25, WH50 and WH51 also contain 'new' C-S planes of cataclased mica, asymmetric crenulations (C′-planes) and quartz shape-preferred orientations consistent with a top-to-the-SE/SSE sense of shear (Fig. 6.3C). Cataclased top-to-the-SE/SSE fabric elements clearly post-date well recrystallized top-to-the NW/NNW C-,S-, and C′-planes and porphyroclast tails.

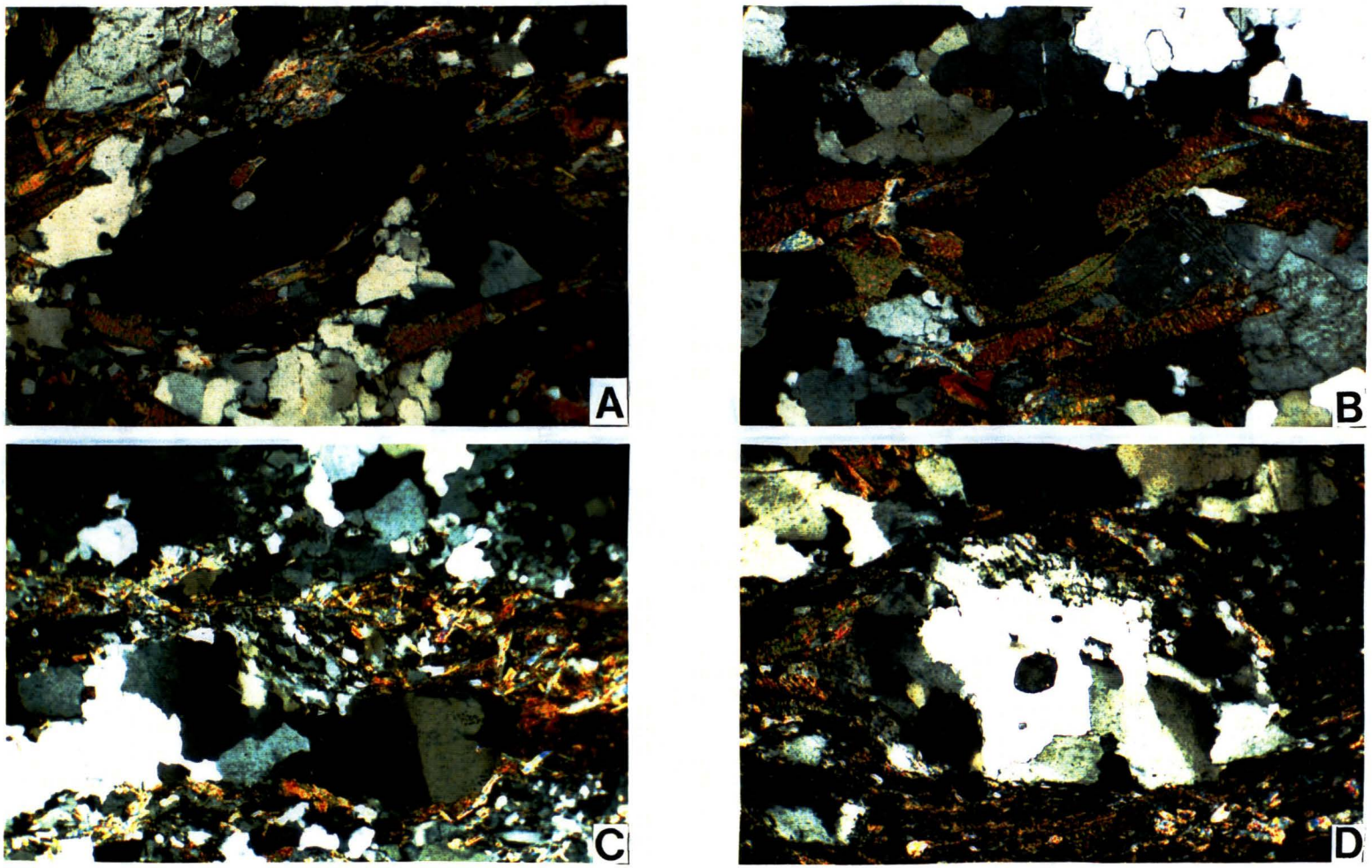

Fig. 6.3 A) and B) K-feldspar porphyroclast systems showing a top-to-the-NW sense of shear; crossed polarised light; viewed to SW; view across=2.9 mm. C) oblique quartz shape preferred orientation and C-S planes recording a top-to-the-SE sense of shear; crossed polarised light; viewed to SW; veiw across=2.9 mm. D) asymmetric pod of quartz showing a top-to-the-SW sense of shear; viewed to the NW; view across=2.9 mm.

Samples B8 and B27 from north of Belfast Creek are less well mylonitized and do not display well-formed indicators of shear.

Samples containing NE-SW-trending lineations (WH25) and N-S-trending lineations (WH16), contain feldspar porphyroclasts identical in nature to those recorded in outcrops containing NNW-SSE lineations. Recrystallized biotite tails and C-S planes of recrystallized mica record top-to-the-NE and top-to-the-N senses of shear for WH25 and WH16 respectively. Both samples also contain 'new' C-S planes of cataclased biotite and quartz shape-preferred orientations giving an opposing sense of shear to recrystallized biotite C-S planes i.e. top-to-the-SW and top-to-the S. In addition, sample WH25 displays isoclinally folded 'old' S-planes that have been caught up in the 'new' C-S plane development, which suggests that a change in shear-direction has occurred.

6.4.2 Around Belfast Creek

Near Belfast Creek, particularly around the main body of Red Jacket Granite, some NW-SE-trending lineations are subordinate to NE-SW orientations. Mesosomes are favourable sites for mylonitization and samples taken from south of Belfast Creek (B14, B18m and B37) contain NE-SW-trending lineations and some shear-sense indicators.

B37 contains asymmetric σ_a-type plagioclase porphyroclasts with tails of recrystallized biotite that record a top-to-the-NE sense of shear. However, within the same sample 'new' C-planes of cataclased or newly crystallized biotite and associated S-planes orientated approx. 28° to the C-planes record a top-to-the-SW sense of shear. Quartz shape-preferred orientations, asymmetric crenulations and a muscovite fish deformed during the 'new' C-S plane development also record a top-to-the-SW sense of shear. Asymmetric pods of quartz in B14 (Fig. 6.3D) and most plagioclase σ_a-type porphyroclasts in B18m record a top-to-the-SW sense of shear.

Top-to-the-NE shear-senses recorded by porphyroclast systems in mylonitized migmatites south of White Horse Creek are inconsistent with the top-to-the-SSW sense of shear proposed for the southern limb of the core complex by Tulloch and Kimbrough

(1989). The reversal in shear-sense from 'old' top-to-the-NE to 'new' top-to-the-SW in these mylonitized migmatites is discussed further in Chapter 8.

6.5 Quartz c-axis Fabric Analysis

Samples containing both NW-SE and NE-SW trending lineations have undergone intense static recrystallization. Quartz ribbons are coarse-grained and quartz crystals display predominantly sharp extinction. This static recrystallization has randomised quartz c-axis preferred orientations to the point where some samples from between White Horse Creek and just north of Belfast Creek display incoherent quartz fabrics that cannot be interpreted in terms of a sense of shear (Fig. 6.4).

Sample B3, just south of Red Jacket Creek, has undergone severe mylonitization and contains a well developed quartz rodding lineation. Quartz ribbons in thin section are extremely elongate and have been statically recrystallized. However the ribbons have retained a well developed c-axis preferred orientation that can be classed as a type I crossed girdle. This girdle is asymmetric with respect to the foliation consistent with a top-to-the-NW sense of shear (Fig. 6.5). A top-to-the-NW sense of shear is supported in thin section by feldspar porphyroclast systems. Variably mylonitized mesosomes B27 and B5a south of Red Jacket Creek, record a type II crossed girdle and single girdle respectively (Fig. 6.5). The dominant single girdle displayed by B5a is asymmetric with respect to the foliation consistent with a top-to-the-SE sense of shear, which is also recorded by quartz-shape-preferred orientations in thin section. However, porphyroclast systems in B5a record a top-to-the-NW sense of shear.

Sample WH22, just north of Red Jacket Creek, displays a poorly defined girdle that appears to be asymmetric with respect to C-plane, consistent with a top-to-the-SE sense of shear (Fig. 6.5). A top-to-the-SE sense of shear is inconsistent with top-to-the-NW porphyroclast systems both in thin section and in outcrop. Just south of White Horse Creek, WH51 has retained a type II crossed girdle c-axis fabric that cannot be interpreted in terms of a sense of shear.

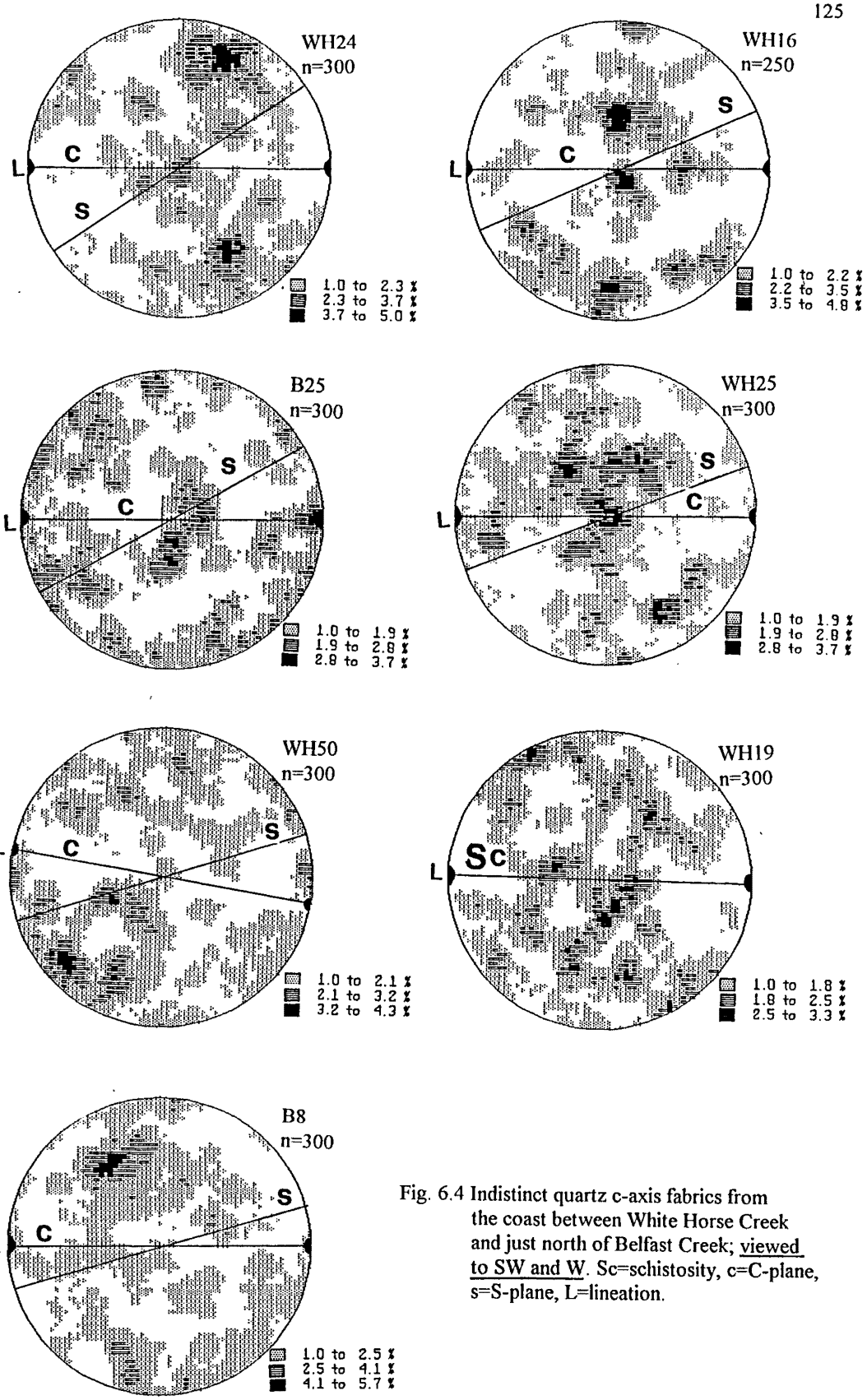

Fig. 6.4 Indistinct quartz c-axis fabrics from the coast between White Horse Creek and just north of Belfast Creek; viewed to SW and W. Sc=schistosity, c=C-plane, s=S-plane, L=lineation.

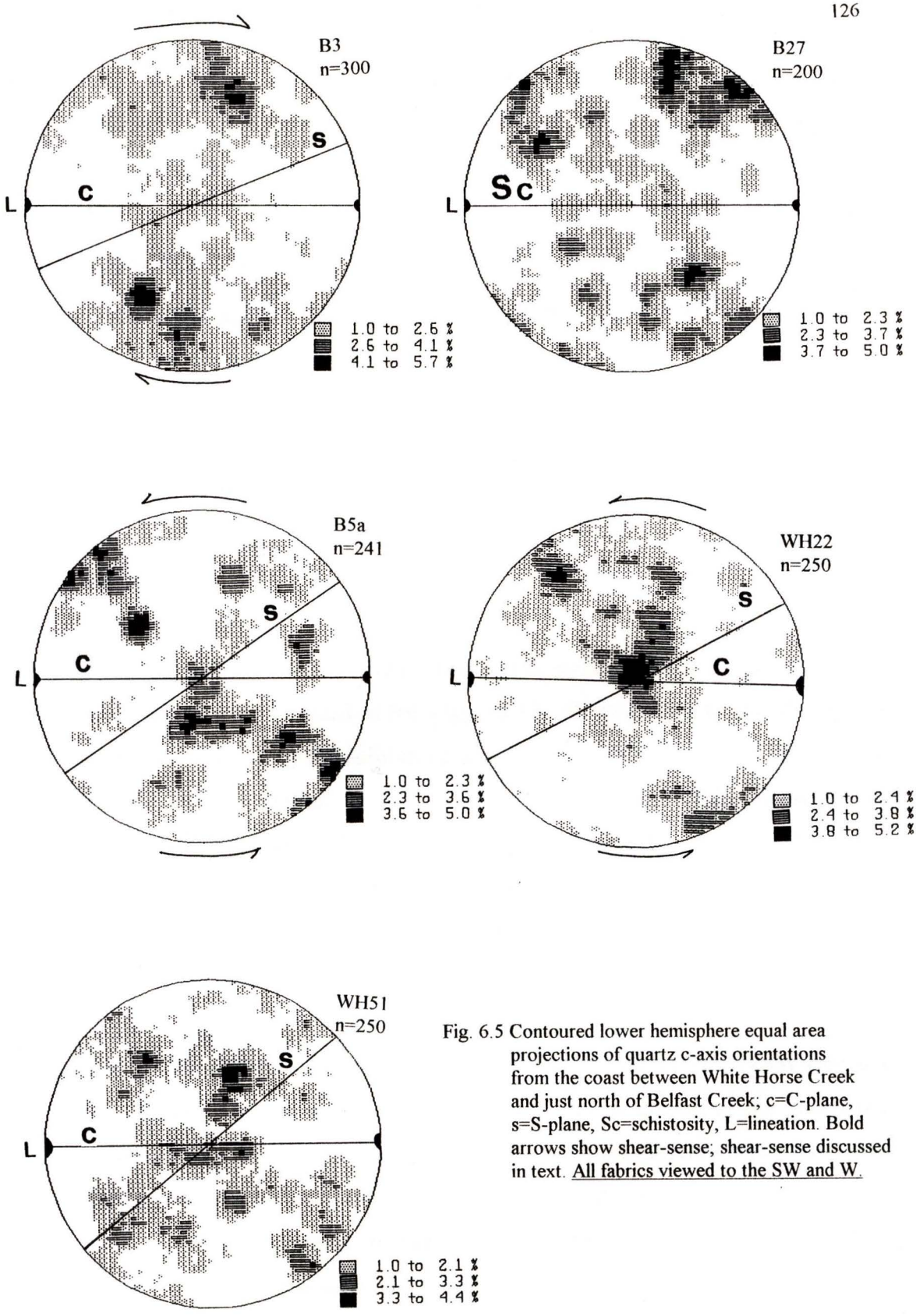

Fig. 6.5 Contoured lower hemisphere equal area projections of quartz c-axis orientations from the coast between White Horse Creek and just north of Belfast Creek; c=C-plane, s=S-plane, Sc=schistosity, L=lineation. Bold arrows show shear-sense; shear-sense discussed in text. All fabrics viewed to the SW and W.

Around Belfast Creek, mesosomes B14, B37 and B18m that record a NE-SW-trending lineation have undergone less recrystallization and retain quartz c-axis preferred orientations (Fig. 6.6). B37 and B18m display a well defined type I crossed girdle and single girdle respectively. These girdles are asymmetric with respect to the C-plane consistent with a top-to-the-NE sense of shear. A top-to-the-NE sense of shear recorded by B37 is supported in thin section by σ_a-type porphyroclast systems. B14 contains a less well defined girdle that appears to be asymmetric with respect to the foliation recording a top-to-the-NE sense of shear (Fig. 6.6).

6.6 Origin of NW/NNW-directed movements

6.6.1 Introduction

Mylonitized migmatites south of White Horse Creek possessing top-to-the-NW/NNW shear-sense indicators are distinquished from typical MCMZ structures by the 90° change in direction of stretching and by the substantial static recrystallization and up-dip sense of shear. The static recrystallization of the mylonites south of the White Horse Creek suggests that they may be older and/or from a deeper crustal level than the mylonites in the MCMZ and have probably been uplifted along the White Horse Creek Fault during a later brittle deformation. Top-to-the-NW/NNW shear-sense indicators are inconsistent with the NNE-SSW-directed extension proposed by Tulloch and Kimbrough (1989).

In coastal outcrops south of White Horse Creek, the timing of NNW-NW-directed movements is broadly constrained between the possible migmatization of the Greenland Group at around 380-400 Ma (Chapter 4; section 4.4) and the development of NE-SW lineations which post-date the intrusion of Red Jacket Grantite at around 110 Ma (Ireland. pers. comm.). NNW-NW-directed movements may therefore be of Paleozoic or Cretaceous ages. Possible Paleozoic and Cretaceous development of the NNW-NW-oriented mylonitic lineations is now discussed further.

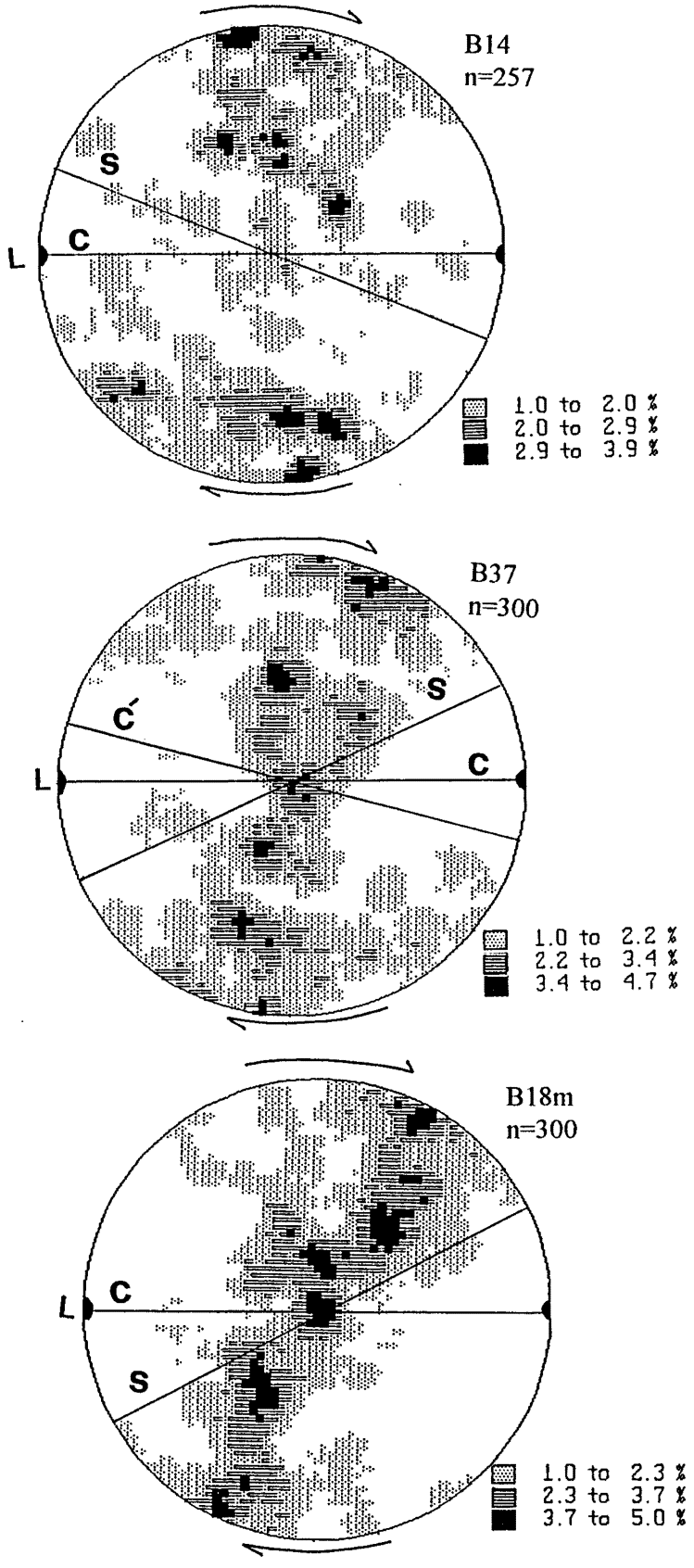

Fig. 6.6 Contoured lower hemisphere equal area projections of quartz c-axis orientations from mesosomes around Belfast Creek; c= C-plane, s=S-plane, c′=C′-plane, L=lineation. All fabrics viewed to the NW; bold arrows indicate shear-sense.

6.6.2 Possible Cretaceous development of NNW/NW-directed movements

Cretaceous development pre-dating emplacement of the Red Jacket Granite

Top-to-the-NW/NNW senses of shear may record the earlier Cretaceous plate convergence movements overprinted by later NE-SW extensional movements. The NW-NNW-trend is at high angles to the trend of subduction-related structures such as the Separation Point Batholith and Median Tectonic Zone and up-dip senses of shear recorded in exposures along the coast south of White Horse Creek possibly reflect a period of reverse thrusting related to convergence. Development of NW-NNW-directed movements during Cretaceous convergence which predated NE-SW extension is consistent with the absense on NW-NNW-oriented structures from the main body of the Red Jacket Granite.

Preservation of top-to-the-NW/NNW structures may be due to intense strain partitioning, or structures of this orientation may have been preserved because they were originally lower in the crust and did not undergo mylonitization associated with Cretaceous core complex development. Softening of the migmatites around Belfast Creek by the mid-Cretaceous intrusion of the Red Jacket Granite may have enabled the migmatites at this locality to take up strain associated with Cretaceous NE-SW-movements.

Cretaceous development post-dating or related to intrusion of the Red Jacket Granite

NW/NNW-trending lineations may represent NE-SW-trending lineations in the MCMZ folded into NW/NW orientations about a nearly E-W-trending fold, or NE-SW-trending lineations rotated into NW/NWW orientations. However, there is no evidence for a macroscopic fold such as fold vergence, or rotation of lineations seen in the field.

Opposing senses of shear on opposite limbs of the Charleston and Parsons Hill arches implies that some Cretaceous ductile deformation of the Charleston Metamorphic Group is controlled by magma intrusion. Around Belfast Creek, lineations are of highly variable trend and include NE-SW, WNW-ESE and NW-SE-trending lineations which appear to rotate around the main body of Red Jacket Granite (Map 3), rather than being simply of NE-SW-trend. Shear-sense indicators associated with NE-SW lineations around Belfast Creek are texturally identical to those associated with NNW/NW-trending mylonitic

lineations, displaying a large amount of static recrystallization. The identical textures and structures in migmatites containing NE-SW lineations and those containing NW/NNW-trending mylonitic lineations suggests that they may be of the same age and related to the same deformational event. The NNW/NW-directed movements may, therefore, be of Cretaceous age associated with the linear or domal uprise of a magma body somewhere to the SE, perhaps the poorly exposed Red Jacket Granite. The up-dip sense of shear now recorded can perhaps be attributed to tectonic tilting along the White Horse Creek Fault, during uplift after ductile deformation ceased.

6.6.3 Possible Paleozoic development of NNW/NW-directed movements

South of White Horse Creek, NNW/NW-directed movements may be of Paleozoic age post-dating the migmatization of the Greenland Group (possibly around 380-400 Ma). A Paleozoic age for the development of top-to-the-NW/NNW movements would be consistent with the absence of NW/NNW-trending structures in the main body of exposed Red Jacket Granite which was emplaced at around 110 Ma (Ireland. pers. comm.).

NNW-SSE-trending lineations are also preserved in the monzogranitic gneisses around Cape Foulwind (section 5.2) and in migmatites of sedimentary origin near Charleston (section 4.3). The preservation of NNW-SSE-trending lineations throughout the field area, and apparent absensce of these lineations from mid-Cretaceous orthogneisses at Charleston and the Red Jacket Granite suggests that these lineations may record a pre mid-Cretaceous event, possibly of Carboniferous age. The timing of NNW/NW-trending lineations is discussed further in Chapter 8.

The NW-SE trend of leucosomes may have developed during migmatization of the Greenland Group, or may be a strain feature imposed upon the migmatites at a later stage.

6.7 The Red Jacket Granite

6.7.1 Introduction

Highly deformed leucogranite of variable composition outcrops south of Belfast Creek and was first named the Red Jacket Granite by Nathan (1975). In the field, the main body of Red Jacket Granite cross-cuts migmatitic layering, and therefore clearly postdates migmatization (Fig. 2.7A). However, the granite sometimes contains a foliation that parallels a similar foliation within the country rock. Although the granite clearly cross-cuts the layering in the migmatites, sills from the granite intrude parallel to migmatitic layering near the periphery of the of Red Jacket Granite.

Discordant Rb-Sr dates on muscovite (212 Ma) and biotite (104 Ma) by Aronson (1968) were thought to indicate emplacement of the granite body prior to 212 Ma and a later metamorphism about 104 Ma. However, zircons of the Red Jacket Granite analysed by Ireland using SHRIMP (pers. comm.) record ages around 110 Ma for two single zircons. No inherited zircons were found . This implies that the granite crystallized in the Cretaceous and contains absolutely no record of Paleozoic magmatism or metamorphism.

The main body of the Red Jacket Granite contains predominantly NE-SW-trending lineations and some WNW-ESE-trending lineations. One NE-SW-trending fold and two WNW-ESE-trending folds were noted in the homogeneous granite. No NNW-SSE-trending structures were observed within the main body of the Red Jacket Granite.

6.7.2 Petrofabric Analysis

Two samples of unequivocal Red Jacket Granite were collected (RJG2 and RJG3). Both samples contained NE-SW-trending lineations defined by a preferred orientation of elongate quartz crystals, muscovite and boudinaged feldspars. RJG2 was taken from the main body of Red Jacket Granite. RJG3 was taken from a smaller body of Red Jacket Granite from the extreme south of the area (sample grid references in Appendix A).

The coarse-grained nature of the granite makes thin-section analysis of textures and shear-sense indicators difficult. Feldspar textures are consistent with magmatic crystallisation (Carlsbad-twinned microcline poikilitically encloses euhedral zoned plagioclase crystals) and no unequivocal shear-sense indicators were noted in thin sections parallel to the NE-SW-trending lineation. However, quartz has undergone plastic deformation and dynamic recrystallization and RJG2 displays a quartz c-axis fabric dominated by a single girdle asymmetric with respect to the schistosity consistent with a top-to-the-NE sense of shear (Fig. 6.7). The quartz c-axis fabric from RJG3 is less distinct and appears to be a type II crossed girdle which is symmetric with respect to the foliation recording a component of coaxial deformation (Fig. 6.7).

Sills of Red Jacket Granite display textures in thin section which differ from those seen in samples RJG2 and RJG3. Plagioclase, quartz and orthoclase lack euhedral crystal form and textures which can be equated with slow cooling but, rather, form an equidimensional mosaic of grains. Within the sills, muscovite displays spherulite-like growth forms (Fig. 6.8A). The lack of feldspar crystal form and the spherulitic growth of muscovite implies a moderate degree of undercooling and suggests that the Red Jacket magma crystallized quickly when it came into contact with relatively cooler (but probably still warm) migmatitic country rock.

Within the sills, quartz has undergone little deformation but does exhibit some undulatory extinction. The quartz c-axis fabric displayed by one such sill (B18f: Fig. 6.7) contains a dominant girdle of c-axes which appears asymmetric with respect to the foliation consistent with a top-to-the-SW sense of shear.

Numerous shear zones which parallel the sill-country rock boundaries are contained within the sills. The shear zones are sites of K-metasomatism and contain abundant muscovite (up to 90%), quartz and rare K-feldspar. Some shear zones contain a sigmoidal muscovite-defined foliation consistent with a top-to-the-SW sense of shear (Fig. 6.8B). Quartz c-axis fabrics from four such shear zones within B18f record indistinct quartz fabrics.

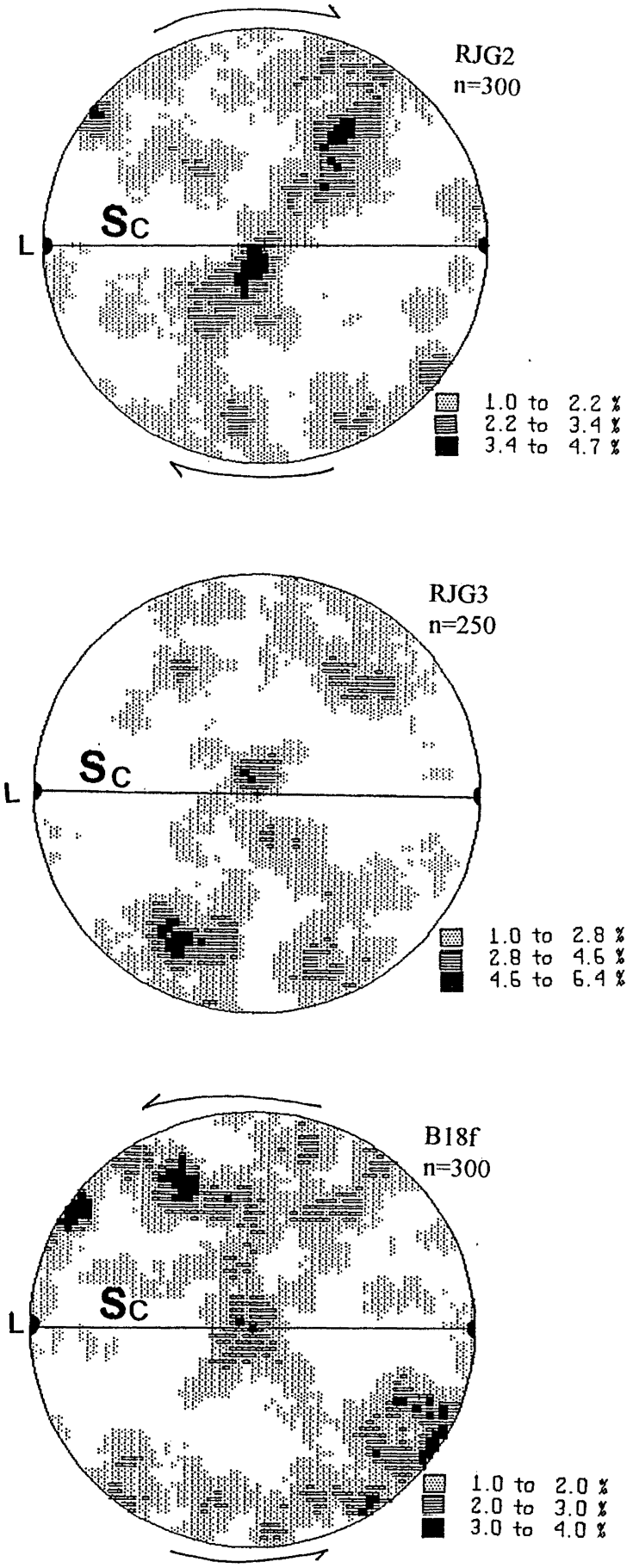

Fig. 6.7 Contoured lower hemisphere equal area projections of quartz c-axis orientations from the Red Jacket Granite (RJG2 and RJG3) and a sill coming off the main body of Red Jacket Granite (B18f); Sc=schistosity, L=lineation. All fabrics viewed to the NW; bold arrows indicate shear-sense.

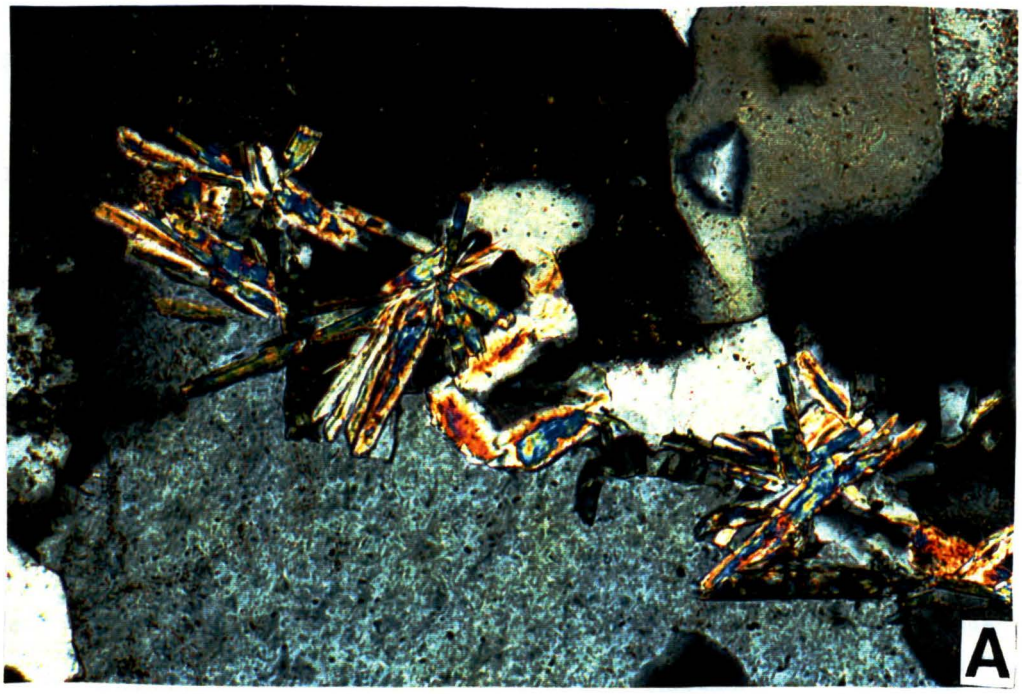

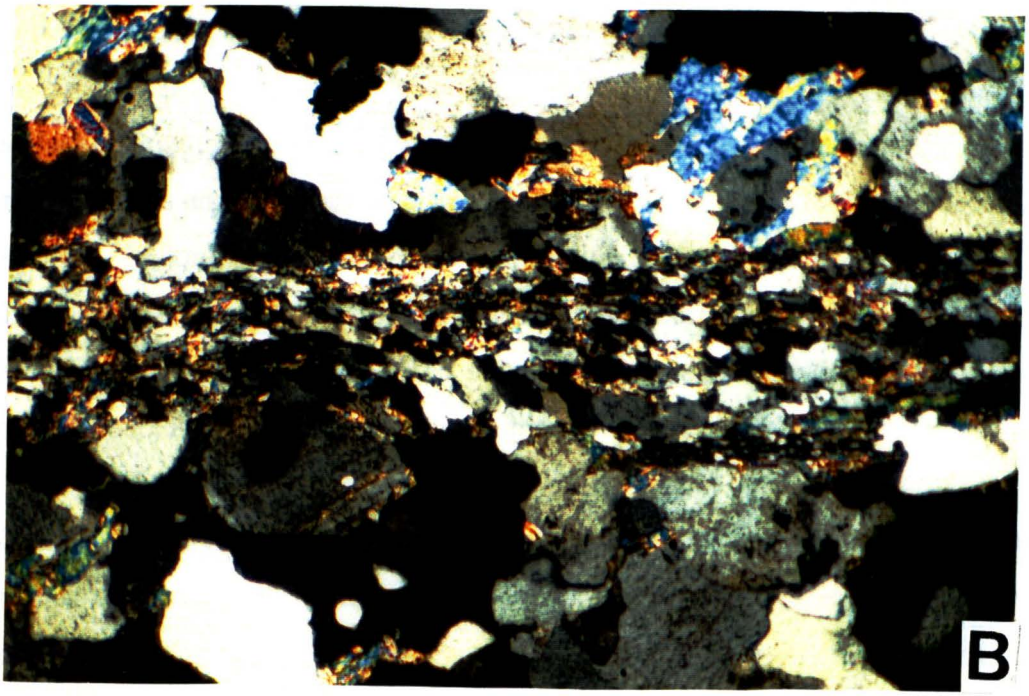

Fig. 6.8 A) Spherulite-like growth forms of muscovite in Red Jacket Granite sills; crossed polarised light; view across=1.24 mm. B) Shear zone showing a sigmoidal foliation consistent with a top-to-the-SW sense of shear; viewed to the NW; view across=2.9 mm.

6.7.3 Geochemistry

Unpublished whole rock X-ray fluorescence analyses of the Red Jacket Granite (Appendix B) by N. Robinson show a range in SiO_2 content from 66.91% to 73.35%. Thin section and geochemical analysis records a range in rock composition from syenogranite to granodiorite and ASI values from the Red Jacket Granite suggest a predominantly S-type designation (1.10 to 1.67).

K_2O-Na_2O-CaO plots of the Red Jacket Granite follow the Karamea Suite trend defined by Tulloch (1983), (Fig. 6.9). However a geochemical similarity with the Karamea Suite of mid-Paleozoic age conflicts with the mid-Cretaceous age for the Red Jacket Granite indicated by SHRIMP analysis of zircons. When the Red Jacket Granite is compared with the trend of the two known Cretaceous granitoid rock groups exposed in Nelson-Westland (subduction-related Separation Point and extension-related Rahu Suite) the Red Jacket Granite contains a much greater proportion of K_2O (Fig. 6.9).

The Red Jacket Granite also possesses a geochemical signature distinct from the I-type Charleston orthogneiss analyses published by Kimbrough and Tulloch (1989), exposed 12 km to the north. Major element differences include significantly higher K_2O, lower CaO and slightly lower Na_2O when compared with the Charleston orthogneiss. Trace elements Sr and Ba are significantly lower in the Red Jacket Granite than in the orthogneiss while Rb is more than double that recorded in the orthogneiss.

The Karamea Suite-type geochemistry but mid-Cretaceous age for the Red Jacket Granite implies that geochemical characteristics alone are not a sufficient parameter to determine the age of a granite when geochronological data is lacking. Perhaps what is most interesting about the Red Jacket Granite is the geochemical similarity to unpublished data from the Siberia Bay Pluton (Smith 1992) which suggests that the Siberia Bay syenogranite-monzogranite may also be of mid-Cretaceous age, rather than mid-Paleozoic

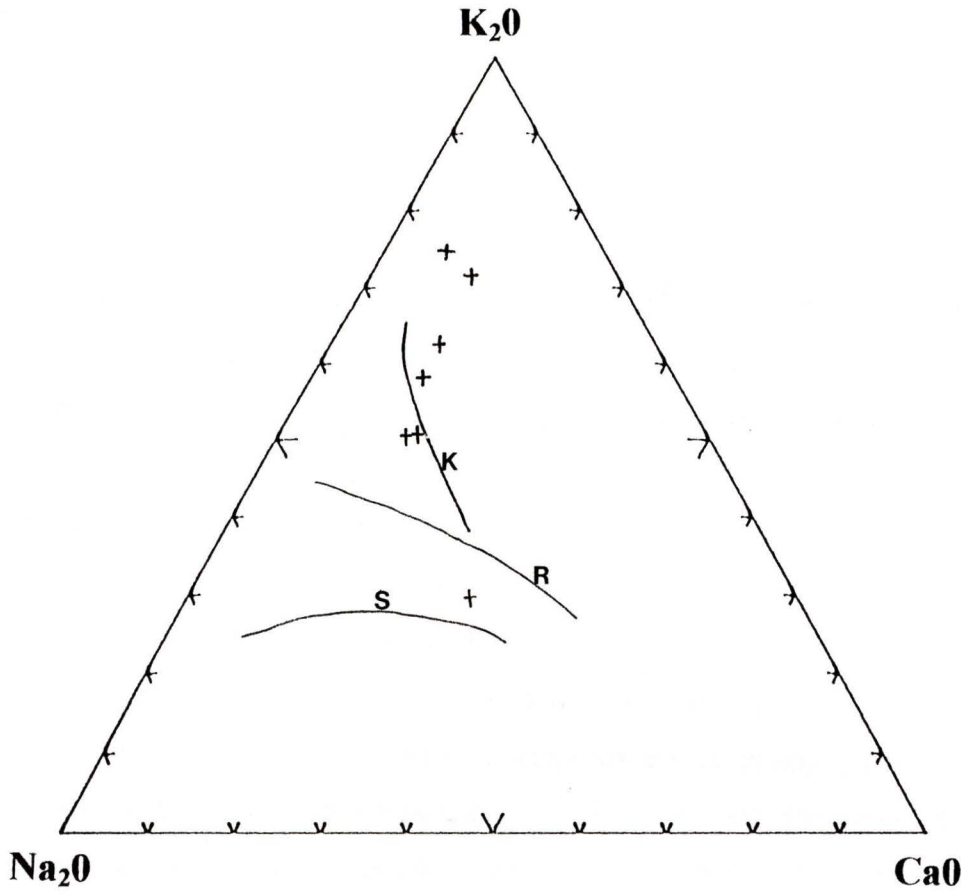

Fig. 6.9 K_2O-Na_2O-CaO plot of the Red Jacket Granite. Trends for the Rahu Suite (R), Karamea Suite (K) and Separation Point Suite (S) after Tulloch (1983).

as previously assumed. A mid-Cretaceous age for the some parts of the Siberia Bay syenogranite-monzogranite is consistent with the presence of some totally undeformed granite at the northern end of Siberia Bay.

6.8 Summary

The coast south of White Horse Creek records a complex series of deformational events. NNW-SSE and NW-SE-oriented mylonitic lineations recording predominantly top-to-the-NW/NNW senses of shear occur in the migmatites of sedimentary origin and are absent from the main body of Red Jacket Granite. These NNW-NW mylonitic lineations may be of Paleozoic age predating the crystallisation of the Red Jacket Granite (approx. 110 Ma). NNW-SSE-trending lineations are also found at Cape Foulwind and in migmatitic lithologies near Charleston. This suggests that the development of NNW/NW-trending lineations may record a widespread, possibly Paleozoic event. Alternatively, the NNW/NW-trending lineations may be of Cretaceous age recording a period of reverse thrusting during an earlier plate convergence, or associated with the uprise of magma to the SE, such as the poorly exposed Red Jacket Granite. WNW-ESE trending structures and NE-SW-trending mylonitic structures which record a predominantly top-to-the-NE sense of shear clearly post-date intrusion of the Red Jacket Granite. The static recrystallization in the mylonites suggests an origin deeper in the crust than the mylonites in the MCMZ and the coast south of White Horse Creek has probably undergone uplift along the White Horse Creek Fault.

NW-SE-trending leucosomes may have developed during migmatization or may be a strain feature imposed upon the migmatites at a later stage.

The Red Jacket Granite of Cretaceous age (around 110 Ma; Ireland. pers. comm.) is geochemically similar to the Karamea Suite of mid Paleozoic age and is geochemically distinct from the Charleston orthogneiss lithologies and the Rahu Suite granitoids of mid-Cretacoeus age. This implies that geochemical similarity alone is not a sufficient parameter to determine the age of granite when geochronological data is lacking. It also implies that

the Siberia Bay syenogranite-monzogranite, which shows a Karamea Suite-type geochemistry may also be of mid-Cretaceous age. A mid-Cretaceous age for the Siberia Bay granitic rocks would support the presence of undeformed granite at the northern end of Siberia Bay.

CHAPTER SEVEN

HORNFELSIC LITHOLOGIES

7.1 Introduction

Biotite-rich fine-grained layers, pods and xenoliths are found within the migmatites, mylonites and Charleston and Cape Foulwind orthogneiss lithologies. In thin sections parallel to a typically weak biotite-defined lineation, biotite imparts a hornfelsic to schistose texture.

In the very south of the field area, the hornfelses occur as discrete layers or lenses in the migmatites or lense-shaped bodies within the Red Jacket Granite which possess biotite-rich schistose margins (Fig. 2.9A). Within the mylonite zones, the same hornfelsic layers display an anomalous lack of boudinage, although some layers appear to have undergone some degree of mylonitization. At the mouth of the Morrisey Creek an apparently undeformed hornfels lense contains a core rich in pyroxene (Shelley 1970). The hornfelsic layers in the MCMZ display a conspicuous lack of boudinage.

In the cliffs on the northern side of Parsons Hill, large rafts of hornfels have been broken up within the more mobile gneiss of tonalitic composition (Fig. 7.1). Although predominantly undeformed, these large rafts contain some internal deformation recorded by folded 1 mm wide felsic layers.

At Tauranga Bay, Siberia Bay and around Cape Foulwind, lenses of biotite-rich rock occasionally contain a complex zonation of mafic and felsic minerals suggesting metasomatic alteration by circulating country-rock fluids (Fig. 7.2A). Abundant xenoliths in Tauranga Bay display either discrete or diffuse boundaries with the orthogneiss country rock and are generally oblate within the plane of the foliation. Some hornfelses lack

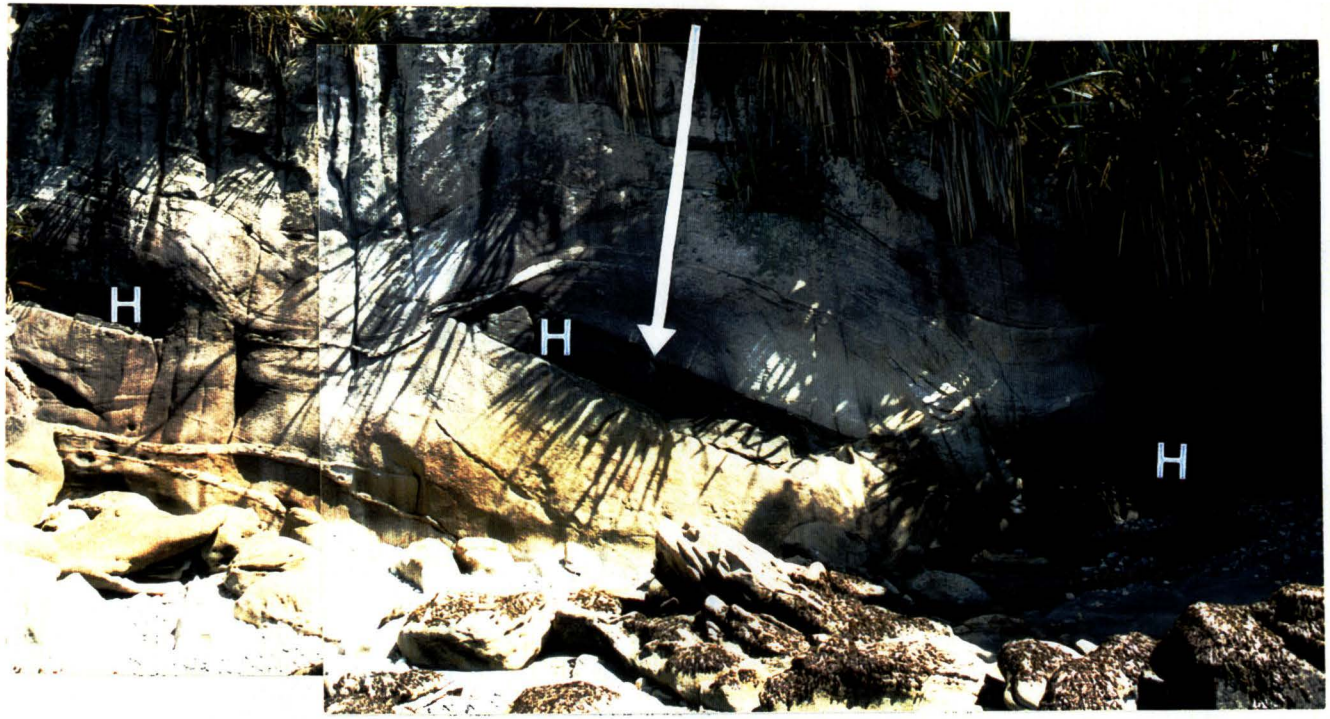

Fig. 7.1 Large rafts of hornfels on the northen side of the Parsons Hill Arch ; note internal deformation (arrow); length of middle raft=4 m.

Fig. 7.2 A) Hornfelsic xenolith from Siberia Bay; view across= 0.5 m.B) Pod with diffuse boundaries from the south Tauranga Bay, note large tourmaline porphyroblasts; pencil length=14 cm.

quartz altogether (sample HFTBA) which suggests removal of more mobile components in the xenoliths. The same sample contained a schistosity defined by the alignment of biotite and a lineation defined by large porphyroblasts of tourmaline (Fig. 7.2B).

7.2 Origin of the Hornfelsic layers, Pods and Xenoliths

The oxidation state of biotite in the hornfelses varies throughout the area. In the southern migmatites and mylonite zones, the biotite is always red-brown in colour. At Parsons Hill the large rafts of hornfels contain green biotite, while at Tauranga Bay the biotite is of an intermediate colour. The biotite oxidation state does not reflect the differing I-type or S-type origin of the xenoliths, but instead reflects the reducing or oxidising state of circulating fluids within the country rock: those hornfelses contained within the I-type orthogneiss display green biotite while those within migmatized sediments display red-brown biotite.

Mineralogically, most hornfelses reflect a sedimentary origin and contain abundant apatite, some tourmaline (Tauranga Bay) and rare sillimanite (southern migmatites). Plagioclase, which ranges from albite (Tauranga Bay) to andesine (southern migmatites), lacks Carlsbad twinning, albite twinning and euhedral crystal shapes which are typical of igneous crystallisation, but may display some crystal zoning (presumably of metamorphic origin). The hornfelses only rarely contain pyroxene, hornblende or titanite and where these minerals occur they appear to be associated with a metasomatic reaction of the hornfelses rather than being of primary origin.

South of White Horse Creek, hornfelsic layers parallel compositional banding within the stromatic migmatites and are considered here to be migmatitic restites from which some mobile material was removed during anatexis (presumably to form leucosomes). The migmatites themselves contain red-brown biotite and display regular layers of leucosome, mesosomes and melanosomes suggesting a sedimentary origin. The hornfelsic restites included in the migmatites are, therefore, also concluded to be of sedimentary origin.

7.3 Quartz c-axis Fabric Analysis

In total, nine hornfels specimens were taken from the study area for fabric analysis. Two specimens were taken from the coast south of the main body of Red Jacket Granite (HFSB2 and B2a), one from the coast dominated by NW-SE-trending lineations north of Belfast Creek (HFSB1), two from the MCMZ (HFWH2 and HFWH3), one from the large rafts of hornfels at Parsons Hill (HFC) and two from the South Tauranga Bay headland (HFTBA and HFTB2). Sample HFTBA does not contain quartz. Sample HFWH3 has undergone mylonitization in the MCMZ and contains a fabric more akin to that of the surrounding mylonites and is not discussed further in this section.

Lineations defined primarily by a preferred orientation of biotite trend NE-SW for all samples except for HFSB1, which contains a ENE-WSW trending lineation, and HFSB2 and B2a, which contain NW-SE trending lineations. All quartz-bearing samples display quartz c-axis fabrics consistent with coaxial deformation with the exception of sample B2a (Fig. 7.3). HFC, HFWH2, HFSB1 and HFSB2 record variably defined type II crossed girdles with an angle between the limbs of up to 90°. HFTB2 contains a symmetric fabric but lacks the girdle distribution of c-axes characteristic of the previous fabrics. Sample B2a appears to record a poorly defined girdle asymmetric with respect to the foliation consistent with a top-to-the-NW sense-of-shear (Fig. 7.3).

Hornfelses which record coaxial fabrics are found surrounded by mylonites formed by non-coaxial deformation in the MCMZ. Predominantly coaxial fabrics suggests that the more refractory hornfels may have undergone a bulk pure shear in contrast to the bulk simple shear of the mylonites. Alternatively, the coaxial fabrics may record a fabric associated with pre-Cretaceous deformation, preserved by intense strain partitioning, though this seems unlikely given the essentially new crystallization recorded in the hornfelsic layers.

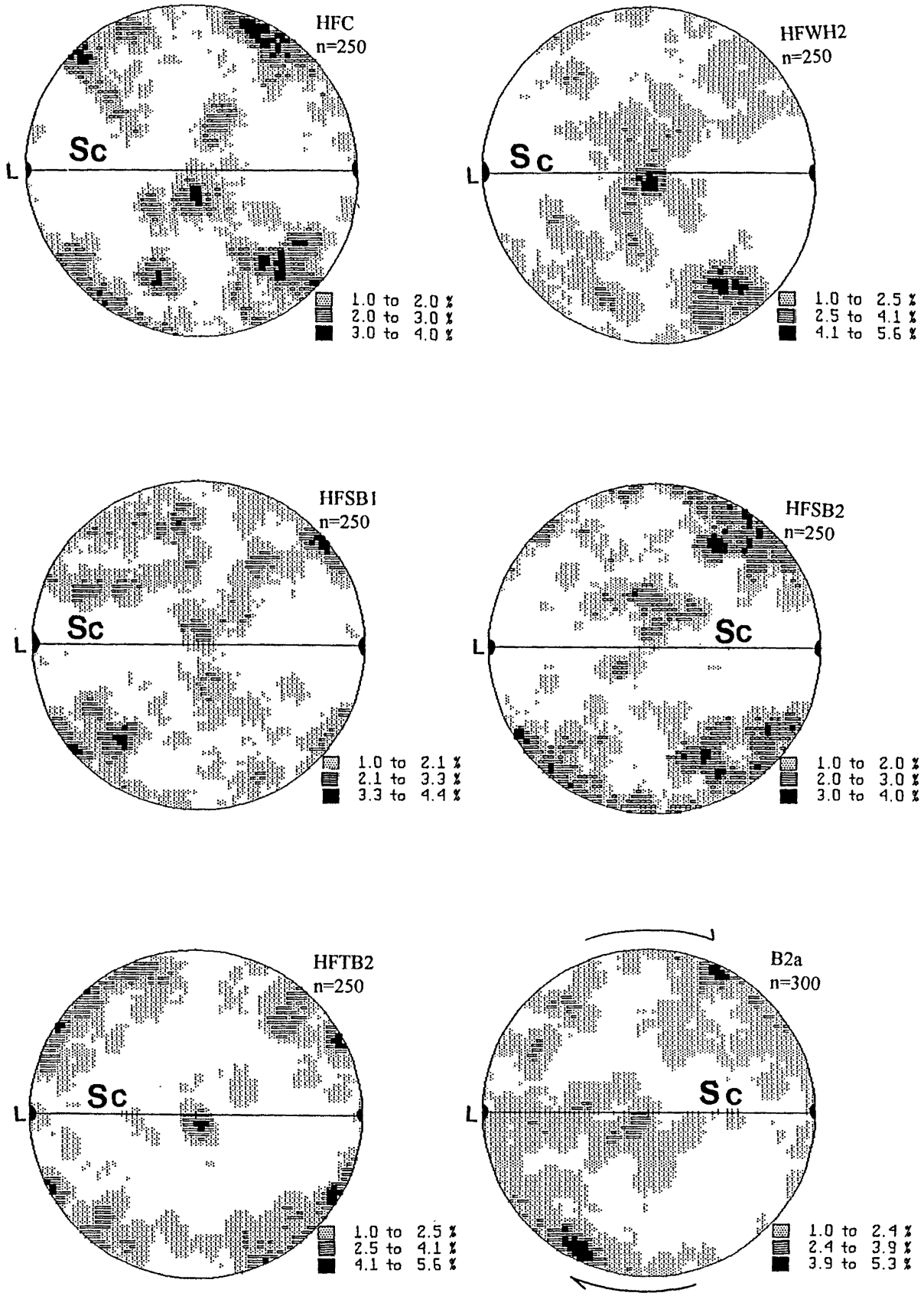

Fig 7.3 Contoured lower hemisphere equal area projections of quartz c-axis orientations from hornfelsic-type lithologies. HFC, HFWH2 and HFTB2 are viewed towards the NW; HFSB1 viewed towards the NNW, and HFSB2 and B2a viewed towards the SW. Sc=schistosity, L=lineation; bold arrow indicates shear-sense.

CHAPTER EIGHT

THE ORIGIN OF TRUE AND APPARENT SHEAR REVERSALS

8.1 Introduction

Examination of quartz c-axis fabrics and microstructures from the mylonitic rocks in the study area has established dominant senses of shear (Chapter 3). However, there are seemingly real reversals in shear-sense where an older generation of C-S planes are overprinted by a younger generation with an opposing sense of shear. These shear-sense reversals complicate the simple core complex model proposed by Tulloch and Kinbrough (1989). Reversals in shear-sense are recorded in the SBMZ and Tauranga Bay monzogranitic gneiss where top-to-the-NE/ENE C-S planes are overprinted by younger top-to-the-SW/WSW C-S planes, and near the mouth of the Four Mile River where top-to-the-SW C-S planes are overprinted by top-to-the-NE C-S planes. True shear reversals are also found in the mylonitized migmatites south of White Horse Creek where top-to-the-NE fabric elements are overprinted by top-to-the-SW fabrics, and top-to-the-NW/NNW fabric elements are overprinted by top-to-the-SE/SSE fabric elements. Shear reversals on a somewhat larger scale are found on opposite sides of the Charleston and Parsons Hill Arches. A summary of these shear reversals is given in Fig 8.1.

In addition to real reversals in shear-sense, some mylonites possess asymmetric quartz c-axis fabrics which seem to give opposing senses of shear when compared to microstructures in thin section. Such apparent shear reversals are found in the MCMZ and DCMZ where apparent top-to-the-NE quartz c-axis fabrics contradict top-to-the-SW shear-sense microstructures found in thin section. Samples DC5 and R20 from the DCMZ possess dubious quartz fabrics possibly suggesting a top-to-the-NE sense of shear, rather than a top-to-the-SW sense of shear recorded by other fabric elements (C-, S- and C′-planes, oblique quartz shape-preferred orientations). Due to the dubious character of the quartz c-axis fabrics, DC5 and R20 have been omitted from this discussion.

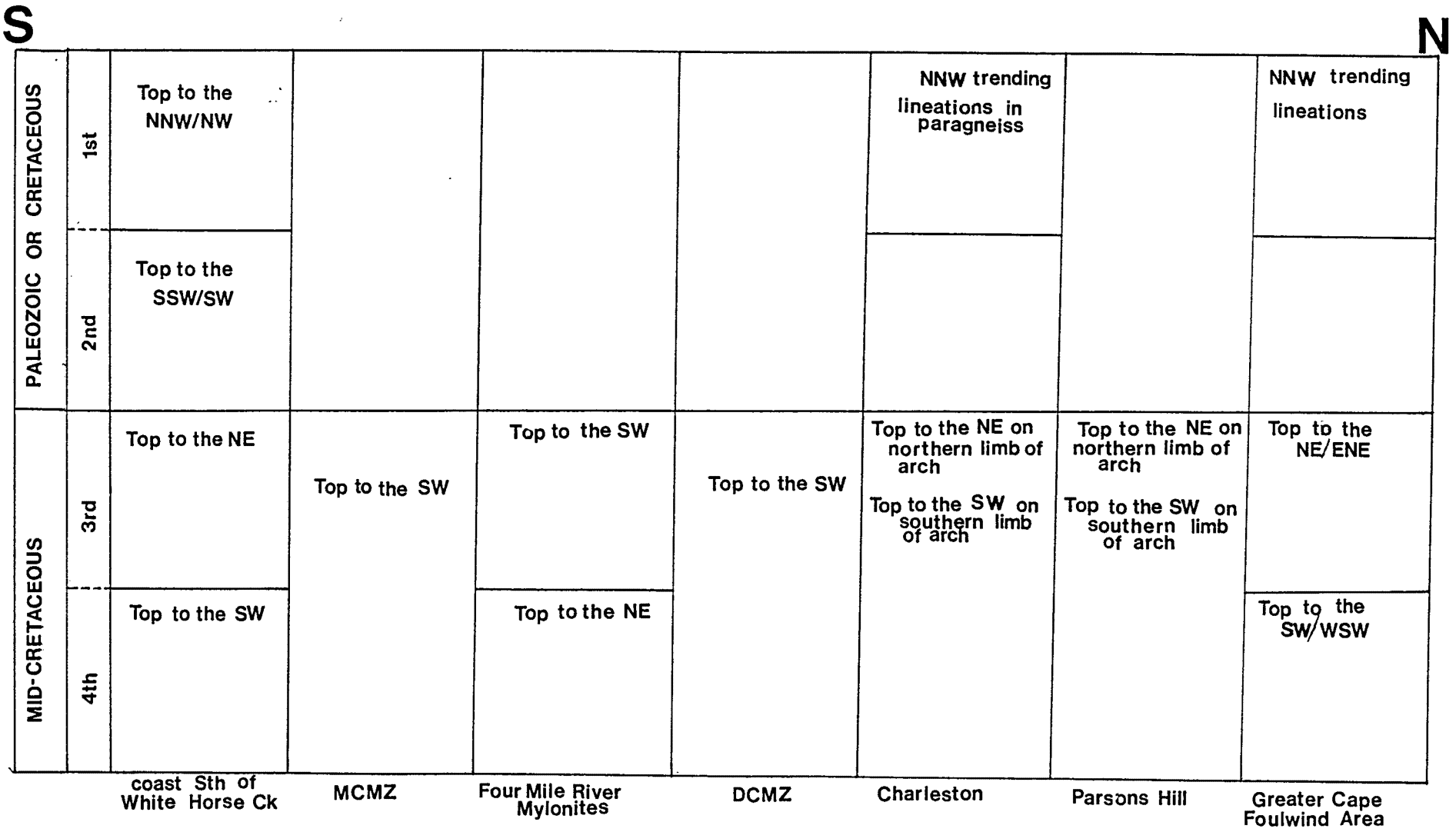

Fig. 8.1 Summary of shear-sense reversals from the coast south of White Horse Creek to Cape Foulwind.

8.2 True Reversals in Shear-sense

8.2.1 Shear reversals in the Tauranga Bay monzogranitic gneiss, SBMZ, Four Mile River mylonites and mylonitized migmatites south of White Horse Creek.

The Tauranga Bay monzogranitic gneiss and mylonites in the SBMZ record true shear reversals. Gross fabric elements in outcrop record a top-to-the-NE/ENE sense of shear. However, in Tauranga Bay, the S-planes associated with the top-to-the-NE/ENE movement have become folded and kinked by the development of 'new' top-to-the-SW/WSW C-S planes. Folding and kinking of 'old' S-planes (Fig. 5.2B and C) suggests that $\sigma 1$ changed in orientation during deformation and that the reversal in shear-sense is genuine. The 'new' C-planes lie along planes sub-parallel to the 'old' S-planes. The same reversal is recorded in the Siberia Bay mylonites where reactivated C-, S and C′-planes and oblique quartz shape-preferred orientations record a top-to-the-SW/WSW sense of shear.

Overprinting of top-to-the-NE/ENE C-S planes and porphyroclast systems by top-to-the-SW/WSW C-S planes and oblique quartz shape-preferred orientations also occur in mylonitized migmatites south of White Horse Creek. In thin section, S-planes associated with top-to-the-NE movements are folded by top-to-the-SW fabric elements. Near the mouth of the Four Mile River a similar scenario occurs, although in this case, recrystallized top-to-the SW C-S planes of mica are deformed by later-developed top-to-the-NE C-S planes.

The change in shear-sense from top-to-the-NE/ENE to top-to-the-SW/WSW in the Tauranga Bay monzogranitic gneiss, SBMZ, and migmatites south of White Horse Creek; and from top-to-the-SW to top-to-the-NE near the mouth of the Four Mile River may possibly be explained in a number of ways. These include overprinting of top-to-the-NE/ENE fabrics associated with top-to-the-NE detachments by fabrics associated with the top-to-the-SW Pike Detachment Fault, the development of broad zones of antithetic shearing or development of conjugate planes of shearing which become flattened with progressive deformation.

Overprinting of shear-sense indicators associated with the Ohika Detachment by indicators associated with the Pike Detachment and the possible development of a third southern detachment.

The reversal in shear-sense from top-to-the-NE/ENE to top-to-the-SW/WSW in the Tauranga Bay monzogranitic gneiss, top-to-the-NE to top-to-the-SW mylonitized migmatites south of White Horse Creek, and the shear reversal from top-to-the-NE/ENE to top-to-the-SW/WSW in the SBMZ may be associated with the relative timing and dominance of the overlying detachment faults. According to Tulloch and Palmer (1990), K-Ar dating of sericite from an altered granite along the Ohika Detachment Fault yielded an age of 98 Ma while sericite from a similar rock underlying the Pike Detachment Fault yielded a significantly younger age of 85 Ma. This suggests that movement along the Pike Detachment continued for some time after the cessation of the movement associated with the Ohika Detachment.

Top-to-the-NE/ENE mylonitization in the SBMZ and at the south Tauranga Bay headland may be attributed to movement of the overlying Ohika Detachment Fault. When the ductile deformation associated with the Ohika Detachment Fault ceased, ductile deformation associated with the Pike Detachment Fault continued, overprinting top-to-the-NE/ENE fabrics in the SBMZ and Tauranga Bay with top-to-the-SW fabrics. A similar scenario can perhaps be advocated to explain the overprinting of top-to-the-NE fabric elements by top-to-the-SW fabric elements south of White Horse Creek. Top-to-the-NE fabric elements at this locality may possibly record the development of an early third detachment zone, situated south of White Horse Creek. Top-to-the-SW fabric elements which overprint top-to-the-NE fabric elements may simply represent to progressive development and eventual dominance of the Pike Detachment over detachments associated with a top-to-the-NE movements with time.

The development of broad antithetic shear zones

Top-to-the-NE/ENE senses of shear in the SBMZ and in the Tauranga Bay monzogranitic gneiss may be due to the development of a broad zone of antithetic shearing on a back-dipping mylonite zone. Reynolds and Lister (1990; Fig 8.2) propose that mylonite zones associated with core complexes are folded so that on one side of the core complex, mylonitic fabrics and the overlying detachment dips gently in the direction of upper plate transport and on the opposite side, the mylonite zone rolls over to dip in the opposite direction of upper plate transport. This folding is accompanied by the development of antithetic shear zones.

When applying Reynolds and Lister's model (Fig. 8.2), top-to-the-SW senses of shear on the northeastern side of the core complex become related to the movement of the overlying plate and top-to-the-NE/ENE shearing is explained by movement associated with an antithetic shear zone. This model requires the overlying Ohika Detachment Fault to record a top-to-the-SW sense of shear and overlying cover of the upper plate on both sides of the core complex to dip in the same direction (Fig. 8.2). According to Tulloch and Kimbrough (1989) the Ohika Detachment Fault records a top-to-the-NE sense of shear and the overlying cover (Pororari Group) dips in opposite directions, toward the axis of the core complex, on opposite sides of the core complex.

Development of conjugate C′-planes which become flattened with time

The reversals in shear-sense recorded in the Siberia Bay mylonites, Tauranga Bay monzogranitic gneiss, mylonitized migmatites south of White Horse Creek and mylonites near the mouth of the Four Mile River may simply record a combination of shear-senses developed during core complex formation and/or development near the axis of the Paparoa Metamorphic Core Complex.

Semi-ductile deformation of rocks undergoing opposing senses of shear on opposite sides of the complex is potentially, at least, extremely complicated. Development of conjugate C′-planes may be expected, each recording opposing senses of shear, synthetic to the gross foliation. Flattening of the conjugate planes of shearing with a progressive

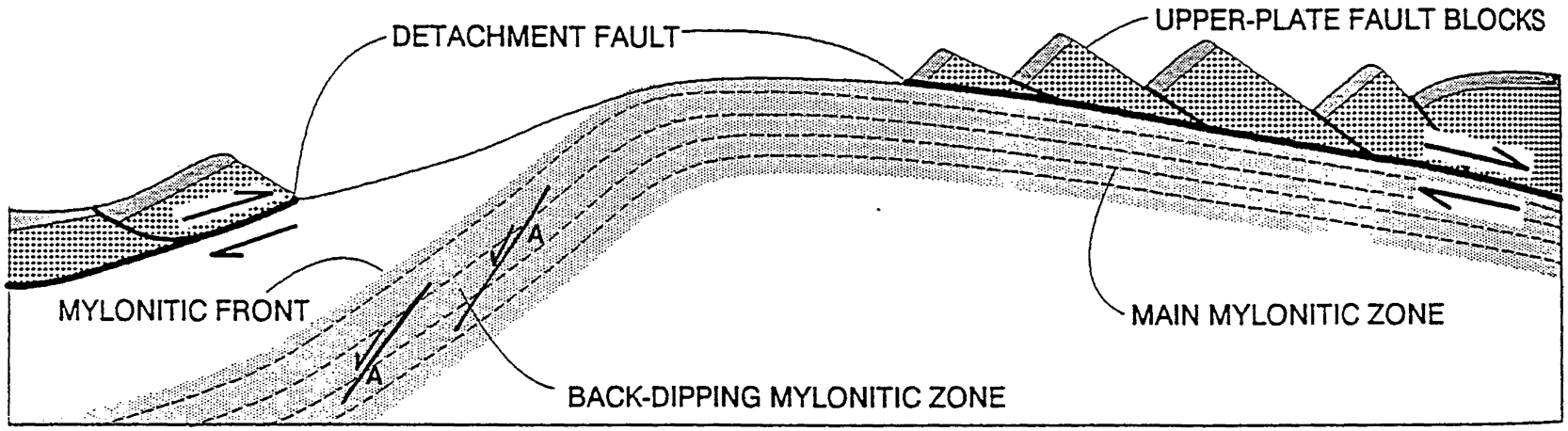

Fig. 8.2. A model for core complex development after Reynolds and Lister (1990) based on the development of a back-dipping mylonite zone and antithetic shear zones (A).

coaxial deformation may produce opposing senses of shear, on the similar apparent planes of shearing (Fig. 8.3). Opposing senses of shear such as those recorded in the SBMZ, Tauranga Bay monzogranitic gneiss and mylonitized migmatites south of White Horse Creek, may record the development of an early C′-planes, associated with a top-to-the-NE or NE/ENE sense of shear overprinted by a later C′-plane associated with a top-to-the-SW or SW/WSW sense of shear. Progressive flattening of both the C′-planes during a progressive coaxial deformation may have then resulted in the C′-planes lying within similar planes of shearing. The reversal of shear-sense from top-to-the-SW to top-to-the-NE recorded by mylonites near the mouth of the Four Mile River may record a similar scenario. However, in this case, C′-planes associated with top-to-the-SW shearing have been overprinted by C′-planes associated with top-to-the-NE shearing.

The development of conjugate C′-planes which become flattened with progressive deformation is particularly appealing in the case of the Tauranga Bay monzogranitic gneiss and the SBMZ which, according to the model proposed by Tulloch and Kimbrough (1989), lie close to the axis of the core complex. Close proximity to the core complex axis accounts for the static recrystallization of mica and quartz within these rocks. Development of conjugate C′-planes is further supported by the difference in dip between 'old' and 'new' C-S planes in sample TB5: the 'new' C-plane is nearly parallel to the 'old' S-plane.

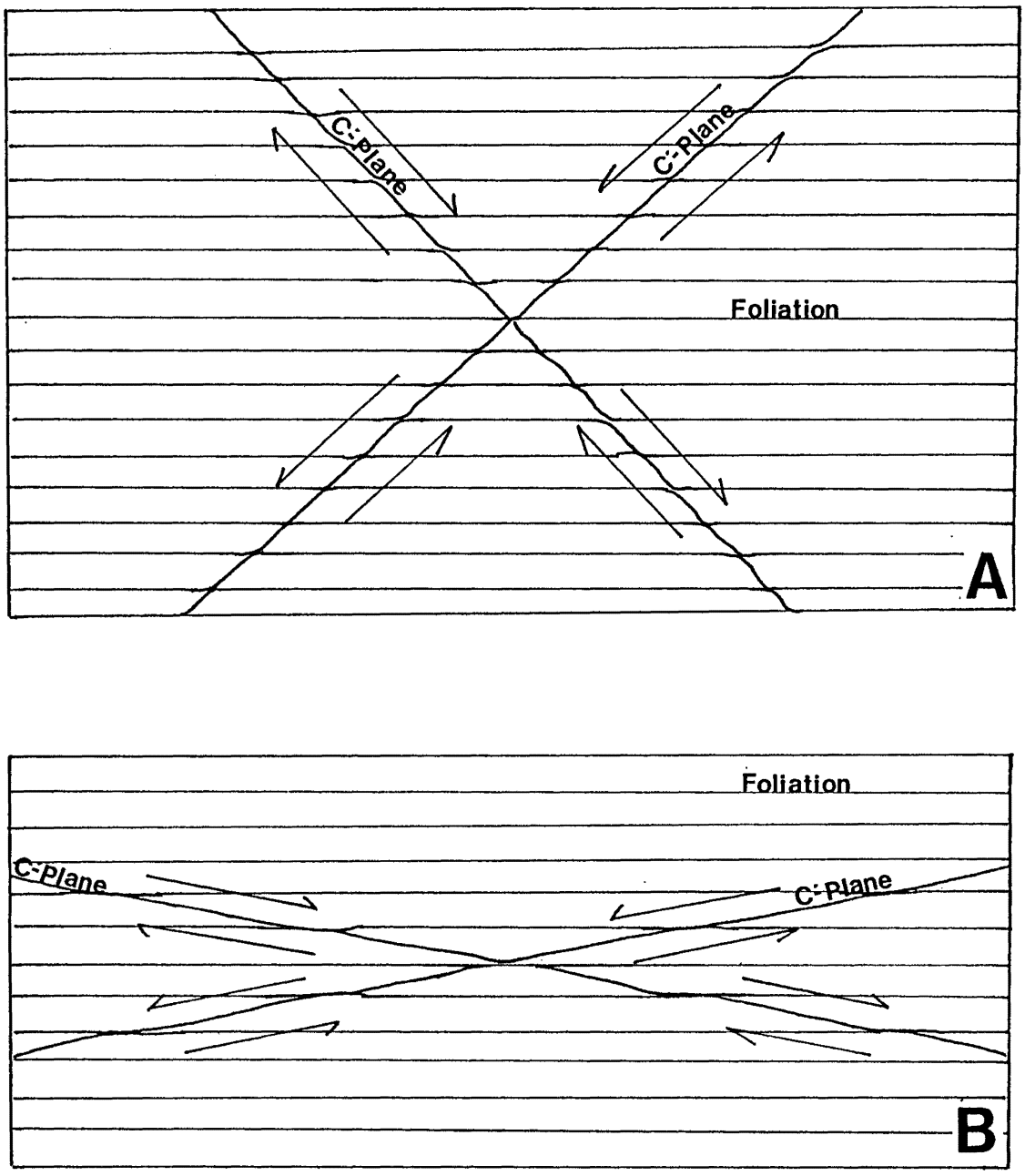

Fig. 8.3 Reversals in shear-sense due to the progressive flattening of conjugate shear planes (C′-planes). A) conjugate shears initiated at a high angle to the foliation, B) conjugate shears after flattening lying sub-parallel to the foliation.

South of White Horse Creek, NW/NNW-trending lineations which record a top-to-the-NW/NNW sense of shear are overprinted by later-developed top-to-the-SE/SSE fabric elements. The NW/NNW-trend of such lineations is inconsistent with the NNE-SSW extension direction proposed for core complex formation by Tulloch and Kimbrough (1989) and timing of NNW/NW-trending fabric elements is discussed in section 6.6. Although the relationship of NW/NNW-trending structures to Cretaceous core complex development is uncertain, the shear reversal of top-to-the-NNW/NW to top-to-the-SE/SSE recorded by fabric elements in thin section may possibly be attributed to the overprinting of conjugate planes of shearing.

8.2.2 Shear Reversals associated with the Uprise of Magma.

Intrusion of granodioritic, tonalitic and granitic magmas along WNW-ESE lines near Charleston and Parsons Hill has formed WNW-ESE-trending arches of the foliation at these localities. On the NNE limb of the Charleston and Parsons Hill arches, granitic and granodioritic gneisses record a top-to-the-NE sense of shear, while on the SSW limbs, the gneisses record top-to-the-SW senses of shear.

Brun and van den Driessche (1994) suggest that strain patterns directly related to the detachment zone in core complexes must be distinguished from strain patterns associated with gneiss domes underlying the detachment zone. According to Brun and van den Driessche (1994) detachment-related mylonitization within the ductile non-molten crust is characterised by the development of extensional C′-planes. However, in the dome-shaped core of the core complex, development of C-S planes which lack associated C′-planes suggests a retrograde path from high to medium temperatures as commonly observed in syn-tectonic granites.

The presence of C-S planes and absence of well developed C′-planes in the granitic gneiss near Charleston suggests deformation of the granitoids during a change from high temperatures to moderate temperatures as the magma cooled (Brun and van den Driessche 1994). The presence of broad C′-planes on the south side of Parsons Hill records deformation of a slightly lower temperature. However, the broad C′-planes record a top-

to-the-SW sense of shear on the SW side of the Parsons Hill arch and are considered to be a consequence of the uprise of magma at Parsons Hill. Granodioritic magma at Parsons Hill may have intruded at a slightly later stage than the two-mica granite and tonalitic magmas at Charleston.

Opposing senses of shear on opposite limbs of the Charleston and Parsons Hill arches implies that the intrusion of magma is intimately associated with ductile deformation of the lower plate during core complex development and that shear-senses associated with such arches may not neceassarily simply be attributed to the movement of the overlying detachment faults.

8.2.3 Summary of True Shear Reversals

C-, S- and C′-planes recording a top-to-the-NE/ENE sense of shear have been overprinted by top-to-the-SW/WSW fabrics in the Tauranga Bay monzogranitic gneiss and SBMZ. Mylonitzed migmatites south of White Horse Creek contain top-to-the-NE shear-sense indicators overprinted by top-to-the-SW. These record a true reversals in shear-sense and may be attributed to the overprinting of fabrics associated with movement on top-to-the-NE detachment faults by fabrics associated with movement on the top-to-the-SSW Pike Detachment Fault. Alternatively, the shear-sense reversals may be due to the development of conjugate, but temporally distinct C′-planes which became flattened with progressive coaxial deformation.

Opposing senses of shear on opposite limbs of the Charleston and Parson Hill arches may be attributed to the uprise of magma along WNW-ESE lines.

8.3 Apparent Reversals in Shear-sense

Quartz c-axis fabrics that record anomalous senses of shear occur in the MCMZ and DCMZ where apparent top-to-the-NE quartz c-axis fabrics contradict top-to-the-SW shear-sense indicators found in thin section. Quartz fabrics recording anomalous senses of

shear are not restricted to any particular type of mylonite, but occur in fine-grained dynamically recrystallized mylonites (WH42 and WH231), coarse-grained recrystallized mylonites (WH38, WH36 and WH35), and mylonites rich in feldspar (DC3). The quartz fabrics which show top-to-the-NE senses of shear are either type I crossed girdles (WH231 and DC3; Figs. 3.10 and 3.13) or single girdles (WH38, WH36, WH35, WH42; Figs. 3.10 and 3.11).

In the MCMZ and DCMZ quartz c-axis fabrics that appear to record a top-to-the-NE sense of shear may have a range of origins. Many quartz c-axis fabrics in the literature are measured in mylonites which contain a high percentage of quartz. Fabric development in mylonites containing abundant mica and feldspar are more poorly studied. Schmid and Casey (1986) suggest that the presence of more than one mineral in a mylonite may disperse the c-axis preferred orientation of quartz. However, the c-axis fabrics recording anomalous senses of shear show definite asymmetric girdles. In addition, MC2, a deformed leucogranite which contains approx. 50% feldspar exhibits a moderately well defined asymmetric type I crossed girdle with a top-to-the-SW sense of shear (Fig. 3.10). This suggests that the presence of rigid grains alone is not enough to significantly disperse quartz c-axis fabrics.

Alternatively, the single girdles may represent the reorientation of quartz c-axes during a late stage deformation (Brunel 1980; Lister and Price 1978) or a heterogeneous simple shear. These two suggestions are now discussed further.

8.3.1 Quartz c-axis Reorientation during a Late-stage Deformation.

If the quartz fabrics recording a top-to-the-NE sense of shear are a result of a late stage deformation, the single girdles could represent a change from simple shear to pure shear during which $\sigma 1$ remained constant in orientation. This would produce a single girdle of c-axes with an apparent opposite sense of asymmetry when compared to fabric elements such as C-, S- and C′-planes, porphyroclast systems and oblique quartz shape-preferred foliations (Fig. 8.4). Coarse grained mylonites WH38, WH36 and WH35 are spatially associated with numerous syn- and post-tectonic pegmatites. Pegmatite intrusion may

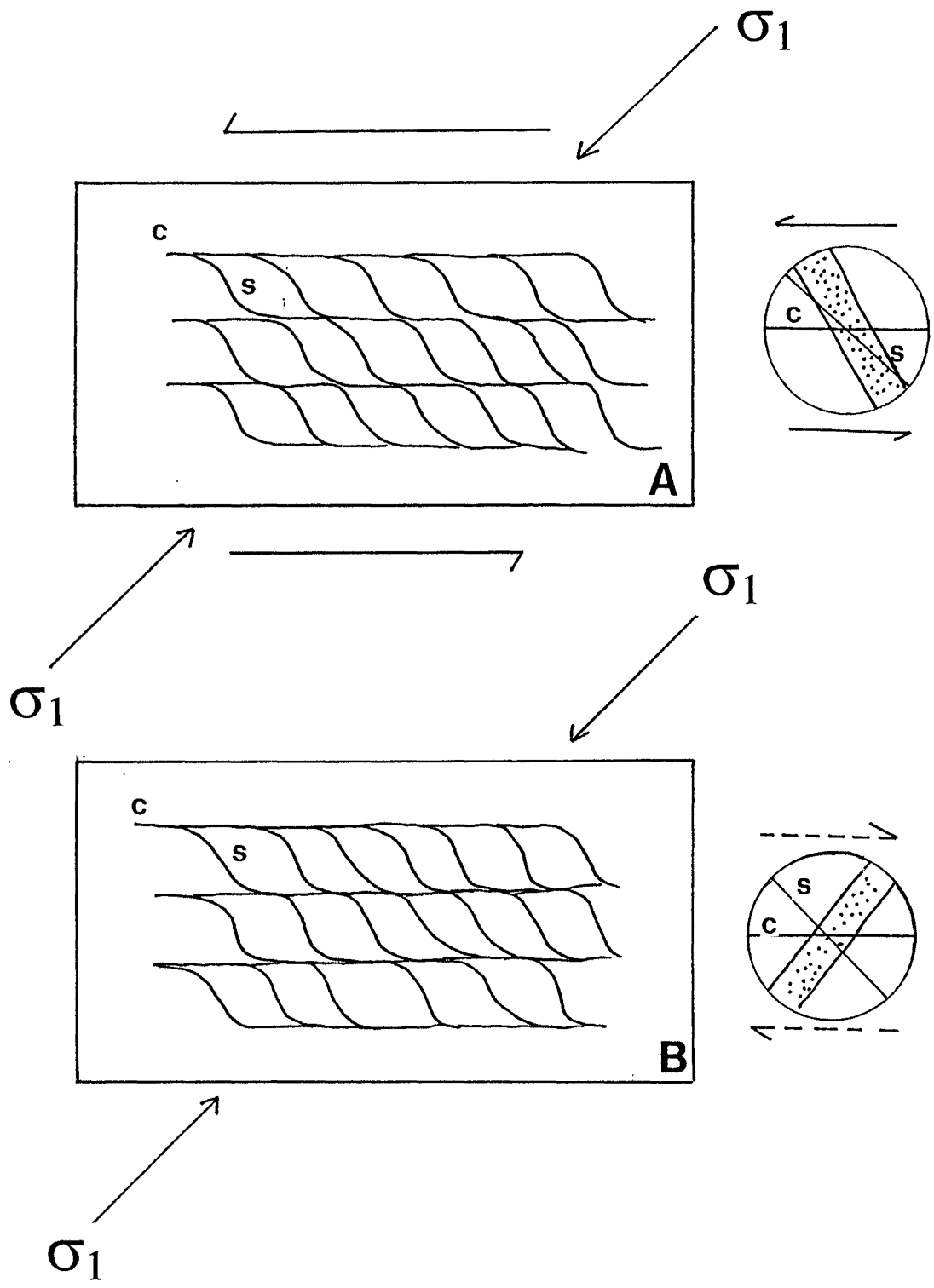

Fig. 8.4 Diagrammatic representation of a pure shear overprint on a simple shear. A) C-S planes and quartz c-axis fabric developed during simple shear (bold arrows=true shear-sense). B) pure shear overprint on simple shear and rotation of quartz c-axes (broken arrow=apparent shear-sense). Note that C-S planes from previous simple shear retained.

have softened the surrounding mylonites enabling the recrystallization of mica and plastic deformation of quartz to continue to a late stage.

One cannot attribute the c-axis fabric asymmetrys shown by WH38, WH36 and WH35 to a switching of simple shear from top-to-the-SW to top-to-the-NE because the single girdles lack an internal asymmetry, no fabric elements except quartz c-axes are reoriented, and buckling of older S-planes, which might be expected, does not occur.

8.3.2 Heterogeneous Simple Shear

The single c-axis girdles may simply record a partitioning of deformation into simple shear along the C-planes and pure shear along the S-planes (Fig. 8.5A). In this scenario, quartz ribbons or grains aligned along the S-plane would undergo a coaxial deformation rather than a simple shear.

Two mylonites which record a top-to-the-SW sense of shear, consistent with shear-sense indicators in thin section record a weak partitioning of strain into C- and S-planes. MC5 is a dynamically recrystallized vein of quartz which contains a well defined single girdle c-axis fabric (Fig. 3.10). MC5 differs from mylonites displaying top-to-the-NE senses of shear in that the dynamically recrystallized quartz in MC5 displays no clear S-plane development but does possess a foliation defined by muscovite flecks which parallels the C-plane of surrounding mylonites. MC2, a mylonitized leucogranite possesses a type I crossed girdle which shows a clear top-to-the-SW sense of shear (Fig. 3.10). In thin section, the partitioning of strain into S- and C-planes is complicated by the presence of large feldspar porphyroclasts and quartz ribbons are aligned along both S- and C-planes.

C-planes in sample WH42 are defined by a concentration of cataclased mica and a lack of quartz (Fig 8.5B). Measurement of c-axes in WH42 preferentially sampled quartz aligned along S-planes rather than C-planes. Strain partitioning of pure shear along the S-plane can therefore be invoked to explain the quartz c-axis fabric of WH42.

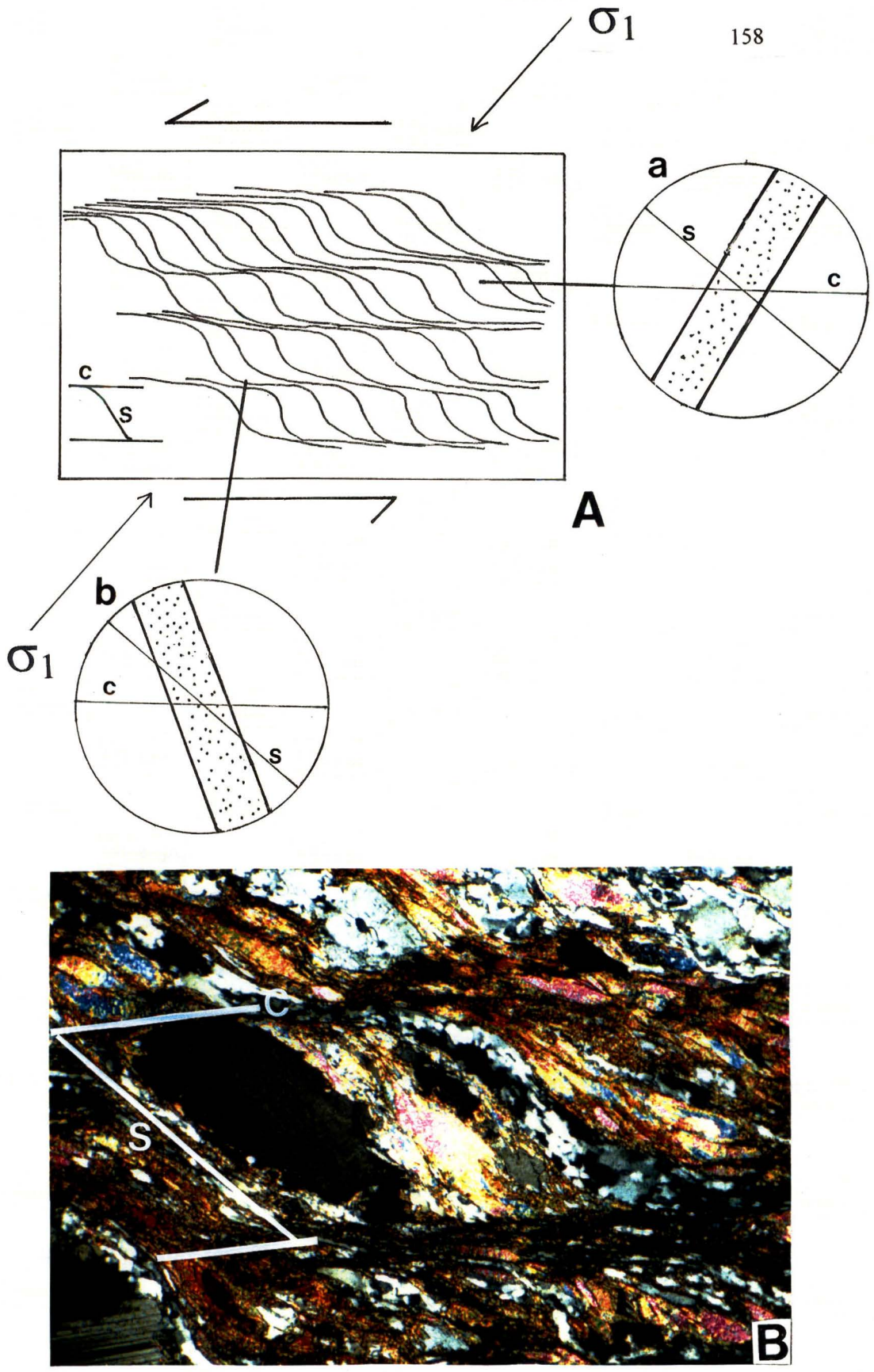

Fig. 8.5. A) Diagrammatic representation of a partitioning of deformation into simple shear along the C-planes and a pure shear along the S-planes. Quartz fabrics preferentially measured from S-plane (a) give the apparent opposite sense of asymmetry to those measured from the C-plane (b).

B) Sample WH42 showing preference of quartz to lie along the S-plane (discussed further in text); crossed polarised light; viewed to the NW; view across=2.9 mm.

However, coarse-grained mylonites WH35, WH36 and WH38 do not show such a clear relationship between quartz aligned along the S-plane and anomalous c-axis girdles. Although some pods of quartz which lie along the S-plane in these samples show a crystallographic preferred orientation consistent with a top-to-the-NE sense of shear, quartz ribbons lying along the C-planes show the same c-axis preferred orientation. It is therefore difficult to invoke a simple strain partitioning to explain the quartz c-axis fabrics.

The apparent top-to-the-NE shear-sense recorded by asymmetric quartz c-axis fabrics in the coarse grained mylonites, which contain microstructures possessing a top-to-the-SW sense of shear, can be attributed to a late stage change in the deformation regime from simple shear to pure shear rather than strain partitioning along C-S planes.

Samples DC3 from the DCMZ and WH231 from the MCMZ display asymmetric type I crossed girdles which appear to record a top-to-the-NE sense of shear (Figs. 3.10 and 3.13), while fabric elements in thin section record a top-to-the-SW sense of shear. Quartz ribbons in DC3 and WH231 do not show any preference to lie along S-plane rather than the C-plane and the fabrics cannot be attributed to the preferential sampling of quartz that has undergone a pure shear along the S-planes. In addition, the internal asymmetry exhibited in the quartz c-axis fabric of DC3 suggests that this fabric is not due to a late pure shear.

Switching of the shear direction from top-to-the-SW to top-to-the-NE cannot be invoked to explain the asymmetric type I crossed girdles because no other fabric elements have been affected and S-planes show no evidence of kinking or folding.

8.3.3 Summary of Apparent Shear Reversals

Quartz c-axis fabrics that record a top-to-the-NE sense of shear in the MCMZ conflict with top-to-the-SW C-, S-, and C′-planes, oblique quartz shape-preferred orientations and porphyroclast systems in thin section. The top-to-the-NE senses of shear are only apparent shear-reversals and can be attributed to a late pure shear overprint in coarse-grained

recrystallized mylonites, and to the partitioning of simple shear into pure shear (S-planes) and simple shear (C-planes) in sample WH42. The origin of asymmetric type I crossed girdles which record a top-to-the-NE sense of shear (DC3 and WH231) remains unresolved.

CHAPTER NINE

DISCUSSION

9.1 Evidence for mid-Cretaceous Crustal Extension

Microscopic structures such as boudinage, the development of C-, S- and C′-planes and porphyroclast systems are not necessarily indicative of an extensional tectonic setting. All microscopic and macroscopic structures found in the Charleston Metamorphic Group can be found in orogens undergoing compression. However, several independent lines of evidence which indicate regional and sometimes local NNE to ENE oriented extension, and the fact that senses of shear within the Charleston Metamorphic Group are down-dip and that the foliation is subhorizontal are most easily explained in terms of extension in the Western Province during the mid-Cretaceous. These issues are discussed further in the following sections.

9.1.1 Down-dip or 'normal' senses of shear

SW-dipping foliation in the MCMZ contains shear-sense indicators which show a top-down-to-the-SW sense of shear. This normal sense of shear is most easily reconciled with extension. Normal senses of displacement are also recorded on both sides of the Charleston and Parsons Hill arches such that the ENE dipping limbs contain top-to-the-NE shear-sense indicators and WSW-dipping limbs contain indicators recording a top-to-the-SW senses of shear. Although the analysis of shear-sense associated with extensional gneiss domes must be treated separately from the kinematics of the detachment zone (Brun and van den Driessche 1994), the normal senses of shear on either sides of the Charleston and Parsons Hill arches indicate a localised extension associated with the uprise of magma.

In the southern Paparoa Range, low grade metasedimentary rocks of the Greenland Group are juxtaposed on top of high grade metamorphic rocks along the Pike Detachment

Fault. According to Tulloch and Kimbrough (1989) the Pike Detachment Fault dips to the SSW and is associated with top-down-to-the-SSW fabrics in the mylonitic basement. In the Buller Gorge, the Ohika Detachment Fault dips to the NE and mylonitized basement below the fault contains top-down-to-the-NE shear-sense indicators (Tulloch and Kimbrough 1989). Both detachment faults record normal senses of shear, which are most readily interpretable in terms of a regional extensional tectonic setting.

9.1.2 Development of other Cretaceous Core Complexes in New Zealand

Core complexes recording a mid Cretaceous extensional event are found in deeper crustal high grade gneisses exposed east of the Alpine Fault in Fiordland. According to Gibson et al (1988) the stretching lineation in one such core complex trends NE-SW, parallel to the predominant stretching lineation in the Charleston Metamorphic Group exposed at Cape Foulwind and the greater Charleston area.

9.1.3 WNW-ESE-trending sedimentary basins

Laird (1994) describes WNW-ESE-trending fault-bounded half-graben sedimentary basins which formed between 100 and 105 Ma. WNW-ESE extensional half-grabens are orientated parallel to the future spreading axis in the Tasman Sea. These fault-bounded basins are infilled with Pororari Group sediments (non-marine carbonaceous mudstone, vitric tuffs and sandstone overlain by a coarse breccia-conglomerate). Evidence of rapid uplift of the crystalline lower plate is recorded in the Pororari Group by an upward change of clast composition from predominantly Greenland Group to a mixture of Greenland Group and two-mica granite (probably from the extensive Buckland Granite) (Muir et al 1994b).

SHRIMP zircon dating of the volcanogenic sediments (Stitts Tuff member) at the base of the Pororari Group has yielded an age of 101 Ma (Muir. pers. comm). This implies that the extensional half-grabens of the upper plate were forming by 101 Ma.

In addition to a 100-105 Ma extensional event, Laird (1994) also proposed that a separate extensional event took place between 95 and 100 Ma, based on dates from the West Coast and Tasman Sea that show a noticeable peak at this time. This was followed by initiation of sea floor spreading and the formation of the Tasman Sea at about 82 Ma which continued until 60 Ma (Laird 1994).

9.1.4 Emplacement of an A-type Granite

The French Creek Granite, exposed in the Hohonu Range possesses an A-type geochemistry consistent with emplacement during an extensional tectonic setting (Tulloch et al 1994). A conventional U-Pb zircon age of 83 Ma and a zircon SHRIMP age of 81.7 Ma (Waight pers. comm) suggests the French Creek Granite was emplaced at the same time as the initiation of sea floor spreading in the Tasman Seas and the separation of New Zealand from Australia at c. 82 Ma (Weissel and Hayes 1977).

9.1.5 Intrusion of Alkali-lamprophyre dykes

Alkali-lamprophyre dykes are exposed in the lower Buller Gorge and in the Hohonu Range. The dykes trend WNW-ESE, at right angles and consisitent therefore to the regional extension direction proposed by Tulloch and Kimbrough (1989). K-Ar whole rock analyses by Adams and Nathan (1978) on undeformed lamprophyre dykes in the Buller Gorge obtained ages of 80-86 Ma. Field evidence from the Hohonu Batholith indicates emplacement of similar alkali-lamprophyre dykes preceding and contemporaneous with the 81.7 Ma French Creek Granite (Waight 1995).

9.2 Paleozoic events and the mid-Cretaceous development of the Paparoa Metamorphic Core Complex

9.2.1 Paleozoic Events

The earliest event recorded in the study area is the migmatization of the Greenland Group. Rb-Sr geochronology of the Greenland Group by Adams (1975a) attained an age of 495 ± 11 Ma for sedimentation of the Greenland Group, which is supported by the presence of lower Ordovician graptolites (Cooper 1974). Ion microprobe analysis of paragneiss zircons near Charleston reveals the youngest zircon rims to be 380-400 Ma or late Silurian/early Devonian in age (Ireland 1992). Presuming the gneisses and associated migmatites represent metamorphosed Greenland Group, this age indicates migmatization of the Greenland Group may have occurred in the lower-Devonian. Additional evidence for metamorphism at this time is provided by K-Ar ages of the Greenland Group greywackes in the Paparoa Range which apparently record two thermal episodes at 298-370 Ma and 395-438 Ma (Adams et al 1974).

Alternatively, the migmatites may have formed during Cretaceous core complex development. However, if this were the case, one would expect zircon rims of mid-Cretaceous rather than Paleozoic age. Migmatization of the Greenland Group, therefore, probably accompanied the emplacement of Devonian Karamea Suite granitoids such as the O'Sullivans granite at 377.7 ± 4.1 Ma (Muir et al 1994a), which comprises a large part of the Karamea Batholith. Possible Paleozoic events recorded in the study area are summarised in Fig. 9.1.

Devonian granitic activity was followed by the early Carboniferous emplacement of the Cape Foulwind monzogranite (327.3 ± 6.2 Ma, Muir et al 1994a), probably the Tauranga Bay monzogranite and, in the Buller Gorge, the Windy Point Granite (328.6 ± 4.4 Ma, Muir et al 1994a). The early Carboniferous granitoids were intruded immediately prior to,

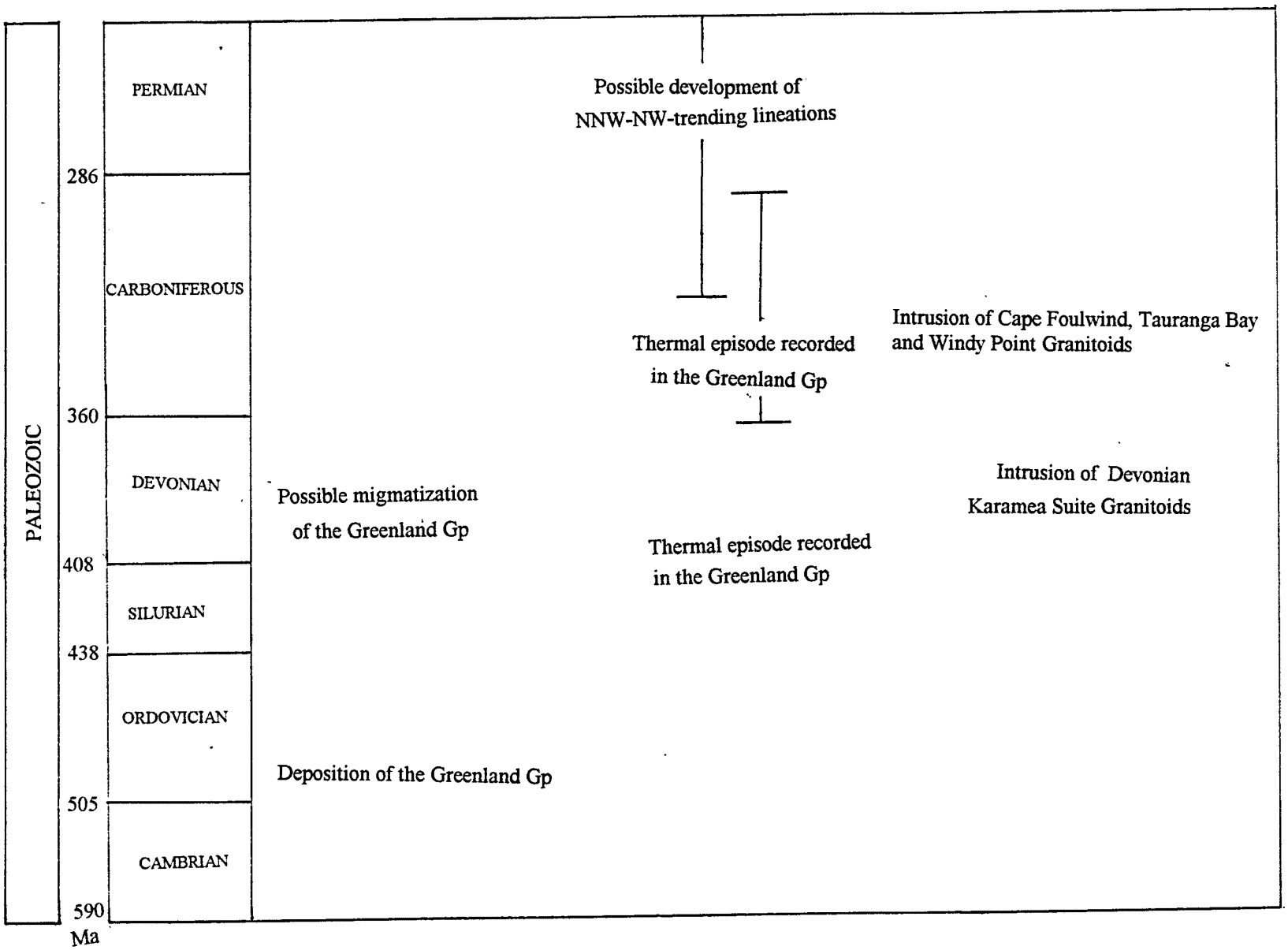

Fig. 9.1 Summary of Paleozoic events recorded in study area.

or during tectonism which appears to be recorded in the Cape Foulwind monzogranite and Tauranga Bay monzogranite as a combined magmatic and solid-state foliation.

9.2.2 The Timing of NNW-SSE and NW-SE-trending Lineations

NNW-SSE-trending lineations occur at Siberia Point near Cape Foulwind where they are associated with a magmatic-solid state foliation. Shelley (1972) also noted NNW-SSE lineations in the Tauranga Bay monzogranitic gneiss. However, NNW-SSE lineations are not recorded in the Siberia Bay syenogranite-monzogranite which is variably mylonitized, or undeformed. Around Charleston, NNW-SSE trending lineations are present in migmatites of sedimentary origin on cliffs below the Charleston Cemetery, but absent from the neighbouring Charleston orthogneiss lithologies. South of White Horse Creek, NNW-SSE and NW-SE-trending lineations are dominant and appear to pre-date the Cretaceous NE-SW-trending lineations.

NNW-SSE lineations at Cape Foulwind and in the migmatites at Charleston are of uncertain age. Potentially, at least, the lineations may be of Carboniferous age, Cretaceous age or any age intermediate between the emplacement of the Cape Foulwind monzogranite and the development of the later NE-SW-trending lineations. However, little evidence is recorded in the Buller Terrane for significant deformational events post dating intrusion of the Cape Foulwind granitoid at 327.3 ± 6.2 Ma (Muir et al 1994a) and predating the early Cretaceous. The possibility of the Carboniferous or Cretaceous development of NNW-SSE and NW-SE lineations is outlined in the following discussion.

Cretaceous development of NNW-SSE and NW-SE-trending lineations

The NNW-SSE trending lineations may be of Cretaceous age predating the intrusion of granitic, tonalitic and granodioritic magmas at Charleston, syenogranitic-monzogranitic magmas in Siberia Bay, and the main body of Red Jacket Granite south of White Horse Creek. However, it is also possible that NNW-SSE trending lineations may have post-dated the intrusion of these magmas but been destroyed by a later mobilisation of the granitic gneisses during the pervasive deformation associated with later NE-SW lineations. In the latter scenario, NNW-SSE and NW-SE-trending lineations may simply be preserved

in the migmatites of sedimentary origin due to their more refractory nature. Strain during this Cretaceous event may have been initially taken up along the pre-existing magmatic-solid state foliation in the monzogranite at Cape Foulwind.

Top-to-the-NW/NNW senses of shear recorded in mylonitized migmatities south of White Horse Creek may possibly be of Cretaceous age, perhaps recording a reverse shearing associated with plate convergence which pre-dates NE-SW-directed Cretaceous extension; or of mid-Cretaceous age imposed upon the migmatites during the emplacement of the Red Jacket Granite. However, NW-SE trending leucosomes associated with migmatization may be significantly older.

Carboniferous development of NNW-SSE and NW-SE-trending lineations

The absence of the NNW-SSE and NW-SE-trending lineations from granioitds intruded during the mid-Cretaceous, and development of this trend of lineation from south of White Horse Creek to Cape Fouwlind suggests that these lineations may record an earlier widespread deformational event. This event may be of Carboniferous age associated with a syn-tectonic emplacement of the Cape Foulwind and Tauranga Bay monzogranites. In this scenario, NNW-SSE lineations in the migmatites of sedimentary origin at Charleston, and NNW-SSE and NW-SE-trending lineations south of White Horse Creek would be attributed to the same tectonic event. The absence of NNW-SSE lineations in the Charleston orthogneiss lithologies and from the main body of Red Jacket Granite would simply be a result of emplacement of the magmas after deformation associated with the NNW-SSE and NW-SE lineations. Some support for this proposal is suggested by K-Ar dating of Greenland Group by Adams (1975b), which records a thermal event affecting the Greenland Group between 298-370 Ma (section 9.2.1). This age represents the resetting of the K-Ar system by granite intrusion at high levels and the possibility is that there was a contemporaneous and more fundamental metamorphic event at deeper crustal levels.

The moderate dip of the foliation containing NNW-SSE and NW-SE-trending lineations and the predominantly up-dip sense of shear south of White Horse Creek suggests that the event recorded by NNW-SSE and NW-SE lineations is not related to the development of a Paleozoic core complex.

9.2.3 Cretaceous Deformation and Metamorphism

Development of the Charleston and Parsons Hill Arches and the Red Jacket Granite

The first event which is unequivocally of mid-Cretaceous age is the intrusion of tonalitic, granitic and granodioritic magmas at Charleston prior to the 108 Ma intrusion of undeformed pegmatite (recalculated from Aronson 1968). Emplacement of the Red Jacket Granite to the south occurred at about 110 Ma (Ireland pers. comm. SHRIMP zircon data). Intrusion of tonalitic, granitic and granodioritic magmas around Charleston and south of White Horse Creek is intimately related to some of the mylonitic deformation in the Charleston Metamorphic Group. Spatial association of plutonic bodies with the WNW-ESE-trending Charleston and Parsons Hill arches, and down-dip senses of shear on the limbs of the arches, imply that mylonitization at this level in the crust was initiated by or synchronous with plutonic intrusion.

The stretching lineation recorded in the orthogneisses forming the Charleston and Parsons Hill arches is somewhat oblique to the trend of the arches and may imply that NE-SW oriented extension imposed only a weak control on the uprise of magma, or that the NE-SW stretching lineation is a later-stage lineation developed after the initial intrusion of the plutons.

The least deformed granitoids are porphyritic biotite-tonalites exposed in the bed of Deep Creek. Here the foliation is subvertical and may record the uprise of magma in the centre of the Charleston arch, perhaps along a pre-existing basement discontinuity such as a subvertical fault.

Development of the Mylonitic Rocks

The Siberia Bay syenogranite-monzogranite which occurs as both mylonitized and undeformed outcrops in Siberia Bay suggests emplacement perhaps prior to mylonitization, during mylonitization and after mylonitization ceased. Local uprise of magma is recorded by two 2m-wide domal structures in the centre of Siberia Bay. However, opposing senses of shear are not recorded on opposite sides of the pluton and

C′-planes are well developed, both in the SBMZ and Tauranga Bay monzogranitic gneiss. Although the small areas of outcrop makes interpretation difficult, feldspar megacrysts show only brittle deformation and the temperature during mylonitization has remained moderate, suggesting that massive syn-tectonic emplacement of magma at this locality has not occurred. However, most mica and quartz in the SBMZ and Tauranga Bay monzogranitic orthogneiss displays static recrystallization implying that the temperature remained moderate after mylonitization. This recrystallization may have been facilitated by granitoid emplacement after mylonitization and/or close proximity to the centre of the core complex. The presence of undeformed granite in Siberia Bay suggests that local post-mylonitic emplacement of granite did occur.

The lack of opposing senses of shear on either side of the Siberia Bay pluton and the presence of well developed C′-planes, particularly in the Tauranga Bay monzogranitic gneiss suggests that the top-to-the-NE/ENE mylonitization recorded in the SBMZ and Tauranga Bay orthogneiss is associated with the overlying Ohika Detachment Fault which records a top-to-the-NE sense of shear (Tulloch and Kimbrough 1989). Although some local uprise of syenogranitic-monzogranitic magma probably occurred in Siberia Bay during mylonitization, the magma was emplaced into an already established tectonic regime associated with detachment. The top-to-the-SW/WSW senses of shear which post-dates top-to-the-NE/ENE senses of shear in Siberia Bay and Tauranga Bay can be attributed either to the overprinting of fabrics associated with movement on the Ohika Detachment Fault by fabrics associated with movement of the Pike Detachment Fault, or the shear reversal may perhaps be due to the development of conjugate, but temporarily distinct C′-planes near the axis of the core complex which became flattened with progressive deformation (Chapter 8).

Mylonitization associated with the formation of the MCMZ and Four Mile River mylonites is spatially associated with the intrusion of syn- and post-mylonitic pegmatites and affects leucogranite of the same composition as that exposed at Charleston. However, the MCMZ, Four Mile River mylonites and DCMZ contain intensely dynamically recrystallized mylonites with well developed C′-planes that have undergone little thermal annealing. The MCMZ and DCMZ, and sample FM17 from the mouth of the Four Mile

River, record a top-to-the-SW sense of shear which sub-parallels top-to-the-SSW senses of shear displayed by mylonites underlying the Pike Detachment Fault described by Tulloch and Kimbrough (1989). The presence of well developed C′-planes and the top-to-the-SW direction of shear suggests the mylonitic rocks south of Charleston record a regional deformation associated with movement on the overlying Pike Detachment Fault.

At around this time, uplift of the mylonitized migmatites south of White Horse Creek and overprinting of NNW-SSE and NW-SE lineations by NE-SW lineations ocurred. Around Beflast Creek, mylonitized migmatites possessing NE-SW trending lineations display top-to-the-NE porphyroclast systems and C-S planes which have been overprinted by top-to-the-SW fabric elements. Early top-to-the-NE shear-senses are inconsistent with the top-to-the-SW senses of shear recorded in the MCMZ and the SSW shear-sense associated with the Pike Detachment (Tulloch and Kimbrough 1989), and may possibly imply the presence of an early third detachment fault. Top-to-the-SW fabrics which overprint top-to-the-NE fabrics south of White Horse Creek may record the progressive development and eventual dominance of the Pike Detachment over this third top-to-the-NE southern detachment.

The deformation of orthogneiss at Charleston ceased prior to the intrusion of pegmatite which remained undeformed at 108 Ma (recalculated from Aronson 1968). Mylonites at the mouth of the Four Mile River and in the MCMZ are also cut by post-mylonitic pegmatites which suggest that mylonitization at these localities may also have ceased at around 108 Ma. In Siberia Bay, the intrusion of post-mylonitization pegmatites was accompanied by localised intrusion of syenogranitic-monzogranitic magmas. However, no dating of the undeformed or mylonitized syenogranite-monzogranite has been undertaken to date, and the timing of these events remains largely unconstrained. The cessation of mylonitic deformation at Charleston and probably the MCMZ by 108 Ma does not preclude the continuation of ductile deformation at deeper levels in the crust.

A summary of Cretaceous metamorphic and structural events is given in Fig. 9.2.

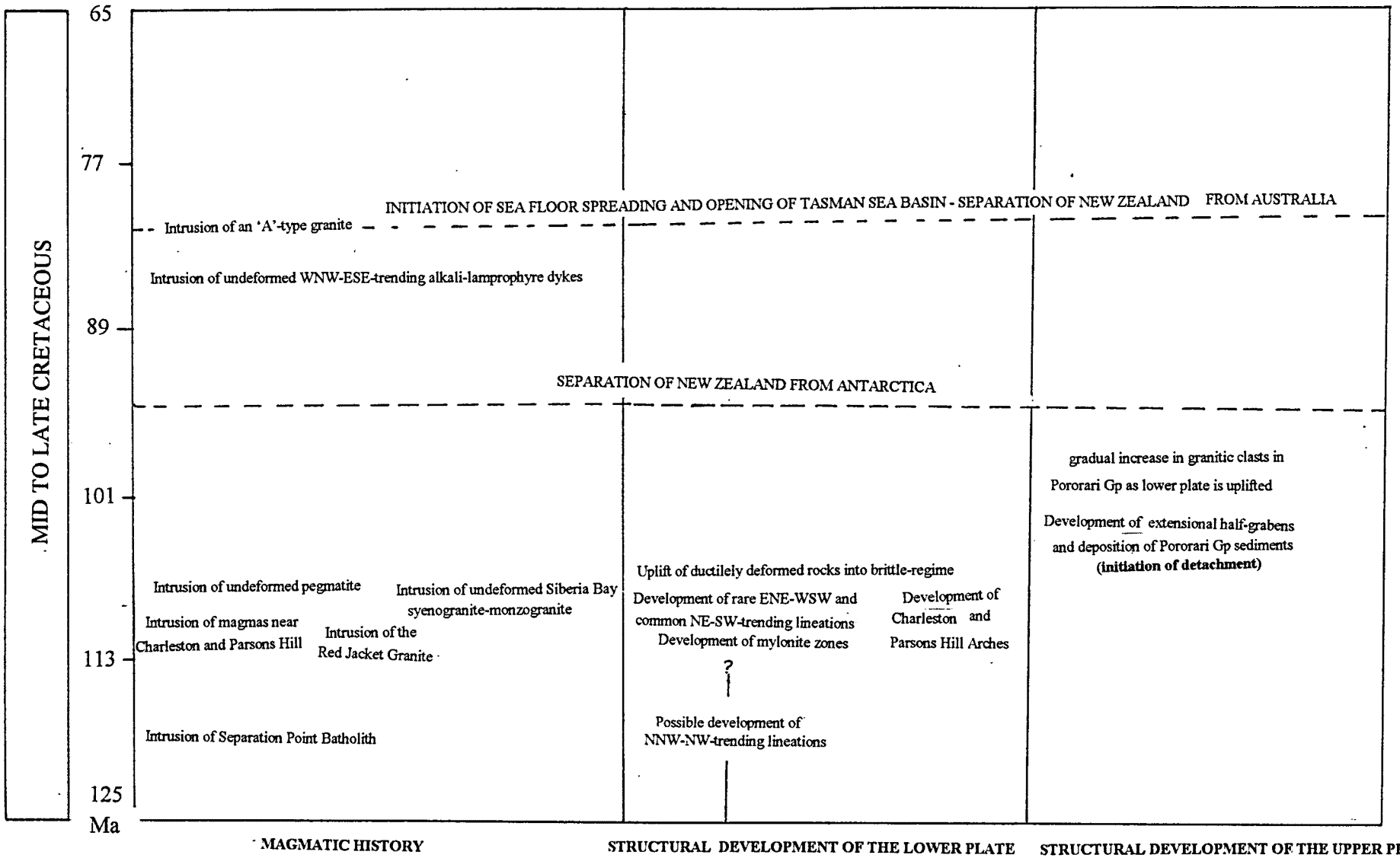

Fig. 9.2 Summary of Cretaceous events recorded in this study area and in the greater West Coast area.

Overprinting of Ductile Fabrics by Brittle Fabrics

During the later stages of core complex development uplift of the core complex continued (at this stage, probably by tectonic denudation), bringing the coastal section around and south of White Horse Creek into the brittle-regime where small scale faulting, brecciation and associated hematitic alteration overprinted previously-formed ductile fabrics. Less pervasive brittle deformation is recorded in the MCMZ and SBMZ. The sometimes extreme brittle deformation suffered by rocks outcropping south of White Horse Creek suggests that the rocks lay in a zone of brittle deformation associated with the southern Pike Detachment Fault when deformation of the lower plate at this locality was arrested.

K-Ar data recorded from muscovite in altered granite along the Ohika and Pike Detachment Faults suggests that movement along the Pike Detachment Fault continued after movement on the Ohika Fault had ceased (Tulloch and Palmer 1990) and that uplift associated with the Pike Detachment may have been occurring as late as 85 Ma.

9.3 Tectonic Setting of the Paparoa Metamorphic Core Complex

From the Permian to the early Cretaceous, the Western Province of New Zealand formed part of an extensive arc system located on the southwest Pacific margin of Gondwana (Muir et al 1995). During this time, the tectonic regime was dominated by compression along a series of westerly dipping subduction zones. The products of convergent margin tectonics compose the Eastern Province of New Zealand, and include magmatic arcs, forearc basins, trench slope basins and accretionary complexes (Bradshaw 1989). According to Muir et al (1995) the NNE-SSW-trending Separation Point Batholith of early Cretaceous age (118 ± 3 Ma) represents the final stage of magmatism associated with subduction. The Separation Point Batholith is attributed to the melting of a basaltic protolith beneath a continental arc, initially thickened by the collision of the Median Tectonic Zone volcanic arc complex with the Western Province (Muir et al 1995).

In the mid-Cretaceous, at around 105 ± 5 Ma (Bradshaw 1989), the tectonic regime in New Zealand changed abruptly from one dominated by compressonal tectonics to one of extension culminating in the onset of rifting of New Zealand from Australia at around 82 Ma (Weissel and Hayes 1977). This abrupt onset of extension has been attributed to the arrival of a spreading ridge at a subduction zone (Bradshaw 1989). This interpretation has found support from Muir et al (1994b), who suggest that the geochemical signature from the Separation Point Batholith indicates that a spreading centre was in close proximity during the Cretaceous.

The development of the Paparoa Metamorphic Core Complex immediately post-dated a period of crustal thickening, perhaps caused by the collision of the Median Tectonic Zone with the Western Province (Muir et al 1995). The onset of extension and intrusion of the granitic, granodioritic and tonalitic magmas at Charleston may have been initially related to a high heat flow in the lower crust associated with the preceding crustal thickening. Intrusion of the magmas near Charleston at around 110 Ma facilitated ductile deformation in the lower crust and initially, at least, uplift associated with core complex development at Charleston was probably caused by pluton intrusion. A similar scenario can be proposed for the larger part of the core complex exposed in the Paparoa Range, where high heat flow associated with the intrusion of the massive Buckland Granite (109 Ma; Muir et al 1994a) probably facilitated uplift and ductile deformation at this time and locality. Uplift along the Pike Detachment Fault and Ohika Detachment Fault post-dating the intrusion of magmas was probably a result of tectonic denudation. Zircon SHRIMP analysis of the Stitts Tuff member of the Pororari Group yields an age of 101 Ma (Muir pers. comm.) implying that uplift and basin formation had begun in the upper plate at this time.

Core complexes found in the North American Cordillera, Aegean Sea and in Papua New Guinea also post-date significant periods of crustal thickening (Coney and Harms 1984; Hill et al 1992; Lee and Lister 1992). In all these cases, the orientation of extension which post dated crustal thickening was at a high angle to the trend of the previously active subduction zones. A genetic relationship between preceding crustal thickening and extensional tectonics leading to core complex formation has been proposed for the Cordilleran metamorphic core complexes by Coney and Harms (1984). These workers

suggest that overthickening of the crust during subduction led to the formation of a gravitationally unstable mass which, during Cenozoic time, spread laterally, resulting in deep seated crustal extension aided by the thermal pulse of Cenozoic magmatism. This proposed link between subduction and later core complex formation could also possibly be applied to complexes of the Aegean Sea and the D'Entrecasteaux Islands of Papua New Guinea. Waight (1995) proposes a similar scenario for the Paparoa Metamorphic Core Complex suggesting that mid-Cretaceous crustal extension is a consequence of crustal collapse and thinning of overthickened crust following the cessation of subduction, rather than being directly related to the opening of the Tasman Sea. Although Waight (1995) does not suggest a direction of spreading, if spreading of the overthickened crust was simply triggered by the cessation of subduction-related compressional forces one would expect the extension direction to be orientated at a high angle to the trend of the previously active subduction zone.

However, in the Charleston Metamorphic Group, the NE orientation of stretching lineations in the MCMZ, Four Mile River mylonites and DCMZ, NE/ENE trend of stretching lineation in the SBMZ and Tauranga Bay monzogranitic gneiss of the lower plate, and NNE-oriented extension implied by WNW-ESE-trending sedimentary basins and lamprophyre dykes of the upper plate, is nearly parallel to structures emplaced as a result of subduction subparallel to the Mesozoic Gondwana margin. Structures that subparallel the Mesozoic Gondwana margin are the NNE-trending Separation Point Batholith, which developed as a result of subduction and underplating parallel to the Gondwana margin (Muir et al 1995), and the Median Tectonic Zone. The parallelism between linear structures associated with subduction and the later extension directions is difficult to reconcile with a spreading of overthickened crust such as that proposed by Coney and Harms (1984), although this does not preclude the high heat flow associated with the over thickened crust as being a factor in the initiation of extension.

A similar scenario to the apparent parallelism between the extension direction and subduction-related structures in the Western Province of New Zealand is found in the Himalayas where N-S-directed shortening and crustal thickening associated with the convergence of the Indian and Asian plates has been accompanied by W-E-directed

extension (Royden and Burchfiel 1987). E-W-directed extension in the Himalayan mountain belt undergoing N-S-directed compression has been attributed to continental escape as material in the collision zone escapes laterally towards a zone of lower compressive strain (Royden and Burchfiel 1987), essentially driven by gravity collapse of the Himalayan topographic front. Applying a similar model to the development of the Paparoa Metamorphic Core Complex would require crustal thickening contemporaneous with extension. However, there is no evidence that extension associated with core complex formation accompanied crustal thickening.

J. Bradshaw (pers. comm.) proposes two explanations for the parallelism between the trend of subduction and extension. The first possibility is that extension was parallel to the local continental margin and not necessarily related to continental breakup. However NE-SW-oriented extension is oriented nearly perpendicular to the trend of Tasman Sea rifting associated with the separation of New Zealand from Australia which began about 82 Ma ago (Weissel and Hayes 1977). In addition, there are no core complexes recorded in the literature where extension occurred parallel to the trend of the previously active subduction zone margin.

Bradshaw proposes the other possibility of major oroclinal bending between the time of intrusion of the Separation Point Batholith (118 Ma), and the beginning of the impression of extensional lineations after crystallisation of the Buckland Granite (109 Ma). NNW-SSE-trending lineations recorded in the Cape Foulwind monzogranitic gneiss and in migmatites of sedimentary origin near Charleston may possibly be of Cretaceous age predating the development of NE-SW-trending lineations (section 9.2.2). If this is the case, NNW-SSE lineations may record deformation prior to oroclinal bending, although there is little evidence for a rotation of these lineations into NE-SW orientations.

9.4 Models for Core Complex Development

9.4.1 Models described in the Literature

Models advocating a pure-shear flattening accompanied by igneous dilation (Miller et al 1983 and Anderson 1971) envisaged the transition between the brittlely deforming upper crust and ductilely deforming lower crust as a flat fault essentially representing the brittle-ductile transition (Fig. 9.3A). Pure shear models involving flat faults separating brittlely and ductilely deforming rocks have been largely invalidated by the recognition of low angle normal detachments between normal fault systems of the upper crust and ductile shear zones of the lower crust. Pure shear models, such as those illustrated in Fig. 9.3A, are not capable of predicting uplift or doming of the lower crust or the diachronous nature of the ductile and brittle deformation described in many core complexes (Wernicke 1985).

In an attempt to explain the dome or arch-shape of many shear zones and detachment faults, and the decrease in ductile deformation with depth in the lower plate, Davis and Coney (1979) and Davis and Hardy (1981) proposed a model based on an internally distended crustal-scale megaboudin. Davis and Coney (1979) proposed that the basement stretched and necked in a manner akin to megaboudinage and that layers above the megaboudins flowed passively during metamorphism.

Field studies of Cordilleran core complexes suggest that simple shear predominates in shear zones immediately below the detachment faults, and that the sense of shear associated with detachment is unidirectional over large areas. This led Wernicke (1981, 1985) to propose a model based on simple shear along detachment faults that initiate at shallow depth (Fig. 9.3B). Normal-sense displacement along such low angle narrow zones of movement which pass through the crust or lithosphere brings the lower ductile crust into contact with the brittle upper crust and accounts for the diachronous nature of ductile and brittle deformation. Doming of the detachment fault and upwelling of the asthenosphere is attributed primarily to tectonic denudation of the upper crust. The uniform-sense simple-shear theory of Wernicke (1985) does not specifically predict the

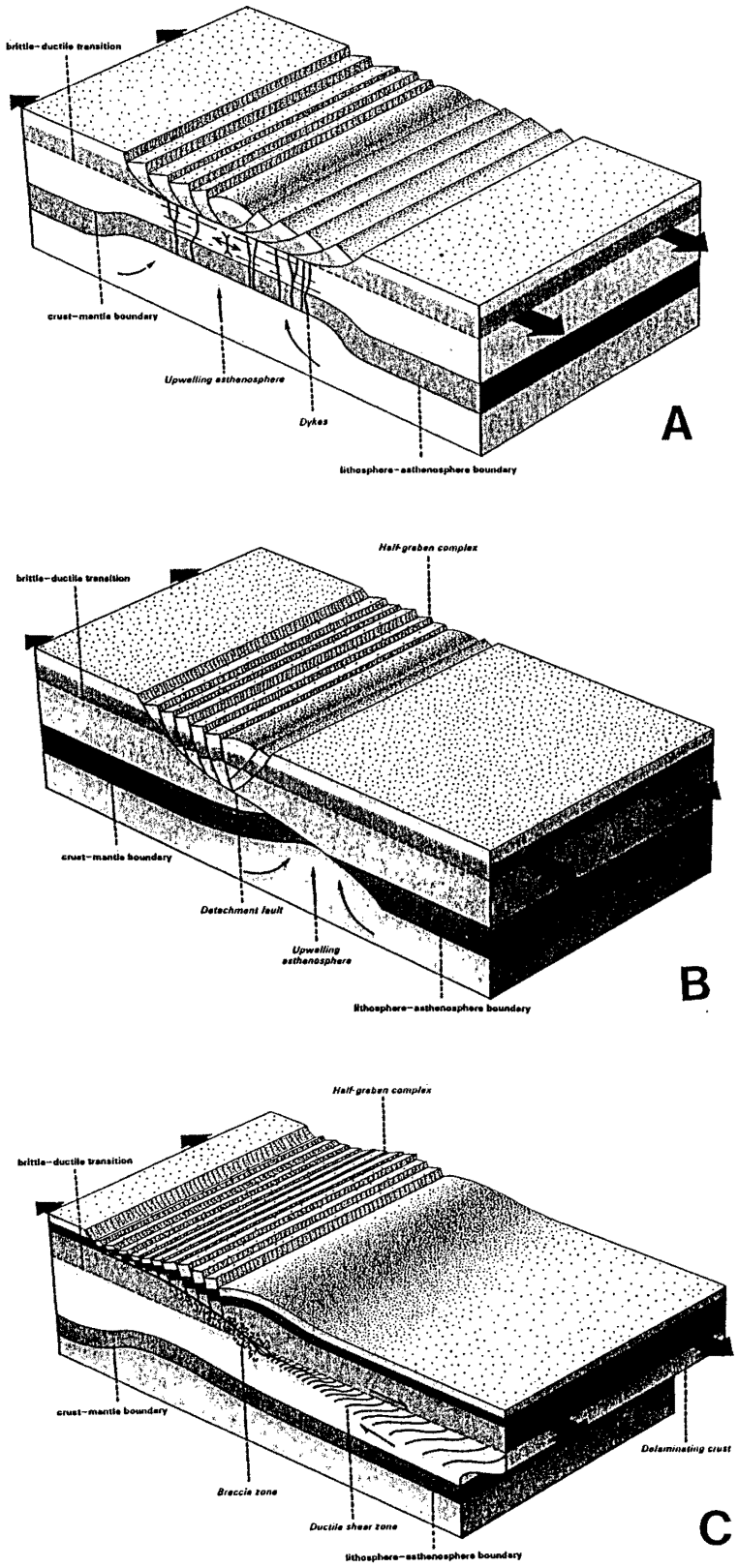

Fig. 9.3 A) Example of a symmetric pure shear model for continental extension from Lister and Davis (1989).
B) Extension of the continental crust using a single lithospheric dislocation (from Lister and Davis 1989; after Wernicke).
C) Crustal shear zone model of Lister and Davis (1989).

association of igneous activity with core complex development and magmatism is only viewed as a "passive" response to extensional strain of the lithosphere.

An alternative to Wernicke's model was proposed by Lister and Davis (1989). The alternative model of Lister and Davis involves a shallow-dipping detachment fault that disappears with depth into zones of brecciation, cataclasis and at deep levels, a ductile shear zone (Fig. 9.3C). The ductile shear zone terminates at depth in a zone of complex anastomosing shear zones involving bulk pure shear in the middle and lower crust. This evolving crustal shear zone model envisages continental extension as the result of a combination of detachment faulting and the effects of the shallow-dipping ductile shear zones, and that detachment faults are simply upper crustal manifestations of such zones. The movement zone is folded as the result of the bowing upwards of lower crust to form a broad basement culmination, the result of a combination of isostatic rebound due to tectonic denudation, and granite intrusion in the middle crust.

In contrast to the uniform-sense simple shear model of Wernicke (1985) where the detachment fault initiates at a low angle, Buck (1988) and Wernicke and Axen (1988) proposed that high angle normal faults rotate to become nearly horizontal during extension due to the upward flexuring of the footwall. This progressive rotation of normal faults toward the horizontal results in an upward folding of the detachment zone and produces an asymmetric core complex that is steeply dipping on one side and flat lying on the other (Brun and van den Driessche 1994). Brun and van den Driessche (1994) apply this model to the Montagne Noire gneiss dome and detachment fault system and conclude that although the gneiss dome itself has opposing senses of shear on opposite sides of the dome, the overlying detachment fault itself records a uniform sense of shear.

9.4.2 A Model for the Development of the Paparoa Metamorphic Core Complex

This study of the lower plate mylonitic rocks of the Paparoa Metamorphic Core Complex records a top-to-the-SW sense of shear for the MCMZ, Four Mile River mylonites and DCMZ on the SW side of the core complex. This direction of shear is sub-parallel to a top-to-the-SSW sense of shear displayed by indicators underlying the Pike Detachment in

the southern Paparoa Range (Tulloch and Kimbrough 1989). The top-to-the-NE sense of shear recorded by the Ohika Detachment Fault (Tulloch and Kimbrough 1989) appears to be supported by top-to-the-NE/ENE senses of shear in the SBMZ and Tauranga Bay monzogranitic gneiss. Development of later top-to-the-SW/WSW shear-sense indicators can perhaps be attributed to the overprinting of fabrics associated with the Ohika Detachment Fault by fabrics associated with the Pike Detachment Fault. Top-to-the-NE senses of shear south of White Horse Creek imply the presence of a third southern top-to-the-NE detachment fault. Top-to-the-SW senses of shear which overprint top-to-the-NE senses of shear south of White Horse Creek may record the overprinting of fabrics related to the possible third southern detachment by fabrics related to the Pike Detachment Fault.

Opposing senses of shear on opposite sides of the Charleston and Parsons Hill arches are related to the uprise of magma in the ductile lower crust and are not necessarily related to the movement of the overlying detachment. The opposing senses of shear do not, therefore, imply extension in a coaxial regime (Brun and van den Driessche 1994).

However, the top-to-the-NE sense of shear recorded by the Ohika Detachment Fault and top-to-the-SW sense of shear recorded by the Pike Detachment Fault precludes the application of simple shear models where the detachment records a uniform sense of shear, such as those proposed by Wernicke (1985) and Lister and Davis (1989). Support for opposing senses of shear on opposite sides of the core complex is found in the upper plate, where the Pororari Group sediments apparently dip towards the axis of the core complex so that in the NE of the Paparoa Range the sediments dip to the SW, and in the SW the sediments dip to the NE (Fig. 1.1). The change in dip recorded by the Pororari Group across the core complex is also inconsistent with uniform-sense detachment models that record a uniform dip in the overlying cover rocks (Fig. 9.3B and C).

Pure shear models such as that proposed by Miller et al (1983) (section 9.4.1; Fig. 9.3A) cannot be reconciled with the formation of low-angle detachment faults and the outward displacement of the upper plate along such detachments. In addition, the dip of the Pororari Group is not consistent with the displacement of the upper plate in such models.

The alternative two stage model proposed here (Fig. 9.4) is based on the early regional development of conjugate listric normal faults which flatten with depth. During stage one, top-to-the-NE/ENE fabric elements in the SBMZ, Tauranga Bay monzogranitic gneiss, and top-to-the-NE shear-sense fabric elements from mylonitized migmatites south of White Horse Creek are considered to be associated with movement along early top-to-the-NE/ENE detachment faults. Top-to-the-NE/ENE shear-sense indicators in the SBMZ and Tauranga Bay monzogranitic gneiss are associated with the Ohika Detachment Fault, while top-to-the-NE shear-sense indicators south of White Horse Creek may possibly be associated with the early development of a third southern detachment. Top-to-the-SW senses of shear recorded in the MCMZ, DCMZ and in the Four Mile River mylonites are associated with movement along the Pike Detachment Fault.

The second stage of core complex development envisages the progressive growth and eventual dominance of the Pike Detachment Fault, overprinting top-to-the-NE/ENE fabric elements associated with the Ohika Detachment and the third southern detachment with top-to-the-SW fabric elements. Tulloch and Palmer (1990) suggest that movement along the Pike Detachment Fault may have continued for some time after movement along the Ohika Detachment. In this model, the Greenland Group tectonic cover has essentially slid off the Pike and Ohika detachments, forming half-grabens which have been infilled with terrestrial deposits (Pororari Group).

Doming of the core complex and ductile deformation of the lower crust was probably initiated by plutonic intrusion, and continued after intrusion by tectonic denudation. However, the initiation of extension itself may be related to the production of overthickened crust during the preceding period of subduction. Opposing senses of shear on opposite sides of the Charleston and Parsons Hill arches are a consequence of magma intrusion and do not reflect the movement of the overlying detachment fault.

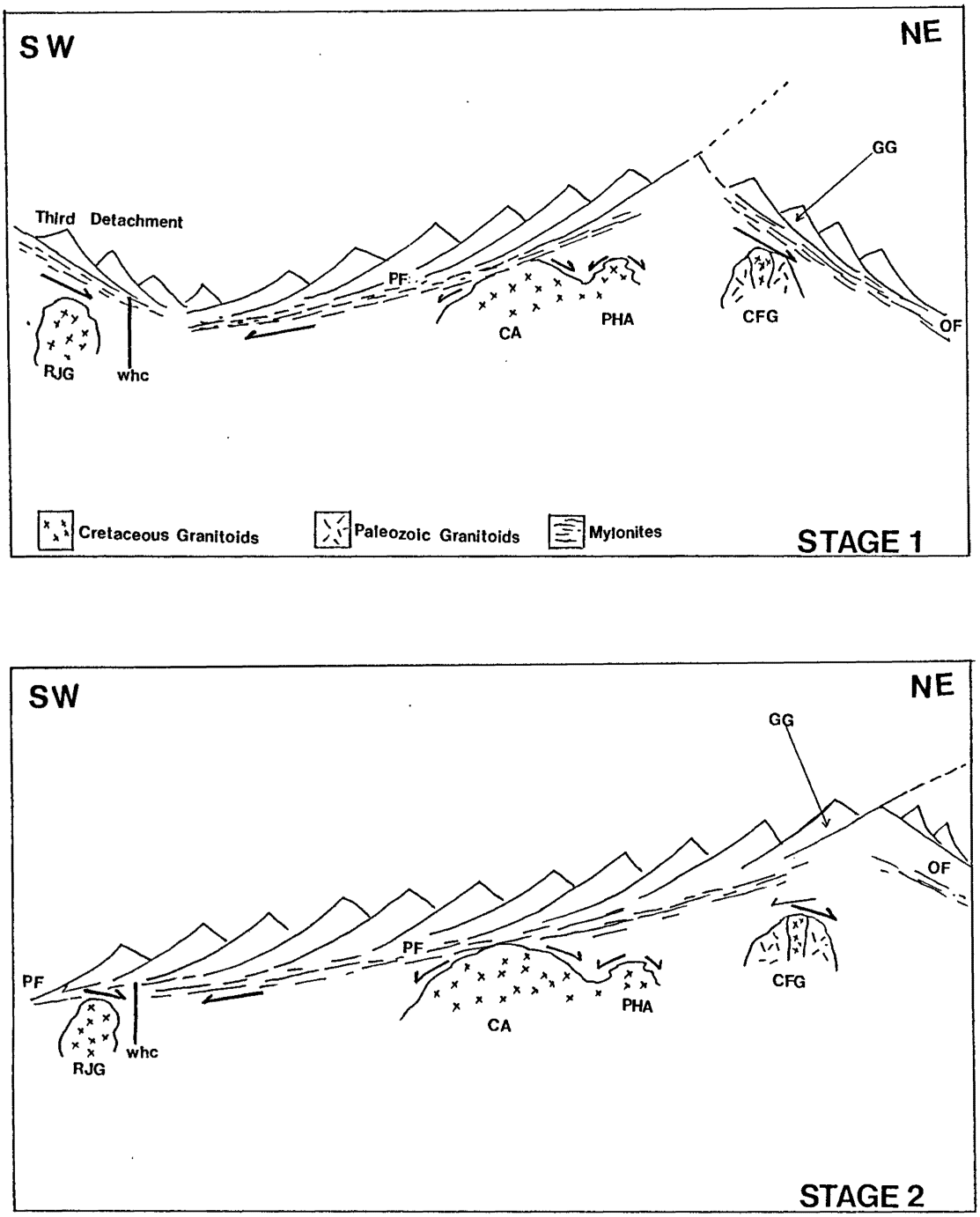

Fig. 9.4 Schematic drawing of a two stage development of the Paparoa Metamorphic Core Complex (not to scale).

PF=Pike Detachment Fault, OF=Ohika Detachment Fault, third possible detachment shown to the SW. RJG=Red Jacket Granite, CA=Charleston Arch, PHA=Parsons Hill Arch, CFG=Cape Foulwind Granitoids, GG=Greenland Group, whc=White Horse Creek Fault.

STAGE 1: Conjugate detachment faults; OF imposes top-to-the-NE sense of shear on CFG; PF imposes top-to-the-SW sense of shear on mylonites south of the CA; the possible third detachment imposes a top-to-the-NE sense of shear on mylonitized migmatites in the SW, adjacent to the Red Jacket Granite. Shear reversals developed on opposite sides of CA and PHA due to uprise of magma.

STAGE 2: Further development and eventual dominance of the PF. Shear reversals south of the White Horse Creek Fault due to overprinting of fabrics associated with the third possible detachment (bold arrow) by fabrics associated with the PF (thin arrow). Shear reversals in the SBMZ and Tauranga Bay monzogranitic gneiss due to overprinting of fabrics related to the OF (bold arrow) by fabrics related to the PF (thin arrow).

9.4.3 Comparison of the Paparoa Metamorphic Core Complex with core complexes described in the Literature

Features common among core complexes from the Aegean Sea, North American Cordillera and Papua New Guinea are the development of low angle detachment faults and a low-dipping foliation. Lower plate foliations are characteristically warped into one or more broad asymmetric arches or dome structures that have been attributed to isostatic rebound by mid-crustal flow in response to tectonic denudation (Wernicke and Axen 1988), the development of a back-dipping mylonitic front (Lister and Davis 1989), syn-tectonic emplacement of granitoids into the lower plate (Anderson 1971) and as a result of megaboudinage (Davis and Coney 1979). Stretching lineations in the lower plate of Cordilleran and Aegean core complexes possess a remarkably consistent trend and uniform sense of shear (Coney 1980: Lee and Lister 1992). Of particular interest is that the same sense of shear is recorded on both sides of the broad arch or dome structures (Yin and Dunn 1992; Spencer 1984; Wernicke 1985). Uplift results in the progressive overprinting of ductile fabrics by brittle fabrics. Brecciated basement rocks are characterised by retrograde chlorite and a distinctive hematitic red-staining (Coney 1980).

Core complexes from the Aegean Sea, North American Cordillera and Papua New Guinea are spatially and temporarily related to plutonic and/or volcanic activity. The intrusion of garnet-bearing two-mica granite, such as that exposed around Charleston is particularly common in core complexes of the North American Cordillera (Coney 1980). Although some authors have recognised a genetic link between plutonism, volcanism and the development of Cordilleran core complexes (Gans et al 1989), uplift during core complex development has been largely attributed to isostatic rebound due to tectonic denudation.

Core complexes on the D'Entrecasteaux Islands of Papua New Guinea clearly demonstrate a strong link between core complex development and plutonism (Hill et al 1992). The islands comprise gneiss domes that reach a topographical height of 2.5 km and which have undergone a major deformational event culminating in the formation of ductile shear zones known to be active during extension. The lower plate of the core complexes

contain two zones of rocks: a core of migmatites, eclogites, amphibolites, gneisses and granodioritic intrusions and mylonitic shear zones which mantle the core zone (Hill et al 1992). Mylonitic shear zones are curved around the gneiss domes and dip at angles between 0° and 45°. The orientation of shear zone lineations vary markedly from shear zone to shear zone (Hill et al 1992). On the north-eastern flanks of the gneiss domes, major NE-dipping shear zones underlie detachment faults recording a down-dip top-to-the-NE sense of shear.

Although the core complexes of D'Entrecasteaux Islands have some characteristics in common with Cordilleran and Aegean core complexes (development of a detachment faults with a uniform sense of shear, the evolution of ductile to brittle deformation in the lower plate shear zones and an association with igneous intrusion), there appear to be marked differences too. According to Hill et al (1992) these include the complex arrangement of shear zones and stretching lineations on the D'Entrecasteaux Islands, the extreme topographical expression of the gneiss domes, and the steepness of dip of some dome bounding shear zones which can be up to 45°. To account for the extreme topographical height, and control of plutonism on the formation of ductile shear zones, Hill et al (1992) proposed that uplift of the mylonitic shear zones was due to the inflation of sills during magmatism.

The Paparoa Metamorphic Core Complex possesses many features characteristic of other core complexes. These features include a mylonitic foliation of low dip deformed into broad arch structures orientated at high angles to the extension direction, a fairly consistent NE-trending stretching lineation and the overprinting of ductile fabrics by brittle fabrics and hematitic alteration in the south of the study area. The intimate link between plutonism and core complex development suggests the Paparoa Metamorphic Core Complex may be akin to those of the Aegean Sea and D'Entrecasteaux Islands of Papua New Guinea. However, there is a striking difference between the Paparoa Metamorphic Core Complex and those described in the literature. Cretaceous stretching lineations, while being of fairly consistent trend do not record the unidirectional sense-of-shear recorded by stretching lineations of other core complexes, particularly those of the North American Cordillera. In the Paparoa Metamorphic Core Complex, the relative displacement of the

upper plate is complicated with detachment faults (Ohika Detachment and a possibly third southern detachment) recording a top-to-the-NE or ENE senses of shear overprinted by top-to-the-SW senses of shear associated with the Pike Detachment.

9.5 Future Work

Timing of the mylonitization of syenogranite-monzogranite at Siberia Bay is unconstrained and undeformed granite in Siberia Bay is likely to post-date mylonitization. SHRIMP zircon analysis of both undeformed and deformed portions of the Siberia Bay syenogranite-monzogranite could potentially pin point the timing of ductile deformation at this locality. Dating of the White Horse Creek and Four Mile River pegmatites that cross-cut the mylonitic foliation would place a minimum age on ductile deformation at these localities.

Although zircon analysis of paragneiss near Charleston implies migmatization of the Greenland Group metasedimentary rocks at around 380-400 Ma (Ireland 1992), further zircon SHRIMP work needs to be done to confirm this suggestion. SHRIMP dating of zircons from a leucosome that parallels the foliation cut by the Red Jacket Granite around Belfast Creek would give an age for migmatization of the Greenland Group. This may also enable the age of NW/NNW trending lineations to be better constrained.

Much of the late history of the Paparoa Metamorphic Core Complex is recorded in the Pororari Group sediments. In addition to the varying clast composition within the Pororari Group, the Pororari Group and Greenland Group must undergo a detailed structural study. If the model for core complex development proposed herein holds, the Pororari Group sediments should thicken towards the centre of the core complex and blocks of Greenland Group should be tilted towards the centre of the core complex.

According to Tulloch and Kimbrough (1989), another detachment fault which separates Greenland Group metasedimentary rocks from the Charleston Metamorphic Group lies to the north of the Ohika Detachment Fault. Kinematic analysis of the Charleston

Metamorphic Group northeast of Westport could have implications for the model proposed herein for the Paparoa Metamorphic Core Complex. The detachment fault north of the Ohika Detachment may be similar to the Pike Detachment and record a down-dip top-to-the-SW sense of shear.

Quartz c-axis fabric analysis in this study has shown c-axis fabrics to be unreliable indicators of shear-sense. To better understand the origin of c-axis girdles giving an opposing sense of shear to the direction of movement in mylonite zones recorded by other microstructures, future quartz c-axis studies should concentrate on the effect of strain partitioning and late coaxial overprints on c-axis fabrics.

CHAPTER TEN

CONCLUSIONS

1. Stretching lineations in the mylonite zones south of Charleston are oriented generally NE-SW. Microstructural shear-sense indicators in mylonites from the MCMZ, DCMZ and one sample from the Four Mile River mouth display top-to-the-SW senses of shear which can be associated with movement on the overlying Pike Detachment Fault.

2. Near Cape Foulwind, gross fabric elements in the Tauranga Bay monzogranitic gneiss and SBMZ record top-to-the-NE/ENE senses of shear which can be attributed to movement associated with the overlying Ohika Detachment Fault. However, these fabric elements are folded and kinked by later top-to-the-SW/WSW movements which may be related to the overprinting of structures associated with the Ohika Detachment Fault by the structures associated with the Pike Detachment Fault, or the development of C′-planes near the axis of the core complex which become flattened with progressive coaxial deformation. Top-to-the-NE shear-senses south of White Horse Creek are overprinted by top-to-the-SW senses of shear and possibly represent the early development of a third southern detachment which was overprinted by fabrics associated with the Pike Detachment Fault.

3. Quartz c-axis fabrics are the least reliable shear-sense indicators used in this thesis. Single girdles with an apparent sense of asymmetry recording a top-to-the-NE sense of shear in the MCMZ contradict top-to-the-SW microstructures in thin section and may be attributed to either a reorientation of quartz c-axes during a late stage deformation, or a partitioning of strain between the S-plane (pure shear) and C-plane (simple shear). The origin of type I crossed girdles which possess an asymmetry consistent with a top-to-the-NE sense of shear in mylonite samples containing top-to-the-SW shear-sense indicators, and quartz c-axis girdles at right angles to the foliation and containing the lineation in the SBMZ are also not understood.

4. 'V'-pull-aparts record localized senses of shear which may or may not represent the bulk shear-sense. 'V'-pull-aparts, therefore cannot be used as sole indicators of shear-sense.

5. The mid-Cretaceous intrusion of granitic, granodioritic and tonalitic magmas around Charleston and south of White Horse Creek has imposed important local controls on the ductile deformation forming WNW-ESE-trending arches. Opposite senses of shear on opposite limbs of the Charleston and Parsons Hill arches is not related to the movement of the overlying detachment, but is a consequence of the uprise of magma.

6. The timing of NNW/NW-oriented lineations near Cape Foulwind and in migmatites of sedimentary origin is constrained between the crystallization of the Cape Foulwind monzogranitic gneiss (327 Ma; Muir et al 1994a) and the development of NE-SW-trending lineations which postdate crystallization of granitic, granodioritic and tonalitic magmas at Charleston (around 110 Ma; Muir. pers. comm.) and the intrusion of undeformed pegmatite at 108 Ma (recalculated from Aronson 1968). NNW-NW-trending lineations south of White Horse Creek and top-to-the-NW/NNW senses of shear may be of Paleozoic or Cretaceous age.

7. A two stage model is proposed for the development of the Paparoa Metamorphic Core Complex. The first stage involves the formation of regional, conjugate listric normal faults. The second stage envisages growth and eventual dominance of the Pike Detachment Fault, overprinting earlier fabrics. The Paparoa Metamorphic Core Complex does not fit commonly advocated models for core complex development such as uniform-sense simple shear models, or models involving pure shear.

8. The NE to ENE-trend of stretching lineations in the lower plate of the core complex is perpendicular to the Tasman Sea rift and nearly parallel to structures emplaced subparallel to the trend of subduction along the Mesozoic Gondwana margin (Separation Point Batholith and Median Tectonic Zone). This anomaly has yet to be adequately explained.

REFERENCES

Adams, C.J.D. (1975a) Discovery of Precambrian Rocks in New Zealand: Age variation of the Greenland Group and Constant Gneiss, West Coast, South Island. *Earth and Planetary Science Letters* 28, 98-104.

Adams, C.J.D. (1975b) New Zealand K-Ar age, List-2. *New Zealand Journal of Geology and Geophysics*, 18, 433-467.

Adams, C.J.D. and Nathan, S. (1978) Cretaceous Chronology of the Lower Buller Valley, South Island, New Zealand. *New Zealand Journal of Geology and Geophysics* 21, 455-462.

Adams, C.J.D., Harper, C.T. and Laird M.G. (1974) K-Ar ages of low grade metasediments of the Greenland and Waiuta Groups in Westland and Buller, New Zealand. *New Zealand Journal of Geology and Geophysics*, 18, 39-48.

Anderson, R.E. (1971) Thin Skin Distension in Tertiary Rocks of Southeastern Nevada. *Geological Society of America Bulletin*, 82, 43-58.

Aronson, J.L. (1965) Reconaisance Rubidium-Strontium Geochronology of New Zealand Plutonic and Metamorphic rocks. *New Zealand Journal of Geology and Geophysics*, 8, 401-423.

Aronson, J.L. (1968) Regional geochronology of New Zealand. *Geochimica et Cosmochimica Acta.*, 32, 660-697.

Bartrum, J.A. (1914) Some intrusive igneous rocks from the Westport district. *Transactions*, Vol. XLVI pp 262-269, Article XXXIV.

Behr, H. J. (1980) Polyphase shear zones in the granulite belts along the the margins of the Bohemian Massif. *Journal of Structural Geology*, 2, 249-254

Bell, T.H. (1985) Deformation partitioning and porphyroblast rotation in metamorphic rocks: a radical reinterpretation. *Journal of Metamorphic Geology*, 3, 109-118.

Bell. T. H. and Hammond, R.L. (1984) On the internal geometry of Mylonite Zones. *Journal of Geology*, 92, 367-686.

Bell, T.H. and Cuff, C. (1989) Dissolution, solution transfer, diffusion versus fluid flow and volume loss during deformation/metamorphism. *Journal of Metamorphic Geology*, 7, 425-447.

Bell, T.H. and Johnson, S.E. (1992) Shear sense: a new approach that resolves conflicts between criteria in metamorphic rocks. *Journal of Metamorphic Geology*, 10, 99-124.

Berthe', D. and Brun, J. P.(1980) Evolution of folds during progressive shear in the South Amorican Shear Zone. *Journal of Structural Geology*, 2, 127-133

Berthé, D., Choukroune, P. and Jegouzo, P. (1979) Orthogneiss, mylonite and non-coaxial determination of granites: the example of the South Armorican shear zone. *Journal of Structural Geology*, 1, 31-42.

Blumenfeld, P. and Bouchez, J.L.(1988) Shear criteria in granite and migmatite deformed in the magmatic and solid states. *Journal of Structural Geology*, 10, 361-372

Bowen, F.E. (1964) Geological Map of New Zealand, Buller, sheet 15, scale 1:250,000. New Zealand Department of Scientific and Industrial Research, Wellington.

Bradshaw, J. D. (1989) Cretaceous Geotectonic Patterns in the New Zealand Region. *Tectonics*, 8, 803-820.

Bradshaw, J. D. (1993) A review of the Median Tectonic Zone: terrane boundaries and terrane amalgamation near the Median Tectonic Line. *New Zealand Journal of Geology and Geophysics*, 36, 117-125.

Brun, J.P and Van Den Driessche, J. (1994) Extensional gneiss domes and detachment fault systems: structure and kinematics. *Bulletin de la Societe geologique de France.* 165, 519-530.

Brunel, M. (1980) Quartz fabrics in shear-zone mylonites, evidence for a major imprint due to late Strain increments. *Tectonophysics*, 1964 T33-T44.

Buck, W.R. (1988) Flexural rotation of normal faults. *Tectonics*, 7, 959-973.

Cobbold, P. R. and Quinquis, H. (1980) Development of sheath folds in shear regimes. *Journal of Structural Geology*. 2, 119-126.

Coney, P. J. (1980) Cordilleran metamorphic core complexes: an overview. *Geological Society of America Memoir*, 153, 17-28

Coney, P.J. and Harms, T.A (1984) Cordilleran metamorphic core complexes: Cenozoic extensional relics of Mesozoic compression. *Geology* 12, 550-554.

Cooper, R. A. (1974) Age of the Greenland and Waiuta Groups, South Island, New Zealand. *New Zealand Journal of Geology and Geophysics*, 17, 955-962.

Cooper, R.A. (1989) Early Paleozoic Terranes of New Zealand, *Journal of the Royal Society of New Zealand*, 19, 73-112.

Cox, S. H. (1882) Notes on the mineralogy of New Zealand. *Transactions and Proceedings of the New Zealand Institute*, XV, 361-409.

Davis, G. H. and Coney, P. J (1979) Geologic development of the Cordilleran metamorphic core complexes. *Geology*, 7, 120-124.

Davis, G.H. and Hardy, J.J. (1981) The Eagle Pass detachment, southeastern Arizona: product of mid-Miocene listric (?) normal faulting in the Southern Basin and Range. *Bulletin of the Geological Society of America*, 92, 749-762.

Etchecopar, A . (1977) A plane kinematic model of progressive deformation in polycrystalline aggregates. *Tectonophysics* 39, 121-139.

Etchecopar, A ., Vasseur, G. (1987) A 3-D Kinematic model of fabric development in polycrystalline aggregates: comparisons with experimental and natural examples. *Journal of Structural Geology*, 9, 705-717.

Fletcher, J.M. and Bartley, J.M (1994) Constrictional strain in a non-coaxial shear zone: implications for fold and rock development, central Mojave metamorphic core complex, California. *Journal of Structural Geology*, Vol 16, 555-570.

Fueten, F. (1992) Tectonic interpretations of systematic variations in quartz c-axis fabrics across the Thompson Belt. *Journal of Structural Geology*, 14, 775-789.

Gans, P.B., Mahood, G.A. and Schermer, E. (1989) Synextensional magmatism in the Basin and Range Province; A case study from the eastern Great Basin. *Geological Society of America Special Paper* 233, pp53.

Gapais, D. and White, S.H. (1982) Ductile shear bands in a naturally deformed quartzite. *Textures and Microstructures*, 5, 1-17.

Ghosh, S. K. and Sengupta, S. P (1987) Progressive development of structures in a ductile shear zone. *Journal of Structural Geology*, 9, 277- 287.

Gibson, G.M., McDougall, I. and Ireland, T.R. (1988) Age constraints on metamorphism and the development of an metamorphic core complex in Fiordland, Southern New Zealand. *Geology*, Vol. 16, 405-408.

Grindley, G.W. (1959) The Geological Map of New Zealand 1:2 000 000. *New Zealand Geological Survey Bulletin* 66.

Grindley, G.W., Harrington, H. J., and Wood, B. L. (1961) The geological map of New Zealand, scale 1: 2,000,000, New Zealand Department of Scientific and Industrial Research, Wellington, 1961.

Haast, J. von (1865) Jurors Report on the New Zealand Expedition. P257

Hanmer, S. and Passchier, C (1991) Shear-sense indicators: a review. *Geological Survey of Canada Paper* 90-17.

Hector, J. (1865) Jurors Report on the New Zealand Expedition. P266, 437.

Henderson, J. (1917) The Geology and Mineral Resources of the Reefton Subdivision: *New Zealand Geological Survey Bulletin*, 18, 233p.

Hill, E.J., Baldwin, S. L.and Lister, G.S. (1992) Unroofing of active metamorphic core complexes in the D'Entrecasteaux Islands Papua New Guinea. *Geology* 20, 907-910.

Hippert, J.F. (1993) 'V'-pull-apart microstructures: a new shear-sense indicator. *Journal of Structural Geology*, 15, 1393-1403.

Hippert, J.F. (1994) Microstructures and c-axis fabrics indicative of quartz dissolution in sheared quartzites and phyllonites. *Tectonophysics*, 229, 141-163

Hume, B.J. (1977) The relationship between the Charleston Metamorphic Group and Greenland Group in the Central Paparoa Range, South Island, New Zealand. *Journal of the Royal Society of New Zealand*, 7, 379-392.

Ireland, T.R. (1992) Origin of gneisses in the Charleston Metamorphic Group. *Geological Society of New Zealand Miscellaneous Publication* 63A p83.

Keep, M. and Hansen, V.L. (1994) Deformational Styles in the Proterozoic Pinal Schist, Pinal Peak Arizona: Microstructural and Quartz Analyses. *Journal of Structural Geology*, 102, 229-242.

Kimbrough, D.L., and Tulloch, A.J. (1989) Early Cretaceous age of orthogneiss from the Charleston Metamorphic Group, New Zealand. *Earth and Planetary Science Letters*, 95, 130-140

Laird, M.G. (1967) Field Relations of the Constant Gneiss and Greenland Group of the Central Paparoa Range, West Coast, South Island. *New Zealand Journal of Geology and Geophysics* 10, 247-256.

Laird, M.G. (1988) Geological map of New Zealand Punakaiki, sheet S37, Scale 1:63,360 New Zealand Department of Scientific and Industrial Research, Wellington.

Laird, M. G. (1994) Geologic aspects of the opening of the Tasman Sea. *In:* van der Lingen, G.J., Swanson, K. M., and Muir, R. J. (eds) Evolution of the Tasman Sea Basin: proceedings of the Tasman Sea Conference, Christchurch, New Zealand, 27-30 Nov 1992. A.A Balkema, Rotterdam, 1-17.

Law, R.D., Knipe, R.J. and Dayan, H. (1984) Strain Path partitioning within thrust sheets: microstructural and petrofabric evidence from the Moine Thrust Zone at Loch Eriboll, Northwest Scotland: *Journal of Structural Geology*, 6, 477-497.

Law, R.D., Casey, M. and Knipe, R.J., (1986) Kinematic and tectonic significance of microstructures and crystallographic fabrics within quartz mylonites from the Assynt and Eriboll regions of the Moine Thrust Zone, North West Scotland. *Transactions of the Royal Society of Edinburgh: Earth Sciences* 77, 99-125.

Law, R.D., Schmid, S.M. and Wheeler, J. (1990) Simple shear deformation and quartz cystallographic fabrics: a possible natural example from the Torridon area of North-West Scotland. *Journal of Structural Geology*, 12, 29-45.

Law, R.D., Miller, E.L, Little, T.A. and Lee, J. (1994) Extensional origin of ductile fabrics in the Schist Belt, Central Brooks Range, Alaska-II, Microstructural and petrofabric evidence. *Journal of Structural Geology*, 16, 919-940.

Lee, J. and Lister, G. S. (1992) Late Miocene ductile extension and detachment faulting, Mykonos, Greece. *Geology*, 20, 121-124.

Lister, G. S. and Snoke, A. W. (1984) S-C mylonites. *Journal of Structural Geology*, 6, 617-38.

Lister, G.S. and Williams, P.F. (1979) Fabric development in shear zones: theoretical controls and observed phenomena. *Journal of Structural Geology*, 1, 283-297.

Lister, G.S. and Hobbs, B.E. (1980) The simulation of fabric development during plastic deformation and its application to quartzite: the influence of deformation history. *Journal of Structural Geology*, 2, 1039-1044.

Lister, G.S. and Dornsiepen, U.F. (1982) Fabric transitions in the Saxony granulite terrain. *Journal of Structural Geology*, 4, 81-92.

Lister, G.S. and Davis, G.A. (1989) The origin of metamorphic core complexes and detachment faults during Tertiary continental in the northern Colorado river region, U.S.A. *Journal of Structural Geology*, 11, 65-94.

Lister, G.S., Patterson, M.S. and Hobbs (1978) The simulation of fabric development in plastic deformation and its application to quartzite: the model. *Tectonophysics*, 45, 107-158.

Lloyd, G.E., Law,R.D., Mainprice,D. and Wheeler, J. (1992) Microstructural and crystal fabric evolution during shear zone formation. *Journal of Structural Geology*, 14, 1079-1100.

Mainprice, D., Bouchez, J. L. and Blumenfeld, P. *et al* (1986) Dominant c slip in naturally deformed quartz: implications for dramatic plastic softening at high temperature. *Geology*, 14, 819-822

Malavielle, J. (1987) Extensional shearing deformation and kilometer-scale "a-type" folds in a Cordilleran metamorphic core complex. *Tectonics*, 6,423-448.

Miller, E.L., Gans, P.B. and Garing. J. (1983) The Snake range decollement: and exhumed mid-Tertiary brittle-ductile transition. *Tectonics.*, 2, 239-263.

Morgan, P.J. and Bartrum, J.A. (1915) The Geology and Mineral Resources of Buller-Mokihinui Subdivision. *New Zealand Geological Journal*, Bulletin 17, 210p.

Muir, R.J., Bradshaw, J. D. and Weaver, S. D. (1994b) Crustal extension prior to the opening of the Tasman Sea Basin: Evidence from New Zealand granites. *In:* van der Lingen, G. J., Swanson, K. M., Muir, R. J. (Eds) Evolution of the Tasman Sea Basin: Proceedings of the Tasman Sea Conference, Christchurch, New Zealand, 27-30 November 1992. A.A.Balkema, Rotterdam, 55-64

Muir, R.J., Ireland, T.R., Weaver, S.D. and Bradshaw, J.D. (1994a) Ion microprobe U-Pb zircon geochronology of granite magmatism in the Western Province of the South Island, New Zealand. *Chemical Geology*, 113, 171-189.

Muir, R.J., Weaver, S.D., Bradshaw, J.D., Eby, G.N. and Evans, J.A. (1995) Geochemistry of the Cretaceous Separation Point Batholith, New Zealand: granitoid magmas formed by melting of mafic lithosphere. *Journal of the Geological Society of London.*, 152 (In Press).

Nathan, S. (1975) Geological map of New Zealand, Foulwind and Charleston, sheets S23 and S30, scale 1:63,360, New Zealand Department of Scientific and Industrial Research, Wellington.

Passchier, C.W. and Simpson, C. (1986) Porphyroclast systems as kinematic indicators. *Journal of Structural Geology*, 8, 831-843.

Paterson, S. R., Vernon, R. H. and Tobish, O. T. (1989) A review of criteria for the identification of magmatic and tectonic foliations in granitoids. *Journal of Structural Geology*, Vol. 11, 349-363

Phillips, E. R., Ransom, D. M., Vernon, R. H. (1972) Myrmekite and muscovite developed by retrograde metamorphism at Broken Hill, New South Wales. *Mineralogical Magazine*, 38, 570-578.

Platt, J.P. and Vissers, R.L.M. (1980) Extensional structures in anisotropic rocks. *Journal of Structural Geology*, 2, 397-410.

Ramsay, J.G. (1967) Folding and Fracturing of Rocks. McGraw-Hill Inc. 569p

Reed, J.J. (1958) Granites and mineralisation in New Zealand. *Journal of Geology and Geophysics*, 1, 47-64.

Reynolds, S. J. and Lister, G.S. (1990) Folding of mylonitic zones in Cordilleran metamorphic core complexes: Evidence from near the mylonitic front. *Geology*, 18, 216-219.

Royden, L.H. and Burchfiel, B. C. (1987) Thin-skinned N-S extension within the convergent Himalayan region: gravitational collapse of a Miocene topographic front. *From* Cowards, M.P., Dewey, J.F. and Hanckock, P.L. (eds) Continental Extensional Tectonics, *Geological Society Special Publication* No. 28, 99 611-619.

Sawyer, E.W. and Robin, P.Y.F. (1986) The subsolidus segregation of layer-parallel quartz-feldspar veins in greenschist to upper amphibolite facies metasediments. *Journal of Metamorphic Geology*, 4, 237-260.

Schmid, S.M. and Casey, M. (1986) Complete fabric analysis of some commonly observed quartz c-axis patterns. *American Geophysical Union Monograph* 36, 263-286.

Shelley, D. (1970) The structure and petrography of the Constant Gneiss near Charleston, South-West Nelson, New.Zealand. *Journal of Geology and Geophysics,* 13, 1370-1391.

Shelley, D (1972) Structure of Constant Gneiss near Cape Foulwind, Southwest Nelson and its bearing on the regional tectonics of the West Coast. *Journal of Geology and Geophysics,* 15, 33-48.

Shelley, D. (1985) Optical Mineralogy (2nd Ed). Elsevier Science Publishing Co., Inc. New York. 321p

Shelley, D. (1993) Igneous and metamorphic rocks under the microscope: classification, textures, microstructures and mineral preferred orientations. Chapman and Hall, London. 445 pp.

Shelley, D. (1995) Asymmetric shape preferred orientations as shear-sense indicators. *Journal of Structural Geology*, 17, 509-517.

Simpson, C. (1986) Determination of Movement Sense in Mylonites. *Journal of Geological Education*, 34, 246-261.

Simpson, C. and Schmid, S.M. (1983) An evaluation of criteria to deduce the sense of movement in sheared rocks. *Geological Society of America Bulletin*, 94, 1281-1288.

Smith., J. B. (1992) The geochemistry petrology and structure of granites from Cape Foulwind, southwest Nelson, New Zealand. Unpublished BSc (hons) project, housed in the University of Canterbury.

Spencer, J. E. (1984) Role of tectonic denudation in warping and uplift of low-angle normal faults. *Geology*, 12, 95-98.

Starkey, J. and Cutforth, C. (1978) A demonstration of the interdependence of the degree of quartz preferred orientation and the quartz content of deformed rocks. *Canadian Journal of Earth Science,* 15, 841-847

Suggate, R.P. (1957) The Geology of the Reefton Subdivision. *New Zealand Geological Journal*, Bulletin 56.

Tullis, J. And Yund, R.A. (1987) Transition from catacalstic flow to dislocation creep of feldspar: mechanisms and microstructures. *Geology.*, 15, 606-609.

Tulloch, A.J. (1983) Granitoid rocks of New Zealand- a brief review. *Geological Society of America Memoir*, 159, 5-19.

Tulloch, A.J. (1988) Batholiths, plutons and suites: Nomenclature for the granitoid rocks of Westland-Nelson. *New Zealand Journal of Geology and Geophysics*, 31, 505-509

Tulloch, A.J. and Brathwaite, R.L. (1986) Granitoid Rocks and associated mineralisation of Westland and West Nelson, New Zealand. International Volcanological Congress, New Zealand, South Island Igneous Rocks tour guides A3, C2, C7. *New Zealand Geological Survey, Record B*, 65-92.

Tulloch, A.J.and Kimbrough, D.L. (1987) Cretaceous Plutonic/tectonic provinces in the Westland Nelson Foreland, and a 'Metamorphic Core Complex' origin for the Charleston Metamorphic Group. *Geological Society of New Zealand, Miscellaneous Publication* 37A.

Tulloch, A.J. and Kimbrough, D.L. (1989) The Paparoa Metamorphic Core Complex, New Zealand: Cretaceous Extension associated with fragmentation of the Pacific Margin of Gondwana. *Tectonics*, 8, 1217-1234

Tulloch, A.J. and Palmer, K. (1990) Tectonic implications of the granite cobbles from the mid-Cretaceous Pororari Group, southwest Nelson, New Zealand. *New Zealand Journal of Geology and Geophysics*, Vol. 33, 205-217.

Tulloch, A.J., Kimbrough, D.L. and Waight, T.E. (1994) The French Creek Granite, North Westland, New Zealand - Late Cretaceous A-type plutonism on the Tasman passive margin (extended abstract). *In:* van der Lingen, G. J., Swanson, K. M. and Muir, R.J. (eds). Evolution of the Tasman Sea Basin: Proceedings of the Tasman Sea Conference, Christchurch, New Zealand, 27-30 November 1992. A.A. Balkema , Rotterdam , 65-67.

Vauchez, A. (1987) The development of discrete shear-zones in a granite: stress, strain and changes in deformation mechanisms. *Tectonophysics*, 133, 137-156.

Waight, T. E.(1995) The Geology and Geochemistry of the Hohonu Batholith and adjacent rocks, North Westland, New Zealand. Unpublished PhD thesis, housed in the University of Canterbury.

Weissel, J.K. and Hayes, D.E. (1977) Evolution of the Tasman Sea reappraised. *Earth and Planetary Science Letters*, 36, 77-84.

Wellman, H.W. (1956) Structural Outline of New Zealand, *New Zealand Department of Scientific and Industrial Research, Bulletin* 121.

Wernicke, B. (1981) Low-angle normal faults in the Basin and Range Province: nappe tectonics in an extending origin. *Nature*, 291, 645-648.

Wernicke, B. (1985) Uniform-sense normal simple shear of the continental lithosphere. *Canadian Journal of Earth Science*, 22, 108-125.

Wernicke, B. and Axen, G. J. (1988) On the role of isostacy in the evolution of normal fault systems. *Geology*, 16, 848-851.

White, P.J. (1994) Thermobarometry of the Charleston Metamorphic Group and implications for the evolution of the Paparoa Metamorphic Core Complex, New Zealand. *New Zealand Journal of Geology and Geophysics*, 37, 201-209

White, S.H., Burrows, S.E., Carreras, J., Shaw, N.D.and Humphreys, F.J.(1980) On mylonites in ductile shear zones. *Journal of Structural Geology*, 12, 175-187.

Yin, A. and Dunn, J.F. (1992) Structural and stratigraphic development of the Whipple-Chemehuevi detachment fault system, southeastern California: Implications dor the geometrical evolution of domal and basinal low-angle normal faults. *Geological Society of America Bulletin*, 104, 659-674.

APPENDIX A: Thin section/sample grid references and descriptions

Thin section/sample field number	Canterbury University Collection number	Location NZMS 260 K29	Description
CF50	15133	820383	deformed pegmatite
CF51		819383	deformed granite
CFS3		817373	granitoid mylonite
CFS2		817373	mylonitized syenogranite-monzogranite.
CFS4	15134	817373	"
CFS33	15135	822377	"
CFS27	15136	822377	"
CFS31	15137	822377	"
CFS38		822378	"
TB3b	15138	814357	deformed monzogranite
TB5	15139	813358	deformed monzogranite
C1	15140	796210	granitic gneiss
C3	15141	796211	granitic gneiss
DC8		798203	tonalitic gneiss
C10		798213	granodioritic migmatite
PH3	15142	812228	granodioritic gneiss
PH1	15143	811227	granodioritic gneiss
C40		814229	tonalitic gneiss
C28	15144	802222	migmatite
HFTB2	15145	813359	hornfels
HFTBA	15146	813357	hornfels
HFC	15147	813229	hornfels
		NZMS 260 K30	
DC15	15148	791200	biotite tonalite
DC5	15159	793179	mylonitized leucogrante
DC3	15150	792173	granitoid mylonite
R20		798176	granitoid mylonite
FM12	15151	783155	granitic gneiss
FM22		783155	granitic gneiss
FM15	15152	782154	granitoid mylonite
FM17	15153	781153	granitoid mylonite
MC1	15154	782132	granitoid mylonite
MC2	15155	782133	mylonitized leucogranite
MC5	15156	783133	mylonitized vein
WH31	15157	776126	granitoid mylonite
WH2	15158	776125	"
WH231		776126	"
WH32a		776127	"
WH233	15159	776128	granitoid mylonite

WH234		776128	"
WH35	15160	776130	"
WH36	15161	776130	"
WH37		776131	"
WH38	15163	776131	"
WH42	15164	776137	"
WH44		777134	"
WH43		776133	"
WH41		776133	"
DS833		777133	"
B29		772111	Red Jacket Granite
B3	15165	775113	granitoid mylonite
B5a		774113	mylonitized migmatite
B25		772111	"
B27		772108	"
WH24	15166	773112	"
WH50	15167	777118	"
WH51		777119	"
WH25		773113	"
B8	15168	772112	"
WH16		777120	"
B14	15169	771103	mylonitized mesosome
B18m	15170	772108	mylonitized mesosome
B37	15171	770104	mylonitized mesosome
WH22		777118	mylonitized migmatite
RJG2	15172	771106	Red Jacket Granite
RJG3		771102	Red Jacket Granite
B18f	15173	772108	Sill of Red Jacket Granite
HFSB2		771102	hornfels
B2a		771102	hornfels
HFSB1	15162	772111	hornfels
HFWH2		776127	hornfels
HFWH3		776127	hornfels

APPENDIX B: Red Jacket Granite XRF Analyses by N. Robinson

Major Results (as percent oxides)

	24695	24696	24697	24699	24700	24702	24703
SiO_2	71.80	73.08	62.08	72.79	66.91	73.35	71.12
TiO_2	0.11	0.17	0.80	0.26	0.66	0.11	0.23
Al_2O_3	15.37	14.76	16.75	14.78	15.69	14.67	14.28
Fe_2O_3	0.98	1.20	6.80	1.75	5.17	0.99	1.91
MnO	0.01	0.02	0.08	0.03	0.06	0.01	0.04
MgO	0.35	0.38	3.32	0.62	1.78	0.14	0.43
CaO	0.52	1.37	0.77	1.13	1.84	0.99	1.46
Na_2O	1.83	3.29	1.28	2.17	3.05	3.02	3.20
K_2O	6.95	4.83	5.50	4.82	3.02	5.58	4.71
P_2O_5	0.14	0.11	0.14	0.21	0.26	0.19	0.14
LOI	1.31	0.83	1.94	1.05	1.07	1.38	1.25
TOTAL	99.37	100.05	99.46	99.61	99.49	100.43	99.76

Trace Results (as parts per million)

Ga	21	21	20	24	19	21	21
Pb	63	46	20	25	42	58	57
Rb	185	182	329	265	200	159	171
Sr	64	78	62	80	104	61	78
Th	9	13	17	15	5	8	6
Y	11	20	32	39	24	11	26
V	10	21	112	71	25	14	20
Cr	6	11	91	61	18	6	8
Ni	6	7	41	25	15	6	7
Zn	24	35	98	82	35	29	25
Zr	64	87	137	110	86	80	68
Nb	8	5	13	28	5	9	6
Ba	180	215	556	111	484	168	218
La	14	21	45	34	15	17	12
Ce	44	45	84	65	46	38	30
Nd	18	24	38	37	23	21	17